THE UNIVERSITY
of EDINBURGH

Cost and Uncertainty in the Design of Offshore Wind Farms

Esteve Borràs Mora

2020

A thesis submitted in partial fulfilment of the requirements for the award of an Engineering Doctorate, jointly awarded by the University of Edinburgh, the University of Exeter and the University of Strathclyde.
The work presented has been conducted under the industrial supervision of EDF Energy R&D UK Centre as a project within the Industrial Doctoral Centre for Offshore Renewable Energy (IDCORE).

THE UNIVERSITY
of EDINBURGH

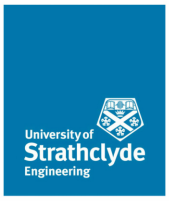

Declaration

I declare that this thesis has been composed solely by myself and that it has not been submitted, either in whole or in part, for any other degree or professional qualification except as specified. Except where otherwise acknowledged, the work presented is entirely my own. Parts of the work in this thesis have been published:

- Thought only a small fraction, Chapter 3 is based on Esteve Borras Mora, James Spelling, Adriaan H. van der Weijde. Transition from deterministic to stochastic cost models for offshore wind farms. Offshore Wind Energy 2017, London, United Kingdom.
- Chapter 5 is based on Esteve Borras Mora, James Spelling, Adriaan H. van der Weijde. Benchmarking the PAWN distribution-based method against the variance-based method in global sensitivity analysis: Empirical results. Environmental Modelling and Software 122 (2019) 104556
- Chapter 6 is based on Esteve Borras Mora, James Spelling, Adriaan H. van der Weijde. Global sensitivity analysis for offshore wind cost modelling. This paper has been recommended for publication in Wind Energy.
- Chapter 7 is based on Esteve Borras Mora, James Spelling, Adriaan H. van der Weijde, Ellen-Mary Pavageau. The effects of mean wind speed uncertainty on project finance debt sizing for offshore wind farms. Applied Energy 252 (2019) 113419.
- Chapter 8 is based on Esteve Borras Mora, James Spelling, Adriaan H. van der Weijde. How does risk aversion shape overplanting in the design of offshore wind

farms? Journal of Physics: Conference Series 1356 012026 as well as Esteve Borras Mora, James Spelling, Adriaan H. van der Weijde. Cost and uncertainty in overplanting the design of offshore wind farms. 42nd International Association for Energy Economics (IAEE) International Conference 2019 - Local Energy, Global Markets. Montreal, Canada.

All publications written as part of this thesis are appended in Chapter 10.

Esteve Borràs Mora

Lay Summary

The goal of the Engineering Doctorate is to develop new methodologies to optimise the design of offshore wind farms subject to uncertainty, simultaneously considering cost and risk aspects. This thesis describes the methodology of a cost modelling tool to evaluate the financial performance of offshore wind assets, as well as the development, validation and deployment of a framework for quantitative uncertainty management with several applications relevant to the offshore wind industry. The application of the quantitative uncertainty management framework to the cost modelling tool highlights: key parameters when building financial models for offshore wind farms, guidance on additional efforts towards reducing their uncertainties and recommendations when choosing among uncertainty analysis techniques. In addition it provides management with a method to arrive at optimal solutions to complex decision-making problems; this is demonstrated through the analysis of case studies that can lead to further optimisation of offshore wind farms by linking the financial valuation to the engineering design.

Abstract

Offshore wind cost modelling seeks to understand and quantify how different project specifications, technology choices and market trends contribute to the overall project finances; linking extensive financial valuation to the engineering design and supporting investment decisions at the initial stages of development. This offers a basis for objective communication and decision-making; allowing for a greater number of cases to be analysed; and when considering new ideas, offering the option to assess the economic feasibility and potential.

Cost modelling involves a heavy reliance on models. As models become more realistic, they also become more complex and difficult to understand; especially where model inputs are subjected to sources of uncertainty. The goal of the Engineering Doctorate is to develop new methodologies to optimise the design of offshore wind farms subject to uncertainty, simultaneously considering cost and risk aspects. This thesis describes the methodology of a cost modelling tool to evaluate the financial performance of offshore wind assets, as well as the development, validation and deployment of a framework for quantitative uncertainty management with several applications relevant to the offshore wind industry.

This framework is key for risk analysis, producing metrics for the spread of the project performance. However, due to model complexity and input uncertainty, modellers find it difficult to grasp the response of the risk metric to variation in cost drivers based, solely, on intuition. For this reason, global sensitivity analysis is used to identify key

cost drivers and neglect the contribution of those that are not relevant. To accomplish this, a toolbox is built to benchmark two techniques: the variance-based and distribution-based method against a set of well-known test functions. This comparison provides new insights on the applicability of the methods. In addition, the application of the framework to the cost modelling tool highlights: key parameters when building financial models for offshore wind farms, guidance on additional efforts towards reducing their uncertainties and recommendations when choosing among global sensitivity analysis techniques.

The application of this framework to offshore wind cost modelling equips management with a method to arrive at optimal solutions to complex decision-making problems. For example, it provides a competitive advantage when performing strategic and competitive tender analysis, comparative evaluation of multiple sites, detailed evaluation of specific project layouts and sensitivity studies on both design/technology choices and cost variations.

Finally, two techno-economic applications are dealt with in this thesis. While the first one provides a framework to answer the question: does the deployment of additional advanced sensing technology, which presumably reduces wind speed uncertainty, compensate for the incurred development expenditure? The second aims at answering the question: given the fact that most of the time the wind farm is not generating at full power, is there any economic benefit to install additional wind turbines for a given export capacity?

Acknowledgements

This EngD thesis is the result of three years of work at the EDF Energy R&D UK Centre, during which time I have received help and support from a wide range of people.

First and foremost, I would like to thank my industrial and academic supervisors Dr. James Spelling and Dr. Harry van der Weijde. This thesis would not have been possible without their continuous advice and support. James granted me the opportunity to join EDF Energy R&D UK Centre, involved me from the very beginning in the industrial context and deeply inspired me with his scientific rigour and understanding. Harry guided me through each stage of the process, always providing useful insights and giving me countless opportunities to develop and expand my knowledge of the topic, both in terms of breadth and depth.

I would also like to express my gratitude to EDF Energy R&D UK Centre for hosting me over those three years and for letting me be part of the cost modelling team, EDF Renouvelables for helping me understand how to assess the financial viability of offshore wind farms in the real world and EDF R&D in France for their collaboration. Special thanks go to my line managers Dr. Ellen Marie Pavageau and Dr. Marie Berthelot for their support and trust. To my colleagues at EDF Energy R&D UK Centre, a big thanks for the sense of community, for building a culture of constant learning and for all the great moments we have had together.

I am also grateful to my fellow IDCOREians and especially to Alex, with whom I have exchanged a great deal of ideas, support and advice throughout the course of the engineering doctorate. To Albert and Bernat and to my friends in the UK, Spain, France, Russia, the US, Peru, Germany, Czech Republic and around the world, thank you for always being there. You always give me reasons to go away from work and see things from different angles. Last but not least, I would like to thank my family for their unconditional love and support throughout my academic studies.

For all this, I am extremely grateful.

Funding from the Energy Technologies Institute (ETI) and the RCUK Energy Programme for the Industrial Doctoral Centre for Offshore Renewable Energy (Grant number EP/J500847/1) is gratefully acknowledged.

Contents

List of Tables

List of Figures

List of Abbreviations

AEP Annual Energy Production

AIS Air Insulated Switchgear

ANOVA Analysis of Variance

AR Allocation Round

ASP Administrative Strike Price

BHHMM Below Hub Height Met Mast

BI Business Interruption

BSUoS Balancing Services Use of System

CAPEX Capital Expenditure

CAR contractors all risk

CCA Climate Change Act

CCDF Conditional Cumulative Distribution Function

CDF Cumulative Distribution Function

CER The Irish Commission for Energy Regulation

CFADS Cash Flow Available for Debt Service

CfD Contract for Difference

CTV Crew Transfer Vessel

CVaR Conditional Value at Risk

DECC Department of Energy and Climate Change

DECEX Decomissioning Expenditure

DEVEX Development Expenditure

DSCR Debt Service Coverage Ratio

DSU Delayed Start-Up insurance

ECN the Energy Research Centre of the Netherlands

EMR Electricity Market Reform

EPCM Engineering, Procurement, and Construction Management

ESReDA European Safety, Reliability and Data Association

FID Final Investment Decision

FIDER Final Investment Decision enabling for Renewables

FLIDAR Floating Light Detection and Ranging

FORM First-Order Reliability Method

FV Future Value

GIS Gas Insulated Switchgear

GSA Global Sensitivity Analysis

HAFLIDAR High Accuracy Commercial Floating LIDAR

HDMR High Dimensional Model Representation

HHMM Hub Height Met Mast

HLDP Heavy Lift Dynamic Positioning vessel

HLJU Heavy Lift Jack-Up vessel

HVAC High Voltage Alternating Current

HVDC High Voltage Direct Current

HVOS High Voltage Offshore Substation

IRR Internal Rate of Return

ISO GUM ISO guide to the expression of uncertainty in measurement

KDE Kernel Density Estimation

KS Kolmogorov-Smirnov statistic

LAFLIDAR Low Accuracy Commercial Floating LIDAR

LCCC Low Carbon Contracts Company

LSA Local Sensitivity Analysis

LV Low Voltage

MARR Minimum Acceptable Rate of Return

MEC Maximum Export Capacity

MEC Maximum Export Capacity

MP Monopile

MVAC Medium Voltage Alternating Current

NDT Non-destructive Testing

NPV Net Present Value

O&G Oil & Gas

O&M Operation and Maintenance

OEM Original Equipment Manufacturer

OFTO Offshore Transmission

OPEX Operational Expenditure

OTB Offshore Transportation Barge

OTM Offshore Transformer Module

OWCAT Offshore Wind Cost Analysis Tool

PDF Probability Distribution Function

PD Property Damage

PINS Planing Inspectorate

PPA Power Purchase Agreement

PV Present Value

QR Quasi-random

ROC Renewable Obligation Certificate

RO Renewable Obligation

ROV Remotely Operated Vehicle

SCADA Supervisory Control and Data Acquisition

SEU Subjective Expected Utility

SORM Second-Order Reliability Method

SPJU Self-propelled Jack-up Vessel

SPV Special Purpose Vehicle

SQSS Security and Quality of Supply Standards

SVC Static Var Compensator

TCE The Crown Estate

TNUoS Transmission Network Use of System

TP Transition Piece

TSO Transmission System Operator

TSO Transmission System Operator

UCDF Unconditional Cumulative Distribution Function

UPS Uninterruptible Power Supply

UXO Unexploded Ordnance

VaR Value at Risk

VBSA Variance-based Sensitivity Analysis

VCA Value Chain Assessment

WACC Weighted Average Cost of Capital

XPLE Cross-linked Polyethylene cables

Part I

Specifying the Research Question

Chapter 1

Introduction

This first chapter sets the stage for the rest of the thesis. It begins with the context in which this thesis has been performed, followed by a problem statement that needs to be addressed. Then, the aims and objectives of the study are stated and a brief overview of the contributions is given. Finally, the layout of the rest of the thesis is presented.

1.1 Think Globally, Act Locally – UK Offshore Wind

With the advent of anthropogenic climate change, energy system's objectives have shifted from mainly focusing on security of supply to decarbonisation. The introduction of legally-binding carbon targets in the UK, as stated in the Climate Change Act (CCA), committed the UK government by law to reducing greenhouse gas emissions by at least 80% by 2050, compared with 1990 levels [1]. The CCA marked the beginning of a strong push for decarbonisation. However, both decarbonisation and security of supply have to be achieved simultaneously in a time- and cost-effective manner. Whereas the timescale is dictated by the battle against anthropogenic climate change and measured against appropriate climate change targets, its costs can be seen as a binding constraint, as the government has to ensure that customers are able to pay their energy bills. In addition, energy systems, and electricity generation in particular, are increasingly facing growing energy demand associated with human population growth and stricter carbon emission constraints [2]. Therefore, the quest for affordable, clean and reliable energy is more pressing than ever, and has led to a renewed interest

in the development of renewable energy technologies, of which offshore wind has played, plays and will play a leading role.

The first offshore wind farm in the world was installed in 1991 in Videnby, Denmark. The project was located at approximately 2 km from shore at water depths ranging from 3 to 7 meters. It consisted of 11 wind turbines with an overall capacity of 4.95 MW [3], approximately half of the size of a current 10 MW wind turbine. Since Vindeby, the offshore wind sector has grown at an unprecedented pace and has become one of the leading contenders for the future provision of renewable energy.

The growth of total installed capacity has gone hand-in-hand with the downward trajectory of its costs, which, to a large extent, can be attributed to supportive policy frameworks. These policy frameworks have enabled the development of a robust industrial structure, giving confidence to a broad range and type of organisations to make the necessary investment decisions for the industry to flourish [4]. Government intervention has helped the offshore wind industry at the initial stages, providing market scale and clarity, de-risking private sector investment and allowing for technological development. As a result of capital grants to support innovative demonstration projects, fixed remuneration systems to increase investor confidence, and the more recent competitive auctions, offshore wind sits in the energy mix as one of the most promising technologies to lead the energy transition.

At a very early stage, the UK government decided to take an open door approach to site identification and let developers identify potential sites for offshore wind, given the low levels of information on wind conditions, seabed geology, wave height, etc. The Crown Estate (TCE), an independent organisation responsible for managing offshore renewable energy development rights, awarded development rights through a series of licensing rounds: Round 1 in April 2001 with 1.6 GW, Round 2 in December 2003 with 7.3 GW, Round 1 & 2 Extensions in May 2010 with 1.6 GW, Scottish Territorial Round in January 2009 with 4.8 GW and Round 3 in January 2010 with over 32 GW [5] . More recently, TCE held in 2019 the UK Round 4 with the aim of providing up

to 7GW in offshore wind leasing rights [6].

The UK is characterised by a highly decentralised model of site development, where the only activity taken at government level is the zone identification carried out by TCE. This zone identification is based on site characteristics criteria such as wind speed, seabed conditions, water depth, and known site constraints such as environmental impacts, shipping routes and grid connection. If developers are successful in bidding for the exclusivity of a given zone, they can proceed with the selection of a site within the awarded zone, negotiate the lease with the Planing Inspectorate (PINS) (Or Marine Scotland when applicable), acquire grid permits from National Grid and design and construct the electrical infrastructure, which will eventually be sold through the Offshore Transmission (OFTO) regime. Once a project is consented and fully permitted, the project can apply for support mechanisms.

Two support mechanisms have been put in place in the UK for the development of offshore wind farms, the Renewable Obligation (RO) and the Contract for Difference (CfD) schemes. The RO scheme, which came into effect in 2002 in England, Wales and Scotland, followed by Northern Ireland in 2005, was designed to encourage the deployment of renewable energy in the UK. It placed an obligation on UK electricity suppliers to source an increasing proportion of the electricity they supply from renewable sources through Renewable Obligation Certificates (ROC). ROCs are green certificates issued to electricity generators and bought by suppliers to show that they have fulfilled the RO. This gave incentives to all qualifying developers by providing a fixed level of support, in addition to the wholesale market price for a period of 20 years. Although the level of ROC support depends on the technology and the date of accreditation, the offshore wind industry benefited from a high level of support compared to other qualifying technologies. However, the RO was phased out on the 31st of March 2017, after a transitional period where developers could apply for either ROC or CfD support mechanisms [7].

In 2012, the UK electricity market went through a series of reforms under the Electricity Market Reform (EMR) programme [8]. Under this programme, the CfD was set to replace the ROC. Long-term CfDs are private law contracts between a low carbon electricity generator and the Low Carbon Contracts Company (LCCC), a government-owned company. The purpose of the CfD is to provide greater certainty and stability of revenues to electricity generators by reducing the exposure of electricity generators to volatile wholesale prices. This is achieved through a two-way payment mechanism. If the strike price is greater than the wholesale price, the generator is paid by the LCCC a top-up above the wholesale price up to the set strike price. Otherwise, the generator is required to make payment back to the CfD counterparty, as displayed in Figure 1.1. Developers are paid a flat (indexed to inflation) rate for the electricity they produce over a 15-year period. Therefore, CfDs incentivise investment in renewable energy projects faced with high upfront costs and lengthy projected cash flows by offering them direct protection from volatile wholesale electricity prices, while protecting consumers from paying increased support costs when electricity prices are high.

CfDs are awarded through Allocations Rounds (ARs), whereby renewable generators can apply for a CfD by submitting what is a form of "sealed bid". In these auctions, different renewable technologies compete against each other for the contract. The frequency of auctions is established by the government. The government also sets out an Administrative Strike Price (ASP) for each AR based on technology specific factors, market conditions and policy considerations. ASPs set out the maximum support, presented on a price per MWh basis for each technology in a given delivery year, reflecting the maturity of the technology. For example, in the AR 3, offshore wind CfD-awarded projects for delivery in 2023/2024 received an ASP of £56/MWh (in 2012 prices), which meant that a successful generator would receive, at its maximum, £56 for every MWh of energy generated. The competitive nature of these auctions are typically reflected in strike prices much lower than ASPs, resulting in lower costs incurred by consumers.

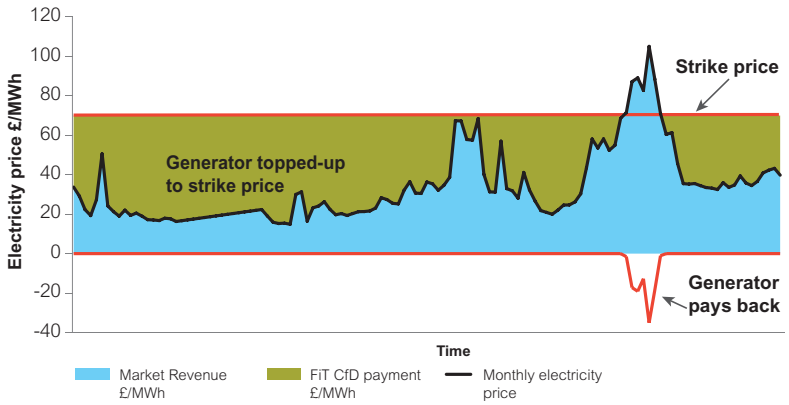

Figure 1.1: Contract for Difference [9]

The UK awarded early CfDs under the Final Investment Decision enabling for Renewables (FIDER) programme and held three allocation rounds: AR1, AR2 and AR3. Figure 1.2 shows the evolution of ASP as well as the auction results AR1, AR2 and AR3 for given delivery years. Dots for CfD ARs represent when the auction took place, while the end of the lines signals the project delivery year. Figure 1.2 has been compiled from several governmental sources [10, 11, 12]. ASP are shown in blue, CfD AR 1 in green, CfD AR 2 in red and CfD AR 3 in black. The strike price in AR1 almost halved in AR2 and decreased ever further in AR3, showing how rapidly the cost of offshore wind has gone down.

The success story of offshore wind is not only attributed to the UK government and its support mechanisms, but also to the many industrial actors within the sector committed to reducing the cost of energy. As the offshore wind market grew, so did the average wind turbine rated capacity, the distance from shore and the water depths. With the departure from small capacities new challenges and opportunities appeared to develop optimised projects and benefit from economies of scale. The size of the turbines kept growing, resulting in balance of plant and installation cost reductions due to the reduced number of units. The move from 33 to 66 kV in inter-array cables allowed for the connection of more turbines per string or the possibility to design inter-array configurations in ring layouts rather than in radial strings, thus increasing reliability. Bespoke vessels and equipment which can operate in a wider range

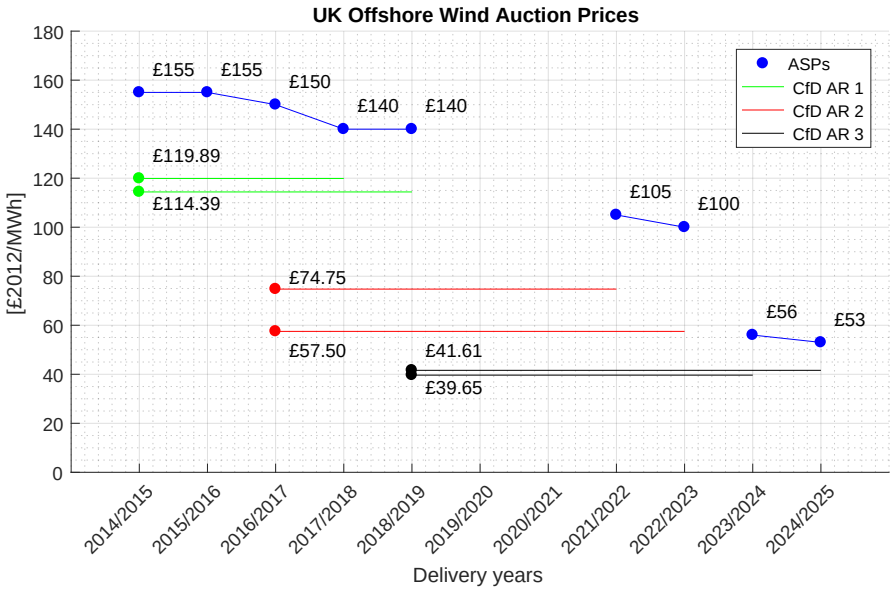

Figure 1.2: UK Contract for Difference Allocation Round Results

of conditions resulted in lower Operation and Maintenance (O&M) costs. This is just to name a few innovations; a comprehensive list on innovations in the offshore wind sector can be found in [13]. There is no doubt that technology innovation has been the cornerstone of steep cost reductions in the sector.

By the end of 2018, the European offshore wind market had installed a cumulative total capacity of more than 18GW. Within Europe, the UK is the market leader for offshore wind, responsible for 43% of the total number of all grid-connected turbines [14]. To sustain this leading position in the market, a Levelised Cost of Energy (LCOE) target of £100/MWh was set jointly by the UK government and industry in 2012 [15], which was expected to be met by 2020. However, four years ahead of schedule, wind farms taking final investment decisions in 2015/2016 were already achieving prices lower than this target. Record-low contracts for offshore wind farms were awarded to Borsselle 3 and 4 offshore wind project in the Netherlands at 54.5€/MWh in July 2016 [16] and Kriegers Flak in Denmark at 49.9€/MWh in November 2016 [17]. Following that, competitive tenders in Germany resulted in bid prices of 0€/MWh in April 2017 [18]. Although

those bids cannot be compared directly with UK prices, since they are associated with different support revenue mechanisms and do not bear the cost of the electrical transmission system, the bid levels were lower than expected. Support revenue mechanisms vary from country to country, as a result zero bids mean different things depending on which country we are referring to. As an example, if we consider Germany, the German subsidy scheme offers developers a 20-year price floor which is not inflation linked. Developers keep any upside should market prices rise above the level of their subsidy, however no protection is offered against inflation risk. This essentially means that the owners did not request any output subsidy on top of wholesale electricity prices. Another peculiarity of Germany is that German developers must build the offshore substation, but not the link to shore. This is very different to UK developers, who will need to price in the cost of the transmission link in the bid price. In addition to that, different schemes have different rules which make it very difficult to compare and interpret offshore wind bid prices across different countries. In the UK the Contract for Difference (CfD) Allocation Round (AR) 2 resulted in the lowest strike price seen at that moment with a value of £57.5/MWh in September 2017 [19], down from a lowest £114.39/MWh in CfD AR 1 in February 2015 [20]. In April 2018 in the second German auction, results included zero bids once again. In September 2019 in the UK CfD AR 3, prices dived to a staggering value of £39.65/MWh, 60% lower than the target imposed to be met by 2020 [21]. In addition, the UK government has committed to a series of CfD auctions starting in May 2019 and then every other year from then on, providing a greater level of certainty for the UK offshore wind industry [22].

The offshore wind industry has entered a maturation phase and a strong group of actors has emerged. This strong group of actors are the winners of recent tenders and range from developers to independent power producers, from institutional banks to commercial banks, from suppliers of wind turbines to cables, giving birth to a new hierarchy of players in the offshore wind industry. At the same time, the central auctioning system has scared off the group of actors who have not got experience over the recent tenders with such record-low clearing prices. Whereas this can be seen as a barrier to market entry, it reflects the fact that this strong group of players has acquired experience and

knowledge about what it takes to bring a project to commissioning or to deal with the marine construction risk, all of this supported by a strong track record of projects being delivered on time and on budget. There is a clear difference between the players who have acquired this experience and those who have not. Thus, this is reflected in the bids. This strong group feels much more confident about pricing what can be done and how and when to do it. They can either take the same risk at lower cost of capital because they are comfortable with it or consider that the risks are lower since they have already done it and know how to manage it.

As shown with record-low auctions results together with a basket of potential innovations and the emergence of well-established players in the sector, the transition to competitive central auctions has pushed developers to make predictions further into the future, increasing the level of uncertainty in their estimates and challenging the way offshore wind cost modelling had previously been addressed. In addition, offshore wind dominates the future growth of renewables in the UK, as shown across the different future energy scenarios from National Grid. Figure 1.3 shows the Two Degrees Future Energy Scenario from National Grid which achieves the 2050 decarbonisation target with large-scale centralised solutions. The success of future offshore wind projects is conditioned, more than ever, upon linking extensive financial valuation and uncertainty quantitative management techniques to the engineering design of offshore wind farms.

1.2 Problem Statement: Offshore Wind Techno-Economic Modelling

As the offshore wind market continues to thrive, a wider range of products is being offered to developers; more reliable sensing devices to measure the wind speed, taller, bigger and more powerful wind turbines, higher voltage inter-array systems, new bottom-fixed and floating foundation designs, longer export cables, better O&M strategies and data-driven solutions to operate the farms, advanced types of financing, etc. This increased variety of technology and product choices has resulted in an increased

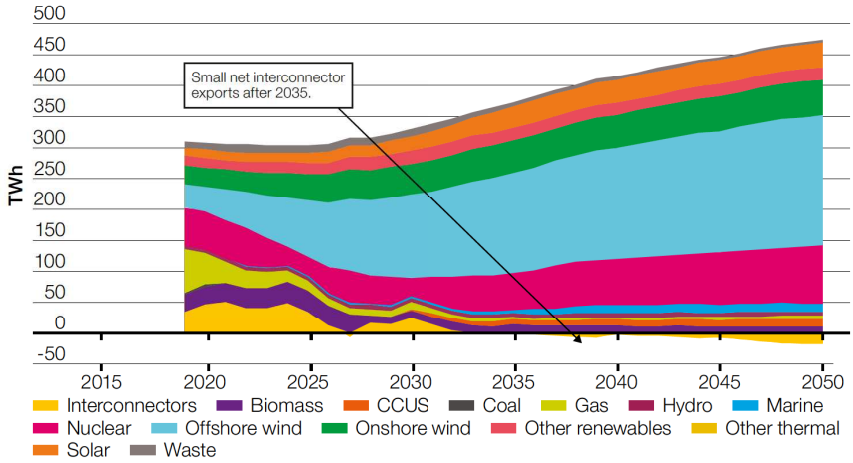

Figure 1.3: Electricity output by technology under Future Energy Scenario Two Degrees from National Grid [23]

complexity for project developers to make decisions regarding the optimal selection of technology and products for a given site. In addition to the increased variety, the unprecedented pace of the sector is pushing developers to conduct periodical market research reports to keep up with the latest technological trends, as there is room for accommodating innovations in the design of the farms due to long development periods before commissioning.

The evaluation of the financial viability of an offshore wind project is a multidisciplinary task, since it involves elements of engineering economics, capital budgeting, financial management and strategic planning as well as expert domain knowledge. Producing a cost estimate for a particular project is an enormous undertaking and requires interaction between teams from different disciplines. Therefore, there is a clear need to standardise and streamline the procedure to evaluate offshore wind projects by the creation of techno-economic cost modelling tools. Elements of economics, engineering and business need to be brought together to offer a basis for objective communication and decision-making, allowing for a greater number of cases to be analysed and when considering new ideas, offering the option to assess the economic feasibility and potential.

As offshore wind techno-economic models become more realistic, they also become more

difficult to understand, especially where model inputs are subjected to sources of uncertainty which impose a limit on the confidence of the model output. The problem not only lies in building cost modelling tools with the right level of granularity and sets of assumptions, but also to understand and quantify its sensitivities, which is key to understanding the risks and profitability for the next generation of offshore wind farms.

The application of uncertainty propagation techniques via Monte Carlo simulation usually requires a large number of model runs (in the order of thousands); this becomes prohibitive for most of the models. These additional computational costs need to be addressed by efficiently parallelising the computer code and the use of a high performance computing cluster.

Although methods have been developed in the academic literature to quantify uncertainties for complex models as shown in Chapter 2, these have not been applied in the offshore wind industry. In addition, and given the nature of the techno-economic modelling activities, studies tend to be either very detailed in the engineering design while putting aside financial valuation principles or they make use of sound financial models that do not take into consideration the engineering design. The current thesis is an attempt to remedy this lack of complex and computationally demanding analysis by linking the financial valuation and uncertainty quantitative management methods to the engineering design of offshore wind farms on a high-performance computing cluster.

1.3 Thesis Aim and Contributions

The work presented as part of this thesis aims to develop advanced analytical methods for offshore wind cost modelling in order to assess the financial viability of offshore wind assets and support its investment decisions at early stages of development. The developed approach builds on a leading industrial cost modelling tool by incorporating new methodologies to optimise the design of offshore wind farms subject to uncertainty,

simultaneously considering cost and risk aspects. In the development of this work, the objectives have been:

- extend the development of an existing cost modelling tool to reflect current technology choices and market trends as well as validate its assumptions
- investigate the latest techniques in stochastic and uncertainty analysis as well as provide a framework whereby the impacts of cost and uncertainty can be analysed
- identify key sources of uncertainty in assessing the overall project finance for offshore wind farms
- apply this framework to new designs and methodologies that can lead to further optimisation of offshore wind farms by linking the financial valuation to the engineering design

This thesis can be broken down into the following contributions, as displayed in Figure 1.4.

Part II - Methodology

Chapter 3 : Validation of the Cost Modelling Tool

The development of the cost modelling tool was extended to account for current technology choices and market trends. A validation of its assumptions was carried out in conjunction with several groups of experts and based on best practices in the industry. Aspects of project development, consenting, wind resource assessment, marine operations and civil, mechanical, reliability, electrical and financial engineering were scrutinized and challenged. The validation phase used a comparison of each department benchmark costs against the cost outputs from the cost modelling tool to make sure that they were in the same order of magnitude and within the tolerances established.

Chapter 4 : Overarching Stochastic Module

A quantitative uncertainty management framework was developed to help quantify how

different technology choices or market trends affect the spread of possible project performance. Model inputs were modelled by probability distribution functions, representing their inherent uncertainty. By propagating these uncertainties to the model output via Monte Carlo simulation or Sobol sequences, the probability distribution of the output can be obtained. The stochastic module allows modellers to analyse the impacts of cost and uncertainty based on a risk metric within a probabilistic framework.

Chapter 5 : Global Sensitivity Analysis Benchmark

In the search of the state-of-the art Global Sensitivity Analysis (GSA) techniques applicable to the cost modelling tool, two techniques came as potential solutions: the variance-based method and the PAWN distribution-based method. A GSA toolbox was built to benchmark the PAWN distribution-based method against the variance-based method for a set of well-known test functions. This comparison demonstrates the application of these two methods and provides new insights which can be shared across the applied mathematics community.

Chapter 6 : Global Sensitivity Analysis Module

The stochastic module is key for risk analysis, however, due to model complexity and input uncertainty modellers cannot longer grasp the response of the model output risk metric to variations in cost drivers based on sole intuition. Instead, GSA techniques allow modellers to study how the different sources of uncertainties in the risk metric can be apportioned to the different sources of uncertainty in the cost drivers, identifying key cost drivers and neglecting the contribution of those that are not important. The state-of-the-art methods in Chapter 5 were applied to the cost modelling tool and provided insight into key variables affecting the overall project finances.

Part III - Applications

Chapter 7 : Application I - Mean Wind Speed Uncertainty and Debt Sizing

The internal GSA study revealed the importance of the wind speed and financial parameters uncertainty. Developers need to understand the trade-off between the estimated

uncertainty in the wind resource assessment and the development expenditure incurred. For this reason, this work focused on a new way of understanding the effects of wind resource assessment campaigns by integrating project finance constraints into cost calculations and highlighting the importance of detailed cost modelling for optimal design of offshore wind farms. This research provided a framework to answer the question: does the deployment of additional advanced sensing technology, which presumably reduces wind speed uncertainty, compensate for the incurred development expenditure?

Chapter 8 : Application II - Overplanting

To date the connection of offshore wind farms is subjected to a Maximum Export Capacity (MEC) set in their connection agreement with the Transmission System Operator (TSO). Generators can export up to their contracted MEC, with any additional generation curtailed by the TSO. However, the share of time an offshore wind farm is generating at its MEC tends to be low. This application takes advantages of the stochastic capabilities of the cost modelling tool and aims at answering the question: given the fact that most of the time the wind farm is not generating at full power, is there any economic benefit to install additional wind turbines for a given export capacity?

1.4 Layout of the Thesis

This thesis has been divided into 9 chapter and 4 parts. The relationship among thesis chapters is shown in Figure 1.4 and Figure 1.5.

Part I is the point of departure of this work where the research question is specified. The first chapter began with an overview of the context of the work, the problem statement as well as its aims and contributions to knowledge. Chapter 2 provides a literature

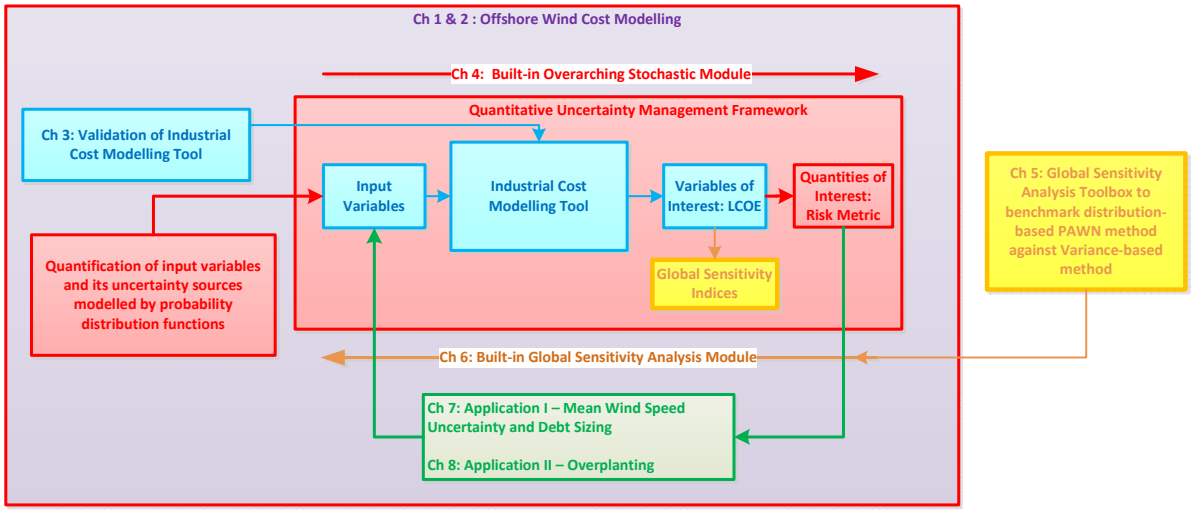

Figure 1.4: Thesis Contributions

review of the current methodologies for offshore wind cost modelling, taking into consideration techno-economic models and uncertainty quantification techniques.

Part II concerns the core methodology of this thesis. Chapter 3 introduces the cost modelling tool, covering aspects of project development, wind resource assessment, wind turbines, foundations and electrical components' expenditures, operation and maintenance and financial assumptions. Chapter 4 sets up the quantitative uncertainty quantification framework used throughout this thesis; this includes uncertainty analysis and propagation techniques, global sensitivity analysis, risk metrics, sampling techniques as well as a brief description of its practical implementation and access to a high performance computing cluster. Chapter 5 benchmarks two chosen global sensitivity analysis techniques against a set of well-known test functions to understand its applicability and scalability. Chapter 6 presents the application of these two global sensitivity analysis techniques to the cost modelling tool; key cost drivers are presented and recommendations for building offshore wind financial models are given.

Part III focuses on two industrial applications in the offshore wind industry that bridge the gap between financial valuation and engineering design and where the tools developed in this thesis can be applied to deliver value to a developer. Whereas Chapter 7 examines the effects of mean wind speed uncertainty to the debt sizing for project finance, Chapter 8 investigates the cost and uncertainty in overplanting the design of offshore wind farms.

Part IV presents the concluding remarks of this thesis. Chapter 9 concludes the work of this thesis and sets the stage for future studies, with academic, industrial and policy-making recommendations. The same chapter describes the academic and industrial impact of this work, given its industrial context within EDF Energy R&D UK Centre.

1.5 Formulating the Research Question

All research begins with a question. In order to formulate the research question a literature review was conducted in Chapter 2. We found enough material to define the following research questions:

- What are the latest techniques in stochastic and uncertainty analysis that can provide a framework to evaluate the techno-economic and financial performance of offshore wind assets in terms of cost and uncertainty? This question will address the gap in the literature regarding the use of quantitative uncertainty management techniques for offshore wind techno-economic models.
- What are the key sources of uncertainty in assessing the overall project finances for offshore wind farms? No literature that we know of identifies the key drivers in building complex offshore wind investment models.
- Can we apply a quantitative uncertainty framework that can lead to further optimisation of offshore wind farms by linking the financial valuation to the engineering design?

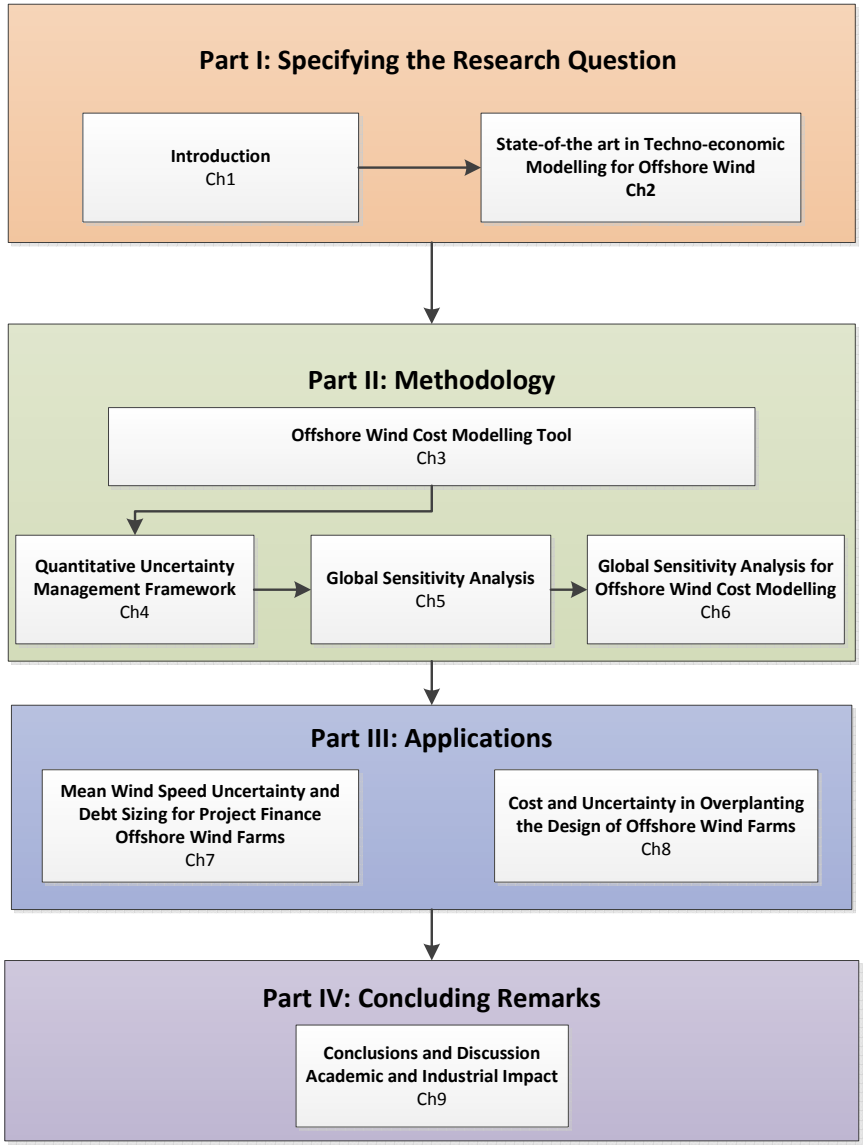

Figure 1.5: Relationship among thesis chapters

Chapter 2

Literature Review

This chapter provides a literature review summarising the most up to date research and practices in offshore wind cost modelling and quantitative uncertainty analysis; this lays on a strong basis to be able to identify potential gaps in the literature and formulate the research question. Section 2.1 presents the state of the art for offshore wind cost modelling, while Section 2.2 covers the quantitative uncertainty analysis. Finally, Section 1.5 discusses existing gaps in the literature and formulates the research questions, which forms the backbone of this work.

2.1 Cost Modelling

2.1.1 Key Objectives of Cost Modelling

Estimating the life cycle costs of an offshore wind project is a time-consuming and multidisciplinary endeavour. Cost modelling takes into consideration assumptions from development to decommissioning phases, enabling to identify key cost drivers and provides a solid basis for discussions. Estimates obtained from cost modelling practices are used to authorise offshore wind project's budgets and manage its costs. Even if the project is at early stages of development, i.e. when there is too much uncertainty to provide a reliable estimate for how profitable the project would be, cost modelling is still beneficial for the following reasons [24]:

- **track performance against targets**

  It enables management to set targets and metrics to track performance as well as to be able to compare different project configurations' costs

- **provide advanced decision-making**

  It equips management with a tool to answer very complex questions such as - which turbine should be used? what is the optimal installation method? what are the key risk drivers? which zone should be developed within a given area?

- **identify key cost drivers**

  It enables management to break down cost components, identify key cost drivers and the causal factors driving profitability for offshore wind projects

- **make uncertainties explicit**

  It is a blend of both art and science; there are different ratios between science and art depending on the level of design of the project. Estimating involves complex calculations but it also requires imagination, assumptions and judgement. It is precisely the subjective elements involved in producing an estimate that are referred to as the art element. The earlier the stage of the project is at, the higher the judgement/art needs to be. It is important to characterise and flag up cost components and uncertainties that are not well understood

- **bound with theoretical limits**

  The limits of offshore wind projects are governed by a number of different factors, which can be investigated through the cost model; stress testing the cost model can help to understand these extreme cases

- **establish a data flow**

  It provides a structured way of thinking about techno-economic variables, their associated uncertainties and how they affect the metric outputs

- **enhance negotiation skills**

  It enables management to have a solid basis for discussion with contractors/suppliers to be able to acquire products at a fair value

With these objectives in mind, we will now review existing practices in offshore wind cost modelling.

2.1.2 Offshore Wind Cost Modelling

The first studies that used offshore wind costs models were based on projecting onshore data to offshore [25]. By doing so the models did not account for specific offshore parameters and consequently, did not represent the harsh environmental conditions offshore wind farms operate in. Later, based on real offshore wind experience from developers, contractors and suppliers, new cost models were specifically created to explain the specificities of the offshore industry; the Energy Research Centre of the Netherlands (ECN) was one of the first research centres to develop a computer programme to quantify the investment costs of offshore wind energy [26]. In parallel, probabilistic methodologies were developed to quantify key cost drivers and uncertainties around those models, as seen in the work of [25, 26, 27]. One of the earliest studies to combine detailed techno-economic modelling and uncertainty analysis can be found in [25]. This PhD thesis develops an integrated cost model for offshore wind projects that bridges the gap between conventional technical and economic assessments, where its inputs are represented by probability density functions and uses @ Risk Monte Carlo simulation to propagate the uncertainty to the model output.

In 2012 the UK Government published a simple LCOE model, which calculates the impact of innovations for an offshore wind farm reaching Final Investment Decision (FID) in 2020 [28]. This was developed by BVGA for the Department of Energy and Climate Change (DECC) Offshore Wind Programme to enable the identification of high-impact (in terms of LCOE reduction) technological developments. That very same model was extended using, once again, the @ Risk Monte Carlo simulation to propagate the uncertainty to the model output [29]. That same year, 2012, a prominent book on offshore wind cost modelling was published; the purpose of the book was to develop models for the installation and decommissioning costs of offshore wind projects [30].

Given the stochastic nature of the environmental conditions and multidisciplinary content of an offshore wind farm, many approaches have been followed to develop new cost models. Whereas cost modelling engineers tend to focus more on a detailed breakdown of the different offshore wind farm components, as shown in [31], investors typically take a high level perspective on technology and focus more on the risks associated with them, as has been shown in [32]. Despite these attempts to capture offshore wind technicalities, the introduction of new environmental regulations, economic policies, technological advancements and financing structures has resulted in a new set of relationships that need to be considered in order to define risks and profitability for the next generation of offshore wind farms. For these reasons, simple cost models are no longer suitable to accurately represent these relationships, when using them as decision-making tools. Instead, tailored techno-economic models should be developed having the best of both worlds - technology specificities and financial modelling expertise. This thesis fills the gap in the literature by providing an advanced stochastic decision-making tool for offshore wind cost modelling that integrates both technology and financial modelling.

It is important to keep in mind that cost models are partially based on imagination, assumptions and judgement. Even with complex algorithmic models, it is often up to (senior) management to weight certain values over others, making these models even more subjective. As a result, (senior) managers can make mistakes just as easily when using a cost model than when working without one. In addition, markets are far from being constant and technology is always moving forward, in particular in such a dynamic sector like offshore wind. As a result, prices offered to developers change constantly, which means that costs have to be frequently updated. This can be very time consuming, especially in complex decision-making models.

The purpose of this thesis is to explore the techno-economic feasibility of large-scale commercial bottom-fixed offshore wind projects and therefore floating offshore wind literature is not considered. While there is a huge potential market for floating offshore wind, this has not reached the stage of maturity of its bottom-fixed counterpart; therefore floating is out of the scope of this work. In 2016 a life cost analysis framework

for offshore wind farms with bottom-fixed foundations was proposed by [31]. That life cycle cost model was divided into 5 phases: predevelopment and consenting, production and acquisition, installation and commissioning, operation and maintenance and decommissioning and disposal; finance costs were not included. The model was later updated in 2018 with the most up-to-date parametric equations in the literature and it also integrated the use of the industry standard ECN O&M tool for the prediction of operation and maintenance costs in conjunction with the latest reliability data [33]. Later on, a stochastic version of the same model was developed in [34] in an attempt to account for their uncertainties. More recently, the work of [35] has taken the previous research one step further - it has established a methodology to aid decision-making at the initial stages of an offshore wind farm investment by combining life cycle analysis with multi-objective optimisation algorithms for Round 3 offshore wind projects. However, the model lacks technology specificities and financial modelling expertise to be able to fully reflect the LCOE of offshore wind projects.

Commercial software has also been developed by different players in the sector. For example, DNV GL uses a Value Chain Assessment (VCA) software to support investment decisions for offshore wind [36]. VCA uses a probabilistic analysis taking into account the link between technology and finance as well as the interactions between several parts of the value chain. However, VCA is a proprietary software which cannot be used for research purposes. It is precisely this link between technology and finance that it is important to investors and shareholders. Likewise, BVGA utilises an internal offshore wind cost model [13]. The purpose of the cost model is to track the impact of innovations on the LCOE and produce reports on how technology innovation is anticipated to reduce the cost of energy from European offshore wind farms in the future [13].

Finally it is worth noticing that other authors have focused on reviewing existing literature and commercial reports to provide researchers with up-to-date cost data. Examples of these are: review of offshore wind farm cost components [37], a guide to an offshore wind farm [38] and a review of investment model cost parameters for VSC HVDC

transmission infrastructure [39]. Cost parameters, which constitute the backbone of profitability assessments, are gathered from an extensive collection of techno-economic sources.

Building on the cost modelling capabilities, two industrial applications that bridge the gap between financial valuation and engineering design are investigated in line with the latest information. First, developers need to find the right balance between an increase in the development expenditure associated with better wind speed predictions and a decrease in the financing costs to minimise their LCOE. No previous literature has attempted to explain how a reduction in mean wind speed uncertainty can be translated to both an increase in the development expenditure and a reduction in the cost of financing. It is the trade-off between these two ingredients that determines their aggregated contribution to LCOE. Chapter 7 addresses this in more detail and provides a framework that can deliver value to a developer. Second, the connection of offshore wind farms is subjected to a maximum export capacity (MEC) set in their connection agreement with the Transmission System Operator(TSO). Generators can export up to their contracted MEC, with any additional generation curtailed by the TSO. For this reason, it has been common practice to size the capacity of offshore wind farms to its MEC, even though the majority of the time they are not generating at full power. Little thought has been put into designing offshore wind farms which optimise its farm capacity in regard to the fixed electrical connection capacity. Chapter 8 addresses overplanting in more detail, which is defined as the process of installing additional wind farm capacity compared to its MEC.

2.2 Quantitative Uncertainty Modelling

The solution to offshore wind cost modelling involves the creation of dedicated decision support models. These decision support models are often very complex, resulting in relationships between inputs and outputs that are poorly understood. Additionally, with the advent of higher computational power, the mathematical models in use capture

greater level of sophistication, bringing more complexity into the codes, and as a result, not allowing modellers to grasp the response of the model output to variations in model inputs based soley on intuition. This is especially true for models subjected to sources of uncertainty which impose a limit on the confidence of the response or output of the model. Therefore, good modelling practice requires that the modeller provides an evaluation of the confidence of the output under different scenarios. Assuming that a first quantification of uncertainties in the inputs has been undertaken, the evaluation can be done in a two-way iterative process. On the one hand, uncertainties from the input factors are propagated to the outputs by means of uncertainty propagation techniques. On the other hand, an evaluation of how much the uncertainty of the input factors affects the uncertainty in the model output is assessed. Sensitivity analysis techniques address the second of these issues and are classified into two groups or methods: Local Sensitivity Analysis (LSA) and Global Sensitivity Analysis (GSA). Whereas LSAs analyse the behaviour of the system response locally by means of partial derivatives or similar approaches around a chosen point, GSA determine all the system's critical points in the combined space formed by the parameters [40].

While building, using and maintaining simulation cost models is important, the use of sensitivity analysis is key across the modelling process. Sensitivity analysis methods allow modellers to study how the different sources of uncertainties in the model output can be apportioned to the different sources of uncertainty in the model inputs. This, in turn, guides the process of determining the most relevant input variables to an output behaviour by screening out those variables whose contribution can be neglected. A Stochastic Framework, also called the quantitative uncertainty management methodology from the European Safety, Reliability and Data Association (ESReDA)[41] is considered for the development of this work. One of the key objectives for uncertainty management which is closely linked with sensitivity analysis is "to understand the influence or to rank the importance of uncertainties, thereby to guide any additional measurement, modelling or R&D efforts".

Sensitivity Analysis is a research domain which is gaining popularity in different fields.

An increased share of articles that use sensitivity analysis has been found in the literature, of which its fractional share in the use of GSA has also been expanded [42]. Further information on GSA techniques can be found in [43, 44, 45, 46, 47]. In the context of this work, the GSA guides the process of determining the most relevant input variables to an output behaviour as well as identifies those variables whose contribution can be neglected. By ranking the model inputs in order of importance, useful insight into the model can be gained, especially when the system is not well known or the model is at the early stages of development. The process of ranking these inputs is also referred to as **Factor Prioritization**[43]. Prioritization leads naturally to the idea of important inputs but also to negligible inputs or factors whose variability has a negligible effect on the output. Very often the inputs of the model follow very asymmetric distributions of importance, with few inputs accounting for most of the output uncertainty and most inputs playing little or no role [41]. By identifying those parameters that have no significant contribution to the model output, the complexity of the model can be reduced. This is also known as **Factor Fixing**[43]. Significant contribution is subjective, it is important to keep in mind the shortcomings of the cost models mentioned earlier in this chapter. As important as this is, it is also important to define a risk metric. Variance has been widely used as a risk metric, but it is not always a good proxy for uncertainty.

Global sensitiviy analysis techniques are powerful for model-building and decision-making processes. As far as those questions are concerned, our interest will lie in **Factor Prioritization** and **Factor Fixing**. Therefore, it is important to define and characterize a mathematical index that looks after these two processes. Desirable properties of such index can be found in the work of [48] and displayed in Table 2.1. It is for this reason that, in the search of the most convenient method or combination of methods to be applied in a complex offshore wind techno-economical model, these properties have been taken into consideration.

Complex techno-economic models consist of many input variables that tend to be

Table 2.1: Good properties of a sensitivity index

Property	Description
Global over local	It considers variations over the entire feasible space, rather than local variations around a point in the domain.
Quantitative over qualitative	It can be calculated through a numerical, reproducible procedure.
Model independent	It can be applied regardless of the structure of the problem. Linear or non-linear, additive or non-additive.
Unconditional on any assumed value	The results of the sensitivity index should not be conditioned upon an assumed value. For example, the density-based entropy method takes into consideration the change of the pdf, given a fixed value. If this fixed value was to be changed, the results would also differ. This means that this method is not unconditional.
To be easy to interpret	The simpler the interpretation of the index is, the better for comparing it in different models and applications. For instance, the variance-based sensitivity method provides the user with a tangible interpretation of the index: expected reduction in variance that would be obtained if the variable was fixed.
To be easy to compute	This is synonym for being easy to implement rather than being concerned with the execution time.
To be stable	Dealing with sensitivity indices that are calculated by means of stochastic techniques might suggest a lack of confidence in the results. In order to avoid this, it is important to obtain consistent or robust results with confidence intervals.
To be moment independent	This means that, without prior knowledge of the output pdf, one shouldn't take any statistical moment to fully characterize the output uncertainty.

represented by a computer code. An example of GSA methods applied to a techno-economic model can be found in [49]; this study applies the variance-based, δ density-based and entropy density-based GSA methods to a simple biodiesel production model. Other authors have used a combination of methods at different stages of modelling; an example of those can be found in [50], where the author applies different GSA methods to the aero-elastic time domain response of an offshore wind turbine. As far as offshore

wind techno-economic models are concerned, an O&M model was investigated by means of the Morris method in [51] and a life-cycle cost model was interrogated by means of the variance-based Sobol method in [29]. An extensive review of different sensitivity analysis methods has been carried out and displayed in Table 2.2. From that, a flowchart has been drawn and displayed in Figure 2.1. The aim of the flowchart is to facilitate the choice of sensible sensitivity analysis techniques for a particular model, based on the following questions:

- Properties of the pre-existing model. Is the model linear or non-linear? is the model monotonic or non-monotonic?
- The number of inputs or CPU time. This will, to some extent, condition the number of model evaluations that can be undertaken in order to characterize the behaviour of the model.
- The goal of the study. Does the study need to be qualitative or quantitative? local or global? does it need to capture the interactions between parameters?
- The methodology to represent uncertainty. Is variance a good measure to represent the uncertainty in the model? This concerns the moment independent property.

In particular for this work, the model under study, Offshore Wind Cost Analysis Tool (OWCAT), is considered to be non-linear and non-monotonic and hence, no a priori assumptions can be stated. Since the model is composed of many different inputs, a screening technique has been considered appropiate for Factor Fixing, as Figure 2.1 suggests. However, more recently, in the work of [52], it has been proved that it is better to use the total sensitivity indices of the variance-based method at low sample size than the Morris method, which implies many modelling assumptions. The same work suggests a unified practice when transitioning from screening to quantitative sensitivity analysis, using the same design and sample to move from the former to the latter. This is the reason why in Figure 2.1 we have linked the screening techniques with the variance-based Sobol method. The same Figure starts off by requesting assumptions on model properties. If our model was linear or non-linear but monotonic, several sensitivity

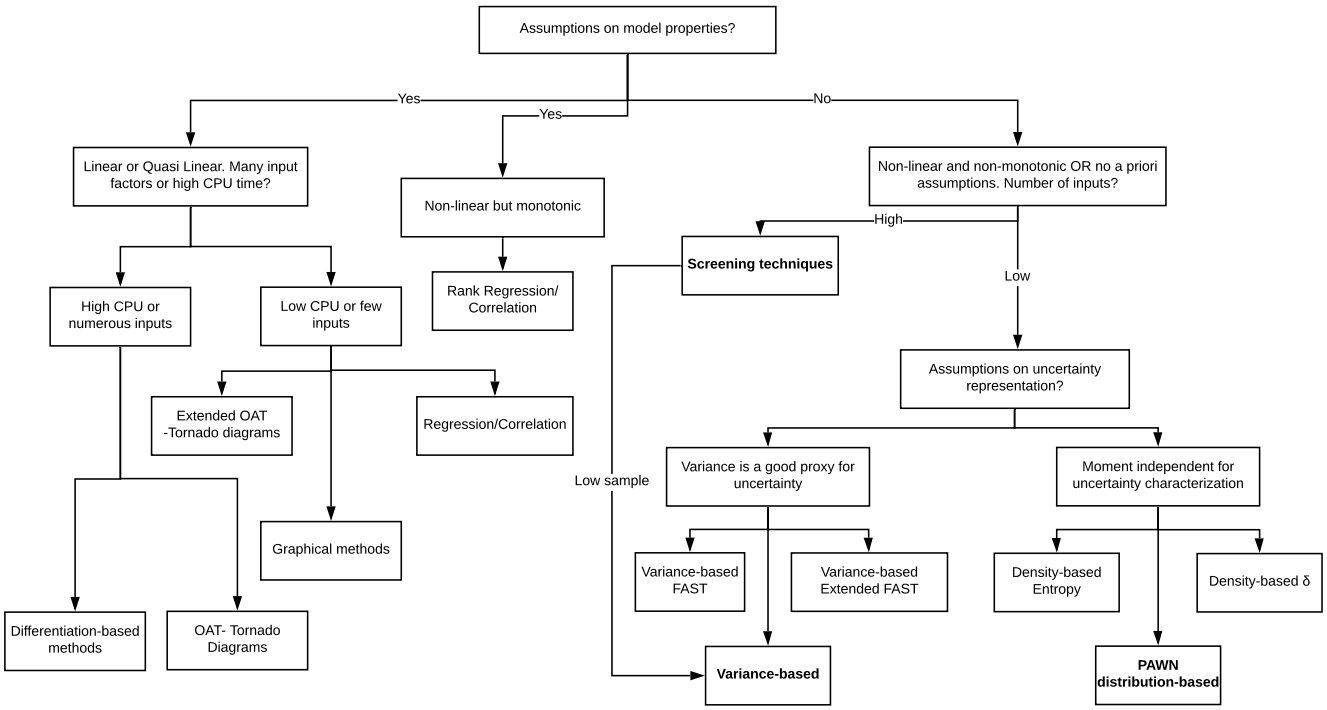

Figure 2.1: Decision diagram guiding the choice of SA techniques, expanded from [41]

analysis techniques could be applied in a very efficient manner by exploiting the internal structure of the problem. However, as it has been reiterated, there is no prior knowledge on the behaviour of cost modelling tool. The tool is made up of different modules with highly non-linear functions and internal iterative processes. A few examples of them are (a)cost modelling functions depending on exponents. (b)mass foundation and electrical components correlations also depending on exponents. (c) double loop iterative process for advance project finance modelling requirements. As a result, only the right hand side of Figure 2.1 is appropriate. We are interested in using a global quantitative assessment that takes into consideration interactions between the different input parameters. Also, we would like to see how the contribution of model inputs to the output might change when considering the cumulative distribution function instead of variance to represent output uncertainty.

After reviewing the current state-of-the-art in GSA methods, it has been considered

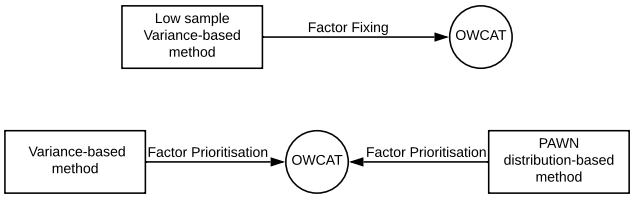

Figure 2.2: Application of global sensitivity analysis methods to the offshore wind cost modelling tool (OWCAT) in two stages. First (top) factor fixing by variance-based method at low sample size, second (down) factor prioritisation by variance-based method and the PAWN distribution-based method.

appropriate to apply GSA methods to the cost modelling tool in two stages. The first stage applies the variance-based method at low sample size so as to screen out irrelevant inputs, whereby the complexity of the input domain is reduced - Factor Fixing. Then, the second stage applies the variance-based method and the PAWN distribution-based method to the subset of relevant inputs to identify which key inputs drive the response of the model - Factor Prioritisation. It has been regarded appropriate to benchmark the PAWN distribution-based method against the variance-based method in the cost modelling tool, given that the latter is model independent. A benchmark of these two methods is conducted in Chapter 5 and [53] as an intermediate step to then be applied to the cost modelling tool. This process is displayed in Figure 2.2. Global sensitivity analysis techniques are applied to the cost modelling tool in Chapter 6.

Table 2.2: Review of the different sensitivity analysis methods

SA name	Description	References
One-at-a-time methods (OAT) and Tornado diagrams	Simplest form of SA. Study the model output when we vary one model input at a time, while quantifying the effect of the shift in x_i from the base case to the sensitivity case. The graphical representation of OAT is often a Tornado diagram. This SA technique has the following properties: local, quantitative, conditional, moment independent, easy to interpret and implement and stable. However, it neglects interaction effects and is strongly dependent on the chosen point. The computational complexity is $2N+1$,where N is the number of inputs. OATs are widely used in the industry due to its ease of implementation.	[54]
Extended OAT and Tornado diagrams	It is the generalization of OAT by including the interaction effects. Results are still strongly dependent on the chosen point. This SA technique has the following properties: local, quantitative, conditional, moment independent, easy to interpret and implement and stable. The computational complexity is $2N+2$ for first, interaction and total order indices. Therefore, the cost of a generalised tornado diagram is $4N+3$.	[54]
Graphical methods - spider plots and one way SA	This approach registers the values of the model output while the input varies over the entire predetermined range. The method results prohibitive for more than 10 inputs.	[54]
Differentiation-based	The aim of differential methods is to quantify the rate of change due to small variations in the uncertain model inputs, namely, capturing the estimation of the local gradients. They are appropriate for computationally intensive or high dimensional models. This SA technique has the following properties: local, quantitative, model dependent, conditional, easy to interpret and implement and stable. The problem with this method is that the interactions are only characterized by the use of expensive second or higher order analysis and they work only with continuous inputs. In addition, it is deemed to be local and conditional, since the choice of the base case might significantly influence the outcomes of the SA. The computational complexity of differentiation-based techniques is considered to be low, making the analysis feasible in most practical applications for which the model output is smooth.	[41] and [54]

Table 2.2: Review of the different sensitivity analysis methods

SA name	Description	References
Screening methods - Morris	Screening methods foresee the evaluation of the model at a limited number of locations in the input space. The goal of screening techniques is to identify the least important model inputs. The Morris methods has been chosen over other screening methods such as the supersaturated design and sequential bifurcations due to its completeness [55]. This SA technique has the following properties: global (by averaging and taking the variance of many local values), quantitative, model independent, unconditional, easy to interpret and implement and stable. One of the main issues with Morris method is the fact that it does not quantify how much interactions the inputs have.	[56],[57], [58],[59]and [54]
Regression-Correlation	The use of regression-based methods in GSA represents a simple and intuitive assessment of the decomposition of variance for linear models. For this reason, they were the first class of GSA to be extensively analysed. This SA technique has the following properties: global, quantitative, model dependent, unconditional,easy to interpret and implement and stable. The main issue with this method is that it can only be applied when the model is linear or quasi-linear. The computational complexity is N, which is equal to the number of model evaluations.	[41]
FAST	The Fourier Amplitude Sensitivity Test (FAST) was developed in the 70s. The main principle was to use a multidimensional Fourier transformation of the function of study. In this way, this led to a mono-dimensional Fourier decomposition along a curve exploring the input space. This SA technique has the following properties: global, quantitative, model independent, moment dependent, unconditional, easy to interpret and stable. However, it does not calculate the interaction effects and it is quite complex to implement.	[60] and [61]
Extended FAST	FAST was extended by Saltelli in order to compute the total order effects. The method is also referred as eFAST. This SA technique has the following properties: global, quantitative, model independent, moment dependent, unconditional, easy to interpret and stable. However, it is still quite complex to implement and, consequently it has rarely been used in the literature.	[62]

Table 2.2: Review of the different sensitivity analysis methods

SA name	Description	References
Variance-based	It measures the decomposition of the output variance in terms of two indices: the first and higher order indices. This SA technique has the following properties: global, quantitative, model independent, unconditional, easy to interpret and implement and stable. However, the model assumes that the variance is a good proxy for uncertainty, leading to the moment dependent property.	[63],[64],[43], [65],[66] and [67]
Entropy Density-based	It measures the divergence between the unconditional and the conditional PDFs by either the Shannon or Kull-back-Leibler entropy. This SA technique has the following properties: global, quantitative, model independent, moment independent, easy to interpret and stable. The model is not that easy to implement since calculating empirical pdfs may be challenging. In addition, the moment is conditional since the results are highly dependent on the choice of the conditioning value.	[68]
δ Density-based	It considers changes in model output by conditioning values x_i and measuring the area enclosed between the conditional and conditional probability distribution function. This SA technique has the following properties: global, quantitative, model independent, moment independent, unconditional, easy to interpret and stable. The model is not that easy to implement since calculating empirical pdfs may be challenging.	[69]
PAWN distribution-based	It considers the changes in model output when fixing a variable x_i, by analysing the distance between the empirical conditional and unconditional cumulative probability distribution functions. This SA technique has the following properties: global, quantitative, model independent, unconditional, moment independent, easy to interpret and implement and stable. The computational complexity is $N_u + n \cdot N_c \cdot k$, where N_u is the evaluations obtained by sampling the entire input feasibility space, N_c is the number of samples obtained by sampling the non-fixed inputs only, while keeping the value of x_i fixed. k is the number of uncertain inputs and n are random samples for the fixed input x_i, or conditioning points.	[48] [70] and [71]

Part II

Methodology

Chapter 3

Techno-Economic Modelling

This chapter introduces the cost modelling tool used throughout this thesis; this includes aspects of project development, wind resource assessment, marine operations to civil, mechanical, reliability, electrical and financial engineering.

3.1 Overview of Offshore Wind Cost Modelling Tool

The Offshore Wind Cost Analysis Tool (OWCAT), developed predominantly by James Spelling at the EDF Energy R&D UK Centre, has been used in the past for comparative evaluation of multiple sites, detailed evaluation of specific project layouts and sensitivity studies on both design/technology choices and cost variations [72]. The tool has been validated against cost data from the Navitus Bay, Courseulles-sur-Mer and Neart na Gaoithe projects and shown to be accurate within ± 15% for these cases. The contribution of the EngD work presented in this Chapter is to explain its inner workings and extend the development of the existing cost modelling capabilities to reflect current technology choices and market trends as well as to validate its assumptions.

The cost modelling tool consists of four main modules: a wind farm design module, a cost calculation module, a financial module and an overarching stochastic module which allows inputs to be represented by probability distribution functions. The first stage of the module concerns the wind farm design. In order to evaluate the costs of

the project, it is necessary to understand the number and type of wind turbines, foundations, inter-array cabling and the export system. In other words, the wind farm itself must be modelled. Designing an offshore wind farm requires interaction between teams from different disciplines; for example, the wind turbine team will have to interact with the foundation team to make sure that the loads of the turbine are correctly passed onto the foundation, and the foundation team will need to make sure that the electrical connections are correctly secured within the foundation. As such, a cost model must capture the same interactions as the design process and cannot be a simple accumulation of models from separate disciplines.

The design outputs of the first module are fed as inputs into the second module, which calculates the costs of the different offshore wind farm components. The cost module can be divided into Development Expenditure (DEVEX), Capital Expenditure (CAPEX), Operational Expenditure (OPEX) and Decommissioning Expenditure (DECEX). DEVEX covers the costs of all the processes up to the financial close or placing firm orders to proceed with the construction. CAPEX calculates the supply and installation costs of the wind farm, including wind turbines, foundations, inter-array cables, offshore substations, export cables and onshore substations. Indirect costs such as Engineering, Procurement, and Construction Management (EPCM) costs and insurance are also included in the CAPEX breakdown. OPEX includes direct costs for the operation and maintenance of the wind farm, as well as transmission charges, insurance, taxes and royalties. DECEX accounts for the decommissioning of the wind turbines, foundations and offshore substations.

The cost outputs of the second module are passed into the third module, which is the financial model of the wind farm project. The financial model takes into consideration the different cash flows throughout the life of the wind farm, as well as the financing structure put in place to supply the initial capital investment. Based on the resulting free cash flows and financing costs, the LCOE can be determined, together with other financial performance indicators. The financial module allows for corporate and project

financing modelling.

The OWCAT structure is shown in Figure 3.1. This information has been divided into:

- (i) Project Specifications
- (ii) Technical Specifications
- (iii) Economic and Financial Specifications
- (iv) Vessel Specifications
- (v) Structural Masses and Electrical Components Database

(i) refers to the project offshore wind farm characteristics such as the capacity of the farm, the wind speed at a given referenced height, the average water depth, the soil conditions, the distance from shore, the wind turbine model, foundation type and export system specifications among others. Since no two projects will have the same characteristics, project specifications attempt to model each particular site. (ii) addresses the details of the offshore wind technology, representing wind turbine, foundation, inter-array cable, export system and grid parameters. For example, as far as the wind turbine is concerned, parameters such as the wind turbine availability, the installation vessel associated with the wind turbine, the average loading, installation and commissioning times are accounted for. In addition, a decommissioning factor is used for all offshore wind farm components to account for a reduction in time from the installation phase; this decommissioning factor adds a reduction in time from the same activities carried out during the installation and it is used at the discretion of the modeller. (iii) concerns the reference year for real prices, the risk-free rate and cost of debt, insurance and insurance premium tax rates, contingency requirements, corporation taxes, depreciation, seabed rent, exchange rates and inflation. (iv) involves the different vessel characteristics used in the installation and decommissioning of the offshore wind farms. As an example, heavy-lift jack-up vessel parameters comprise the day rate, vessel transit speed, vessel positioning time, vessel mobilisation time, operational weather window and carrying capacities in regard to different components. (v) consists of the data used to establish the foundation mass correlations, which are the basis for the CAPEX estimation in

foundation procurement. It also considers the correlations used to estimate the cost of different electrical components.

The final design contains not only the design of the offshore wind farm, where the foundations masses, inter-array and export system are sized, but also the procurement, vessel charter model and the Annual Energy Production (AEP) as displayed in Figure 3.1. The procurement module stores all the information concerning wind turbines, foundations and the electrical system, in terms of the type, number of elements and size (also length if required), giving rise to a procurement catalogue which forms the basis for the cost module. The vessel charter model is based on the work of Kaiser [30], whereas the AEPs is built upon industry's best practices assuming respectively either a logarithmic- or power-law wind profile in conjunction with a Rayleigh or Weibull probability distribution to model the wind speed. Wake losses and electrical losses are also accounted for in the AEP submodule.

A financial metric typically used in the energy sector to evaluate the financial performance of a project is the LCOE. The LCOE is a metric for which an equal-valued fixed revenue delivered over the life of the asset's generating profile would cause the project to break even. In the context of this work, we look at the LCOE of an energy project by fixing a discount rate equal to the Minimum Acceptable Rate of Return (MARR) - making sure that the company is accepting the project when compared to others. Therefore, by imposing the MARR or the minimum internal rate of return of the project, we are able to obtain an LCOE figure. This is defined in Equation 3.1. Further details on the financial computational methodology are given in Section 3.9.4.

$$LCOE = \lambda | \sum_{t=1}^{n} \frac{FCF_t(\lambda)}{(1+MARR)^t} = 0; \tag{3.1}$$

Where FCF_t are the free cash flows incurred at different points in time, $MARR$ is the desired Minimum Acceptable Rate of Return (MARR), n is the total number of periods and λ is an iterative value of the LCOE. λ starts with an initial guess obtained from a simplified financial model, as described in Section 3.9.2 and then, through a complex

financial calculation, described in Section 3.9.4, it converges towards the true LCOE; LCOE is the λ for which the equation on the right hand side is equal to zero.

Lastly, the creation of the stochastic module (depicted in orange in Figure 3.1) allows the model to be embedded in the framework of uncertainty quantification.

3.2 Decision-making Cost Modelling Tool

Offshore wind cost modelling assesses the financial viability of offshore wind assets and support its investment decisions at early stages of development. Cost modelling enables strategic decision making with accurate, precise and high-quality decisions as it takes into consideration a wide range of assumptions such as project development, consenting, wind resource assessment, marine operations and civil, mechanical, reliability, electrical and financial engineering, as shown in Figure 3.2.

Cost estimating is a blend of science and art. Science because it heavily relies on mathematical algorithms or parametric equations to estimate the costs. Art because it also requires imagination, assumptions and a degree of judgement in the process. This combination of objectivity and subjectivity within the cost modelling process is why, given the same offshore wind farm project specifications, technology modifiers and market trends, no two cost modellers come up with the same total project cost. As the project develops with more details, the percentage of art may decrease and the science may increase. Nevertheless, cost estimates are needed across the different phases of project development to guide decision-making.

Building a cost model requires strong expertise in many aspects of offshore wind. For this reason, several meetings were held with a range of experts from EDF Group in order to leverage their expertise and validate the modelling assumptions and cost hypotheses. Cost models need to be at sufficient detailed level to capture the elements that significantly affect cost - key cost drivers. The following sections describe the key ingredients to estimate the cost of an offshore wind project.

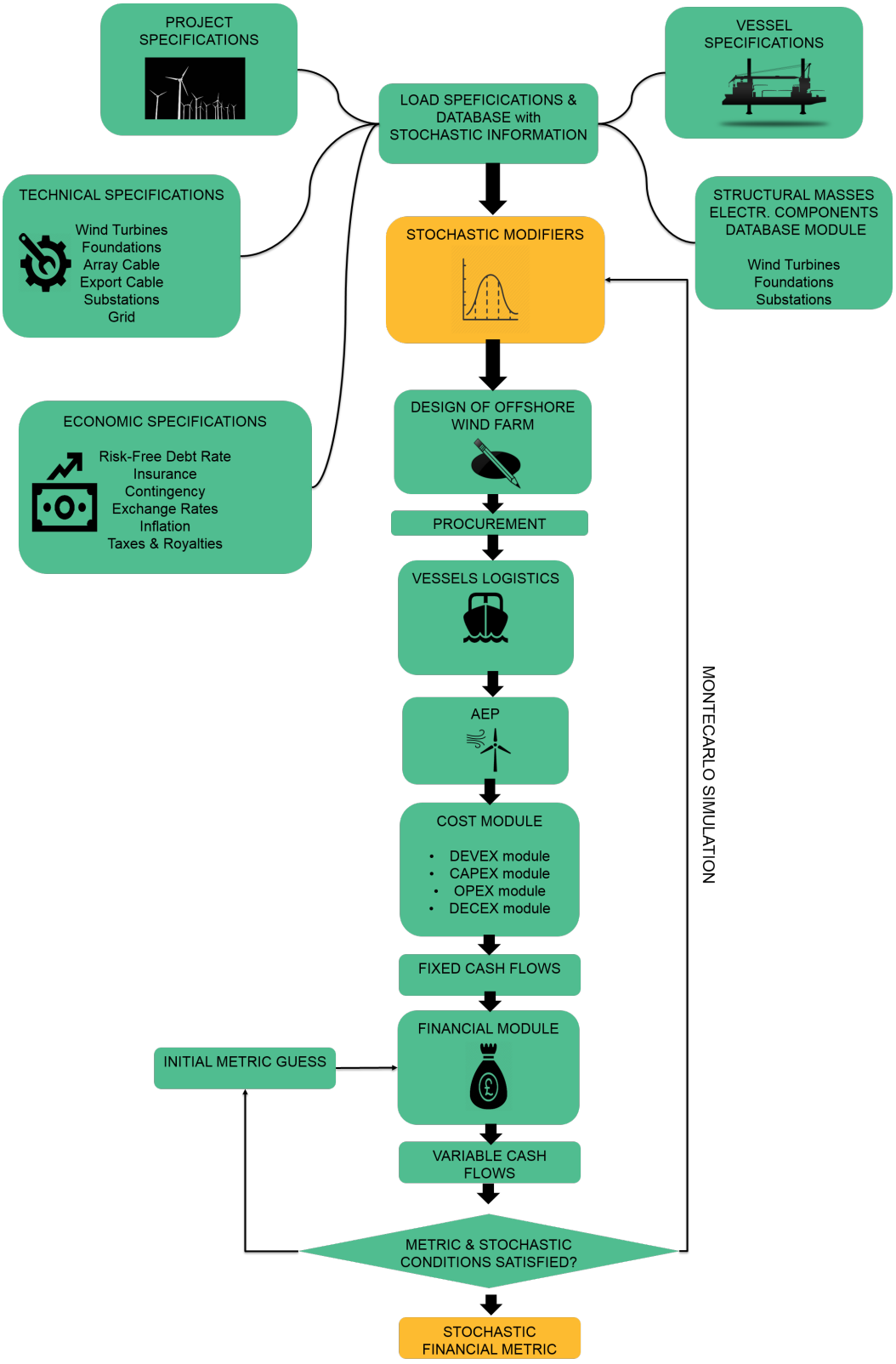

Figure 3.1: Stochastic OWCAT Structure

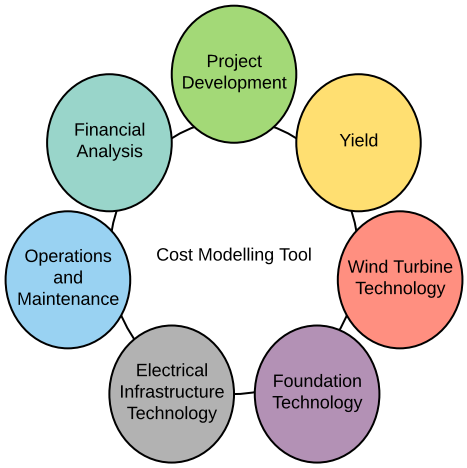

Figure 3.2: Key Areas in Cost Modelling Tool

3.3 Project Development

The development and consenting phase covers the processes up to the point of financial close or placing firm orders to proceed with wind farm construction [73]; this phase is managed by the developer in the UK. As offshore wind projects are very site-specific, specialist advice is typically required during this phase; this consists of:

- Development project management
- Wind resource assessment
- Environmental impact assessment
- Geophysical and geotechnical surveys
- Front-end engineering design
- Legal services
- Due diligence
- Stakeholder engagement

Development project management sets the strategy and coordinates the efforts of the project staff to accomplish the project development objectives. Wind resource assessment is concerned with estimating the future energy production of a wind farm. Environmental impact assessment evaluates any environmental impact a wind farm may have on species that live, use or frequent the offshore wind environment in the sea and in the air; this includes benthic, pelagic, ornithological, sea mammals and onshore environmental surveys. Geophysical and geotechnical surveys analyse the soil characteristics of the proposed wind farm. This part of the development process assists in choosing the foundation design and wind farm layout, as well as minimises risk during installation activities. Front-end engineering design takes into consideration the technical requirements as well as rough investment cost for the project; it includes basic engineering studies regarding the wind turbines, foundations, electrical infrastructure, logistics, etc. Legal services cover the planning process, relevant legislation and procurement contracts. Financial institutions intending to invest in an offshore wind project frequently require an independent third party to carry out a technical due diligence of the project in order to identify any potential risk. Due diligence ensures all critical technical project expectations are independently evaluated as well as any potential issues and associated mitigation measures identified. Stakeholder engagement involves local communities affected by the project in the decision-making process.

At the completion of this phase, the project can either progress to the next phase or be sold on to another company. Development expenditures are estimated to be around 4% of the wind farm capital cost, or what is around £60 million for a 500 MW wind farm (valued at £3 million per MW) [73]. The cost modelling tool estimates the development expenditure components by means of several cost modelling functions governed by standard power law functions; these functions are fitted with cost data obtained from real-world projects and scaled accordingly. A scaling exponent of 0.5 is typically used for indirect costs such as engineering, design and management activities and has therefore been used for the scaling of development expenditure components [74]. Development expenditure cash flows are evenly distributed over the first four years prior to FID.

3.4 Yield

The yield is concerned with estimating the future annual energy production of a wind farm.

3.4.1 Gross AEP

Gross annual energy production is the total amount of electricity generated by an offshore wind farm as if there were no losses incurred in the process; it is defined as a function of the wind speed distribution, power curve and number of turbines.

3.4.1.1 Wind speed distribution

The first step towards estimating the gross annual energy production is to assess the wind resource at a given site. In order to characterise the wind resource, developers employ mean wind speed estimates derived from data representing a long-term period. Developers then fit a probability distribution to the underlying data to characterise its wind speed distribution. As far as the wind speed distribution is concerned, the wind industry standard is the Weibull distribution, defined by two parameters: A and k. A is the Weibull scale parameter in m/s; a measure for the characteristic wind speed of the distribution that is proportional to the mean wind speed. k is the form parameter; it specifies the shape of the Weibull distribution and takes on a value between 1 and 3. Small k values signify very variable winds, while constant winds are characterised by larger k values. It is important to notice that a Rayleigh distribution is a particular case of Weibull where $k = 2$. Weibull probability and cumulative distribution functions are shown in Equation 3.2 and 3.3, respectively. Wind speed is represented by the symbol u.

$$pdf(u) = \frac{u}{A}\left(\frac{u}{A}\right)^{k-1} e^{-(u/A)^k} \tag{3.2}$$

$$cdf(u) = 1 - e^{-(u/A)^k} \tag{3.3}$$

In order to estimate the AEP, measurements need to be given at hub height. When wind speed measurements are given at a referenced height different than hub height, either a logarithmic or power-law is used to estimate the wind speed at hub height, as shown in Equation 3.4 and 3.5, respectively.

$$u(z) = u_{ref}\left(\frac{z}{z_{ref}}\right)^{\alpha} \tag{3.4}$$

$$u(z) = u_{ref}\frac{log\left(\frac{z}{r}\right)}{log\left(\frac{z_{ref}}{r}\right)} \tag{3.5}$$

Where u_{ref} is the measurement available at the referenced height, z is the turbine hub height, z_{ref} is the referenced height, α is the wind shear exponent (normally between 0.1 and 0.2) and r is the roughness coefficient (normally for sea surface 0.0002). Therefore, it is possible to characterise a site given 3 parameters at a referenced height:

- A Weibull parameter
- k Weibull parameter
- α wind sheer coefficient or r roughness coefficient

Only two parameters are needed where Rayleigh is used ($k = 2$). Given that there is a trivial relationship between the mean wind speed and the Rayleigh scale parameter, a mean wind speed and either a wind sheer or roughness coefficient are sufficient to characterise a site modelled by Rayleigh.

3.4.1.2 Power curve

A wind turbine power curve describes the generator power output as a function of the wind speed. Wind turbine power curves can either be provided by the Original Equipment Manufacturers (OEMs) or be estimated. In this work, only theoretical power curves are used. A theoretical power curve is a function of the rated power P_{rated}, cut-in and cut-out speed u_{cut-in} $u_{cut-out}$, wind turbine efficiency C_{eff}, the air density ρ and the rotor diameter D. The rated power is the maximum output the generator is able to produce. The cut-in speed is defined as the speed at which the turbine begins

to rotate, when applying sufficient torque on the rotor to generate power. At the other side of the curve, when the speed increases beyond a given threshold or cut-out speed , putting the rotor integrity at risk, the braking system is employed to bring the rotor to standstill. Both situations result in a nil energy production. In other cases, when the wind speed is found between the cut-in and the cut-off speed, then production is governed by Equation 3.6. It is worth noting that, whereas Betz efficiency is given by the fraction $\frac{16}{27}$, turbine efficiency is given by C_{eff}. Theoretical power curves are calculated according to Equation 3.6:

$$P(u) = min\left[P_{rated}, \frac{1}{2}\rho C_{eff}\frac{16}{27}\pi\left(\frac{D}{2}\right)^2\left(u^3 - {u_{cut-in}}^3\right)\right] \forall u \in (u_{cut-in}, u_{cut-out}) \quad (3.6)$$

Within the cost modelling tool, power curves are stored in an internal database, from where unit load-curve are derived. A unit load-curve P_{unit} is defined as the power curve divided by the rating of the same machine; this curve expresses the percentages of the maximum rating as a function of the wind speed bins, typically ranging from 0 to 40 m/s with a step size of 1 m/s.

To calculate the gross annual energy production, wind speeds are discretised into a number of bins. For each wind speed bin, we calculate its occurrence (based on Weibull/Rayleigh distribution), multiply it by the time lenght of one year (8760 hours), and that with the corresponding power (based on the power curve at the same wind speed bin). After adding up each "power bin" and multiply it by the number of turbines, the gross annual energy production is obtained, as shown in Equation 3.7.

$$AEP_{gross} = N_{WTG}T\int_0^\infty pdf(u)P(u)du \approx N_{WTG}\sum_{u_{bins}} T\left(cdf(u_{n+1}) - cdf(u_n)\right)P(u_n) \quad (3.7)$$

Where n is a dummy variable, N_{WTG} is the number of wind turbines, T is the time length of one year, $cdf(u_{n+1}) - cdf(u_n)$ is the ocurrance of a wind speed bin and $P(u_n)$ is the power curve value at the same wind speed bin n.

3.4.2 Net AEP

To calculate the net annual energy production AEP_{net}, several loss factors are applied to the gross annual energy production AEP_{gross}. Loss factors are broken down into the following categories:

3.4.2.1 Wake losses

A wake is a cylinder of air downwind of a turbine in which the wind speed is reduced because of the wind energy that has been extracted by the turbine. As the flow proceeds downstream, there is a spreading of the wake and the wake recovers towards the free stream conditions. The bigger the inter-turbine distance is, the less the energy yield is impacted. However, longer distances increase the length of subsea power cables to be laid, and thus the cost. In order to investigate all of the possible wake losses arising from hypothetical arrangements of the turbines at a proposed site, the wind development industry uses a variety of computer models that calculate potential wind turbine wake effects and resultant losses in energy production.

In this work, we've used a well-known commercial software (OpenWind) to estimate the wake losses for a large number of scenarios in a square layout. Those scenarios were derived from different number of wind turbines and inter-turbine distances to estimate wake losses. After compiling the results from different simulations, a function was fitted to the data as a function of these two variables. Depending on the stage of the project, OWCAT allows for different methods of wake estimation - it can leverage the function described before when the project is at early stages of development or it can use a given input from more complex wake estimation studies if the project is at more advanced stages.

3.4.2.2 Electrical losses

Electrical losses in offshore wind farms are incurred in both the inter-array and export system. As far as the inter-array system is concerned, array cable configurations are often either radial or ring, as shown in Figure 3.4. In a radial configuration, the cross section of the array cable changes along each wind turbine string in order to minimise

the size (and thus cost) of cables required. At the end of the strings, where the export current is lowest, cables with smaller cross-section are used; this cross-section increases along the string as the total current increases. Conversely, in the ring configuration, the maximum-sized cable is used along the entire length of the wind turbine string and the ends of two adjacent strings are connected by an additional full-sized cable section.

In order to calculate the array losses, the following steps are taken. First, the active P_{WTG} and reactive Q_{WTG} power of the wind turbines are calculated for each wind speed bin, based on the unit-load curve P_{unit}, the rated wind turbine capacity cap_{WTG} and the power factor ψ. This is displayed in Equation 3.8. Then, the unit apparent power S_{unit} and apparent power S_{WTG} is derived for each wind speed bin as shown in Equation 3.9.

$$P_{WTG} = cap_{WTG} P_{unit} \quad ; \quad Q_{WTG} = cap_{WTG} \sqrt{\frac{1}{\psi^2} - 1} \tag{3.8}$$

$$S_{unit} = \sqrt{P_{unit}^2 + \frac{1}{\psi^2} - 1} \quad ; \quad S_{WTG} = \sqrt{P_{WTG}^2 + Q_{WTG}^2} \tag{3.9}$$

Electrical losses are given as the sum of the wind speed-dependant transformer and subsea power cable losses. Transformer losses are a consequence of the electrical current flowing through the coils, as well as the magnetic field alternating in the core. Whereas losses associated with the coils are called load losses, losses incurred in the core are called no-load losses. The total transformer losses L_{trans} are modelled as a function of the load and the capacity of the transformer. Different wind speeds result in different loads, which in turn give rise to different total transformer losses. Subsea cables losses are modelled as a function of the cross section, operating voltage, conductor material and intensity flowing through them. In the same way as transformer losses, different wind speeds result in different loads, which in turn give rise to different subsea cable losses. It is worth noting that the the selection of cross sections is undertaken in the design module, whereby the minimum cross section that meets the system constraints

is chosen.

Power flowing through the inter-array cables P, injected in each of the j wind turbines nodes in each i string, is then multiplied by the probability of the wind speed to occur between this wind speed range. This is shown in Equation 3.10 and aggregated at farm level P_{OWF}. Total losses are calculated in a similar manner in Equation 3.11. Eventually the loss factor for the inter-array cable losses is displayed in Equation 3.12.

$$P_{OWF} = \sum_{i} \sum_{j} \sum_{u_{bins}} \left(cdf(u_{n+1}) - cdf(u_n)\right) P(u_n) \quad ; \tag{3.10}$$

$$L_{OWF} = \sum_{i} \sum_{j} \sum_{u_{bins}} \left(cdf(u_{n+1}) - cdf(u_n)\right) \left(L_{trans}(u_n) + L_{cables}(u_n)\right) \quad ; \tag{3.11}$$

$$f_{elec} = 1 - \frac{L_{OWF}}{P_{OWF}} \tag{3.12}$$

3.4.2.3 Availabilities

Availability is defined in this model as the amount of time a component is able to operate for a certain period, divided by the amount of time in that period. An availability of 99% is assumed for any electrical component (apart from a wind turbine), capturing the fact that by adding more devices the overall system availability decreases. In this way, two electrical components that have a 99% availability lead to an overall system availability of 98.01%. Array cables availability f_{array}, including a ring configuration redundancy, is given in Equation 3.13; where the array cable is in ring configuration, $f_{array_{cnf}}$ takes the value of 1, otherwise is 0. Availability of the inter-array cable per se is represented by $f_{array_{cable}}$

$$f_{array} = 1 - (1 - f_{array_{cable}})(1 - 0.5 f_{array_{cnf}}) \tag{3.13}$$

Offshore wind farms can be connected to the onshore grid directly through High Voltage Alternating Current(HVAC) or High Voltage Direct Current (HVDC). HVAC is made of an offshore and onshore substation. In addition, if there is either a landfall or offshore compensation platform to be installed, the resulting export system availability is multiplied by their respective availabilities. HVDC comprises an offshore substation (AC collector), an AC-DC converter plus the onshore substation that includes an inverter DC-AC. When offshore wind farms are located near-shore and their capacity is small, the Medium Voltage Alternating Current (MVAC) solution appears to be more cost-effective than HVAC. In this case, power is sent directly to shore through the same array cables. As a consequence, the export system availability is assumed to be 1; the export system availability is set in the array cables availability. Last but not least, an average wind turbine availability of 95% is assumed.

3.4.2.4 Commissioning yield

It is well understood that during the commissioning phase of an offshore wind farm, power produced by the wind turbines becomes gradually available to the grid as the project progresses. Depending on the number of years of commissioning N_{comm}, different AEP_{comm} are obtained for each year j within the commissioning phase; this has been modelled in Equation 3.14.

$$AEP_{j,comm} = \frac{1 + 2(j-1)}{2N_{comm}} \forall j \in 1, .., N_{comm} \tag{3.14}$$

As an example, if there was only one year of commissioning, the AEP_{comm} for that year would be 50%. When extending the commissioning phase to two years, the expected AEP_{comm} would be 25% for year one and 75% for year two. This means that the energy produced at a given year j accounts for half of the install capacity on that year plus the capacity installed up until that date.

At this stage, the net AEP AEP_{net} can be calculated in Equation 3.15 based on the previous coefficients.

$$AEP_{net} = AEP_{gross}(1 - f_{wakes}) f_{elec} f_{WTG} f_{array} f_{exp} \tag{3.15}$$

3.4.3 Degradation factor

Real annual yield is calculated as the AEP_{net} modified by a yearly degradation factor f_{degr}. This degradation factor accounts for the loss in energy production as a result of wear and tear of wind turbines as well as leading edge erosion on the coatings. As the $(1 - f_{degr})$ is powered to the year of operation j, it is expected that the project yield will be reduced as the project progresses towards the last year of operation N_{oper}. Evidence of decline in wind turbine performance can be found in [75] and is modelled as shown in Equation 3.16.

$$AEP_{real} = AEP_{j,net}(1 - f_{degr})^{j} \forall j \in 1, .., N_{oper} \tag{3.16}$$

3.4.4 Capacity Factor

The capacity factor is defined as the unitless ratio of the wind energy output over a given period of time to the maximum possible energy output during that period; this is expressed in Equation 3.17. Due to technical constraints, such as availability of the wind farm, economic reasons, and availability of the wind resource, capacity factor are always lower than 100%. For offshore wind farms capacity factors range typically between 40% and 45% [76] with future developments by 2022 aiming at around 50% [77].

$$CF_{net} = \frac{AEP_{net}}{(daysinayear)(hoursinaday)OWF_{capacity}} \tag{3.17}$$

3.5 Wind Turbine Technology

Wind turbine costs are a significant factor in the overall wind farm costs and are broken down into supply and installation costs, the models for which are presented separately in Subsection 3.5.1 and 3.5.2, respectively.

3.5.1 Wind Turbine Supply

The first cost component concerns the supply of the wind turbines, which includes the following sub-components: rotor blades, hub, nacelle, generator (including any power electronics), transformer and tower. Wind turbine supply costs include the cost of all components situated above the attachment point of offshore foundations. The total cost of the wind turbines supplied to the installation port C^{S}_{WTG} is calculated using Equation 3.18, based on a specific cost C^{ref}_{WTG}, the rated power cap_{WTG} of the wind turbine and the number N_{WTG} of wind turbines required. C^{ref}_{WTG} is an offer quote from an OEM at the fabrication yard and it typically does not include the transportation costs of the wind turbine components C^{trans}_{WTG} from their production facilities to the pre-assembly facility. These unit costs from the fabrication yard to the pre-assembly location, assumed to be the same as the installation port, are given by C^{trans}_{WTG} and depend on the size of the wind turbines. The larger the wind turbines are, the more deck space is needed to fit the same number of turbines. As a result, the number of trips from the fabrication yard to the pre-assembly location increase, giving rise to higher transportation costs. It has been assumed that no savings are expected for larger turbine orders, therefore no scaling factors have been considered.

$$C^{S}_{WTG} = N_{WTG}\left[cap_{WTG}C^{ref}_{WTG} + C^{trans}_{WTG}\right] \tag{3.18}$$

3.5.2 Wind Turbine Installation

The second cost component is the installation of the wind turbines offshore. Wind turbines are first pre-assembled and pre-commissioned at quayside and prepared for lifting onto the installation vessels. The vessels then transport the wind turbine components to the wind farm site where they are installed on the foundations. Finally, mechanical completion activities are performed and the wind turbines are commissioned. The total installation cost C^{I}_{WTG} is given by Equation 3.19 as the sum of the pre-assembly and pre-commissioning costs C^{prep}_{WTG}, the installation vessel charter costs $C^{vessels}_{WTG}$, the commissioning and completion costs C^{comm}_{WTG}, and the overhead costs $C^{overheads}_{WTG}$ related to design engineering for the installation process.

$$C^{I}_{WTG} = C^{prep}_{WTG} + C^{vessels}_{WTG} + C^{comm}_{WTG} + C^{overheads}_{WTG} \tag{3.19}$$

The pre-assembly, pre-commissioning and preparation of the wind turbines to be ready for lifting onto the transportation vessel are represented by C^{prep}_{WTG}.

Vessel costs $C^{vessels}_{WTG}$ depend upon the duration of the charter period, which in turn depend upon the installation method adopted. The current approach is based on the Kaiser-Snyder 'self-transport' model [30], which assumes the use of a single wind turbine installation vessel capable of transporting the required components from port to the wind farm site and then assembling them on a pre-installed foundation. This model is consistent with contemporary turbine installation techniques using purpose-built wind turbine installation vessels.

The total vessel charter time h_{WTG} required for the installation of a single wind turbine can be determined using Equation 3.20, as the sum of the time h_{load} required to load the components onto the vessel and perform sea-fastening, the time h_{pos} needed to position the vessel at the installation site (including jacking-up and down) and the time $h_{install}$ required to install all the components of the wind turbine onto the foundation. The time h_{travel} needed to travel to-and-from the supply port and the offshore wind farm and the time h_{move} required to move between installation sites within the wind farm are also included; these are allocated between the number of turbines that are installed in a single trip, given by the transport capacity cap_{WTIV} of the installation vessel. The travel and moving times can be calculated based on the loaded and unloaded speed $v_{loadWTIV}$ and $v_{unloadWTIV}$ of the vessel. The travel and moving times are given in Equation 3.21 as a function of the distance d_{SP} of the offshore wind farm from the supply port, and the spacing sp_{WTG} between the wind turbines in the array.

To take into account weather delays, weather windows are considered for each operation. A weather window w represents a limited interval when weather conditions are expected to be suitable for a particular offshore task. In this work, weather windows are dimensionless and expressed in percentages. We could think of a weather window as

a multiplier. For example, if the weather window is 50%, it means that an activity that typically takes 1h, will take 2h after accounting for the weather conditions. Offshore transit and in-farm moving phases are dependent on the operational weather window w_{WTIV} of the installation vessel, while installation of the wind turbine components is limited by the maximum wind speed v_{max} that can be tolerated during the installation. Assuming a typical Rayleigh wind speed distribution, an estimation of the weather window $w_{install}$ for turbine installation can be obtained using Equation 3.22 as a function of the mean wind speed v_{mean} at the wind farm site.

$$h_{WTG} = h_{load} + \frac{h_{pos} + h_{install}}{w_{install}} + \frac{h_{travel}}{w_{WTIV}} \frac{1}{cap_{WTIV}} + \frac{h_{move}}{w_{WTIV}} (1 - \frac{1}{cap_{WTIV}}) \quad (3.20)$$

$$h_{travel} = \left(\frac{d_{SP}}{v_{loadWTIV}} + \frac{d_{SP}}{v_{unloadWTIV}} \right) \quad h_{move} = \frac{sp_{WTG}}{v_{loadWTIV}} \quad (3.21)$$

$$w_{install} = 1 - exp \left[-\frac{\pi v_{max}^2}{4 v_{mean}^2} \right] \quad (3.22)$$

The total vessel costs for the wind turbine installation can then be determined using Equation 3.23, based on the duration of each individual turbine installation process, the number N_{WTG} of wind turbines that need to be installed, and the rate c_{WTIV} of the wind turbine installation vessel (including any spread vessels if required). Additional time for vessel mobilisation and demobilisation n_{mob}, required for the installation vessels to prepare for operation and transit from their previous ports, also needs to be considered, and is included in Equation 3.23.

$$C_{WTG}^{vessels} = [n_{mob} + h_{WTG} N_{WTG}] \, c_{rate_{WTIV}} \quad (3.23)$$

Commissioning costs C_{WTG}^{comm} are broken down into offshore works crew costs C_{crew} and CTV (Crew Transfer Vessel) costs C_{CTV}. Commissioning covers all the activities after all wind turbine components have been installed and usually involve standard electrical

tests for the electrical components and turbines, as well as inspection of routine civil engineering quality records. Those costs are modelled in Equation 3.24, where h_{comm} is the duration of the commissioning activities.

$$C_{WTG}^{comm} = C_{crew} + C_{CTV} \quad C_{crew} = h_{comm} C_{rate_{crew}} \quad C_{CTV} = h_{comm} C_{rate_{CTV}} \tag{3.24}$$

The duration of the installation and commissioning process is subject to learning-by-doing, with the total duration reducing as the number of turbines installed increases. This effect can be modelled using a one-factor learning curve [78], as given in Equation 3.25, where the learning rate LR is the reduction in installation time when the number of installation doubles.

A study as part of the ORECCA project [79] has examined learning rates for turbine and foundation installation; ignoring the data-points for very small projects (less than 10 units), a learning rate of around 15% is obtained for wind turbine installation for a reference number of 70 turbines N_{WTG}^{ref}.

$$h = h^{ref} \left(\frac{N_{WTG}}{N_{WTG}^{ref}} \right)^{\frac{ln(1-LR)}{ln2}} \tag{3.25}$$

Overhead costs for design engineering of the wind turbine installation process is determined using a standard power-law cost function, as shown in Equation 3.26. This costs are based on a reference cost obtained from real-world projects and scaled using a 0.5 coefficient, as suggested in [74].

$$C_{WTG}^{overheads} = C_{overheads}^{ref} \left(\frac{N_{WTG}}{N_{WTG}^{ref}} \right)^{0.5} \tag{3.26}$$

3.6 Foundations Technology

Foundation technology connects the wind turbine to the seabed, and transfers the loads applied to the wind turbine to the surrounding soil. Foundation costs represent a significant fraction of the wind farm balance of plant costs. A number of different foundation options exists for offshore wind turbines, with the optimum choice depending on the size of the wind turbine (and thus the loads on the structure), the water depth at which the

turbine is to be installed and the seabed soil conditions. In this work, only bottom-fixed monopiles and jackets are considered given its commercial maturity.

Monopiles are made up of a thick steel cylinder that is anchored (piled or driven) directly to the seabed, as shown in Figure 3.3 (a). Its shape is simple to design, straighforward to fabricate and leads to tight packing on transport vessels - a cost-effective solution for shallow waters where soil conditions are suitable. However, monopiles have often required extra scour protection around their base, mitigation measures for noisy piling during the installation process or post-installation remedial works in the grout connection with the transition piece. Scour is a type of erosion where a significant section of the soil around the pile of a bottom-fixed offshore structure is removed, as described in more detail in Section 3.6.2.3. Bigger monopiles in terms of size and weight, typically referred as "XL monopiles", have emerged with the aim of being deployed at water depths in excess of 40 m. However, technical challenges such as greater wall thickness in order to cope with wave forces and resist buckling loads during piling, limiting diameter pipe sections and thickness in manufacturing and limiting hidraulic grippers and crane vessel capacities in installation need to be addressed.

Jackets are time-consuming to build and coat with anticorrosion treatments, given their A-shaped, truss-like lattice structure of low-diameter steel tubes, resting on piles, as shown in Figure 3.3 (b). Jackets are typically custom-made to given seabed soil conditions and water depths and cannot easily be stacked for sea transport. However, for deep waters or complex soil conditions, jackets have a proven track record over decades of use in Oil & Gas (O&G).

3.6.1 Foundation Supply

The first cost component concerns the supply of the foundations to the installation port. As is the case with wind turbine supply costs, foundation supply costs do not include the cost of installation, which is covered in a separate submodel, presented in Section 3.6.2. Total foundation supply costs C^S_{fnd} are calculated using Equation 3.27.

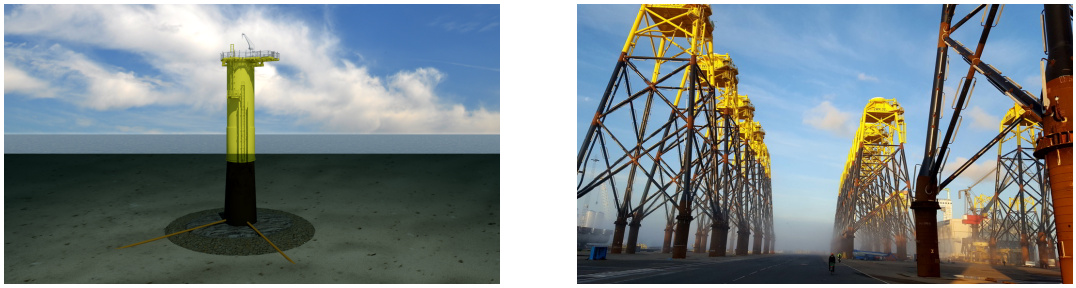

(a) **(b)**

Figure 3.3: (a) Monopiles for the the Gemini offshore wind project designed by Ramboll [80] (b) Jackets for the Wikinger offshore wind project at Bladt's facilities in Lindø [81]

At current time, no savings are expected for larger foundations orders, so no scaling factors have been considered.

$$C_{fnd}^{S} = N_{fnd}\left[C_{fnd}^{proc} + C_{fnd}^{loadout} + C_{fnd}^{trans}\right] + C_{fnd}^{overheads} \tag{3.27}$$

Where N_{fnd} is the total number of foundations, $C_{fnd}^{proc}, C_{fnd}^{trans}$ and $C_{fnd}^{loadout}$ are the costs of procurement, transportation and load-out, respectively for a single foundation and $C_{fnd}^{overheads}$ is the overheads costs for designing and managing construction. Procurement costs can be broken down in turn in primary steel, secondary steel, corrosion protection and fittings costs, as shown in Equation 3.28.

$$C_{fnd}^{proc} = C_{fnd}^{PS} + C_{fnd}^{SS} + C_{fnd}^{corr} + C_{fnd}^{fit} \tag{3.28}$$

In order to determine the procurement costs, foundation masses are estimated so as to evaluate the amount of primary steel that is required for manufacturing. Foundation masses are estimated by means of the following parameters: water depth (at which the foundation is to be installed) d_{water}^{cj}, wind turbine rotor diameter d_{rotor}^{dj} and the mass of the topside $m_{topside}^{ej}$, as shown in Equation 3.29. The coefficients of these equations a_j, b_j, c_j, d_j and e_j are worked out for each foundation type based on fitting Equation 3.29 to internal EDF proprietary data and using least square methods. It is found that monopiles are very sensitive to water depth (d_{water}^{cj} is greater than 1).

$$m_j = a_j + b_j \left[d_{water}^{c_j} d_{rotor}^{d_j} m_{topside}^{e_j} \right] \tag{3.29}$$

Foundations masses can be then converted into primary steel costs by multiplying the foundation masses by the unit primary costs c_{fab}, as shown in Equation 3.30. Unit primary costs depend on material and fabrication costs. While it is understood that monopiles have a balanced repartition between these two cost components, jackets are predominantly driven by fabrication costs due to the complexity of their structure. The more complex the structure, the less the fabrication can be automated in large offshore wind farms. Consequently, jackets benefit less than monopiles from economies of scale given its complex manufacturing process [82, 83].

$$C_{fnd}^{PS} = m_j c_{fab_j} \tag{3.30}$$

In addition to primary steel costs, the costs for secondary steel C_{fnd}^{SS} (boat-landings, ladders, internal platforms, etc.) must be accounted for, as well as the costs for corrosion protection C_{fnd}^{corr}(cathodic protection) and the cost for foundation fittings C_{fnd}^{fit} (such as davit cranes, internal power supply, navigation lights, etc.).

External secondary steel includes boat-landings, rest-platform, external ladders and external platform, including all handrails, gates and flooring. Internal secondary steel covers the internal platform including all handrails and gates as well as the internal ladders. For every item, the steel supply and fabrication including welding and corrosion protection and Non-destructive Testing (NDT), is included. It also includes supply and installation of the infield cable to the foundation entry system (e.g. external J-tubes), supply and installation of an external fall arrest system, a foundation Davit crane and electrical fittings such as a Low Voltage (LV) system including LV power supply, external and internal lighting, navigational aids and a Uninterruptible Power Supply (UPS) system.

The load-out costs from the fabrication yard onto the transport/installation vessel,

including labour, plant and equipment are represented by $C_{fnd}^{loadout}$. Given that jackets cannot be easily stacked for sea transport, load-out jacket foundation costs are considered twice the costs of monopiles. Total costs from the fabrication yard to the pre-assembly location, assumed to be the same as the installation port, are given by C_{fnd}^{trans}. Both costs C_{fnd}^{trans} and $C_{fnd}^{loadout}$ are given per foundation.

As mentioned in the beginning, jackets need to be coated with anticorrosion treatments. This is modelled in Equation 3.31 based on dimensional analysis. As the cost of the corrosion protection is proportional to the area exposed and the area is proportional to the volume to the power of two-thirds, and in turn volume is proportional to mass, this results in the following relationship. This costs are added to C_{fnd}^{corr} when jacket foundations are considered.

$$C_{fnd_{JKT}}^{corr} = C_{CCP_{REF}} \left(\frac{m}{m_{REF}} \right)^{2/3} \tag{3.31}$$

Overhead costs for design engineering of the wind turbine foundation is determined using a standard power-law cost function as explained in other sections.

3.6.2 Foundation Installation

The second cost component concerns the installation of the foundations. According to each foundation type: monopiles or jackets, different installations methods are described.

3.6.2.1 Monopile Installation

Monopiles (MPs) are installed on-site before the Transition Piece (TP) Installation begins. A Heavy Lift Jack-Up (HLJU) vessel is used to install the MPs, while a Heavy Lift Dynamic Positioning (HLDP) vessel is required for the installation of the TPs. It is widely accepted that scour protection is required for MPs foundations.

The foundation installation costs are driven primarily by the vessel charter costs; the

total installation cost C^I_{MP} is given by Equation 3.32. MPs and TPs installation vessel costs are represented by $C^{vessels}_{MP}$and $C^{vessels}_{TP}$, respectively. Scour Protection Costs C^{scour}_{MP} are calculated in a separate submodule: 3.6.2.3 Scour Protection Cost Modelling. This value considers scour protection for a MP Vestas 164-8MW turbine [84]. Eventually, overhead costs $C^{overheads}_{MP}$ related to design engineering and installation management are accounted for. All the vessel charter costs are again based on the Kaiser-Snyder 'self-transport' model [30], which assumes that the installation vessels are capable of transporting the required components from port and installing them on-site.

$$C^I_{MP} = C^{vessels}_{MP} + C^{vessels}_{TP} + C^{scour}_{MP} + C^{overheads}_{MP} \tag{3.32}$$

MP installation is performed by a HLJU vessel; the transport capacity of the HLJU vessel enables it to transport a number of MPs cap_{HLJU} out to the wind farm and then install them. The vessel needs to be equipped with a hydraulic pile-driving hammer in order to complete the installation. The vessel charter time h_{MP} needed to complete the installation of a single MP foundation can be determined using Equation 3.33, the loading and installation times, h_{load} and $h_{install}$ respectively as well as the travel and moving times h_{travel} and h_{move} determined, based on the speed of the heavy lift vessel v_{HLV}), the distance d_{SP} of the offshore wind farm from the construction port and the spacing sp_{WTG} between the wind turbines in the array. Operational weather windows w_{HLJU} are considered for the installation vessel. MP installation is subject to learning-by-doing in a similar manner to the wind turbines and support piles; this effect can thus be modelled using the learning curve approach presented in Equation 3.34. However, no learning rate has been assumed for this study, as this is accounted for in the installation times.

$$h_{MP} = h_{load} + \frac{h_{pos} + h_{install}}{w_{HLJU}} + \frac{h_{travel}}{w_{HLJU}} \frac{1}{cap_{HLJU}} + \frac{h_{move}}{w_{HLJU}} (1 - \frac{1}{cap_{HLJU}}) \tag{3.33}$$

Additionally, the installation time for the MPs depends upon whether or not drilling is

required. The average installation time is increased by an additional duration Δh_{drill}, based on the fraction f_{drill} of installation sites that will require drilling.

$$h_{install} = h_{install}^{ref} \left(\frac{N_{MP}}{N_{MP}^{ref}} \right)^{\frac{ln(1-LR)}{ln2}} + f_{drill} \Delta h_{drill} \tag{3.34}$$

The cost of the MP installation vessel can be determined using Equation 3.35 based on the rate c_{HLJU} of the heavy lift vessel and the duration of the installation process, which is a function of the number of foundations N_{MP} to be installed. Additional costs for the piling hammer c_{hammer} and for the drilling equipment (if needed) c_{equip} are also included, as well as additional charter time for vessel mobilisation and demobilisation $n_{mob_{HLJU}}$.

$$C_{MP}^{vessels} = \left[n_{mob_{HLJU}} + h_{MP} N_{MP} \right] c_{rate_{HLJU}} \tag{3.35}$$

TP installation is performed by a HLDP vessel; the large transport capacity of the HLDP vessel enables it to transport a number of TPs cap_{HLDP} out to the wind farm and then install them. The vessel charter time h_{TP} needed to complete the installation of a single TP foundation can be determined using Equation 3.36, the loading and installation times, h_{load} and $h_{install}$, respectively as well as the travel and moving times h_{travel} and h_{move} determined, based on the speed of the heavy lift vessel v_{HLV}, the distance d_{SP} of the offshore wind farm from the construction port and the spacing sp_{WTG} between the wind turbines in the array. Operational weather windows w_{HLDP} are again considered for the installation vessel. TP installation is subject to learning-by-doing in a similar manner to the wind turbines and support piles; this effect can thus be modelled using the learning curve approach presented in Equation 3.34 (left term). However, no learning rate has been assumed for this study, as this is accounted for in the installation times.

$$h_{TP} = h_{load} + \frac{h_{pos} + h_{install}}{w_{HLDP}} + \frac{h_{travel}}{w_{HLDP}} \frac{1}{cap_{HLDP}} + \frac{h_{move}}{w_{HLDP}} (1 - \frac{1}{cap_{HLDP}}) \tag{3.36}$$

The cost of the TP installation vessel can be determined using Equation 3.37 based on

the rate c_{HLDP} of the heavy lift vessel and the duration of the installation process, which is a function of the number of foundations N_{TP} to be installed. Additional costs for the piling hammer c_{hammer} and c_{equip} for the grouting equipment are also included [85], as well as additional charter time for vessel mobilisation and demobilisation $n_{mob_{HLDP}}$.

$$C_{TP}^{vessels} = [n_{mob_{HLDP}} + h_{TP} N_{TP}]\, c_{rate_{HLDP}} \tag{3.37}$$

3.6.2.2 Jacket Installation

The support piles are assumed to be pre-installed on-site before jacket installation begins in order to allow jacket installation to proceed as smoothly as possible. A jack-up vessel equipped with a hydraulic pile-driving hammer is assumed to be used for support pile installation, while a dynamic positioning 2 (DP2-class) heavy lift vessel is used to install the jackets and grout them into place on the piles. It is currently assumed that scour protection is required for jacket foundations.

The foundation installation costs are driven primarily by the vessel charter costs; the total installation cost C_{JKT}^{I} is given by Equation 3.38. Support pile and jacket installation vessel costs are represented by $C_{PP}^{vessels}$ and $C_{JKT}^{vessels}$, respectively. Scour Protection Costs C_{JKT}^{scour} are calculated in a separate submodule 3.6.2.3. This value considers scour protection for a Vestas 164-8MW turbine [84]. Eventually, overhead costs $C_{JKT}^{overheads}$ related to design engineering for the installation process are accounted for. Whereas the vessel charter costs for the jackets are again based on the Kaiser-Snyder 'self-transport' model [30], which assumes that the installation vessels are capable of transporting the required components from port and installing them on-site, the vessel charter costs for the support-piles have been considered differently. As a consequence, the installation method for the support-piles is detailed below:

$$C_{JKT}^{I} = C_{PP}^{vessels} + C_{JKT}^{vessels} + C_{JKT}^{scour} + C_{JKT}^{overheads} \tag{3.38}$$

Pre-piling is performed by a self-propelled jack-up vessel (SPJU) equipped with a piling hammer. To be able to transport a large number of the support-piles out to the wind farm site, an Offshore Transportation Barge (OTB) is used as a component supply

vessel. Since these two vessels have different vessel characteristics, the most restrictive values will be taken into account to estimate the charter duration, resulting into an operational weather window w_{OP} and vessel velocity v_{OP}. Equation 3.40 displays these constraints. In addition to this, the loading time is only accounted for the first barge $h_{OTB_{load}}$. In other words, the SPJU vessel will not need to return to port until all the support-piles have been installed, given the fact that the OTB will be carrying the remaining pin-piles from the port to the farm, while SPJU is installing others at the same time. Consequently, the total loading time is calculated as the minimum between the number of foundations N_{fnd} to be installed and the capacity of the OTB cap_{OTB}, times the loading time for each individual foundation h_{load}. This is also displayed in Equation 3.40.

$$w_{OP} = min\left(w_{OTB}, w_{JUV}\right)\ z; v_{OP} = min\left(v_{OTB}, v_{JUV}\right) \tag{3.39}$$

$$n_{load} = min\left(N_{fnd}, cap_{OTB}\right)\ z; h_{OTB_{load}} = h_{load} n_{load} \tag{3.40}$$

The vessel charter time h_{PP} needed to complete the installation of the support-piles can be determined using Equation 3.41, based on the number of piles n_{PP} required by each jacket and the loading, positioning and installation times, $h_{OTB_{load}}$, h_{pos} and $h_{install}$ respectively. The travel time h_{travel} and movement time h_{move} can again be determined, based on the operational speed vessel v_{OP}, the distance d_{SP} of the offshore wind farm from the construction port and the spacing sp_{WTG} between the wind turbines in the array. As was the case previously, the equivalent duration of the installation process is increased by the consideration of the operational weather window w_{OP}.

$$h_{PP} = h_{OTB_{load}} + \frac{h_{pos} + h_{install}}{w_{HLDP}} + \frac{h_{travel}}{w_{HLDP}} \frac{1}{cap_{HLDP}} + \frac{h_{move}}{w_{HLDP}} (1 - \frac{1}{cap_{HLDP}}) \tag{3.41}$$

The installation of the support piles is subject to learning-by-doing, which is modelled using a one-factor learning curve as given in Equation 3.42. The installation time for the support piles depends upon whether or not drilling is required. The average

installation time is increased by an additional duration Δh_{drill}, based on the fraction f_{drill} of installation sites that will require drilling.

$$h_{install} = h_{install}^{ref} \left(\frac{N_{PP}}{N_{PP}^{ref}} \right)^{\frac{ln(1-LR)}{ln2}} + f_{drill} \Delta h_{drill} \tag{3.42}$$

Jacket installation is performed by a dynamic positioning 2 (DP2-class) heavy lift vessel; the large transport capacity of the heavy lift vessel enables it to transport a number of jackets cap_{HLV} out to the wind farm and then install them on the previously-installed support piles. The vessel needs to be equipped with grouting equipment in order to complete the installation. The vessel charter time h_{JKT} needed to complete the installation of a single jacket foundation can be determined using Equation 3.43, the loading and installation times, h_{load} and $h_{install}$ respectively as well as the travel and moving times h_{travel} and h_{move} determined, based on the speed of the heavy lift vessel v_{HLV}, the distance d_{SP} of the offshore wind farm from the construction port and the spacing sp_{WTG} between the wind turbines in the array. Operational weather windows w_{HLV} are again considered for the installation vessel. Jacket installation is subject to learning-by-doing in a similar manner to the wind turbines and support piles (but without the requirements for drilling); this effect can thus be modelled using the learning curve approach presented in Equation 3.42 (left term). However, no learning rate has been assumed for this study, as this is accounted for in the installation times.

$$h_{JKT} = h_{load} + \frac{h_{pos} + h_{install}}{w_{HLJU}} + \frac{h_{travel}}{w_{HLJU}} \frac{1}{cap_{HLJU}} + \frac{h_{move}}{w_{HLJU}} (1 - \frac{1}{cap_{HLJU}}) \tag{3.43}$$

The cost of the jacket installation vessel can be determined using Equation 3.44, based on the rate c_{HLV} of the heavy lift vessel (including any spread vessels) and the duration of the installation process, which is a function of the number of foundations N_{fnd} to be installed. Additional costs c_{equip} for the grouting equipment are also included [85], as well as additional charter time for vessel mobilisation and demobilisation $n_{mob_{HLDP}}$.

$$C_{JKT}^{vessels} = \left[n_{mob_{HLDP}} + h_{TP} N_{TP} \right] c_{rate_{HLDP}} \tag{3.44}$$

3.6.2.3 Scour Protection Modelling

Scour is a type of erosion where a significant section of the soil around the pile of a bottom-fixed offshore structure is removed. Seabed scour, driven by the interaction between the foundation and the local flow pattern and velocities, may pose a risk on the structural integrity of foundations. Consequently, scour protection is required for bottom-fixed offshore foundations.

Total scour protection costs C_{scour} are given in Equation 3.45, as the sum of material and installation costs. Material costs are a function of the total scour protection material m_{tot} and its associated unit costs C_{mat}^{unit}. Total scour protection material is dependent on the total number of foundations N_{fnd}, the volume of protection material per foundation or unit V_{mat}^{unit} and the density of the rock armour ρ_{mat}, assumed to be 2.6 t/m^3 [86]. This is shown in Equation 3.46. Total vessel costs for scour protection installation are determined, based on the duration of the rock dumping installation process h_{RDV} and its rate c_{RDV}. Additional time for vessel mobilisation and demobilisation $n_{mob_{RDV}}$ is also required for the installation vessel to prepare for operation and transit from its previous ports.

$$C_{scour} = C_{mat} + [n_{mob_{RDV}} + h_{RDV}]\, c_{rate_{RDV}} \tag{3.45}$$

$$C_{mat} = C_{mat}^{unit} m_{tot} \;\; m_{tot} = N_{fnd} V_{mat}^{unit} \rho_{mat} \tag{3.46}$$

Vessel installation duration h_{RDV} takes into account weather windows w_{RDV} for each operation: offshore transit and in-farm moving phases, as shown in Equation 3.47. The rock dumping vessel is characterised by its capacity cap_{RDV}, loading speed $v_{loadRDV}$ and installation speed $v_{installRDV}$.

$$h_{RDV} = \frac{m_{tot}}{v_{loadRDV}} + \frac{\frac{m_{tot}}{v_{installRDV}}}{w_{RDV}} + \frac{h_{travel} N_{trips}}{w_{RDV}} + \frac{h_{move}}{w_{RDV}}(N_{fnd} - N_{trips}) \tag{3.47}$$

Where N_{trips} is the number of transport trips to and from the construction port as shown in Equation 3.48 and h_{travel} and h_{move} are the travel and moving times given by

Equation 3.49, as a function of the construction port distance d_{SP}, and the inter-turbine spacing sp_{WTG}.

$$N_{trips} = ceil\left(\frac{m_{tot}}{cap_{RDV}}\right) \tag{3.48}$$

$$h_{travel} = 2\frac{d_{SP}}{v_{RDV}} \;\; h_{move} = \frac{sp_{WTG}}{v_{RDV}} \tag{3.49}$$

3.7 Electrical Infrastructure Technology

Electrical costs are a significant part of the balance of plant costs. Although electrical equipment is needed both for onshore and offshore wind, care has to be taken when comparing offshore costs with their onshore counterparts, due to differences arising from: larger arrays of larger machines, less frequent scheduled maintenance, further distance to the network connection points, more aggressive environment, and, what's more important, less space available for equipment [87]. Offshore electrical equipment is more costly than on land, due to the harsh environmental conditions they operate in. In addition, reliability and availability are much more critical, because faults may be more frequent and could take much longer to locate and repair offshore. As a result, a deeper understanding of the cost modelling functions for each component is required for a good cost estimate.

Electrical costs are divided into several categories: inter-array cable, export cable, offshore substation and onshore substation. For each category, supply and installation costs are also broken down, enabling a detailed assessment of their cost components. These costs need to be constantly reviewed in conjunction with economies of scale, learning rates and innovations taking place in the industry.

3.7.1 Inter-Array Cable

The direct costs of the inter-array cables typically represent only a small fraction of the final electrical costs; the design of these components is thus targeted to reduce losses

and maximise reliability, to avoid the much higher indirect costs resulting from lost production. The cost modelling tool includes the option for both radial and ring array configurations, as described below in Subsection 3.7.1.1. The cost of the inter-array cable are broken down into equipment supply and installation costs, which are presented separately in Subsection 3.7.1.2 and 3.7.1.3.

3.7.1.1 Array Cable Design Aspects

Figure 3.4 shows two different array cable configuration: radial and ring. In a radial layout, the cross section of the array cable changes along each wind turbine string, minimising the size (and thus the cost) of cables required. At the end of the strings, where the export current is lowest, cables with smaller cross-section are used; this cross-section increases along the string as the total current increases.

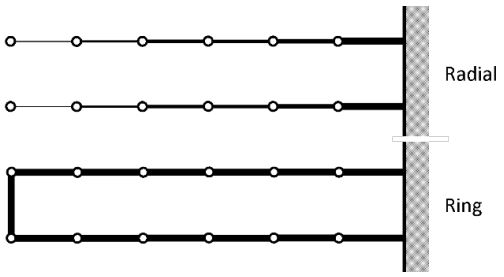

Figure 3.4: Radial and Ring Wind Turbine String Configurations

The total number of wind turbines N_{WTG}^{string} that can be connected to a single string can be determined using Equation 3.50, as a function of the current carrying capacity I_{max} of the largest cable section that can be used in the array, the array voltage V_{array} and the rated output P_{nom}^{WTG} of the wind turbines. If the wind turbines participate in the supply of reactive power to the offshore substation, additional capacity is required in the array cables; this is accounted for with the f_{react} factor, which is the ratio of the reactive power output to the rated active power output of the wind turbines. In the

array configuration, the different cross-sections are determined by obtaining the minimum current carrying capacity required to bring power from one turbine to the other.

$$N_{WTG}^{string} = \frac{\sqrt{3} V_{array} I_{max}}{P_{nom}^{WTG} \sqrt{1 + f_{react}^2}} \tag{3.50}$$

An alternative configuration is the ring layout, where the maximum-sized cable is used along the entire length of the wind turbine string and the ends of two adjacent strings are connected by an additional full-sized cable section. This layout significantly increases redundancy; should a cable failure occur, current can continue to be exported from turbines situated beyond the failure, albeit limited by the maximum carrying capacity of the string. The ring configuration is more expensive than the radial alternative, but the added value of higher reliability makes it an economically attractive option. Cross sections of copper and aluminium are typically used for inter-array cables.

3.7.1.2 Array Cable Supply Costs

The supply cost of the inter-array cable network includes the cost of the cables, as well as a number of additional costs for auxiliary components. The cable cost C_{cable}^{SS} for three-core copper-conductor subsea AC cable is given by Equation 3.51 as a function of the rated voltage V_{op} (in kV) and the cross-section A_{sect} of the conductor cores (in mm2). An additional factor f_{mat} is used to account for the material conductor, taking a value of 0 for copper and 1 for aluminium. This correlation is derived through interpolation of internal cost data sources (EDF data), adjusted for exchange rate and inflation. The available data covers cables ranging from 33 to 275 kV with cross-sections ranging from 95 to 2500 mm2 and can thus also be used for the export cable cost calculation. Coefficients a, b, c, d, e are obtained by minimising the difference between the predicted costs to actual costs from an internal database.

$$C_{cable}^{SS} = a + b A_{sect}^{c} V_{op}^{d} (1 - e f_{mat}) \tag{3.51}$$

Total subsea cable supply costs are determined using Equation 3.52, by summing the

product of the total length l_{sect} (in m) of each of the N_{sect} cable sections by the specific cost of that cable section C^{SS}_{cable}. A certain extra length of spare cable is ordered, to accommodate potential damage during the installation process; this is accounted for using the spare cable factor f_{spare}. Since the cable is assumed to be installed directly in the offshore wind farm, there is no need to account for transportation costs to the installation port.

$$C_{cable} = \sum_{N_{sect}} l_{sect}(1 + f_{spare})C^{SS}_{cable} \tag{3.52}$$

The lengths of each cable section can either be obtained from detailed wind farm simulation software (such as OpenWind), or be estimated using the simple relationship in Equation 3.53. The cable length is estimated as a function of the horizontal inter-turbine distance sp_{WTG}, the vertical direction (to-and-from the seabed), based on the water depth d_W, as well as an additional length l_{int} between the water level and the transformer platform. The total length is increased by a small factor f_{slack} which takes into account the added length needed for cable slack and snaking.

$$l_{sect} = (sp_{WTG} + 2(d_W + l_{int}))(1 + f_{slack}) \tag{3.53}$$

In addition to the direct cost of the cables, a number of auxiliary components are required. The cost of these components C_{aux} is based on the costs of the hang-off assemblies C_{hang} (one for each cable end), cable protection systems (one for each cable end) C_{prot} and cable termination kits (one per phase for each cable end) C_{term}. This is shown in Equation 3.54. Total inter-array cable supply costs are then calculated in Equation 3.55. Overhead supply costs can be determined using a standard power-law cost function, based on the total length of the cable and a scaling exponent of 0.5 [74].

$$C_{aux} = 2N_{sect}(C_{hang} + C_{prot} + 3C_{term}) \tag{3.54}$$

$$C_{supply} = C_{cable} + C_{aux} + C_{overheads} \tag{3.55}$$

3.7.1.3 Array Cable Installation Costs

The second component of the array cable costs concerns the installation of the inter-array cables and their connection to the wind turbines. Array cable installation typically takes place after foundation installation but before wind turbine installation. Array cable installation costs depend upon the installation method chosen; the model presented here is based on surface-laying of the cable, followed by post-lay burial using a separate vessel. The total installation cost $C_{install}$ is given by Equation 3.56, as the sum of the cost $C_{pre-lay}$ of pre-laying activities, the cost C_{vessel}^{lay} and C_{vessel}^{burial} of the vessel spreads for cabling-laying and burial processes, the cost C_{term} of cable termination activities and the overhead costs $C_{overhead}$ related to design engineering for the installation process.

$$C_{install} = C_{pre-lay} + C_{vessel}^{lay} + C_{vessel}^{burial} + C_{term} + C_{overhead} \tag{3.56}$$

Pre-laying activities include the cable-route seabed survey, including Unexploded Ordnance (UXO) survey and the pre-lay grapnel run to remove any debris on the cable route, which are typically performed by smaller vessels. These costs can be determined using Equation 3.57, based on the specific costs of the survey and grapnel-run activities C_{survey} and $C_{grapnel}$ and the total length l_{route} of the cable route. The total length of the cable route is calculated in Equation 3.58, using the parameters described in Equation 3.53.

$$C_{pre-lay} = (C_{survey} + C_{grapnel}) l_{route} \tag{3.57}$$

$$l_{route} = \sum_{N_{sect}} (sp_{WTG} + 2(d_W + l_{int}))(1 + f_{slack}) \tag{3.58}$$

The cost of cable-laying depends upon the duration of the vessel charter period; the required vessels include the principal cable laying vessel (typically dynamic positioning 2(DP2)-class), equipped with a light work-class Remotely Operated Vehicle (ROV), as

well as a number of offshore support vessels to allow tower access and support pull-in operations. For each array cable section, the process begins with preparation activities at the foundations, which includes the installation of winches, messenger wires, etc. by the tower preparation team. The pull-in team is then transferred to the tower and the first end of the array cable is pulled into the foundation and secured, with monitoring provided by the ROV. The cable is then laid-out between the two foundations, cut off at the required length and the other end of the cable pulled in at the second foundation. The vessel charter time h_{lay} needed to complete the laying of a single cable section can thus be determined using Equation 3.59, based on the time $h_{prep}$for tower preparation, the duration h_{pull} of the pull-in process, the length l_{sect} of the cable section and the cable laying speed v_{lay}. The operational weather window of the cable laying vessel w_{CLV} also needs to be considered. Both the tower preparation and pull-in activities are subject to learning by doing, which is modelling using one-factor learning curve as displayed in the wind turbine section based on [78], using a 5% learning rate.

$$h_{lay} = \left(h_{prep} + 2h_{pull} + \frac{l_{sect}}{v_{lay}} \right) \frac{1}{w_{CLV}} \tag{3.59}$$

The cost of the vessels for the cable-laying process C_{vessel}^{lay} can be determined using Equation 3.60, based on the day-rate c_{CLV} of the cable laying spread (including teams and vessels), the day-rate of the CTV auxiliary vessel c_{CTV} and preparation team $c_{prepteam}$, the total duration of the cable-laying process h_{lay} and the number of cable sections N_{sect} to be installed, as well as the additional time for vessel mobilisation and demobilisation n_{mobCLV}. Furthermore, before cable-laying can begin, the cable must be loaded onto the vessel, and the cost of this process $C_{load-out}$ is based on the total length l_{cable} of cable (including spares.)

$$C_{vessel}^{lay} = (n_{mobCLV} + h_{lay} N_{sect})\, c_{CLV} + h_{lay} + (c_{CTV} + c_{prepteam}) + C_{load-out} l_{cable} \tag{3.60}$$

The cost of cable-burial also depends upon the duration of the vessel charter period;

cable burial is performed by a DP3-class offshore construction vessel equipped with a trenching ROV. The time h_{bury} needed to complete the burial of a single cable section can be determined using Equation 3.61, based on the launch and recovery times for the ROV, h_{launch}^{ROV} and $h_{recover}^{ROV}$, and the trenching speed v_{trench} of the ROV; monitoring of the burial process is performed by the ROV during trenching. The operational weather window w_{OCV} of the vessel also needs to be considered.

$$h_{bury} = \left(h_{launch}^{ROV} + \frac{l_{sect}}{v_{trench}} + h_{recover}^{ROV} \right) \frac{1}{w_{OCV}} \tag{3.61}$$

The cost of the vessels for the cable-burial process C_{vessel}^{burial} can be determined using Equation 3.62 based on the day-rate c_{OCV} of the cable burial vessel (including the trenching ROV), the total duration of the cable-burial process and the number of cable sections N_{sect} to be buried, as well as the time for vessel mobilisation and demobilisation n_{mobOCV}.

$$C_{vessel}^{burial} = \left(n_{mobOCV} + h_{bury}^{ROV} N_{sect} \right) c_{OCV} \tag{3.62}$$

Cable termination is performed by a separate termination crew, who access the foundations using a crew transfer vessel once cable-laying has been completed. The cost of cable termination can be determined using Equation 3.63, based on the duration of termination activities h_{term} and the day-rate of the termination crew c_{term}. Termination activities are subject to learning-by-doing, which is modelled using the one-factor learning curve [78], using a 10% learning rate.

$$C_{vessel}^{burial} = 2 h_{term} N_{sect} c_{term} \tag{3.63}$$

The cost of installation overheads (design and engineering of the installation process as well as vessel management) are determined using a standard power-law cost function with a scaling exponent of 0.5 which is commonly used for scaling up overhead costs [74].

3.7.2 Export Cable

Transmission infrastructure is vital in order to export the power from the offshore wind farm to the terrestrial power grid. The cost model includes the option for both HVAC and HVDC subsea power cables, as described in Subsection 3.7.2.1. Export cable system costs are broken down into supply and installation costs, which are presented separately in Subsection 3.7.2.2 and Subsection 3.7.2.3.

3.7.2.1 Export Cable Design Aspects

The export cables can be designed with a certain degree of redundancy, in order to avoid losing the entire export capacity due to a single cable fault. The active current that needs to be transmitted per cable I_{cable}^{active} can be calculated using Equation 3.64, as a function of the number of cables N_{cable}, the total number N_{WTG} of wind turbines in the offshore wind farm and the voltage V_{export} of the export cable. The capacity is selected in order to ensure that in the event of a cable failure, the export capacity of the remaining cables is sufficient to continue to export a certain fraction f_{red} of the total wind farm capacity.

$$I_{cable}^{active} = max\left[\frac{f_{red}}{N_{cable}-1}, \frac{1}{N_{cable}}\right] \frac{N_{WTG} P_{nom}^{WTG}}{\sqrt{3} V_{export}} \tag{3.64}$$

The total current carried by the export cable can be determined using Equation 3.65, as the sum of the active power export current and the reactive charging current. The cable needs to be rated for the maximum value of the total current that it is required to carry; the subsea and underground cables require different ratings.

$$I_{cable}^{active} = \sqrt{I_{active}^2 + I_{charging}^2} \tag{3.65}$$

The reactive power required by the cable can be supplied at one or both ends, and is consumed along the entire length of the cable. As such, the intensity of the charging current is highest at the cable ends where the current is supplied, and it is this maximum value that needs to be taken for the cable rating. A schematic illustration of the intensity of the charging current in a typical export cable setup is shown in Figure 3.5. The majority of the charging current is supplied from the onshore substation; a certain

amount of charging current may be provided at the other end of the cable by the wind turbines, in order to reduce the peak intensity of the charging current and reduce the required cable rating.

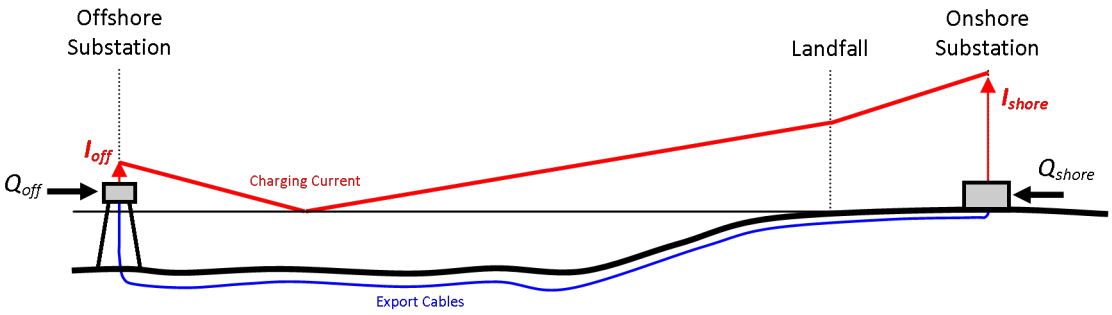

Figure 3.5: Charging Currents for a Typical HVAC Export Cable Configuration

The intensity of the charging current is proportional to the length of the export cable l_{cable}, the export voltage V_{export} and the system frequency f_{export}, as shown in Equation 3.66; exact values for the charging current of subsea and underground export cables have been obtained from manufacturer's data.

$$I_{charging} \propto l_{cable} V_{export} f_{export} \tag{3.66}$$

3.7.2.2 Export Cable Supply Costs

Export cable supply costs differ whether the system is HVAC or HVDC. Whereas the HVAC is divided into onshore and offshore cables, the HVDC system is divided between the AC and DC cable parts. The cable from the substation to the converter is responsible for transferring the power from the farm to the converter. Given that electric power is generated at the wind turbines in AC, this needs to be transferred in AC form to the converter. The cable linking the offshore converter to the onshore substation is considered to be the HVDC link. As was the case for the inter-array cable, some additional slack and spare cable is needed to account for contingency when installing the export cables. Export cable costs are calculated using the same formula as for the inter-array cables, a shown and described in Equation 3.51. The total supply cost for HVAC export cables is then determined using Equation 3.67, based on the

lengths l_{subsea} and $l_{onshore}$ and specific costs (cost per meters) C_{cable}^{SSHVAC} and C_{cable}^{SSUG} of the subsea and onshore cables, respectively, and the total number of export cables N_{cable} that are required. Likewise, the total cost for the HVDC export cables takes into account the AC and DC cable specific costs C_{cable}^{SSHVAC} and C_{cable}^{SSHVDC} of the AC and DC cables and their corresponding lengths, as shown in Equation 3.68.

$$C_{cables} = \left(l_{subsea} C_{cable}^{SSHVAC} + l_{onshore} C_{cable}^{SSUG}\right) N_{cable} \tag{3.67}$$

$$C_{cables} = \left(l_{HVAC} C_{cable}^{SSHVAC} + l_{HVDC} C_{cable}^{SSHVDC}\right) N_{cable} \tag{3.68}$$

3.7.2.3 Export Cable Installation Costs

Export cable installation costs have been broken down into two - offshore and onshore installation activities. These are presented separately in Subsection 3.7.2.4 and Subsection 3.7.2.5. Export cable installation costs are assumed to be the same for both HVAC and HVDC export systems.

3.7.2.4 Offshore export cable installation costs

Subsea export cables are installed using a cable-laying spread followed by a cable burial vessel, in a similar manner to the array cables. The total installation cost $C_{CBLinst}^{off}$ is given by Equation 3.69, as the sum of the cost of pre-laying activities, the cost C_{vessel}^{lay} and C_{vessel}^{burial} of the vessel spreads for cabling-laying and burial processes, the cost C_{term} of cable termination activities at the offshore substation, the cost of cable landfall $C_{landfall}$ and the overhead costs $C_{overhead}$ related to design engineering for the installation process.

$$C_{CBLinst}^{off} = C_{pre-lay} + C_{vessel}^{lay} + C_{vessel}^{burial} + C_{term} + C_{landfall} + C_{overhead} \tag{3.69}$$

The cost of pre-laying activities can be calculated using Equation 3.57, based on the total length l_{route} of the cable route. Cable laying, burial and termination costs can be determined using Equations 3.60, 3.62 and 3.63, with the minor modification that pull-in and termination are only required at one cable end (the substation side). Same

load-out costs as for inter-array cables have been assumed to load the cable onto the installation vessel. Overheads are modelled in a similar way as for inter-array cables.

3.7.2.5 Onshore export cable installation costs

Costs for the installation of the onshore cables have been taken from an Ecofys study [88] and updated for inflation; using this data, the correlation shown in Equation 3.70 has been established, which gives the onshore installation costs as function of the length of the onshore cables l_{cables} and the total number of cables to be installed.

$$C^{on}_{CBLinst} = a l^{b}_{cables} + C_{overhead}(N_{cables}) \tag{3.70}$$

3.7.3 Offshore Substation Costs

Offshore substation costs can be broken down into supply and installation costs, presented separately in Subsection 3.7.3.1 and Subsection 3.7.3.2. The first cost component concerns the offshore substation supply. In order to determine this cost, the total mass for the support structure is estimated and used to evaluate the amount of primary steel that is required for manufacturing. Foundation masses are given by correlations based on an internal database, following parameters in Equation 3.71; foundation masses might be related with the water depth d^{cj}_{water}, the wind turbine rotor diameter d^{dj}_{Rot} , the mass of the topside $m^{ej}_{topside}$, the equivalent capacity C^{fj}_{eq} and the exporting voltage V^{gj}_{exp}. The coefficients of these equations $a_j, b_j, c_j, d_j, e_j, f_j$ and g_j are worked out for each foundation type based on fitting Equation 3.71 to internal data and using least square methods. It is worth notice that all weights and measures are given in the International System of Units (SI). For further information on the methodology and data regarding this foundation mass correlation, this can be found in [89]. The equivalent capacity has been defined as the mass of the transformer plus two-thirds of the mass of the shunt reactors. The mass of jackets m_{JKT} , pinpiles m_{PP} and HVAC topside $m_{topHVAC}$ is estimated using Equation 3.71.

$$m_j = a_j + b_j d^{cj}_{water} d^{dj}_{Rot} m^{ej}_{topside} C^{fj}_{eq} V^{gj}_{exp} \tag{3.71}$$

The masses of the electrical foundations are derived from Table 3.1. This means that to obtain them, not only previous foundation mass correlation functions from Equation 3.71 have been used, but also some hypothesis on the topside masses are assumed. Further details on how to estimate the mass of the hub m_{Hub} or tower m_{Tower}, when this input in not specified, can be found in [89]. Topside costs for the different platforms are taken into account separately.

Foundation Type	Description	Assumption
m_{HVAC}	Mass of HVAC	$m_{JKT}(m_{topHVAC})$
m_{OTM1}	Mass of OTM w shared foundation	$m_{JKT}(m_{Hub} + m_{Tower} + m_{630t})$
m_{OTM2}	Mass of OTM wo shared foundation	$m_{JKT}(m_{630t})$
$m_{HVDCSVC}$	Mass of HVDC collector	$m_{JKT}(m_{topHVAC})$
$m_{HVDCConv}$	Mass of HVDC converter	$m_{JKT}(m_{10000t})$

Table 3.1: Electrical Mass Correlation for HVAC and HVDC

3.7.3.1 Offshore Substation Supply Costs

Two different strategies are considered as far as the design of an offshore HVAC substation is concerned: either a conventional high voltage offshore substation (HVOS), used in the majority of offshore wind farms, or the offshore transformer module (OTM) designed by Siemens. By default, the OTM substation is assumed to be mounted on a jacket foundation of an existing wind turbine, and as such no foundation costs are needed. If desired, a separate foundation could be used for the substation, with the cost calculated using the models presented in the foundation section. Offshore substation supply total costs are calculated as function of the costs of the topside platform $C_{topsideplat}$, the jacket structure C_{JKT}, the transformers C_{trans}, the Gas Insulated Switchgear (GIS) C_{GIS} for array and export systems, the Supervisory Control and Data Acquisition (SCADA) system C_{SCADA}, the Cross-linked Polyethylene (XPLE)

sets C_{XLPE} and the overhead costs $C_{overheads}$. This is displayed in Equation 3.72.

$$C_{HVACon} = C_{topsideplat} + C_{JKT} + C_{trans}N_{trans} + C_{GIS}\left(N_{MVs} + C_{HVs}\right) + C_{SCADA}$$

$$+ C_{XLPE}N_{cables} + C_{overheads} + \left(N_{MVs} + C_{HVs}\right) + C_{SCADA} + C_{XLPE}N_{cables} + C_{overheads} \tag{3.72}$$

The costs of the topside platform $C_{topsideplat}$ are given based on discussions with the manufacturer. As far as the jacket structure costs C_{JKT} are concerned, these have been calculated using the same supply functions described in the jacket foundation supply section. The only difference is that the mass of the foundation is given in Table 3.1. The cost of the transformers C_{trans} can be determined using Equation 3.73, as a function of the rated capacity P_{rate} and the rated voltage V_{op}. To account for the additional costs for "marinisation" of offshore transformers, the costs are increased by a factor f_{off}, which is set to 1 for offshore units. This relationship has been derived from [90], where a_j,b_j,c_j, d_j and e_j are estimated.

$$C_{trans} = a_j + b_j P_{rate}^{cj} V_{op}^{dj}\left(1 + e_j f_{off}\right) \tag{3.73}$$

The cost of the gas-insulated switchgear C_{GIS} is a function of the rated voltage, and can be determined using Equation 3.74; an offshore factor is again used to account for the marinisation costs. This relationship has been derived from [90], where a_j,b_j and c_j are estimated.

$$C_{GIS} = a_j V_{op}^{bj}\left(1 + c_j f_{off}\right) \tag{3.74}$$

In addition to the equipment above, XLPE cable sets and other accessories are required to connect the array cable strings and export cables to the switchgear aboard the offshore substation. The cables set cost is a function of the voltage, and can be determined

using Equation 3.75. This relationship has been derived from [90], where a_j,b_j and c_j are estimated.

$$C_{XLPE} = a_j V_{op}^{bj} (1 + c_j f_{off}) \tag{3.75}$$

In order to allow the (Offshore Transmission Owner) OFTO to monitor and control the export system, SCADA equipment is to be installed on each offshore substation; the cost of this equipment C_{SCADA} is taken into consideration within the offshore substation supply costs. Overhead costs for system design and engineering management also need to be considered, and can again be determined using a power-exponent cost function; the reference costs are scaled using an exponent of 0.5 and the number of substations employed.

The costs of the offshore HVDC system are made of the AC collector and converter supply costs. The AC collector is responsible for transferring the power from the offshore wind farm to the converter. Then power is converted to DC to be fed into the HVDC subsea power cable. The supply costs for the AC collector are considered to be the same as for the HVAC supply costs above; an OHVS platform is considered as a supporting structure for the AC collector. In addition to the AC collector, costs for the converter need to be considered; these can be calculated using Equation 3.76 based on the total power exported through the onshore substation. This relationship has been derived from [90], where a_j and b_j are estimated.

$$C_{conv} = a_j cap_{conv}^{bj} \tag{3.76}$$

3.7.3.2 Offshore substation installation costs

The offshore substation installation module shares many similarities with the foundation installation module, described in Section 3.6.2. As a result, only a high level description of the model is provided. The types of installation vessels and component installation vessels are displayed in Table 3.2 for each offshore substation type.

Structure Type	Installation Vessel	Component Installation Vessel
PP	SPJU (Self-propelled Jack Up Vessel)	OTB
WTG JKT	HLJU (High Lift Jack Up Vessel)	self
OHVS HVAC	OCV (Offshore Construction Vessel)	self
OTM w shared foundation	HLJU (High Lift Jack Up Vessel)	self
OTM wo shared foundation	HLJU (High Lift Jack Up Vessel)	self
HVDC collector	OCV (Offshore Construction Vessel)	OTB
HVDC converter	OCV (Offshore Construction Vessel)	OTB

Table 3.2: Vessels associated with the installation of HVAC and HVDC substation types

The total costs for installing a HVAC substation are a function of the pin-pile installation cost C_{PP}, the supporting jacket foundation (small C_{sJKT} or big C_{hJKT} jacket structure, depending on OHVS or OTM), scour protection C_{SPJKT}, substation installation itself $C_{OTM/OHVS}$ and overhead costs $C_{overheadsJKT}$. The OTM has the advantage over conventional offshore substations that it can be installed using conventional jack-up vessels, significantly reducing the installation cost compared to the use of crane vessels or semisubmersible heavy-lifts. Additionally, separate foundation installation is no longer required, as the equipment is mounted on a standard wind-turbine jacket. As such, the installation costs are limited to the additional charter time for the foundation installation jack-up vessel to install the substation equipment. It is assumed that the vessel must return to port to collect the pre-assembled substation equipment prior to each installation, and the travelling time is thus included. The different types of substations are displayed in Table 3.3. Pin-pile installation costs, jacket installation costs, scour protection costs and overheads costs are given in the foundation section. In order to calculate the costs for the substation installation itself $C_{OTM/OHVS}$, the same methodology used in the foundation section is taken into consideration, being the commissioning time the only additional time in the charter vessel model.

Description	Modelling
OHVS HVAC	$C_{PP} + C_{hJKT} + C_{SPJKT} + C_{OHVS} + C_{overheadsJKT}$
OTM w shared foundation	C_{OTM}
OTM wo shared foundation	$C_{PP} + C_{hJKT} + C_{SPJKT} + C_{OTM} + C_{overheadsJKT}$

Table 3.3: Offshore HVAC Types

The total costs for installing a HVDC substation are a function of the pin-pile installation costs ($C_{PP_{SS}} + C_{PP_{Conv}}$), the supporting jacket foundation ($C_{hJKTSS} + C_{hJKTConv}$, substation installation itself ($C_{SS} + C_{Conv}$, scour protection $2C_{SPJKT}$ and overhead costs $C_{overheadsJKT}$. Pin-pile installation costs, jacket installation costs, scour protection costs and overheads costs are given in the foundation section. The different types of substations are displayed in Table 3.4. In order to calculate the costs for the substation installation itself C_{OHVS}, the same methodology used in the foundation section is taken into consideration, being the commissioning time the only additional time in the charter vessel model.

Description	Modelling
HVDC(HVAC collector + VSC)	$C_{PP_{SS}} + C_{PP_{Conv}} + ...$
	$C_{hJKTSS} + C_{hJKTConv} + 2C_{SPJKT} + C_{OHVS} + C_{Conv} + C_{overheadsJKT}$

Table 3.4: Offshore HVDC Types

3.7.3.3 Onshore substation costs

Onshore substation costs can be broken down into supply and installation costs, which are presented separately in sections 3.7.3.4 and 3.7.3.5.

3.7.3.4 Onshore substation supply costs

The cost of equipment for the onshore substation (including transformers, shunt reactors, switchgear, etc.) is cheaper than their offshore counterparts, due to the more benign operational environment. Transformer, gas-insulated switchgear and cable set costs can be calculated using Equations 3.73, 3.74 and 3.75, with the offshore factor set to 0.

To meet the Security and Quality of Supply Standards (SQSS) recommendations [91] for offshore wind farms of over 90 MW, at least two transformer units need to be installed at the onshore substation, with each transformer having a maximum export rating of 1000 MW or 50% of the wind farm capacity. For the connection to the National Grid substation, existing switchgear will be used, reducing lead times. In order to compensate for the charging currents in the export cables, shunt reactors are connected to the export cables at the onshore substation; the cost of the reactors can be determined using Equation 3.77 based on the rated capacity Q_{rate} and the rated voltage V_{op}. This relationship has been obtained from [90]. The number of reactors N_{comp} needed to be deployed in the onshore substation, will be equal to the overall number of export cables.

$$C_{shunt} = N_{comp}\left[a_j Q_{rate}^{bj} V_{op}^{cj}\left(1 + d_j f_{off}\right)\right] \tag{3.77}$$

In order to provide fast-acting reactive power on the HVAC link, a Static Var Compensator (SVC) is installed in the onshore substation for any transformer. The cost modelling function for the SVC is displayed in 3.78, with the main cost driver being related with its rated capacity P_{rate}. This has also been derived from [90].

$$C_{civil} = a_j P_{rate}^{bj} \tag{3.78}$$

In addition to the electrical equipment, costs for civil engineering works in the onshore substation need to be considered; these can be calculated using Equation 3.79 based on

the total power exported through the onshore substation.

$$C_{civil} = a_j cap_{OSS}^{bj} \tag{3.79}$$

In the HVDC case, an Air Insulated Switchgear (AIS) and a converter unit are also considered. Whereas the cost of the converter unit C_{conv} is a function of the capacity of the wind farm cap_{OWF}, the cost C_{AIS} of the gas-insulated switchgear is a function of the rated voltage, and can be determined using Equations 3.80 and 3.81. Both relationships have been obtained from [90].

$$C_{conv} = a_j cap_{OWF}^{bj} \tag{3.80}$$

$$C_{AIS} = a_j V_{op}^{bj} \tag{3.81}$$

Finally, the costs for a HVAC onshore substation are given in Equation 3.82. This is based on previous cost components, the number of transformers N_{trans}, high-voltage switches N_{HVs} , ultra-high voltage switches N_{UHVs} and export cables N_{cables}.

$$C_{HVACon} = (N_{trans} + N_{trans})\, N_{trans} + C_{GIS} N_{HVs} + C_{AIS} N_{UHVs} + C_{civil} + C_{shunt} + C_{XLPE} N_{cables} \tag{3.82}$$

Likewise, the costs for a HVDC onshore substation are given in Equation 3.83.

$$C_{HVDCon} = C_{conv} + C_{trans} N_{trans} + C_{AIS} N_{UHVs} + C_{civil} \tag{3.83}$$

3.7.3.5 Onshore substation installation costs

Installation costs for onshore equipment $C_{install}$ are calculated using the factorial methodology, given in Equation 3.84 where $f_{install}$ is the installation cost factor and C_{supply} is the supply cost of the onshore substation equipment (not including civil engineering works). The installation cost factor is set to 19% for power electronics, based on the recommendations of Gerrad [74]. The cost of the electrical equipment together with civil works supply are assumed to be C_{civil}.

$$C_{install} = f_{install} C_{civil} \tag{3.84}$$

3.8 Operations and Maintenance

Having established cost functions for the supply and installation of all the main components of the offshore wind farm, attention can now be turned to the operation and maintenance (O&M) activities. O&M activities typically represent a big part of the total costs (e.g. 25–30% of the total lifecycle costs for offshore wind farms) [92]. This includes direct costs for operation and maintenance of the wind farm, as well as transmission charges, insurance, taxes and royalties. Data concerning wind farm operation and maintenance costs have been taken from studies by Mainstream Renewable Power [93] and GL Garrad Hassan [94]. The data in the original report [93] is provided for a 500 MW wind farm with 138 turbines; it has been assumed that the farm is located 20 km far from shore. In a separate report [95], potential O&M synergies are presented when scaling the same offshore wind project up to 1 GW, shedding light onto the sensitivity of the wind farm capacity and number of wind turbines. Maintenance costs are broken down into overheads, wind turbine and balance of plant costs.

Even though, by their very nature, O&M activities are stochastic processes, as maintenance requirements are at least partially due to random failure events, the current philosophy of the cost modelling tool takes a deterministic top-down analysis. It is understood that state-of-the-art offshore wind O&M tools are based on bottom-up analysis [96, 97], being more realistic and providing a better item-level forecasting. These tools might contain complex modelling on: weather forecasting, reliability and logistics. However, the computational power required to run these tools and their complexity make them prohibitive when thousands of cases may need to be run. Our approach seeks to quantify the typical average costs over the offshore wind project lifetime, based on the minimum number of variables; three main parameters drive the O&M cost model - wind farm capacity, number of wind turbines and distance from shore. It is worth

noting that all costs provided herein are given on annual basis.

3.8.1 Operations and Maintenance Overheads

Operations and maintenance overheads refer to ongoing expenses of operating an offshore wind farm; these are divided into 6 categories. C_{OH_1} covers the costs for the special purpose vehicle management, including activities such as: tax, auditing and accounting, office costs and equipment, a project manager, a financial director, administration, legal support and consultancy services for consents and permits. C_{OH_2} refers to the wind farm asset management and it is based on a total estimated headcount of 16 - 9 engineers, 4 technicians/electricians/mechanical fitters, 1 HSE professional, 1 admin assistant and 1 manager. The third overhead cost, C_{OH_3}, includes owners' equipment and premises such as a port facility with offices, storage, workshop and laydown as well as the ship dues, agency fees and the facility maintenance. In addition, an operation base used by operations monitoring staff and training facilities is included. Environmental monitoring is accounted for in C_{OH_4} and health and safety requirements in C_{OH_5}. It is also assumed that there are expenses to support air sea rescue and associated facilities on annual basis; this is reflected in C_{OH_6}. Further information concerning the costs' breakdown is found in [93].

Equation 3.85 shows the modelling approach to each overhead cost component C_{OH_j}, based on scaling effects and two driving parameters - the wind farm capacity and number of turbines. Total overhead costs C_{OH} are given in Equation 3.86. Some cost components may be scaled on either the wind farm capacity or the number of turbines only; some others may even not scale at all. For instance, the HSE component consists of a lump sum regardless of the size of the farm, while the ongoing environmental monitoring is scaled based on the number of turbines.

$$C_{OH_j} = A_j\left(\frac{cap_{OWF}}{500}\right)^{\frac{log(B_j)}{log(2)}} + C_j\left(\frac{N_{WTG}}{138}\right)^{\frac{log(D_j)}{log(2)}} + E_j \tag{3.85}$$

$$C_{OH} = \sum_{1}^{6} C_{OH_j} \tag{3.86}$$

In order to estimate the scaling factor S for each of the overhead cost components, cost data from a potential O&M 1 GW offshore wind farm has been obtained from [95]. Since the cost component for a 500MW farm C_{500W} and 1GW C_{1GW} are known, as well as the driving parameter k that governs the cost (In this case the wind farm capacity or the number of wind turbines) based on a reference value k_{ref} (500 and 138, respectively), the following formula 3.87 is used:

$$C_{1GW} = C_{500MW} \left(\frac{k}{k_{ref}} \right)^{\frac{log(S)}{log(2)}} \tag{3.87}$$

As an example, if one of the overhead cost component were: C_{1GW} = £2.25m and C_{500W} = £1.5m, and the modelling parameter was assumed to be the capacity of the farm, consequently $k = 1000MW$, $k_{ref} = 500MW$, we would obtain a value of $S = 1.5$. The same procedure is applied to all cost components to obtain the rest of the coefficients. Furthermore, other coefficients may be decided based on discussions with project development experts to take into account potential economies of scale.

3.8.2 Wind Turbine Maintenance Costs

The direct costs for wind turbine maintenance are based on the same dataset and are split into manual turbine resets, first, second and third line maintenance activities. First line maintenance activities include scheduled inspections and checklist activities, second line maintenance activities are work that is carried out to repair small wind turbine components that have failed, and third line maintenance is associated with large component failures and repairs. The wind turbine costs are scaled using the following set of Equations 3.88 to 3.91, based on the distance to the O&M port $d_{O\&M}$, the wind farm capacity cap_{OWF} and the number of wind turbines N_{WTG}. The reference dataset explicitly states the split between transportation and repair costs, allowing the share of distance-dependant costs to be identified as well as the degree of variability with the number of wind turbines. The same procedure that was applied to the overhead

costs is applied to cost data from [95], to derive new scaling factors for wind turbine maintenance costs, represented by d_1 to d_4. Manual turbine resets scaling factor has been considered the same as for the first line maintenance.

$$C_{MR} = b_1 \left(\frac{d_{O\&M}}{20km} \right) \left(\frac{N_{WTG}}{138} \right)^{\frac{log(d_1)}{log(2)}} \tag{3.88}$$

$$C_{1L} = \left(a_2 + b_2 \left(\frac{d_{O\&M}}{20km} \right) \right) \left(\frac{N_{WTG}}{138} \right)^{\frac{log(d_2)}{log(2)}} \tag{3.89}$$

$$C_{2L} = \left(a_3 + b_3 \left(\frac{d_{O\&M}}{20km} \right) \right) \left(\frac{N_{WTG}}{138} \right)^{\frac{log(d_3)}{log(2)}} \tag{3.90}$$

$$C_{3L} = a_4 \left(\frac{cap_{OWF}}{500} \right)^{\frac{log(b_4)}{log(2)}} + c_4 \left(\frac{N_{WTG}}{138} \right)^{\frac{log(d_4)}{log(2)}} \tag{3.91}$$

First line maintenance costs are broken down into three categories: first line maintenance, balance of plant and vessels. As a result, the distance-depend part of it is associated with the vessels. It has been assumed from the same report [93], that 20% of the second line maintenance costs are apportioned to the material costs (and modelled by the number of turbines), whereas 80% fall into the transportation costs (and hence are distance-dependent). As far as the third line maintenance costs are concerned, those are split 50-50 between the wind farm capacity and the number of turbines.

3.8.3 Balance of Plant Maintenance Costs

Balance of plant maintenance costs concerns all the supporting components and auxiliary systems of the offshore wind farm needed to deliver energy, other than the wind turbine units themselves. Balance of plant maintenance costs are typically minor compared to wind turbine maintenance costs. As far as the foundations and inter-array cables maintenace costs are concerned, the reference costs come from the initial study [94] and are again scaled based on the number of turbines. Cost modelling functions are given in Equation 3.92. Since array cable surveys and repairs costs are highly variable with seabed conditions, a conservative estimate is considered. Foundation inspection

costs include scour and structural surveys as well as foundations repairs. The scaling factors are considered to be representative of conservative 8% savings incurred when doubling the number of wind turbines. We have assumed a number of 70 turbines to be representative for a commercial offshore wind farms of 500MW [94].

$$C_{FND} = a_1\left(\frac{N_{WTG}}{70}\right)^{\frac{log(b_1)}{log(2)}};\;\; C_{IAC} = a_2\left(\frac{N_{WTG}}{70}\right)^{\frac{log(b_2)}{log(2)}} \tag{3.92}$$

Export system maintenance costs cover the offshore substation, the subsea and underground export cable and the onshore substation. While offshore substation costs are represented by C_{OSS}, there rest is accounted for by C_{OnSS+C}. These costs account for monitoring, inspecting the electrical cables, transformers and structures associated with the collector system. Typically, with high-voltage GIS and enclosed transformers, the on-going maintenance costs are relatively low. The cost modelling functions are given in Equation 3.93 based again on [94].

$$C_{OSS} = a_1 N_{OSS}^{b_1};\;\; C_{OnSS+C} = a_2 + b_2 \tag{3.93}$$

Unlike many of the system components of an offshore wind farm, the onshore substation maintenance is almost non-offshore wind specific, since it consists of standard high-voltage equipment. In addition, onshore cables are generally very reliable and required little scheduled maintenance. Therefore, the main part of the costs is related to the maintenance of offshore assets.

3.8.4 Transmission Charges in the UK

Transmission charges in the UK are split into two components. First, Transmission Network Use of System (TNUoS) charges. TNUoS charges recover the cost of installing and maintaining the transmission system in England, Wales, Scotland and Offshore [98]. These charges are paid in a £/MW basis and depend on locational pricing; the further from the demand the more expensive they are. Second, Balancing Services Use of System (BSUoS) charges. The BSUoS charge recovers the cost of day-to-day operation

of the transmission system. Generators and suppliers are liable for these charges, which are calculated daily as a flat tariff for all users [99]. BSUoS charges depend on the balancing actions that are taken each day, but we provide, within the cost modelling tool, an annual forecast of BSUoS for every operational year of the project.

3.8.5 Insurance

Four main categories of insurance are considered. Delayed start-up (DSU) insurance and contractors all risk (CAR) insurance are taken out during the construction phase, and apply to the gross annual revenue and the total asset value, respectively. Once operation begins, DSU and CAR insurance are replaced with business interruption (BI) and property damage (PD) insurance, again based on the gross annual revenue and the total asset value, respectively. Finally, it is important to note that in the UK an insurance premium tax may apply, increasing the overall cost of insurance.

3.8.6 Taxes and Royalties

Taxes and royalties different from country to country and must be often updated according to the country's economic policy. In this work, only information concerning the UK is presented. When developing an offshore wind farm, the developer will be subjected to corporation tax on profits at a rate specified by the government. In addition, it has been assumed that the developer has to pay a lease proportional to the revenue and capacity of the offshore wind farm under study.

3.9 Financial Analysis

The financial module assess the financial feasibility of a given offshore wind project, based on the different cash flows throughout the project life, as well as the financing structure put in place to supply the initial capital investment. As far as the financing structure is concerned, two discrete sources of funding are considered: equity and debt,

being the latter subjected to banks requirements.

As explained in more detail in Section 3.1, the deterministic cost modelling tool is made up of three modules: design, cost and financial. In order to run the financial module, cost outputs of the second module are needed. The outputs of the cost modelling tool can be retrieved at any point during the modelling process, as seen in Figure 3.6.

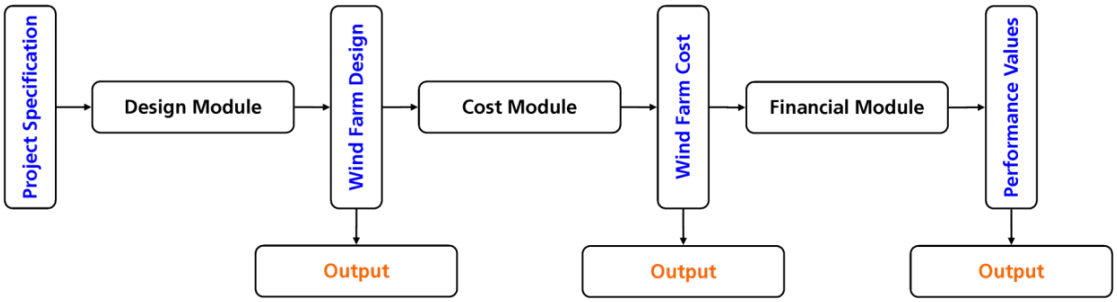

Figure 3.6: Deterministic cost modelling structure

The financial module allows for both corporate and project finance. Corporate finance is the traditional financing process whereby the sponsoring company (the company building the offshore wind farm) procures capital by demonstrating lenders that it has sufficient assets on its balance sheets, to be used as a collateral in case of default. Conversely, project finance concerns those projects financed by a loan where the lender is only entitled to repay from the profits of the project the loan is funding and not from other assets of the borrower, also known as off-balance-sheet financing. Key differences between the two types of financing can be found in [100]. Commercial offshore wind farms are characterized by high capital expenditures, long loan periods and uncertain revenue streams, resulting into more stringent bank requirements when doing project finance; project finance requires the calculation of P50 and P90 wind speeds. Further details on project finance are explained in Chapter 7, which deals with the effects of mean wind speed uncertainty on project finance debt sizing for offshore wind farms.

3.9.1 Financial and Economic Appraisal of Projects

The fundamental principles required to asses the levelised cost of energy for an energy project are outlined in this section.

Time Value of Money

Many financial and investment decisions involve costs and benefits spread out over time. An investment decision involves the commitment of resources on the expectation of future benefits. This implies that it is necessary to quantify the time value of money. 100 pounds today are worth more than 100 pounds tomorrow - money available today can be put to work to earn interest. The time value of money underpins all financial decision-making processes where an investment at the present time is required to benefit from a return on investment in the future.

If we consider the value in the future of a single payment today into an interest bearing investment, this is determined by the compound interest formula given in Equation 3.94. PV is the present value, FV is the future value, n is the number of periods and i is the interest rate. Conversely, calculating the PV from FV is determined by discounting as shown in Equation 3.95; in this case i is understood as the discount rate and could be defined as the opportunity cost of alternative investments.

$$FV = PV(1+i)^n \tag{3.94}$$

$$PV = FV\frac{1}{(1+i)^n} \tag{3.95}$$

Real and Nominal Interest Rates

The rate of inflation R_I is the change in prices for goods and services over time. Although this concept is linked to the time value of money as there is a loss of purchasing power of money with time (assuming positive inflation), it does not relate to the opportunity cost. The same 100 pounds that bought us a basket of things today, will not buy the same things in the future as prices may rise. The average increase in prices is known as the inflation rate. Consequently, when taking into consideration interest

rates for project appraisal, it is important to make a distinction between nominal and real interest rate. While the nominal interest rate R_N is the stated rate of interest and does not take inflation into account, the real interest rate R_R is the nominal interest rate adjusted for the rate of inflation, as shown in Equation 3.96. In the single payment example, this would need to be specified in the i variable as the discount rate.

$$1 + R_R = \frac{1 + R_N}{1 + R_I} \tag{3.96}$$

Project Appraisal

Project appraisal is the process of identifying if the project is viable or not. Although there are several dimensions to project appraisal such as technical, economic, financial, environmental and social, this sections deals with the economic or financial aspects.

The economic viability of an energy project requires the evaluation of multiple cash flows incurring at different points in time. Two performance return metrics form the basis of the evaluation criteria for investment decisions. The net present value (NPV) is the sum of all cash flows discounted to the present using the time value of money; it is used in investment planning to analyse the profitability of a projected investment, as displayed in Equation 3.97. The internal rate of return (IRR) is very similar to NPV except that the discount rate is the rate that reduces the NPV of an investment to zero, as shown in Equation 3.98 . The discount rate is the interest rate used to determine the present value of future cash flows in standard discounted cash flow analysis. If the NPV value is greater than zero, the company's value will increase. However, NPV doesn't tell us which is the minimum company's created value for the commitment of capital the project requires. Therefore, IRR is better suited in this case to guide capital budgeting for competing projects. If the IRR is higher than the required return, we should invest in the project. Otherwise we should pursue other investment opportunities.

$$NPV = \sum_{t=1}^{n} \frac{FV_t(t)}{(1+i)^t} \tag{3.97}$$

$$IRR = i | \sum_{t=1}^{n} \frac{FV_t(t)}{(1+i)^t} = 0 \tag{3.98}$$

The cost of capital is the actual cost of financing business activity through either debt or equity capital. Companies typically include both debt and equity in financing business activity, therefore one must calculate both the cost of debt and the cost of equity to determine the company's cost of capital. Once the cost of debt and the cost of equity are calculated, its weighted average can be obtained - this is referred to as the weighted average cost of capital (WACC). WACC is not necessarily an internal performance return metric; it shows how much interest the company pays for every pound it finances. Companies do not raise specific funds for specific projects. Rather funds are pooled centrally. Therefore, depending on the nature and risk of the project, companies may choose to set a hurdle rate based on the financial cost of capital WACC. The minimum acceptable rate of return (MARR) or hurdle rate is the minimum rate of return the company is willing to accept before starting a project, given its risk and the opportunity cost of forgoing projects. Therefore, the MARR is defined by the company. During project appraisal, projects are evaluated by comparing the IRR against the MARR. If the IRR is greater than the MARR, then the company will be willing to sponsor it.

Capital Recovery Factor

The capital recovery factor CRF is defined as the ratio of a constant annuity to the present value of receiving that annuity for a given length of time. This ratio is useful to convert a simple payment of CAPEX to a stream of cash flows in the future in the simplified financial estimate.

$$CRF = \frac{R_R(1+R_R)^n}{(1+R_R)^n - 1} \tag{3.99}$$

3.9.2 Simplified Financial Estimate

The LCOE is defined as the discounted costs incurred during the operational life of the project divided by the discounted energy produced during the same period of time. Given the fact that this entails a complex financial calculation, an initial LCOE value is required to initiate the financial iterative calculation. The purpose of the Simplified Financial Estimate (SFE) is to provided this initial value as a function of AEP_{net},

CAPEX, OPEX as well as other economic and financial parameters.

Main CAPEX cost components are displayed in Table 3.5 and calculated as Equation 3.100. OPEX is calculated in Section 3.8 and AEP_{net} in Section 3.4.

Variable	Cost Component	Section
DEV	Project development costs	3.3
PORT	Port facilities costs	3.3
PM	Project management costs	3.3
WTG	Wind turbine supply and installation costs	3.5
FND	Foundation supply and installation costs	3.6
IAC	Inter-array cable supply and installation costs	3.7
OSS	Offshore substation supply and installation costs	3.7
EC	Export cable supply and installation costs	3.7
OnSS	Onshore substation supply and installations costs	3.7

Table 3.5: CAPEX cost components for SFE

$$CAPEX = DEV + PORT + PM + WTG + FND + IAC + OSS + EC + OnSS \quad (3.100)$$

Given the uncertainties in the expenditures and to account for unplanned activities, it is a common practice to increase the budget by a certain % during the construction and operation of the offshore wind farm; these construction and operation contingencies are displayed, respectively, $Cont_{CAPEX}$ and $Cont_{OPEX}$ in Equations 3.101 and 3.102.

$$CAPEX = CAPEX_{estimate}(1 + Cont_{CAPEX}) \quad (3.101)$$

$$OPEX = OPEX_{estimate}(1 + Cont_{OPEX}) \quad (3.102)$$

The SFE looks at an average year of operation that represents the cash flow values over the duration of the project, as shown in Figure 3.7. This indicates that the value of CAPEX, incurred at the beginning of the project, is converted, through the capital cost recovery factor, into a stream of equal annual payments for the duration of the project n and given real discount rate R_R .

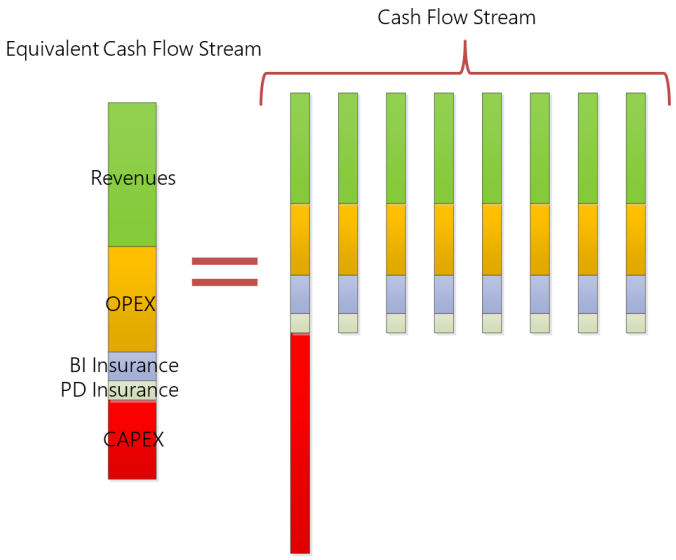

Figure 3.7: Average year of operation

Property Damage (PD) insurance, which is proportional to CAPEX, is depicted as a stream of white bars on the right-hand side of Figure 3.7. Business Interruption (BI) insurance, proportional to OPEX, appears with blue bars. It is worth noting that this SFE tries to consider an equivalent cash flow year to understand the whole project finances. In other words, the left-hand side of Figure 3.7 represents one year, while the right-hand side represents the entirety of the project cash flows. By taking advantage of a simplified financial model where, the expenditures to develop and operate an offshore wind farm are, respectively, CAPEX and OPEX, the insurance-related expenditures account for property damage loss f_{insPD} and business interruption and taxes are considered using f_{tax} corporate tax rate, the first guess $LCOE_{guess}$ is obtained. It is important to notice that whereas property damage insurance is proportional to

CAPEX, business interruption insurance is proportional to the revenue of the farm on a given year $AEP \cdot LCOE(1 - f_{tax})$. Rearranging the terms give rise to Equation 3.103.

$$LCOE_{guess} = \frac{(CRF + f_{insPD})CAPEX + (1 + f_{tax})OPEX}{(1 - f_{tax})(1 - f_{insBI})AEP_{net}} \tag{3.103}$$

3.9.3 Project Phases

The purpose of this section is to associate each cash flow with the point in time at which it is incurred. The different phases of the farm are shown in Table 3.6, representing typical values for a commercial offshore wind farm. It is assumed that any cash flow taking place in more than one year in the construction phase is evenly split between those years.

Variable	Description	Typical value [yr.]
n_{dev}	Development phase	6
n_{comm}	Commissioning phase	2
n_{oper}	Operational phase	25
n_{dec}	Decommissioning phase	2
n_{proj}	Project lifespan	35

Table 3.6: Project Lifespan; data based on EDF internal discussions

It is assumed that the FID takes place on the 5th year. Figure 3.8 displays the development, construction and commissioning cash flows broken down in fixed and variable cash flows.

As far as the fixed cash flows assumptions are concerned, development expenditures take place during the first 4 years of the development phase. Port facilities upgrade costs, onshore supply and installation occur at FID, whereas offshore supply and installation and export cable costs are incurred during the last year of the development phase. Foundation supply and installation starts one year prior to commissioning and finishes one year before the commissioning phase comes to an end. If the duration of

Ref.	Cost Components	Typical Timeline							
		Development & Consent						Commissioning	
		1	2	3	4	FID	6	7	8
	FIXED CASH FLOWS								
1	Development								
2	Port Facilities								
3	Onshore Supply								
4	Onshore Installation								
5	Offshore Supply								
6	Offshore Installation								
7	Export Cable Supply								
8	Export Cable Installation								
9	Foundation Supply								
10	Foundation Installation								
11	Array-Cable Supply								
12	Array-Cable Installation								
13	Wind Turbine Supply								
14	Wind Turbine Installation								
15	Project Management								
16	Construction Contingency								
	VARIABLE CASH FLOWS								
17	Construction Insurance								
18	Construction Interest								
19	Debt Finance								
20	Financing Fees								
21	Electrical Sales								

Figure 3.8: Cash Flows for Development, Construction and Commissioning Phases

the commissioning phase is one year, these cash flows take place during the last year of the development phase. Project management cash flows start on the 5th year of the development FID and finish when the commissioning phase is completed. Turbine supply and installation cash flows are incurred during the commissioning phase. Reference 1 to 15 Cash Flows are calculated from different sections as shown in Table 3.5. Construction contingency, is calculated by adding up all previous cash flows and increase them by a certain % $Cont_{CAPEX}$ as it has been displayed in Equation 3.101 in Section 3.9.2. Apart from the contingency cash flow calculated in the fixed cash flows, none of the other cash flows are calculated in the financial model since they have already been estimated in the cost module. Alternatively, variable cash flows need to be recalculated in conjunction with new LCOE candidates.

As far as the variable cash flows assumptions are concerned, construction insurance is

considered at FID, where the green light for the commissioning phase is given. Debt fees are made up of three categories: arranging, commitment and interest fees. Arrangement fees are the administration charges payable to the lender for preparation of all the documentation required for the loan, as well as finding any other banks involved in setting up the agreement. These fees will vary depending on the complexity of the farm, its size and risk. Secondly, a commitment fee is required and charged by the lender to the developer to compensate the lender for its commitment to lend, and is associated with unused credit lines. Arranging and commitment fees are represented as the financing fees and take place between FID and one year before the end of the commissioning phase. Finally, a standard fee is charged proportional to the debt taken at a given point in time and is represented by the construction interest cash flow. The amount of these fees will be proportional to the size of debt taken on. Interest fees have been split between the construction and operational interest fees.

Finally, electrical sales occur as soon as the first wind turbines of the farm are commissioned. The amount of energy produced by the wind turbines during the commissioning stage is calculated in Subsection 3.4.2.4. If the project is financed via banks, then a decommissioning fund is required. Basically, this is established so that there is no risk faced by the bank in case the developer does not pay for the decommissioning phase after the operational life of the project. When setting up a decommissioning fund, money must be put aside during the operational years so that it is available at the end. The main parameters that govern the decommissioning fund are the interest income and the years for the decommissioning reserve account.

Figure 3.9 shows the project cash flows that take place throughout the operational phase of the offshore wind farm; these cash flows are represented by reference 22 to 28 and calculated in Section 3.8. Electrical Sales and Operational Insurance cash flows also occur during the operational phase. However, the finance measures put in place for the decommissioning fund and for repayment of the debt, take place 10 years prior to decommission phase and during the first 15 years of the operational phase, respectively (being 10 and 15 years, assumptions). The associated interests from that measures are

also considered and represented by the interest income from reserve and operational interest.

While wind turbine decommissioning costs take place during the first year of the decommissioning phase, offshore substation and foundation decommissioning costs are accounted for on the last year. These cash flows are calculated based on the installation methods for the wind turbine, foundations and offshore substation discounted by a time factor, based on expert discussions.

Also, decommissioning contingency is calculated as in the case of CAPEX and OPEX, with a given contingency rate. Figure 3.10 shows the typical timeline for those cash flows. Further information on decommissioning costs can be found in [101]

Ref.	CF Components	Typical Timeline																								
		Operation																								
		9	10	11	12	13	14	15	16	17	18	19	20	21	22	23	24	25	26	27	28	29	30	31	32	33
		FIXED CASH FLOWS																								
22	Overheads O&M																									
23	WTG O&M																									
24	BoP O&M																									
25	Export System O&M																									
26	Grid Connection																									
27	Operational Contingency																									
28	Seabed Rent																									
29	Decommissioning Reserve																1	2	3	4	5	6	7	8	9	10
30	Interest Income from Reserve																									
		VARIABLE CASH FLOWS																								
19	Debt Finance	1	2	3	4	5	6	7	8	9	10	11	12	13	14	15										
21	Electrical Sales																									
31	Operational Insurance																									
32	Operational Interest																									

Figure 3.9: Cash Flows for Operational Phase

Ref.	Cost Components	Typical Timeline	
		Decommissioning	
		Year 34	Year 35
		FIXED CASH FLOWS	
33	Wind Turbine		
34	Foundation		
35	Offshore Substation		
29	Decommissioning Reserve		
30	Interest Income from Reserve		
36	Decommissioning Contingency		

Figure 3.10: Cash Flows for Decommissioning Phase

3.9.4 Formation of the Financial Module

As far as project evaluation is concerned, given a set of cash flows it is relatively easy to calculate several financial metrics such as the Net Present Value, Internal Rate of Return, Payback Period or Profitability Index. These financial metrics are worked out by projecting backwards in time a set of cash flows, resulting into its present value. In addition, they not only depend on the profile of the cash flows but also on a given discount factor.

Equation 3.104 translates the LCOE definition into a mathematical formula, where TOTEX is the total expenditure and NPV is an operator which converts a set of cash flows to present value, given a discount rate. Bearing in mind that the discounted sum of the revenue cash flows should be equal to the discounted sum of expenditures, the right-hand side of Equation 3.104 is obtained. It is important to notice the fact that the LCOE is a constant value, and therefore, $NPV(LCOE \cdot AEP) = LCOE \cdot NPV(AEP)$ and also that the revenue is expressed by $LCOE \cdot AEP$ (in currency units) and accounts for the profit earned by electricity sales.

$$LCOE = \frac{NPV(TOTEX)}{NPV(AEP)} \rightarrow NPV(Revenue) = NPV(LCOE{\cdot}AEP) = NPV(TOTEX) \tag{3.104}$$

The financial module output of the cost modelling tool is the LCOE, which is a universal metric used for comparison of energy costs, and represents a single, constant, inflation-adjusted price available over the entire lifetime of the project, that also takes into consideration the full range of project cash flows based on its characteristics. The LCOE is used for decision making and is made up of Revenue and TOTEX cash flows. TOTEX can in turn be broken down into DEVEX, CAPEX, OPEX, and DECEX. If TOTEX would not depend on the LCOE, then the problem would be trivial and the left-hand side of Equation 3.104 would give us a methodology to work out the LCOE. However, this is not the case. Although DEVEX and DECEX are fixed items, and such can be assessed without any iterative method, CAPEX and OPEX comprise fixed and non-fixed costs, resulting in functions of the LCOE.

In other words, numerical techniques are needed to work out the LCOE. The first step to calculate the LCOE is to define the free cash flows. Although there is more than one way to define the FCF, in this chapter it is assumed that the FCF are calculated as the cash flow from operations minus the offshore wind farm's capital expenditures. In this way, the LCOE can be calculated by finding the zero of the function given by the sum of the discounted FCF, as shown in Equation 3.105.

$$FCF =_{def} LCOE \cdot AEP - TOTEX = 0 \rightarrow NPV(FCF) = 0 \tag{3.105}$$

The financial module consists of fixed and variable cash flows. Fixed cash flows are those that do not depend on the LCOE, whereas variable cash flows are a function of the LCOE. Therefore, whereas variable cash flows need to be recalculated at each iteration, fixed cash flows can be calculated only once at the beginning of the iterative process to improve the efficiency of the tool. Fixed cash flows are shown in Figure 3.11. DEVEX is displayed in red to highlight that different sensing devices will result

in different development expenditure.

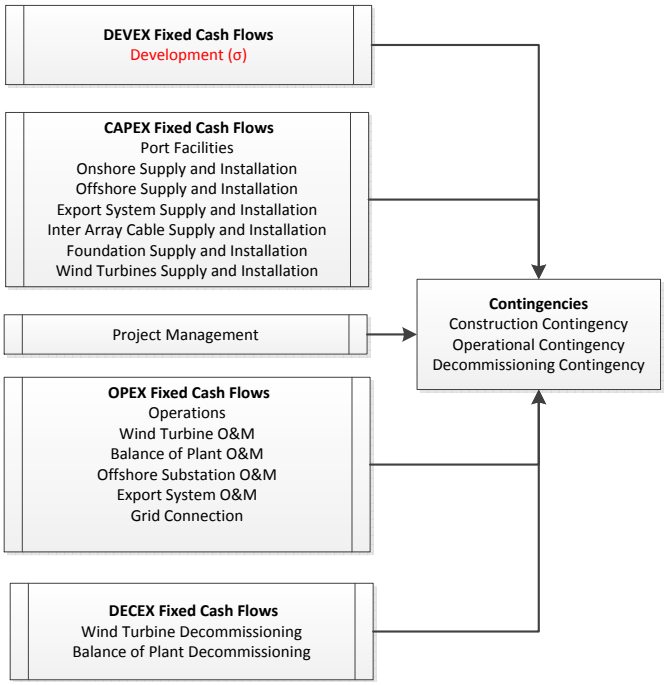

Figure 3.11: Fixed Cash Flows within Cost Modelling Tool

The financial appraisal for project finance arrangements entails not only one but twofold iterative processes. On the first hand, the external loop consists of determining the value of λ that makes Equation 3.1 equal to 0, where its initial guess λ_0 is obtained from a simplified financial module. Each iteration of the external loop is linked with an internal iterative process for debt sizing. The internal loop is only used for project finance arrangements and concerns the debt sizing or sculpting, which determines the maximum amount of project finance debt that the offshore wind farm can sustain based on the bank's requirements. Project lenders usually specify the borrowing capacity on the basis of debt service ratio and covenants. As such, parameters like the DSCR, the maximum leverage and CFADS have been considered. A priori, the variable λ is unknown, meaning that it will take several external and internal iterations to come up with the zero of Equation 3.1. In other words, the LCOE is calculated as the constant real electricity price required to meet the desired Minimum Acceptable Rate of Return,

and not the other way around as usually considered. Given that it is inflation-adjusted, it means that a reference year must be defined (typically FID year is used).

This high-level iterative process is described in Figure 3.12. Further information regarding the details of the different calculations for the internal loop is shown in Figure 3.13.

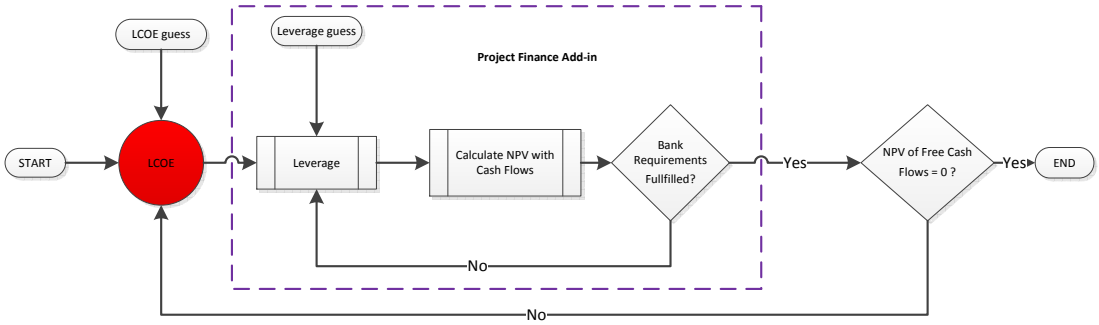

Figure 3.12: Double Loop Iterative Project Finance Modelling

Given the uncertain nature of the wind, developers use probabilistic metrics to characterise the wind resource at a given site. AEP_{P50} is associated with a P50 estimated mean wind speed $\overline{v_{P50}}$, meaning that this is the mean wind speed that is expected to be exceeded in 50% of the estimates. It is important to highlight that this is the estimated mean wind speed and not the measured mean wind speed, which would follow a different probability distribution function such as Rayleigh or Weibull. To put it in other words, this is the median mean wind speed estimate since half of the estimates are expected to be below this value and the other half are predicted to be above it. Although this metric is typically considered from a developer's point of view when doing corporate finance, banks prefer a rather conservative approach; reasons for this are explained in Chapter 7. Thus, banks use the AEP_{P90}, which is the AEP associated with an estimated mean wind speed that is expected to be exceeded in 90% of the estimates $\overline{v_{P90}}$. The mean wind speed estimated uncertainty is assumed

to be characterized by a normal probability distribution, as it is shown in the following relationship 3.106:

$$\overline{v_{PX}} = \overline{v_{P50}} - \sqrt{2} \cdot \sigma \cdot erf^{-1} \left[1 - 2 \cdot F_X\right] \forall X \in [0, 100] \tag{3.106}$$

Where σ is the given level of uncertainty expressed as a percentage of the wind speed representing one standard deviation and X is the level of exceedance requested by the bank. In particular, when looking at a level of exceedance of 90% or P90, Equation 3.107 results in:

$$\overline{v_{P90}} = \overline{v_{P50}} - 1.2816\sigma \tag{3.107}$$

The cost modelling tool calculates both P50 and P90, which are key inputs for the financial model when project finance arrangements are considered.

The OWCAT financial model for a generic offshore wind farm is displayed in Figure 3.13. Two main areas can be identified – the area outside the purple dashed lines, representing a standard corporate finance model based on P50 cash flows and the area inside the purple dashed lines, representing a part of a project finance model or what is referred in this chapter as a Project Finance Add-in based on P90 cash flows. These P50 and P90 cash flows stem from the P50 and P90 AEP values which are the output of the Annual Energy Production module. These P50 and P90 AEP values come in turn from the estimated mean wind speed uncertainty, influenced by several uncertainty drivers. An LCOE value needs to be assumed in order to transform aep values to revenue cash flows. This is represented in Figure 3.13 by a red circle – value that changes from iteration to iteration until the numerical scheme converges (see figure above for the explanation on the two-fold iterative calculation).

The standard corporate finance model calculates the different variable cash flows that are required to work out the NPV of the project – seabed rent, fixed cash flows, construction and operational insurances and taxes. Given a discount rate, an iterative process is required to work out the LCOE that makes the cumulative free cash flows

zero at the end of the project. The standard corporate finance calculation requires one iterative calculation, whereas the Project Finance Add-in adds an additional loop by working out the amount of debt that the financial institution provides to the project. In cases where the offshore farm is financed via corporate finance arrangements, only the left hand side of the financial model is needed. However, this chapter's objective is to understand the effect of the mean wind speed estimated uncertainty on debt sizing for offshore wind farms – so the full financial model needs to be taken into consideration.

The purpose of the Project Finance Add-in (displayed within purple dashed lines) is to estimate the amount of debt that can be reasonably supported by the project based on the probabilistic metric given by the P90 estimated mean wind speed. The output of the Project Finance Add-in is the Debt Finance, Operational and Construction Interest and the Financing Fees cash flows. Without the Project Finance Add-in it would not be possible to estimate the P90 cash flows that are required by the financial institution to support the non-recourse financing of the offshore wind farm. Cash flows in red are key to understand the effect of the estimated mean wind speed on debt sizing for offshore wind farms. These come into play from two sides. On the one side the development expenditure, which is influenced, to some extent, by the cost of the sensing device selected by the developer to characterise the wind speed uncertainty for a given site. On the other side, the changes on the financing costs represented by the four outputs from the Project Finance Add-in: the Debt Finance, Construction and Operational Interest and the Financing Fees. Given the iterative process of the financial modelling, these four cash flows are displayed in blue and are worked out via standard debt sculpting techniques.

It is important to bear in mind that when carrying out an offshore wind farm project evaluation via project finance arrangements, both areas of the financial model need to be taken into consideration. The Project Finance Add-in works out the Debt Finance, Construction and Operational Interest and Financing Fees P90 cash flows and the standard corporate finance calculates all the remaining P50 cash flows that are then fed into the NPV operator. Equation 3.108 splits the cash flows between these two P50

and P90 categories. Therefore, the developer selects a measuring campaign strategy to measure the mean wind speed estimated uncertainty which directly affects the $FCF_t^{P_{50}}$. Equation 3.109 illustrates that the P50 free cash flows are a function of the DEVEX incurred by the developer. At the same time, the mean wind speed estimated uncertainty, represented here with σ, has an indirect effect on the P90 free cash flows - the financing conditions such as Debt Finance, Construction and Operational Interest and Financing Fees cash flows. Equation 3.110 illustrates that the P90 free cash flows are a function of the mean wind speed estimated uncertainty.

This type of modelling integrates the wind resource assessment at the heart of the cost calculations through project finance constraints and allows to quantify and investigate the effect of the mean wind speed estimated uncertainty in debt sizing for offshore wind farms.

$$LCOE = \lambda | \sum_{t=1}^{n} \frac{FCF_t^{P_{50}} + FCF_t^{P_{90}}}{(1 + MARR)^t} = 0; \tag{3.108}$$

$$FCF_t^{P_{50}} = FCF_t^{P_{50}}(DEVEX(\sigma)) \tag{3.109}$$

$$FCF_t^{P_{90}} = FCF_t^{P_{90}}(\sigma) \tag{3.110}$$

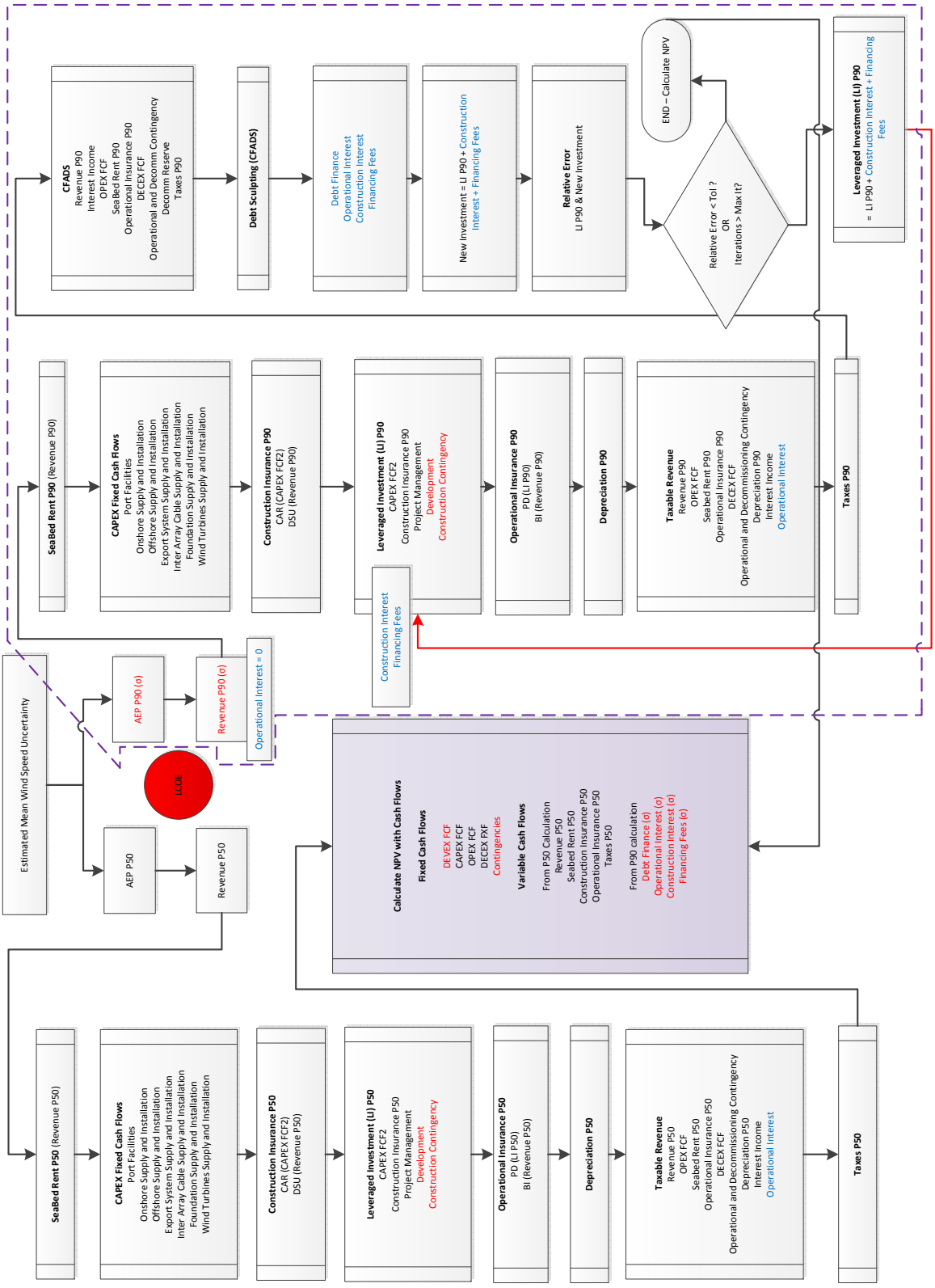

Figure 3.13: Project Finance Structure within Cost Modelling Tool

Chapter 4

Quantitative Uncertainty Management Framework

After describing the cost modelling tool, this chapter introduces the quantitative uncertainty management framework used throughout this thesis; this includes uncertainty analysis and propagation techniques, global sensitivity analysis, coherent risk metrics, sampling techniques as well as a brief description of its practical implementation and access to a high-performance computing cluster.

4.1 Decision-making under Risk, Uncertainty and Ambiguity

There is no clear-cut distinction among risk, uncertainty and ambiguity. Frank Knight was the first to distinguish between risk and uncertainty in his work Risk, Uncertainty, and Profit in 1921 [102].

"The essential fact is that "risk" means in some cases a quantity susceptible of measurement, while at other times it is something distinctly not of this character; and there are far-reaching and crucial differences in the bearings of the phenomenon depending on which of the two is really present and operating...It will appear that a measurable "uncertainty", or "risk" proper, as we shall use the term, is so far different from an

unmeasurable one that it is not in effect an uncertainty at all. We shall accordingly restrict the term uncertainty to cases of the non-quantitative type"

According to Knight risk refers to situations where the classification of states, alternatives or possibilities is objective and known, and their probabilities can be objectively determined. Conversely, for Knight uncertainty arises from the impossibility of exhaustive classification of states; regardless of whether their probabilities can be objectively or subjectively determined, the system under study is so complex that all the possible states are simply not known. As a consequence, any categorisation of events used to predict the future is based on intuition and judgement, implying a degree of subjectivity.

A few decades later, Subjective Expected Utility (SEU) emerged in decision theory. SEU measures the attractiveness of an economic opportunity as perceived by a decision-maker in the presence of risk, based on individual utility functions and subjective believes probabilities [103]. Savage identified risk and uncertainty undistinguishable as long as the subjective believe probabilities and the objectives probabilities were the same. Although the SEU rested on strong assumptions that were consistent across a wide range of situations, Ellsberg's 2-urn paradox added the little nuance between risk, uncertainty and ambiguity by means of a thought experiment involving two urns [104]. The first urn A contained exactly 50 black balls and 50 white balls, while the second B contained 100 black and white balls in an unknown ratio. Ellsberg suggested that, if asked to bet money on a white/black ball being drawn from one or the other urn, people would tend to choose A over B, as the odds are known. He coined this phenomenon as ambiguity aversion and argued that people would prefer taking on risk in situations where they know specific odds rather than an alternative risk scenario in which the odds are completely ambiguous. Ellsberg's paradox violated the principles of SEU. Ellsberg argued that this violation could be explained by ambiguity", which he defined as:

"a quality depending on the amount, type, reliability and "unanimity" of information, and giving rise to one's degree of "confidence" in an estimate of relative likelihoods."

From this brief review of the literature, we can simply characterised each of the three words: risk, ambiguity and uncertainty based on two attributes: (i) exhaustive classification of states, alternatives and possibilities and (ii) its associated probabilities. Risk implies that both (i) and (ii) are clearly defined, ambiguity has only (i) and uncertainty neither of them.

Although there are many uncertainties, ambiguities and risks surrounding the construction and operation of energy projects, we shall consider, in the rest of this work, only risks characterised by a finite classification of states together with known probabilities. It is understood that all risks are uncertainties but not all uncertainties are risks. Risks are uncertainties that matter and, for the sake of simplicity in this work and following the Knightian philosophy, are measurable, or to put it in another way, measurable uncertainties that are linked with certain project objectives. From this point onwards, risks and uncertainties will be considered interchangeably and referred to as measurable uncertainties. In addition, this work will only consider model uncertainty and not the uncertainty (lack of "realism") of the computational model chosen to assess the financial viability of offshore wind farms.

4.2 Quantitative Uncertainty Management

The aim of managing quantitative uncertainties in complex models is to ensure improved performance evaluation and risk control. In order to establish a quantitative uncertainty management framework, the following three requirements are needed, as suggested in the work of Rocquigny [41]. First, a pre-existing model that captures the relationship between inputs and outputs. This can be considered in this thesis as the tools and methodologies that constitute the skeleton of a cost modelling tool designed to assess the financial performance of offshore wind farms. Second, a variety of sources of uncertainty affecting the model inputs, which in this case are represented by probability distribution functions. And finally, industrial stakes and decision-making circumstances motivating the uncertainty assessment; the outcome of the uncertainty assessment provides insights into the cost and uncertainty in the design of offshore wind

farms.

The pre-existing model is a techno-economic model linking inputs (uncertain $\underline{x}$ or fixed variables $\underline{d}$) to outputs $\underline{z}$ (from which decision criteria can be established). This can be formally defined in Equation 4.1.

$$\underline{x}, \underline{d} \Longrightarrow \underline{z} = MODEL(\underline{x}, \underline{d}) \tag{4.1}$$

It is worth noting the difference between these two sets of inputs. Whereas some inputs have uncertainty associated to them, others may be fixed – as they play another role in the model, those are represented with notation $\underline{d}$. This is the case when: (i) model inputs represent variables under full control: for example the vessel associated with the installation of a monopile foundation, (ii) the uncertainties affecting the model inputs are considered to be negligible and (iii) the decision process conventionally fixes some variables for comparative purposes and time constraints: for example the discount rate may be set by the developer. However, it is important to bear in mind that a distinction between "uncertain" and "fixed" variables usually involve an iterative process by means of global sensitivity analysis described in Chapter 5. There is a clear difference in the literature between variables and parameters. A variable represents a model state, and may change during simulation. A parameter is commonly used to describe objects statically. A parameter is normally a constant in a single simulation, and is changed only when you need to adjust your model behaviour. However, for the sake of simplicity we've consider both variables and parameters as those inputs that are constant in a single simulation.

The methodology of quantitative uncertainty management is a staged process. First, the specification of the problem needs to be considered; this is mathematically represented as the central cost model. After that, the uncertainty in the inputs is quantified and modelled by probability distributions. Then, the propagation of uncertainty sources to the quantities of interest in the outputs is carried out via Monte Carlo or other propagation techniques, resulting in a spread of project performance. Finally, the uncertainties in the model output can be apportioned in terms of the uncertainties of the model

inputs through global sensitivity analysis techniques. This methodology is displayed in Figure 4.1.

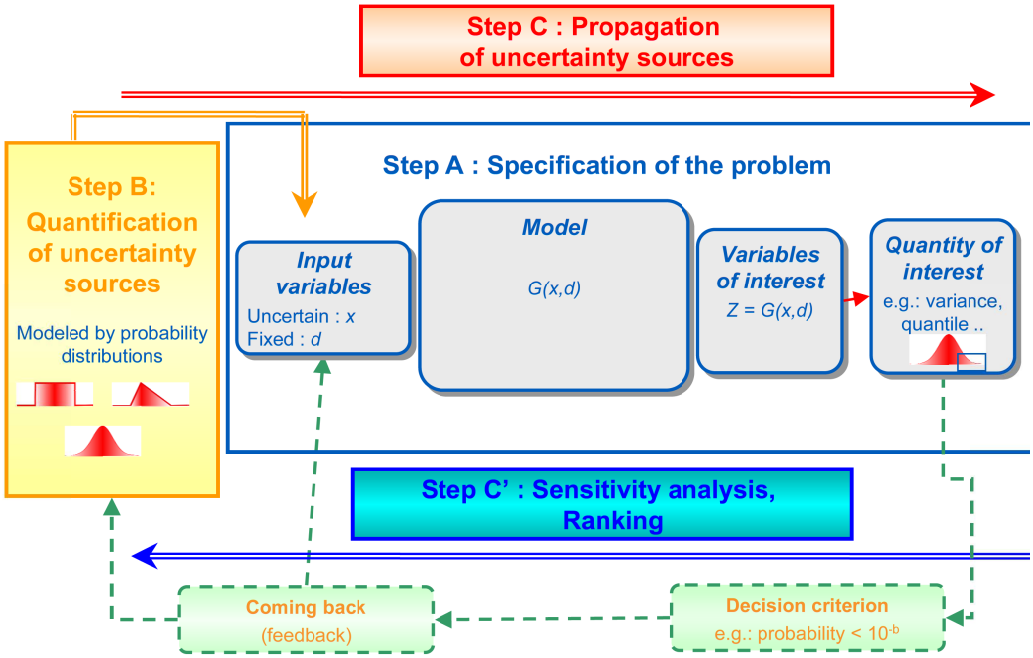

Figure 4.1: Uncertainty management - the global methodology [105]

The main goals of the quantitative uncertainty framework for this thesis are:

First, **Understand (U)** : to understand the influence or rank the importance of uncertainties, focusing on the main cost drivers. This allows the model user to identify the key variables for cost and uncertainty in the different offshore wind farm components. Furthermore, at this stage this could mean that "uncertain" variables could be shifted to "fixed" variables and vice versa.

Second, **Accredit(A)**: to benchmark the model with existing costs, simplify the number of variables that are not required and finally validate it according to the context and stage of the project development process.

Last but not least, **Select (S)**: to compare the different selected quantities of interest

in the outputs to determine which combination of technology choices are optimal for a given site.

The uncertainty modelling can be conducted through a deterministic, probabilistic, extended probabilistic and non-probabilistic framework. Regardless of the framework chosen, the model should include as much information on the measure of uncertainty as possible. There have been many discussions around which the best framework is but no consensus has been reached [41]. From a practitioner's point of view a standard probabilistic setting has been considered, whereby probabilistic distributions are assigned to the components of the input $\underline{x}$. It has also been considered that there is independence between uncertain input variables and hence separate probability distributions are used instead of a joint probability distribution, for which no data and expertise in the offshore wind industry would exist.

Depending on how well the issues are understood, uncertainties can be more or less quantifiable. Figure 4.2 classifies uncertainties in two big groups. Uncertainties inside the dashed box can be, to some extent, influenced by the developer, whereas uncertainties outside the dashed box can be influenced to a lesser extent. Construction and operation of offshore wind assets carries a significant level of technological risk, imposed by its complex engineering systems and pace of technology development. Examples of technological risk are: bigger, taller and more powerful wind turbines which cope with higher loads, newer foundation designs and materials, higher inter-array cable voltages, innovative installation and maintenance techniques, etc. One of the technical risks that has made the headlines several times is cable failures. Such failures are reported to account for 75-80% of the total cost of offshore wind insurance claims [106].

Technology development also puts a lot of pressure onto manufacturers. Demand for a product may change very quickly. Nonetheless, in order for manufactures to stay in business and be able to supply a given product cost-efficiently, significant investments are required. For example, every time that an OEM invests in a new manufacturing plant to produce wind turbines, it has to be very mindful about new sizes coming into the market. Wind turbine technology is one of the key drivers for cost reductions

and developers often attempt to utilise the latest and more powerful units available in the market. This strong desire for the latest units has consequences that trickle down through the entirety of the supply chain. Stronger foundations are required to cope with higher loads, higher voltages are necessary to export power out to shore and, more importantly, new installation and service vessels have to handle bigger sizes and weights. It may well be that a whole fleet of specialised offshore wind installation vessels becomes obsolete in a very short period of time because of the impossibility to handle newer sizes and weights appropriately. In this thesis, risks are taken from a developer perspective. For this reason, it is typically the interactions between components, which are often purchased from different subcontractors, which present the highest level of risk. For instance, foundation designs must be linked not only to wind turbine designs but also to inter-array cables' J-tubes, as wind turbine loads are passed onto the foundations and power has to be transferred to the offshore substation. We will refer to these as unmodelled interactions, as shown in Figure 4.2.

Furthermore, a project may be the only activity or one of many of the activities that constitute a company. Therefore, the project has to be in line with the company strategy, which determines the risk appetite and cost of opportunity of a given project. Based on the company risk strategy, contractual arrangements such as contractor selection and operation and maintenance of offshore assets, are negotiated and agreed upon.

There are even bigger uncertainties in the way offshore wind assets generate electricity and hence revenue, given the conditions under which they operate. Volatile wholesale electricity market prices are driven by market forces. For example, if electricity demand is low or if lots of renewables are currently generating, spot prices tend to be low – this is explained by the low marginal cost of renewables in the merit order, or what is referred to as the price cannibalisation effect. The converse can also be true. When the demand is high or there is scarcity in the supply, spot prices tend to spike.

As a consequence, if an offshore wind asset relied solely on a volatile spot price as its main source of income, the asset would probably not be bankable. Therefore, there

exists several instruments to reduce the exposure to these uncertainties. Power Purchase Agreements (PPA) provide an adequate and predictable revenue stream and are usually a prerequisite to make the project bankable. Also, support mechanisms such as CfD are paramount for the bankability of a project, as they reduce the exposure to volatile wholesale market prices by having a fixed price, called "the Strike Price" for a period of time [107]. Financial markets also contain a huge amount of risk. Fluctuating exchange rates may have a huge impact on the cost of manufacturing as well as on the ability to import certain offshore wind components from continental Europe. Other economic factors such as interest rates and skilled labour can make investing in offshore wind more appealing. For instance, current interest rates imply low borrowing costs, but these may increase in the future.

Weather risk is a major factor to take into consideration both for the installation and operations that take place out in the sea. State-of-the-art weather forecast systems that give exact metocean characteristics of the wind farm area constitute an important part in determining when the best time to carry out an installation or maintenance campaign is. During a windy day, the asset is likely to generate at a higher energy output than during a calm one, suggesting that it would be better to schedule maintenance tasks for periods when the wind is low so as to minimise loss of production. Operators also learn from operating the assets and improve their performance with time. Finally, markets are also influenced in turn by wider political, economic and cultural contexts. The push for decarbonisation has increased the appealing for low-carbon generation technologies and has provided incentives for the deployment of these technologies. Natural disasters such as typhoons, earthquakes and soil liquefaction might pose technical risks on wind turbines that need to be considered by developers.

Layers of uncertainty are another useful way to think about uncertainty. One can imagine an offshore wind project at the centre of concentric circles, each of them representing a layer of uncertainty, as shown in Figure 4.3. The first circle represents the uncertainty related to the technical/project risks such as design, operations, collaboration, etc. This is followed by industry wide and competitive risks, country-specific and fiscal risks, wholesale electricity and financial markets and natural disasters. As we

move from the inner layers to the outer layers, the possibility of mitigating and exploiting the opportunities associated with these risks decreases; the company can decide to change a technology choice for a given site if this reduces the risk exposure, may even try to influence the future electricity regulation through lobbying efforts but has no influence at all on the likelihood of natural disasters.

A comprehensive list of uncertainties surrounding offshore wind energy projects can be found in [108].

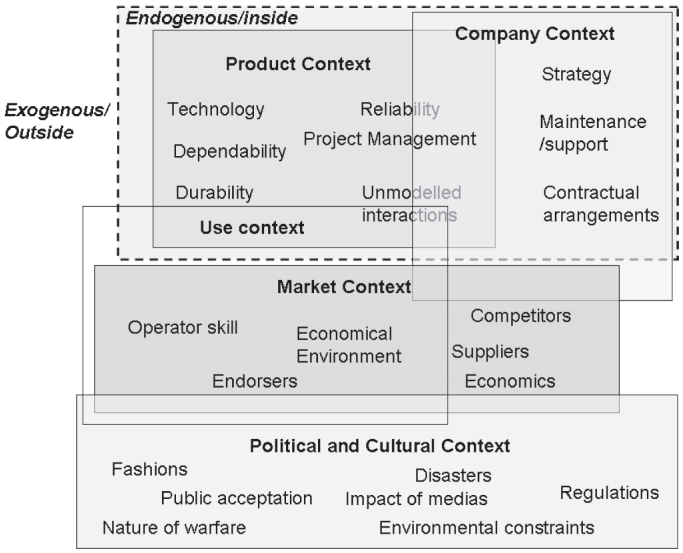

Figure 4.2: Links between uncertainties [41]

4.3 Uncertainty Propagation

Uncertainty propagation consists in estimating the uncertainty in the model outputs due to uncertain model inputs. Although there exists many uncertainty propagation techniques such as deterministic methods, Taylor approximation, ISO GUM, Monte Carlo, First-Order Reliability Method (FORM) and Second-Order Reliability Method (SORM), etc [41], only Monte Carlo simulation allows modellers to extract any desired criteria from the probability distribution of the output. Monte Carlo method is a powerful statistical tool that can deal with a large number of random variables, various types of distributions and highly non-linear models. In addition, it is not sensitive to

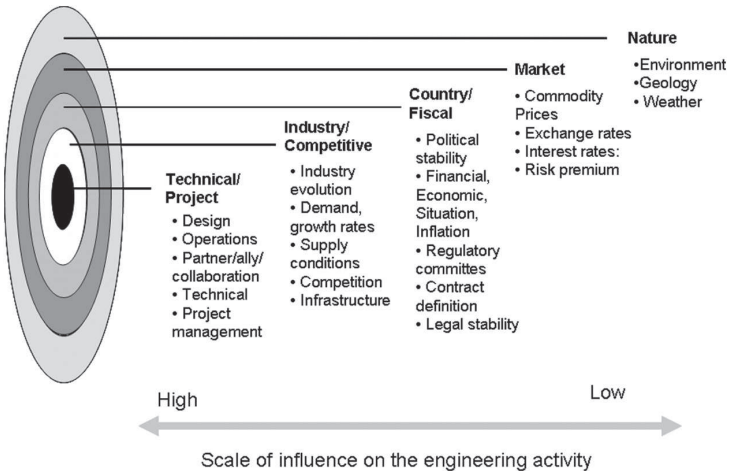

Figure 4.3: Different layers of uncertainty [41]

discontinuities and the model not need to be expressible in a closed analytical form. This makes Monte Carlo the most suited method to solve complex techno-economic problems.

Monte Carlo Simulation

Monte Carlo relies on repeated random sampling to obtain numerical results. Therefore, it is conducted under a probabilistic framework where model inputs are characterised by probability distributions. The following steps are needed to carry out a Monte Carlo simulation, as shown in Figure 4.4. Parameter N is the number of samples needed to estimate the probability distribution of the output.

- Step 1: Generating random variables that are uniformly distributed between 0 and 1.
- Step 2: Transforming the [0,1] uniform variables into random variables that follow a given probability distribution by means of the inverse transformation method.
- Step 3: Calculate model run for a given combination of inputs.
- Step 4: Repeat Steps 1-3 N times to build up a probability distribution function of the output.

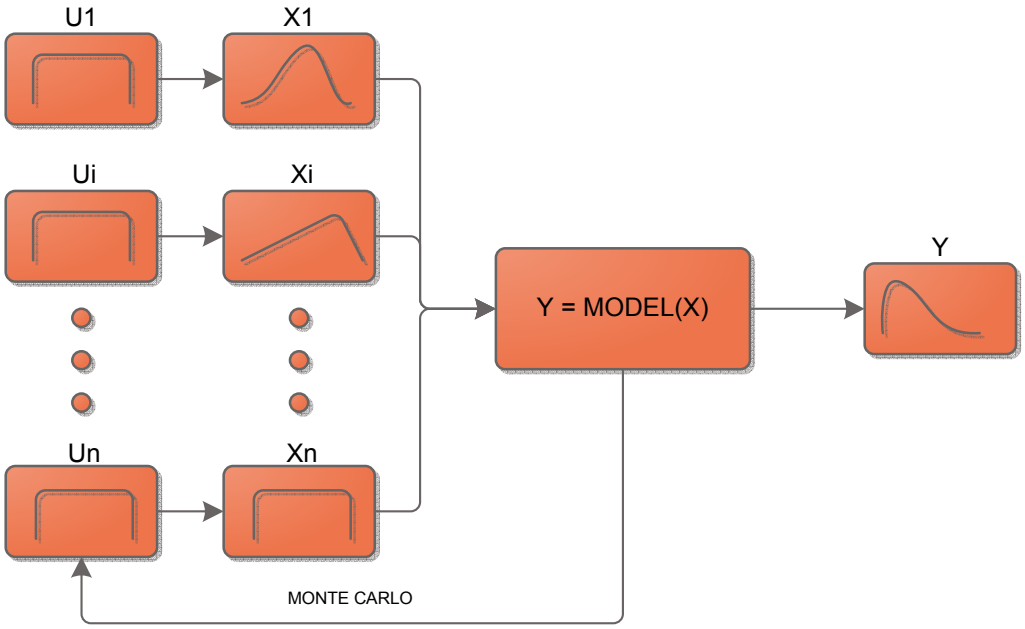

Figure 4.4: Monte Carlo Analysis flowchart

Parallelisation and High Performance Computing

The application of uncertainty propagation via Monte Carlo usually requires a large number of model runs (in the order of thousands). In some cases where the model is computationally expensive to run, it may be desirable to replace the existing model with another which produces similar results, but which is computationally cheaper; this is accomplished by means of a meta-model or surrogate. However, as a downside, the meta-model introduces additional uncertainty as it is an approximation of the existing model. Example of meta-models are polynomial chaos expansions and Gaussian processes. In this thesis, it has been avoided to introduce additional sources of model uncertainty by the construction of a meta-model, despite requiring higher computational costs. These additional computational costs have been addressed by efficiently parallelising the code in conjunction with the use of a high performance computing cluster at the University of Edinburgh - Eddie [109]. Further details regarding the practical implementation are explained in Section 4.7.

4.4 Global Sensitivity Analysis

While building, using and maintaining simulation models is important, the use of sensitivity analysis is key across the modelling process. Sensitivity analysis methods allow to study how the different sources of uncertainties in the output of the model can be apportioned to the different sources of uncertainty in the model input. This, in turn, guides the process of determining the most relevant input variables to an output behaviour or to simply screen out some of the variables whose contribution can be neglected. Further information has been provided in Chapter 2.

Assuming that the progation of uncertainties from model inputs to the quantities of interest in the output has been undertaken, the evaluation can be done in a two-way iterative process. Sensitivity analysis techniques are classified into two groups or methods: LSA and GSA. Whereas LSAs analyse the behaviour of the system response locally by means of partial derivatives or similar approaches around a chosen point, GSAs determine all the system's critical points in the combined space formed by the parameters [43, 40].

A literature review of the global sensitivity analysis techniques can be found in Chapter 2. Two techniques are considered appropriate for application to the offshore wind cost model: the PAWN distribution-based and the variance-based method. It has been shown that the distribution-based method has outperformed the variance-based method for some highly-skewed or multi-modal distributions. However, despite its increasing popularity, there is a lack of understanding about the performance and properties of the distribution-based method. The benchmark presented in Chapter 5 is an attempt to remedy this. We compare the distribution-based method against the variance-based method for a set of well-known test functions. We show that, whereas the distribution-based method can be used as a complementary approach to variance-based methods, it fails to rank different inputs when these have different orders of magnitude in their contribution of the response. Chapter 6 revolves around the application of the distribution-based and the variance-based method to the offshore wind cost model in order to i)improve the understanding of key parameters when building a

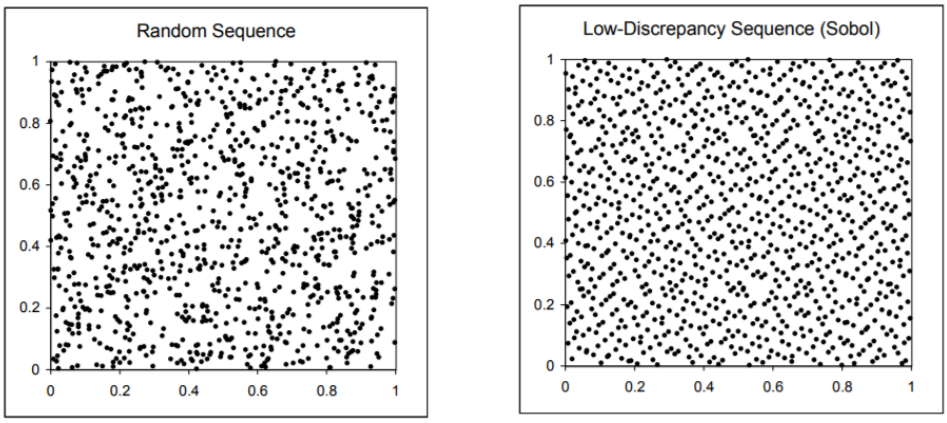

(a) **(b)**

Figure 4.5: (a) First 1024 points in a random sequence and (b) first 1024 points in a low discrepancy Sobol sequence [110]

financial model for an offshore wind farm ii) guide additional efforts towards reducing the uncertainty of those key parameters to drive the financial costs down.

Quasi-Monte Carlo Simulation

Quasi-random(QR) numbers is the term referred as the n-tuples that fill the unit hypercube more uniformly than uncorrelated random points. QR numbers are not random at all, unlike pseudo-random numbers. This means that successive points are placed based on the position of the previous sample points in order to avoid gaps or maximally avoiding each other. Figure 4.5 compares a random number sequence (a) with a QR sequence (b) using 1024 points. As shown, it becomes clear that QR sequences fill up the space more evenly distributed than conventional random numbers.

Many QR sequences have been proposed in the literature as shown in [111], however we will limit ourselves to the ones used in [112], which are an updated version of the Sobol QR low discrepancy sequences; we understand discrepancy as a quantitative measure for the deviation from uniform distribution. The idea of using QR sequences comes down to the numerical difficulties of multidimensional integration. QR sequences tend to outperform conventional random Monte Carlo sampling in the the estimation of multi-dimensional integrals. Replacing these random samples in the Monte Carlo method

by well-chosen deterministic points allows to better approximate multidimensional integrals, by efficiently exploring the input domain; this is the main purpose of QR sequences in this work, with a direct application to the variance-based method.

4.5 Coherent Risk Metrics

Risk metrics are measures of quantitative uncertainty assessments typically used for assessing, comparing and tracking risk. While the risk metric is related to the attribute of risk that is being measured, the risk measure is the operation or procedure that assigns a value to a risk. For example, when calculating the LCOE for an energy infrastructure project, we can look at the 5% worst case realisations of a stochastic model and use Value at Risk (VaR) using 1000 samples. Or we could do the same using 10 000 samples. Therefore, for any risk metric (VaR in this particular example), there may be multiple risk measures.

Risk aversion accounts for the fact that the decision-maker, which in this case may be a developer, will agree to a situation with a more predictable LCOE but possibly higher expected LCOE than another situation with an unknown LCOE but lower expected LCOE.

Risk aversion can be modelled by risk metrics originated in the financial mathematics literature such as the Value at Risk (VaR) and Conditional Value at Risk (CVar). The $\mathbf{VaR}_\alpha$ gives the probability α that a certain outcome is worse than a given threshold. Typically the probability α represents the confidence level and $\mathbf{VaR}_\alpha$ is regarded as the maximum value that will not be exceeded at this given confidence level. Building on $\mathbf{VaR}_\alpha$, $\mathbf{CVaR}_\alpha$ gives the expected outcome given that the value is worse than $\mathbf{VaR}_\alpha$. The concept was first introduced in [113] and further developed in [114]. The mathematical formulation for $\mathbf{VaR}_\alpha$ and $\mathbf{CVaR}_\alpha$ for continuous functions is given in Equation 4.2 and 4.3.

$$\mathbf{VaR}_\alpha(X) = min\left(c : P(X \leq c) \geq \alpha\right). \tag{4.2}$$

$$\mathbf{CVaR}_{\alpha}[X] = \mathbf{E}[X|X \geq \mathbf{VaR}_{\alpha}(X)] \tag{4.3}$$

Where $P(X \leq c)$ is the probability of the variable X being less or equal than c and $\mathbf{E}$ is the mathematical expectation operator. One of the main shortcomings of the $\mathbf{VaR}_{\alpha}$ is that it provides no information on the extent to which values might materialise beyond the threshold amount indicated by the $\mathbf{VaR}_{\alpha}$ itself, whereas $\mathbf{CVaR}_{\alpha}$ does. In addition, $\mathbf{CVaR}_{\alpha}$ has superior mathematical properties since this measure is coherent in the sense of Artzner [115]. Artzner stated a set of four properties that should be desirable for any risk metric. If the risk metric satisfies these 4 properties it is said to be a coherent risk metric. Consider X and Y as random variables representing the losses, $c \in \mathbb{R}$ is a scalar representing loss, and ρ is a risk function which maps the random variable X or Y to $\mathbb{R}$, according to the risk associated with X or Y. Then, the following properties can be defined as:

- (i) Monotonicity: a project that results in higher losses, it also results in higher risk, shown in Equation 4.4.

$$X \leq Y \implies \rho(X) \leq \rho(Y) \tag{4.4}$$

- (ii) Translation Equivariance: increasing the loss, increases the risk in the same amount, shown in Equation 4.5.

$$\rho(X + c) = \rho(X) + c \tag{4.5}$$

- (iii) Subadditvity: diversification decreases risk, shown in Equation 4.6.

$$\rho(X + Y) \leq Y\rho(X) + \rho(Y) \tag{4.6}$$

- (iv) Positive Homogeneity: doubling the variable size doubles the risk, shown in Equation 4.7.

$$\rho(\lambda X) = \lambda\rho(X) \tag{4.7}$$

It is well known that value at risk is not a coherent risk metric as it does not respect the subadditivity property. For this reason, we've selected $\mathbf{CVaR}_\alpha$ as the preferred financial risk metric. In this approach risk aversion is modelled as a weighted average λ of the expected value of X and $\mathbf{CVaR}_\alpha$. Parameter λ can be varied from 0 (in a risk neutrality setting) to 1 (extreme risk aversion), based on the work of Munoz [116] and displayed in Equation 4.8. Figure 4.6 shows how risk aversion changes the decision maker's preferences when varying λ for a simple LCOE distribution that follows a PERT distribution with parameters $\sim$ (60,75,150); an α of 0.95 is assumed as standard practice.

$$\boldsymbol{\rho}_\alpha[\lambda, X] = \lambda \mathbf{CVaR}[X]_\alpha + (1-\lambda)\mathbf{E}[X] \tag{4.8}$$

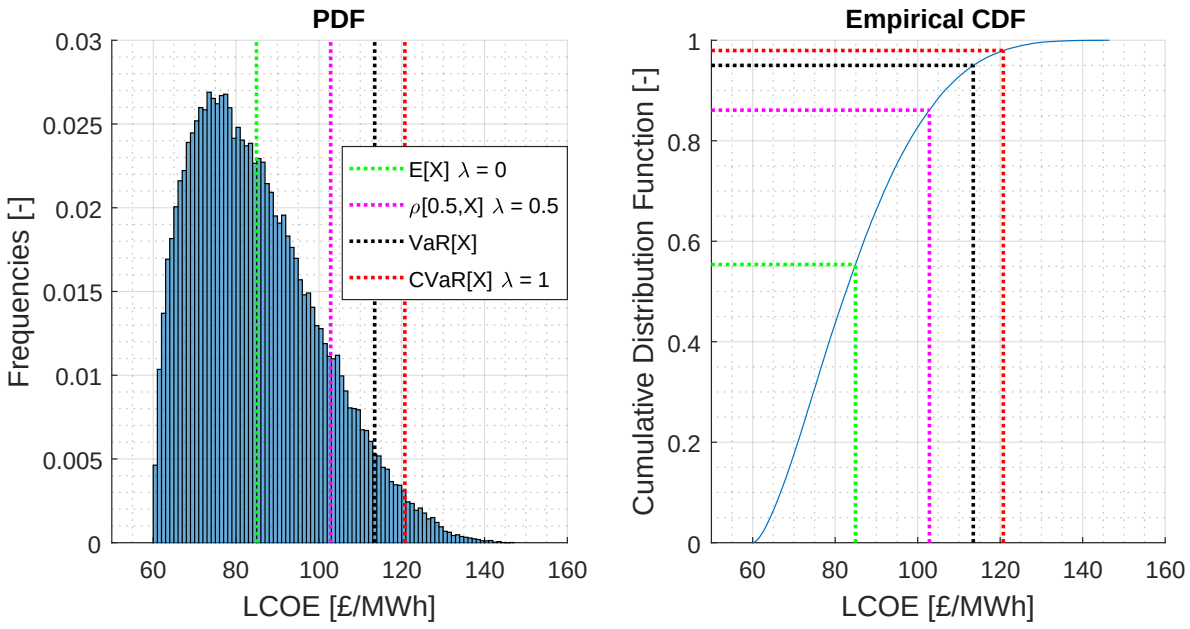

Figure 4.6: Financial risk metrics for a simple LCOE calculation that follows a PERT distribution with parameters PERT $\sim$ (60,75,150) when varying the risk aversion of the decision maker.

4.6 Resampling

Resampling methods are processes of repeatedly drawing samples from a data set. In resampling methods, the simulated samples are drawn from the existing sample of data and not from more model runs. Thus, in resampling methods, there is a given sample size given by computational constraints and we want to analyse and summarise patterns in that sample. The fundamental assumption is that all information about the model that is contained in the original sample of data is also contained in the distribution of these simulated samples. If so, then resampling from the one sample we have is equivalent to generating completely new random samples from the model. In this thesis only bootstrapping is used to assess the confidence intervals for the global sensitivity analysis indices, given that it is considered the most flexible and powerful resampling method [117]. Bootstrapping was formally introduced by Efron in 1979 [118]. Although there are a variety of bootstrap methods, their core is a common process:

- Begin with an observed sample of size N - generate N samples using the computer model
- Generate a simulated sample of size N by drawing observations from your observed sample independently and with replacement.
- Compute and save the statistic of interest
- Repeat this process many times (e.g. 1,000)
- Treat the distribution of your estimated statistic of interest as an estimate of the model distribution of that statistic.

4.7 Practical Implementation

Cost modelling tools involve a heavy reliance on mathematical techniques and complex algorithms linked by different modules. EDF Energy's R&D MATLAB-based cost modelling tool (OWCAT) helps the decision-making process by estimating the LCOE of offshore wind projects. Further information regarding the model, its inputs and outputs can be found in Chapter 3. Without limiting the generality of the foregoing, it

can be assumed that the pre-existing deterministic cost model: G, considered to be the validated baseline model, is divided into N different modules, displayed on the left hand side of Figure 4.7. This section describes the changes carried out to the initial deterministic model G in order to ease the implementation of the quantitative uncertainty management framework from a practical point of view.

The pre-existing model starts off by loading input Data 1 into Module 1, to perform the first set of operations. The subsequent modules require additional information to perform subroutines, namely Module j might require information from input Data j. After completion of Module N, the model output is obtained. It is understood that this refers to any financial metric of interest such as the LCOE. In this context, given that the model is deterministic, the same input data would result into the same output if the model is to be run twice and no change in model inputs is made. Furthermore, input Data j $\forall j = 1, \ldots, k$ are given in m-file format and are embedded inside the main core of the tool. These data structures are based on external Excel cost book files, where cost data is stored. Each Excel file allows for the optimisation of curve fitting coefficients on cost data points. As a result, if new data were made available (for instance, new offshore wind cost components being publicly released), new curve fitting coeffficients would need to be estimated. These coefficients would then need to be manually hard-coded and embedded into the source code. This is time-consuming, hard to maintain and prone to making errors. Moreover, when implementing the stochastic version of the current tool, information would need to be stored within a main structure and be passed along through each of the modules. Each module would then need to have stochastic settings to control which variables need to be updated at each iteration, increasing the complexity of the code across the different modules.

A solution to this approach has focused on restructuring how the different data structures are loaded into the model. If instead of loading data structures separately into each modules, all data were loaded directly from the external Excel files into a central module (referred to as the stochastic module) at the very beginning, stochastic settings would only need to be applied once. In addition, having all the information stored in

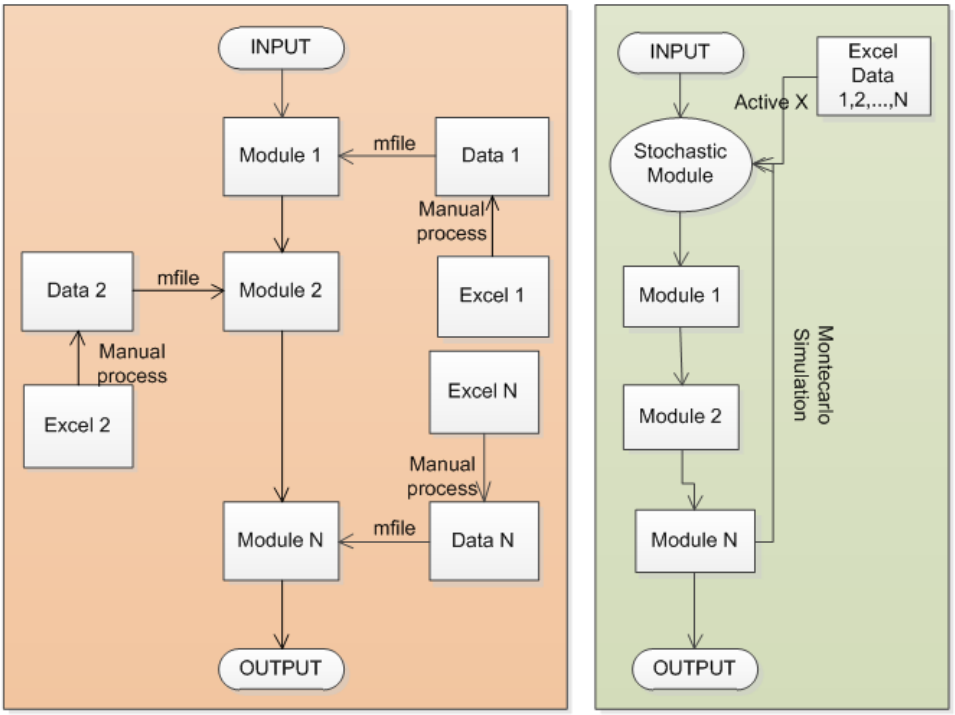

Figure 4.7: Deterministic (left) and Stochastic (right) Cost Model Flowcharts

Excel files, would help model users to communicate the underlying input assumptions with shareholders, share them to confirm their validity and update them when required. For this reason, the approach on the right hand side of Figure 4.7 has been followed in order to deploy a quantitative uncertainty management framework and create a more transparent tool.

The new architecture of the cost modelling tool allows for deterministic and stochastic runs while improving input control. Three main scripts define its architecture:

- Front-end script: loads external data from several Excel files.
- Steering script: separates the different modules: single deterministic run, LSA, stochastic and global sensitivity analysis.
- Deterministic core: runs the design, cost and financial modules.

There are two ways to load the information from the Excel files into MATLAB.

- Using ActiveX software to open Excel files, provides a quick way to exchange information between Excel and Matlab. ActiveX is not dependent on Microsoft Windows operating systems, but in practice, most ActiveX controls only run on Windows.

- Using a xlsread build-in MATLAB function to read information from Excel files to Matlab. Although it might be time-consuming when many Excel files are involved in the calculation, it works for any operating system.

Given that the cost modelling tool is used in a high performance computing cluster at the University of Edinburgh, both ways are implemented.

To run the tool in deterministic mode, the following data fields are required: input description, field name, value and unit. Then, the field "Stochastic" allows the user to select whether or not the variable is run in stochastic mode. If it is, then the following data fields are required: uncertainty type, uncertainty input, data, inputs and units. Uncertainty type concerns the probability distribution function associated with the input. Uncertainty input defines whether the uncertainty is absolute or relative. Absolute uncertainty has the same units as the value of the input. Data reflects the amount of parameters used to describe the probability distribution and Inputs are the value of those parameters. It is important to make sure that the variables selected to run in stochastic mode have a probability distribution function associated to them. In stochastic mode, all the variables selected are stored for post-processing. Therefore it is possible and recommended to check the generated distributions of the model inputs, instead of only checking the outputs.

The new architecture of the stochastic cost modelling tool that has been created as a result of this research allows the user to parallelise the code and run it on a high-performance computing cluster to address the high computational cost of Monte Carlo simulations.

Chapter 5

Global Sensitivity Analysis Toolbox

After establishing the quantitative uncertainty management framework in the last chapter, we will now explore the field of global sensitivity analysis. The search for new and more efficient global sensitivity analysis methods has led to the development of the PAWN distribution-based method. This method has been proven to overcome one of the main limitation of variance-based methods – the moment independent property. In this regard, the distribution-based method has outperformed the variance-based method for some highly-skewed or multi-modal distributions. However, despite its increasing popularity, there is a lack of understanding about the performance and properties of the distribution-based method. The benchmark presented in this Chapter is an attempt to remedy this. We compare the distribution-based method against the variance-based method for a set of well-known test functions. We show that, whereas the distribution-based method can be used as a complementary approach to variance-based methods, which is especially useful when dealing with highly-skewed or multi-modal distributions, it fails to rank different inputs that have different orders of magnitude in their contribution of the response.

5.1 Introduction

GSA methods are used to study how different sources of uncertainty in model output can be apportioned to the different sources of uncertainty in model input by exploring the combined space formed by all parameters in the domain [40] [43]. Before starting a GSA, it is imperative to define which research question needs to be answered and which risk metrics are to be used to quantify uncertainty. Different research questions and risk metrics will lead to different answers, and therefore this is something that has to be established from the very beginning.

In the context of this Chapter, the research question GSA attempts to aswer is to determine the most relevant input variables to an output behaviour, as well as to identify those variables whose contribution can be neglected. The words inputs and factors will be used interchangeably in the context of this work. By ranking the model inputs in order of importance, useful insights into the model can be gained, especially when the system is not well known or the model is in the early stages of development. The process of ranking these inputs is also referred to as **Factor Prioritization**[43]. Prioritization leads naturally to the idea of important inputs but also to negligible inputs or factors whose variability has a negligible effect on the output. Very often the inputs into a model follow very asymmetric distributions of importance, with few inputs accounting for most of the output uncertainty and most inputs playing little or no role [119]. By identifying those parameters that have no significant contribution to the model output, the complexity of the model can be reduced. This is also known as **Factor Fixing**[43].

It is similarly important to define the risk metric. A number of methods have been developed. One of the most well-established and extensively used GSA method is the Sobol or variance-based method, developed in 1990 by Ilya Meyerovich Sobol [64]. The Sobol method decomposes the variance of the model output in terms of the input variances. The method is model independent and therefore, it can be applied to any model regardless of the response function of the input-outputs. In addition, it is easy to interpret and to implement, making it the cornerstone of GSA. However, one of the key limitations of the method concerns the fact that the method needs the second moment

of the output distribution to fully characterize the output uncertainty.

Moment independent techniques arose from the works of Borgonovo [69] and Liu [68], where highly-skewed distributions were analysed to examine how its variance is decomposed. When using conventional variance-based GSA techniques both works concluded that identifying variance with uncertainty might lead to misleading conclusions. The first set of results showed that the unconditional variance was lower that the conditional variance at a given conditioning value, implying that the variance of the output increases when removing the uncertainty from one of the inputs; an example of that can be found in [43] for non-additive models. The second example failed to rank the importance of the different input uncertainties. Therefore, decision makers might be given a false sense of security, whereby attempting to fix/reduce some of the input uncertainty may result in higher variability of the output. These findings prompted the research community to investigate methods that remove the dependence on a single moment. As such, moment independent techniques are not affected by the presence of correlations and can provide a solution for those distributions that are not well represented by its variance, avoiding costly pitfalls.

As a consequence, several GSA methods were developed (citing here just a few) such as the entropy-based and the δ-sensitivity to overcome the moment dependent property [69, 68]. However, the practical implementation of those methods has been quite limited [48]. This is thought to be related with the computational cost of calculating many Probability Density Functions (PDFs). Later on, the PAWN method was published in 2015, coined under the name of "A simple and efficient method for GSA based on CDFs" [48]. The innovative idea was to use the Cumulative Distribution Function (CDF) instead of the PDF in order to apportion the uncertainty of the output into the different inputs. The underlying reason for choosing CDFs over PDFs is based on the fact that CDFs are much easier to approximate than PDFs [48], as explained in the following sentences. PDFs are usually unknown and must be estimated empirically. An easier way to calculate an empirical PDF would be to use a histogram of the data sample, whose resulting shape will be conditioned on both the position of the first bin

and the size of the bin. However, obtaining values that correctly represent the empirical PDF may be difficult. A different way to estimate the PDFs would be to use the Kernel Density Estimation (KDE) methods, which would only require the estimation of a single parameter – the bandwidth. Another approach that has been used in the past is to first estimate the CDFs, and then use derivation techniques to work out the empirical PDFs [68]. Given that the calculation of PDFs has to be repeated many times, it must be as computationally inexpensive as possible. As a result, it seems logical to compute CDFs instead of PDFs at no extra cost and without the need for tuning parameters. Not only does the PAWN method claimed to address the complexity of previous moment independent methods; its authors also provided several examples where the method outperforms the variance-based method for those PDF model output distributions that were highly-skewed or multi-modal, suggesting that, in these cases, variance was not a good proxy for uncertainty.

Findings that more theoretical understanding is needed in order to employ CDF-based sensitivity measures are available in the existing literature as shown in [120, 121, 122]. Nevertheless, given its advantages, moment independent techniques are continously being applied to tackle complex problems. In 2016 the PAWN method was used in a techno-economic optimal wind-energy converter, where its model exhibited an output PDF which was not symmetric but right-skewed [123]. As a result, negative values were obtained for those cases were the conditional variance exceeded the unconditional variance; result of which was driven by a numerical approximation due to the limited sample size. In 2017, the Sobol and PAWN GSA techniques were compared for a hydrological model called Soil and Water Assessment Tool [70]. The comparison was undertaken in terms of the convergence rate, parameter ranking and screening results. It was shown that there were no differences between the two methods as for the convergence rate and screening results. However, PAWN and Sobol came up with a different ranking of the model inputs importance. This chapter emphasises that this was due to the underlying assumption that Sobol considers variance as a good proxy for uncertainty, whereas in reality this may not be the case; at the same time this chapter suggests that the variance-based and PAWN methods may be regarded as complementary approaches to

study the sensitivity of model output.

Although the PAWN method has been widely adopted, a major limitation of PAWN was perceived by the authors regarding the need for a tailored sampling strategy to approximate the sensitivity indices. PAWN required to tune the triplet Nu, Nc and n to compute its PAWN indices, where Nu represented the number of evaluations obtained by sampling the entire input feasibility space, Nc was the number of evaluations obtained by sampling the conditional input space, and n the number of conditioning points. However, no one has yet analysed how to choose the values for the triplet. In addition, given the tailored sampling strategy, it is difficult to apply several GSA methods to the same problem, as PAWN requires dedicated model evaluations. In 2018, the authors addressed these two issues by developing a generic approach of the PAWN method, called the distribution-based global sensitivity analysis. This generic approach provides a solution for these two limitations as shown in [71]. On a separate note, Gamboa et al. investigated in 2018 the generalisation of the so-called Sobol indices to higher moments, where its index appears to be more general than Sobol as it takes into consideration the whole distribution and not the second moment [124].

Given the number of people that use the PAWN distribution-based method in the field of environmental modelling [45], the authors would like to limit the scope of this Chapter to benchmark the PAWN distribution-based against the variance based. Even though the one from Gamboa is well suited for this comparison, this will be considered in future work. Further research is necessary to compare the PAWN distribution-based method against the well-established Sobol method, before the former can be widely adopted by the community. Therefore, a wider set of reference test functions has to be used to benchmark these two methods for those cases where the analytical variances of the test functions are known. In other words, the community needs to know how the PAWN distribution-based method compares to Sobol for those cases where Sobol has worked well and also which are the advantages of the PAWN distribution-based over Sobol. The aim of the current Chapter is to remedy this lack of understanding by providing this

benchmark. We then show its properties, and suggest where the method is appropriate.

The rest of this Chapter is organised as follows: Section 5.2 and 5.3 introduces the fundamentals of variance-based and PAWN distribution-based GSA, respectively. Following this, a set of well-known test functions is introduced in Section 5.4 and used to benchmark the two methods. Results and discussions are shown in Section 5.5. Conclusions are drawn in Section 8.7.

5.2 Sobol Method

5.2.1 Introduction

The Sobol method, or variance-based sensitivity analysis, is a form of global sensitivity analysis that focus on decomposing the variance of the model outputs in terms of the variance of the model inputs. The following formulation is reproduced from [64]. Let us assume that a mathematical model can be represented by Equation 5.1, which is made of summands of increased dimensionality. This is also called a High Dimensional Model Representation (HDMR), where the total number of summands in Equation 5.1 is 2^N. Let us also consider that the model input $\mathbf{X}$ belongs to the n-dimensional unit hypercube domain I^N, which is expressed as: $X_i \in [0,1]\ \forall i \in 1,...,N$. $f(\mathbf{X})$ is the model under study and the number of elements of increasing dimensionality grows as a function of $\binom{N}{i}\ \forall i \in 1,...,N$.

$$Y = f(\mathbf{X}) = f_0 + \sum_i f_i(X_i) + \sum_{i<j} f_{i<j}(X_i, X_j) + ... + f_{12...n}(X_1, X_2..., X_N) \tag{5.1}$$

As a result, the total number of summands (apart from f_0) is given by Equation 5.2.

$$\sum_{i=1}^{N} \binom{N}{i} = 2^N - 1 \tag{5.2}$$

If the following requirement in Equation 5.3 can be satisfied, then the representation of the model is called Analysis of Variance (ANOVA) HDMR. This means that the variables are considered to be mutually independent and it has been proven that this decomposition is unique [66].

$$\int_0^1 f_{i_1 \dots i_s} dX_k = 0 \qquad \text{for } k = i_1, \dots i_s \tag{5.3}$$

From assumption 5.3 and Equation 5.1, it follows the following relationships 5.4 to 5.7, where X_i is the i-th factor, $X_{\sim i}$ denotes all the factors but the i-th and $\mathbf{E}$ is the expectation operator.

$$\mathbf{E}[Y] = \int_{I^N} f(\mathbf{X}) = f_0 \tag{5.4}$$

$$\mathbf{E}_{\mathbf{X}_{\sim \mathbf{i}}}[Y|X_i] = \int_{I^N} f(\mathbf{X}) \prod_{k \neq i} dX_k = f_0 + f_i(X_i) \tag{5.5}$$

$$\mathbf{E}_{\mathbf{X}_{\sim \mathbf{i,j}}}[Y|X_i, X_j] = \int_{I^N} f(\mathbf{X}) \prod_{k \neq i,j} dX_k = f_0 + f_i(X_i) + f_j(X_j) + f_{ij}(X_i, X_j) \tag{5.6}$$

$$\begin{aligned} \mathbf{E}_{\mathbf{X}_{\sim \mathbf{i,j,l}}}[Y|X_i, X_j, X_l] = \int_{I^N} f(\mathbf{X}) \prod_{k \neq i,j,l} dX_k = f_0 + f_i(X_i) + f_j(X_j) + f_l(X_l) + \\ f_{ij}(X_i, X_j) + f_{il}(X_i, X_l) + f_{jl}(X_j, X_l) + f_{ijl}(X_i, X_j, X_l) \end{aligned} \tag{5.7}$$

Equation 5.4 shows that, when integrating the HDMR, all the terms cancel out apart from the constant f_0. The differential x dX_k $\forall k \in 1, ..., N$ concerns the integration of the model respect those k variables. It becomes apparent that when fixing a variable, the integration does not lead to a 0 contribution as per assumption 5.3. The procedure is continued until all $(N-1)$-dimensional summands are defined, and then for the last member $f_{12...N}(X_1, X_2..., X_N)$ Equation 5.1 is used. By regrouping the terms and calculating the multidimensional integrals, the different HDMR functions can be obtained in a recursive way.

5.2.2 Construction of ANOVA in HDMR

If we now assume that the input parameters are independent random variables uniformily distributed over $[0, 1]$, as expressed in 5.8, as well as that $f(\mathbf{X})$ is square integrable (so are all the terms), then the following Equations hold. The expectation of this function is given in Equation 5.9, where $f_X(\mathbf{X})$ is the pdf of x and by construction this is equal to 1.

$$\mathbf{X} = \{X_1, ..., {X_N}^T\}, X_i \sim \mathcal{U}(0, 1), \forall i \in 1, ..., N \tag{5.8}$$

$$\mathbf{E}[f(X)] = \int_{I^N} f(\mathbf{X}) f_X(\mathbf{X}) dX = \int_{I^N} f(\mathbf{X}) dX = f_0 \tag{5.9}$$

The total variance of the function can be defined in Equation 5.10.

$$\mathbf{V}[Y] = \int f(\mathbf{X})^2 dX - {f_0}^2 \tag{5.10}$$

Taking the different functional components of the HDMR $\{f_0, f_i, f_{ij}, ...\}$, partial

variances V_i,V_{ij} can be calculated as in Equations 5.11 and 5.12. In addition, the total variance $V(Y)$ can be decomposed using Equation 5.13.

$$V_i = V(f_i(X_i)) = \mathbf{V}_{X_i}(\mathbf{E}_{\mathbf{X}_{\sim \mathbf{i}}}[Y|X_i]) \tag{5.11}$$

$$V_{ij} = V(f_{i,j}(X_i, X_j)) = \mathbf{V}_{X_i X_j}(\mathbf{E}_{\mathbf{X}_{\sim \mathbf{ij}}}[Y|X_i, X_j]) - \mathbf{V}_{X_i}(\mathbf{E}_{\mathbf{X}_{\sim \mathbf{i}}}[Y|X_i]) - \mathbf{V}_{X_j}(\mathbf{E}_{\mathbf{X}_{\sim \mathbf{j}}}[Y|X_j]) \tag{5.12}$$

$$\mathbf{V}[Y] = \sum_i V_i + \sum_{i<j} V_{i,j} + ... + V_{12...n} \tag{5.13}$$

5.2.3 Sensitivity Indices

The decomposition of variance used in the previous section allows to define the following sensitivity analysis indices: the first and total order sensitivity coefficients. Whereas the first order S_i coefficient measures the part of variance which is caused by X_i, it does not take into account the interaction with the other variables. When considering the order 2 coefficient S_{ij}, it not only takes into account the part of variance caused by X_i and X_j, but also the interaction between X_i and X_j. The order 3 sensitivity coefficient S_{ijk} includes the variance of the output Y, resulting from the interactions of the three variables X_i, X_j and X_k, which is not explained by neither considering the single variables nor by the interaction of two variables. This can be generalised until the highest order.

The first sensitivity index is defined in Equation 5.14. Regardless of the interactions in the model, S_i is a measure of the main effect. In other words, it gives information on how much output variance could be reduced when fixing the input model X_i.

$$S_i = \frac{\mathbf{V}_{X_i}(\mathbf{E}_{\mathbf{X}_{\sim \mathbf{i}}}[Y|X_i])}{V(Y)} = \frac{V_i}{V(Y)} \tag{5.14}$$

Where X_i is the i-th factor and $X_{\sim i}$ denotes all the factors but the i-th. The expectation of Y is taken over all the possible values of $X_{\sim i}$ while keeping X_i fixed. The outer variance is taken over all possible values of X_i. Although the total effects S_{T_i} are a direct consequence from Sobol's decomposition, they weren't explicitly mentioned until the work of Homma and Saltelli [63]. It is worth remembering that the number of coefficients to be computed grows exponentially according to 2^N, where N is the number of uncertain variables. Consequently, computing all Sobol components can be prohibitive if the model has many inputs. For this reason, and as a means to overcome this challenge, the total effect index was introduced, as defined in Equation 5.15. The total effect index takes into account the total contribution of the output variation due to the factor X_i, which includes the first-order effect as well as all higher-order interactions.

$$S_{T_i} = 1 - \widehat{S_{\sim i}} \tag{5.15}$$

Where $\widehat{S_{\sim i}}$ is the sum of all $S_{i_1 \ldots i_s}$ that do not include the index i. A different formalism for it is shown in Equation 5.16 as in the work of Sudret [125].

$$S_{T_i} = \sum_{I_i} \frac{V_{i_1 \ldots i_s}}{V(Y)} \qquad I_i = \{\{i_1, ..., i_s\} \supset \{i\}\} \tag{5.16}$$

In order to be consistent with the first order mathematical definition, the total order index can be defined in Equation 5.17.

$$S_{T_i} = \frac{\mathbf{E}_{\mathbf{X}_{\sim \mathbf{i}}}(\mathbf{V}_{X_i}([Y|X_{\sim i}])}{V(Y)} = 1 - \frac{\mathbf{V}_{\mathbf{X}_{\sim \mathbf{i}}}(\mathbf{E}_{X_i}([Y|X_{\sim i}])}{V(Y)} \tag{5.17}$$

As described in [112], a way to visualise the total order index is to consider $\mathbf{V}_{\mathbf{X}_{\sim \mathbf{i}}}(\mathbf{E}_{X_i}([Y|X_{\sim i}])$ as the first effect order of the $X_{\sim i}$. If we were to subtract this value from $V(Y)$, this would mean that the remaining variance should be the contribution of all terms in the decomposition that include X_i.

A summary of the different statistical measures and its interpretations is given in table 5.1. It is important to notice that the Law of Total Variance can be applied for 1&4 as well as 2&3.

Table 5.1: Statistical measures and interpretation

ID	Mathematical notation	Interpretation
1	$\mathbf{V}_{X_i}(\mathbf{E}_{\mathbf{X}_{\sim \mathbf{i}}}([Y\|X_i]))$	Expected reduction in variance that would be obtained if x_i could be fixed.
2	$\mathbf{E}_{\mathbf{X}_{\sim \mathbf{i}}}(\mathbf{V}_{X_i}([Y\|X_{\sim i}]))$	Expected variance that would be left if all factors but x_i could be fixed.
3	$\mathbf{V}_{X_{\sim i}}(\mathbf{E}_{\mathbf{X}_\mathbf{i}}([Y\|X_{\sim i}]))$	Expected variance that would be obtained if all factors but x_i could be fixed.
4	$\mathbf{E}_{\mathbf{X}_\mathbf{i}}(\mathbf{V}_{X_{\sim i}}([Y\|X_i]))$	Expected reduction in variance that would be left if x_i could be fixed.

5.2.4 Latest Results on the Sobol Method

Since Sobol first published his work, many different estimators have appeared in the literature attempting to increase the efficiency of the method in computing the sensitivity indices. The latest estimators and designs are the radial sampling and the winding stairs. Further information on them can be found in [112] [52]. These show that a radial design outperforms winding stairs. Therefore, this Chapter also adopts the same principle as a comparator.

Given two independent sampling matrices $\mathbf{A}$ and $\mathbf{B}$, a_{ji} and b_{ji} are the generic elements of the matrices, where j is a dummy variables that varies from one to the number of simulations (N) and i is a second dummy variable that varies between one and the number of input variables (k). The generic elements of the matrix are obtained using Sobol's quasi-random numbers, or the so-called shifted LP_t sequences. The use of these low discrepancy series speeds up the performance of conventional Monte Carlo sampling. There are open-source libraries that generate this sequences based on [110]. We can now define $\mathbf{A_B}^{(\mathbf{i})}$ as the matrix $\mathbf{A}$, where the only difference is that column i belongs to $\mathbf{B}$. By using the notation at matrix or component level, the total sensitivity indices S_{T_i} are estimated by Jansen [67] and displayed in 5.18 and 5.19 respectively.

$$\mathbf{E}_{\mathbf{X}_{\sim \mathbf{i}}}(\mathbf{V}_{X_i}([Y|X_{\sim i}]) = \frac{1}{2N}\sum_{j=1}^{N}[f(\mathbf{A})_j - f(\mathbf{A_B}^{(\mathbf{i})})_j]^2 \tag{5.18}$$

$$\mathbf{E}_{\mathbf{X}_{\sim \mathbf{i}}}(\mathbf{V}_{X_i}([Y|X_{\sim i}]) = \frac{1}{2N}\sum_{j=1}^{N}[y({a_1}^{(j)}, {a_2}^{(j)}, ..., {a_k}^{(j)}) - y({a_1}^{(j)}, {a_2}^{(j)}, ..., {b_i}^{(j)}, ..., {a_k}^{(j)})]^2 \tag{5.19}$$

Further information and details on the implementation of Sobol can be found in [112] [52].

5.3 Distribution-based Method

We now describe the distribution-based method. The unconditional cumulative distribution function (UCDF) of the output y is represented by $F_y(y)$, whereas the conditional cumulative distribution function (CCDF) of the output when x_i has been fixed is represented by $F_{y|x_i}(y)$. The logic behind this GSA technique consists of assessing the distance between $F_y(y)$ and $F_{y|x_i}(y)$; this distance accounts for the variability of the output that has been reduced due to fixing input variable x_i, providing an importance

measure of x_i on the output.

Let us imagine that $F_y(y)$ and $F_{y|x_i}(y)$ are almost the same, i.e., that the distance between these two statistics is close to zero. This would mean that the amount of output variability reduction because of fixing the value x_i is negligible, which in turns implies that this parameter has almost no contribution to the output and could well be screened out. Conversely, if the distance of the two CDFs is large, this would mean that almost all the variability of the output can be explained by this parameter. The distance between the UCDF and the CCDF is measured through the Kolmogorov-Smirnov (KS) statistic. Formula 5.20 defines the KS statistic for a given x_i value.

$$KS(x_i) = |F_y(y) - F_{y|x_i}(y)| \tag{5.20}$$

It is important to bear in mind that the KS distance depends on the value upon which it has been conditioned. If we were to use the KS statistic as it is defined in Equation 5.20, this would mean that the model would be conditional on an assumed value, which is not desirable. The metric could give different results based on the conditioning value. As a way to uncondition the previous definition or remove the dependency of x_i, a statistic for the KS (for instance, the median) is used.

$$T_i = stat_{x_i}|KS(x_i)| \tag{5.21}$$

This index T_i, shown in Equation 5.21, has several characteristics: It is global, so the input variations take place in the entire feasible space; it is quantitative, model independent, unconditional, easy to interpret and implement, stable and moment independent. The last property is the main difference between the distribution-based and the variance-based techniques. Considering the fact that the analytical computation of the index T_i is impossible in most cases, the following numerical techniques attempt to estimate it.

$$\widehat{KS(x_i)} = |\widehat{F_y(y)} - \widehat{F_{y|x_i}(y)}| \tag{5.22}$$

Equation 5.22, describes the formulation, where $\widehat{F_y(y)}$ and $\widehat{F_{y|x_i}(y)}$ are the empirical

UCDF and CCDF approximated by a finite number of samples. Whereas the UCDF is approximated using N_u output evaluations by sampling the entire output feasibility space, the CCDF is approximated using N_c output evaluations by sampling all but x_i inputs. Consequently, the conditional KS can be transformed to an unconditional KS by means of a statistic, as displayed in Equation 5.23. However, it is important to notice that the choice of conditioning points will have an effect on the result. Both T_i and S_{Ti} metrics range from 0 to 1.

$$\widehat{T_i} = stat_{x_i = x_i^{(1)}, \ldots, x_i^{(n)}} |\widehat{KS(x_i)}| \tag{5.23}$$

The implementation of PAWN has been made available in [45]. This version of PAWN is now considered as the tailored sampling approach method and futher information can be found in [48, 46]. More recently in 2018, as mentioned in the introduction, a new implementation of PAWN, called the distribution-based method, addressed the limitations of the old version; this can found in [71]. The distribution-based method splits the range of variation of each input factor x_i into n equally spaced intervals I_k and define the conditional samples YC_{ik} accordingly. The unconditional sample YU can coincide with the entire sample Y or with a subsample of it. This is represented in Equation 5.24.

$$\widehat{S_i} = stat_{k=1,\ldots,n} KS(I_k) \; where \; KS(I_k) = |\widehat{F_y(y)} - \widehat{F_{y|x_i}(y) \in I_k}| \tag{5.24}$$

The main difference between the old and new version of PAWN is shown in Figure 5.1, sourced from [71]. "Example of using a tailored sampling strategy (left) and generic sampling (right) to approximate the PAWN index of input x1 in a case of M=3 input factors. Left (tailored): (a) Input samples used to derive the unconditional output sample YU. These are generated by randomly sampling the entire space of input variability. (b) Input samples used to derive three conditional samples YC11, YC12 and YC13. These are generated by fixing x1 at selected conditioning values (for the sake of clarity, only n=3 conditioning values are shown here). (c) Scatter plot of the unconditional (red) and conditional (grey) output samples YU, YC11, YC12 and YC13 against x1. Right (generic): similar to the left hand side but this time the input

samples in (d) and (e) are the same. A random subset (highlighted in red) is used to derive YU, and the three subsets obtained by splitting the variability range of x1 into 3 intervals (grey) are used to derive YC11, YC12 and YC13. After sampling, the approximation of the PAWN sensitivity index follows the same steps: (g) unconditional output distribution (red) and the three conditional distributions (grey) when x1 is fixed to a given value (interval). (h) KS statistic (maximum absolute difference) between the unconditional distribution and each of the three conditional ones, plotted against the conditioning value (centre of the interval)".

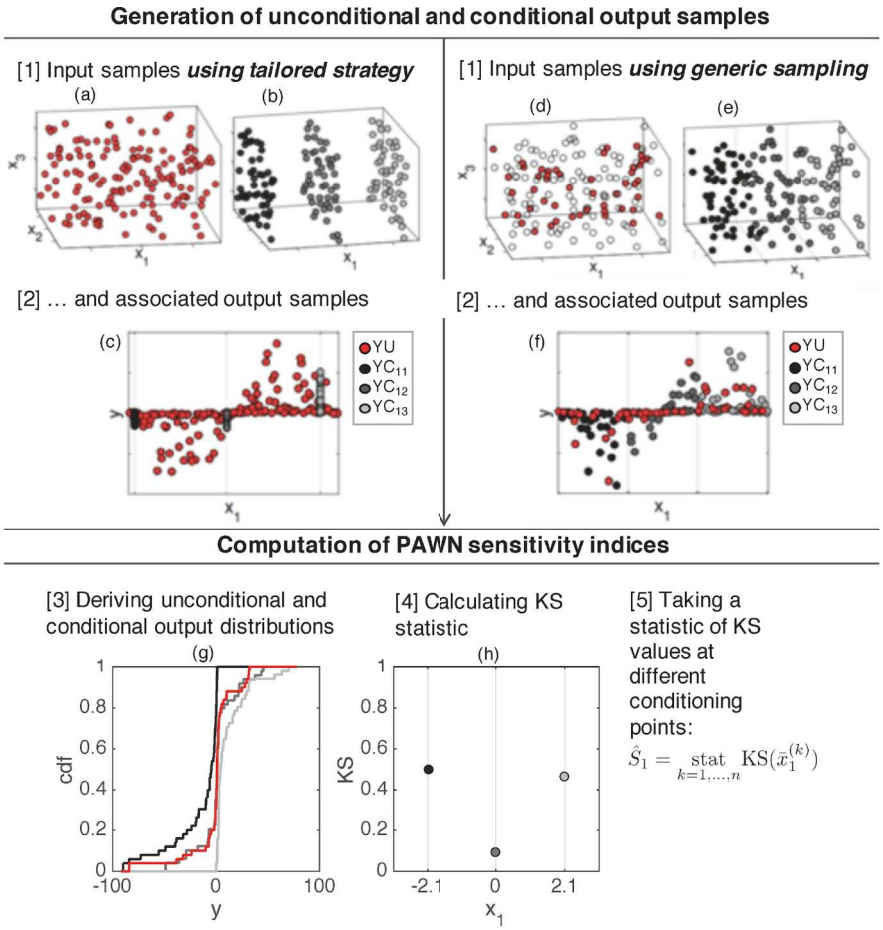

Figure 5.1: Comparison between the tailored and generic approach for the distribution-based method [71]

5.4 Test Functions

A set of well-studied test functions is investigated to benchmark the distribution-based against the reference Variance-based Sensitivity Analysis (VBSA) or also referred to Sobol. The following functions are briefly described below for the sake of completeness.

Function 1: The Ishigami function is one of the most common benchmark test functions because it exhibits strong non-linearity and non-monotonicity [126], as displayed in Equation 5.25. It has already been used as a benchmark by the distribution-based method in [71]. Parameters $a = 7$ and $b = 0.1$ are assumed and $X_i \sim U(-\pi, \pi)$; its analytical variance is displayed in Table 5.2.

$$Y = sin(X_1) + asin^2(X_2) + bX_3{}^4 sin(X_1) \tag{5.25}$$

X_i	ST[%]
1	55.76
2	44.24
3	24.37

Table 5.2: Analytical variance for Ishigami-Homma test function

Function 2: The K function was introduced by Bratley et al. [111] and used for GSA in [112]. The K function is displayed in Equation 5.26.

$$K = \sum_{i=1}^{k} (-1)^i \prod_{j=1}^{i} X_j \tag{5.26}$$

X_i is uniformly distributed in the interval [0,1]. In this test function there are few dominant variables: X_1 and X_2 account for most of the uncertainty band. Moreover, the degree of interaction increases with higher index variables due to the construction

of the function. The analytical variance is displayed in Table 5.3.

Function 3: The non-additive B function was proposed by Saltelli et al. in [43] and displayed in Equation 5.27.

$$B = \sum_{i=1}^{m} X_i \cdot X_{m+i} \tag{5.27}$$

Where $m = k/2$ (k being even), $X_i \sim N(\overline{X_i}, \sigma_{X_i}), i = 1, 2, ..., k$ and $N(\overline{X_i}, \sigma_{X_i})$ concerns the mean and standard deviation of a normal distribution. The choice of the different normal distribution parameters condition the number of important factors. Contrary to the $G*$ and K functions, non-relevant parameters have a non-nihil effect. The same parameters as [52] for the B function are kept and shown in Table 5.3.

Function 4 & 5: The G* function is a modified version of the G-Sobol function and it was introduced in [112]. This function is shown in Equation 5.28 and 5.29.

$$G^*(X_1, ..., X_k; a_1, ..., a_k, \delta_1, ..., \delta_k, \alpha_1, ..., \alpha_k) = \prod_{i=1}^{k} g_i^* \tag{5.28}$$

where g_i^* is defined as:

$$g_i^* = \frac{(1 + \alpha_i) \cdot |2(X_i + \delta_i - I[X_i + \delta_i] - 1|^{\alpha_i} + a_i}{1 + a_i} \tag{5.29}$$

Where X_i are the input factors, uniformly distributed between $[0, 1]$, $a_i > 0$ are the traditional G functional parameters, $\delta_i \in [0, 1]$ and $\alpha_i > 0$ are the shift and curvature parameters, respectively. $\delta_i s$ are randomly chosen since the uncertainties propagate independently of them. The mathematical meaning of $I[X_i + \delta_i]$ refers to the integer part of $X_i + \delta_i$. It is also worth adding that the relative importance of the factors directly depends on the choice of the parameters. For this reason, two functions are

considered for benchmarking purposes with 4 and 10 important factors : 4 (G_4^*) and 10 (G_{10}^*), whose parameters and analytical variance are displayed in Table 5.3.

	K	B		G_4^*			G_{10}^*			
X_i	ST[%]	$\overline{X_i}$	σ_{X_i}	ST[%]	a	α	ST[%]	a	α	ST[%]
1	75.00	0	0.5	0.39	100	1	0	100	1	0
2	25.00	0	0.5	0.62	0	4	67.44	0	4	75.49
3	8.33	0	1	1.55	100	1	0	100	1	0
4	2.78	0	1	1.55	100	1	0	100	1	0
5	0.93	0	2	12.41	100	1	0	100	1	0
6	0.31	0	2	22.34	100	1	0	100	1	0
7	0.10	0	1	3.49	1	0.5	3.19	1	0.4	2.56
8	0.03	0	0.5	1.40	0	3	59.28	10	3	1.24
9	0.01	0	1.5	20.25	100	1	0	0	0.8	23.30
10	0	0	2	36.00	100	1	0	0	0.7	20.00
11	0	1	2	0.31	0	2	46.83	9	2	0.94
12	0	2	2	0.31	100	1	0	0	1.3	37.68
13	0	2	1	0.31	100	1	0	100	1	0
14	0	2	1	0.31	100	1	0	100	1	0
15	0	3	1	1.24	1	0.5	3.19	4	0.3	0.26
16	0	3	3	11.17	100	1	0	100	1	0
17	0	1.5	3	2.79	100	1	0	100	1	0
18	0	3	3	0.70	0	1.5	37.94	7	1.5	1.03
19	0	2	5	17.46	100	1	0	100	1	0
20	0	2	5	31.03	1	0.5	3.19	2	0.6	2.11

Table 5.3: Parameters and analytical variance for K, B, G_4^* and G_{10}^* test functions

Function 6: A highly-skewed test function defined in Equation 5.30 was proposed in [68].

$$y = \frac{x_1}{x_2} \tag{5.30}$$

Where $x_1 \sim \chi^2(d_1)$ and $x_2 \sim \chi^2(d_2)$ follow Chi-square distributions with d_1 equal to 10 and d_2 13.978. The quotient of two Chi-square distributions is F-distributed. Hence

analytical values are shown in Table 5.4 and its formulation is presented in the Appendix 5.8 for the sake of completeness. If d_1 was 10 and d_2 14, the ST would be 54.5454% for both inputs. However, it has been purposely chosen to set d_2 smaller than 14 so that the theoretical variance of input factor 2 is greater than input factor 1.

X_i	ST[%]
1	54.50
2	54.60

Table 5.4: Analytical variance for highly-skewed test function

5.5 Results and Discussion

Ishigami-Homma function:

In order to allow for a fair comparison between the VBSA and the distribution-based, the same number of model evaluations is considered. The benchmark is carried out by taking the distribution-based with $N = 5000$ and $n = 20$ against VBSA with $N = 1250$ samples. Both result into approximately 5000 model evaluations. Results are displayed in Figure 5.2. Total sensitivity indices ST_i (small circles in red) are estimated via Monte Carlo method (by means of the Sobol low-discrepancy sequence) for input factors X_i $i = 1, ..., 3$. 95 % confidence intervals (vertical dashed lines in red) are estimated by bootstrapping 1000 replicas. Analytical variances (crosses in magenta) are given for all input factors. Total Kolmogorov Smirnov (KS) statistics T_i (small circles in blue) are estimated via random Monte Carlo sampling. 95 % confidence intervals (vertical dashed lines in blue) are estimated by bootstrapping 1000 replicas. The level of noise for the distribution-based method (horizontal dashed lines in blue) is calculated by the introduction of a dummy variable. This level of noise is bootstrapped 1000 times and results into the upper and lower horizontal dashed lines in blue. This means that, if the T_i was comprised between the upper and lower bound, we wouldn't be able to say if this is due to the importance of the input or the level of noise of the method.

Figure 5.2 also shows that the analytical variance is inside the confidence level for the variance-based method. If we were to rank the importance of the inputs based on

the two measures, we would obtain different results - the distribution-based method captures the non-linearity of the second input factor X_2 and places more weight on its uncertainty than the variance-based method. Also, the distribution-based method is not able to capture the importance of X_3 as it falls below the upper level of noise. A convergence analysis in VBSA is conducted by increasing the sample size from 125 to 2500 by steps of 125. In addition to this, 95 % confidence intervals are estimated by bootstrapping 1000 replicas in each case. This is shown in Figure 5.3(a). The same process is repeated for the distribution-based . For Figure 5.2 the left axis is used for Sobol with ST_i, whereas the right one is used for distribution-based with T_i. The number of conditioning points has been kept to 20, whereas N is increased from 500 to 10000 by steps of 500, as shown in Figure 5.3(b). As expected, when we increase the number of samples, the range of the confidence intervals is reduced. ST_i and T_i remain stable for the Ishigami-Homma function across the different simulations.

K, B G_4^* and G_{10}^* function:

The same number of model evaluations is considered for the following 4 functions in order to allow for a fair comparison between the VBSA and the distribution-based . The benchmark is carried out by taking the distribution-based with $N = 25200$ and $n = 20$ against VBSA with $N = 1200$ samples. Both result into approximately 25200 model evaluations. Results are displayed in Figure 5.4. Total sensitivity indices ST_i (small circles in red) are estimated via Monte Carlo (by means of the Sobol low-discrepancy sequence) for input factors X_i $i = 1, ..., 20$. 95 % confidence intervals (vertical dashed lines in red) are estimated by bootstrapping 1000 replicas. Analytical variances (crosses in magenta) are given for all input factors. Total Kolmogorov Smirnov (KS) statistics T_i (small circles in blue) are estimated via random Monte Carlo sampling. 95 % confidence intervals (vertical dashed lines in blue) are estimated by bootstrapping 1000 replicas. The level of noise for the distribution-based method (horizontal dashed lines) is calculated by the introduction of a dummy variable. This level of noise is bootstrapped 1000 times and results into the upper and lower horizontal dashed lines in blue, as previously done for the Ishigami - Homma test function.

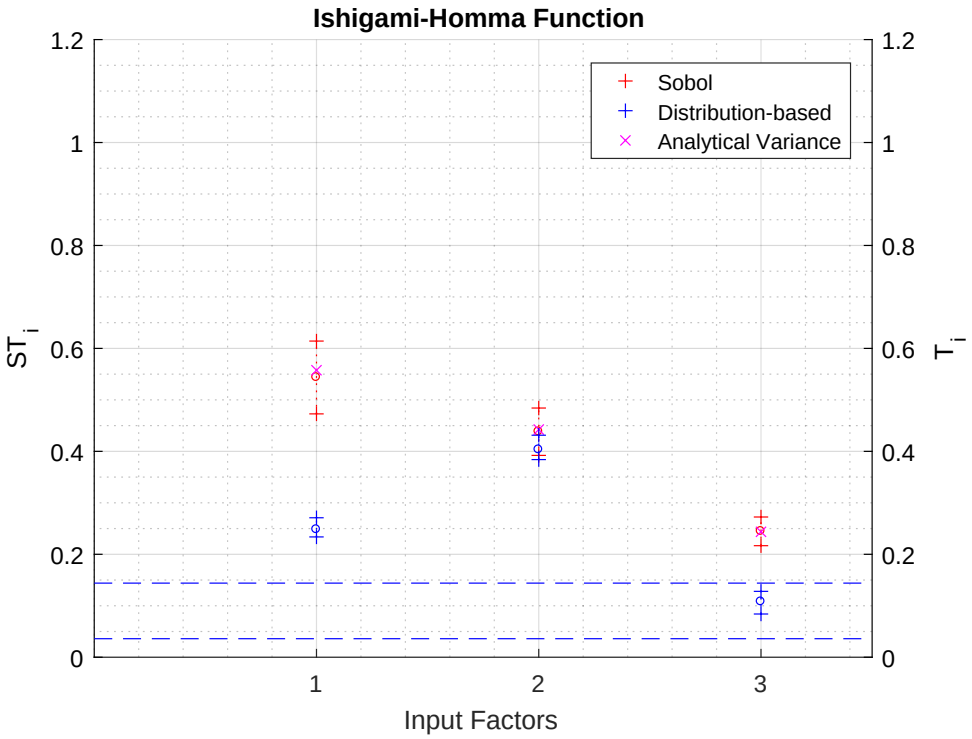

Figure 5.2: Benchmarking the PAWN distribution-based with $N = 5000$ $n = 20$ and $k = 3$ against the VBSA with $N = 1250$ samples for the Ishigami-Homma function. Both result into 5000 model evaluations. Analytical variance is also included to test the accuracy of the VBSA.

As far as the K function is concerned, only the first 9 inputs contribute to the variance of the output, which is reflected in Table 5.2. Input X_1 has a greater contribution than X_2 and X_2 has a greater contribution than X_3, and so on and so forth. However, when the distribution-based method is used, only $X_{1,2,3}$ can be considered within the validity of the method. The level of noise of the method doesn't allow us to say, for example, that input X_4 has a greater contribution than input X_{15}. Consequently, the method fails to rank inputs that have different order of magnitude in the contribution of the response.

When applied to the B function, the distribution-based method allows to identify $X_{5,6,9,10}$ but fails to rank three of the most relevant contributors to the variance: $X_{16,19,20}$. As for the G_4^* function, the distribution-based method allows to identify

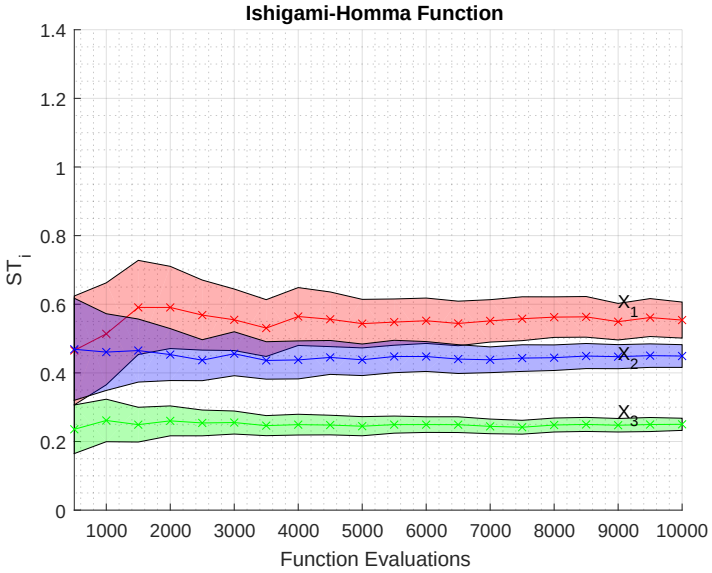

(a)

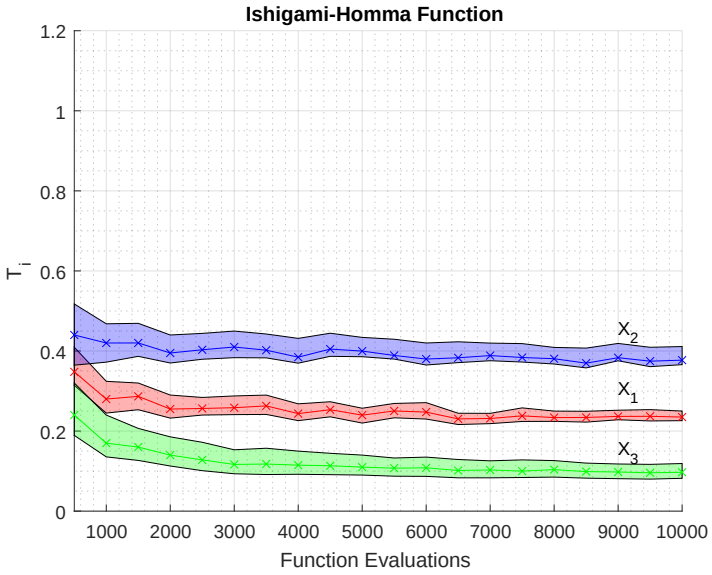

(b)

Figure 5.3: Covergence analysis for Ishigami-Homma function. Comparison of distribution-based T_i and Sobol S_{Ti} indices for input factors X_1, X_2 and X_3.(a): VBSA (b): distribution-based

$X_{2,8,11,18}$ but it does not capture the small contributions represented by $X_{7,15,20}$. Finally as far as the G_{10}^{*} function is concerned, the distribution-based method allows to identify $X_{2,9,10,12}$ but it doesn't capture the small contributions represented by $X_{7,8,11,15,18,20}$.

Figure 5.4 also shows that the analytical variance is inside the confidence level in VBSA for all but one input factor - X_{11} from the B function. It has been checked that increasing the number of model evaluations leads to the analytical variance falling inside the confidence level for all input factors. A convergence analysis in VBSA is conducted by increasing the sample size from 60 to 1200 by steps of 60, leading to a total of 25200 model evaluations in the last case. Confidence intervals are estimated by bootstrapping 1000 replicas in each case. Whereas Figure 5.5 doesn't display the confidence interval for a better interpretation, Figure 5.6 does display it for its main three inputs. The same process is repeated for the distribution-based. The number of conditioning points has been kept to 20, whereas N is increased from 1260 to 25200 by steps of 1260, as shown in Figure 5.5(b,d). ST_i remain stable for both the K and B Function across the different simulations. T_i is also stable and changes only occur in X_5 and X_6 for the B function, as they have similar KS values. This is basically due to the fact that the 20 conditioning points (n) play a role in exploring the search space. These conditioning points are evenly spaced within the domain, but change from simulation to simulation. Finally, it is also worth noticing that in Figure 5.6(d) the main input factors from Sobol cannot be recognised in function B once the confidence levels are plotted.

Highly skewed function:

The empirical PDF of the highly-skewed function (Equation 5.30) is displayed on the left hand side of Figure 5.7. An intuitive derivation of sensitivity indices comes from visual inspection of the scatter plots in Figure 5.7. The ordinate axis is always Y, whereas the abscissa are the various factors X_2 (right) and X_1 (middle). If we divide the total number points in different bins and compute their bin's average, we will obtain an estimate of $\mathbf{E}_{\mathbf{X}_{\sim \mathbf{i}}}([Y|X_i])$. If we now take the variance of the bin's average points, we obtain an approximation of the sensitivity index. Following this method, it is clear

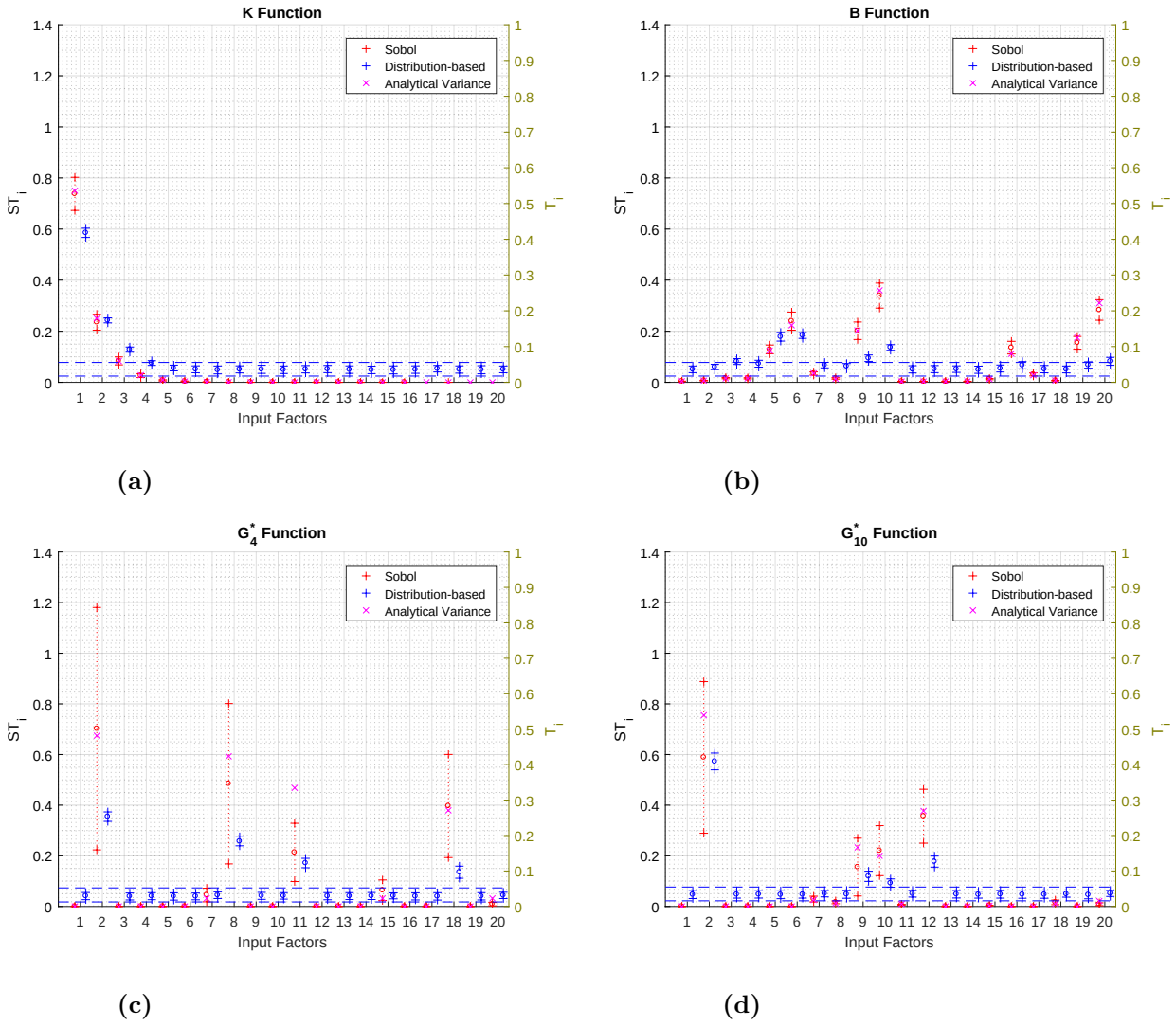

Figure 5.4: Benchmarking the distribution-based with $N = 25200$ and $k = 20$ against VBSA with $N = 1200$ samples. Both result into 25200 model evaluations. (a): K Function (b): B Function (c): G_4^* Function (d): G_{10}^* Function

that X_1 is more important than X_2; this has also been highlighted in the work of [68], where further information can be derived from the conditional PDFs.

Figure 5.8 shows a convergence analysis for the same highly-skewed function using the VBSA and the distribution-based. 95% confidence intervals are represented with coloured patch. It is seen that whereas the Sobol method shows that X_1 and X_2 input factors are equally important, the distribution-based generally recognises the input

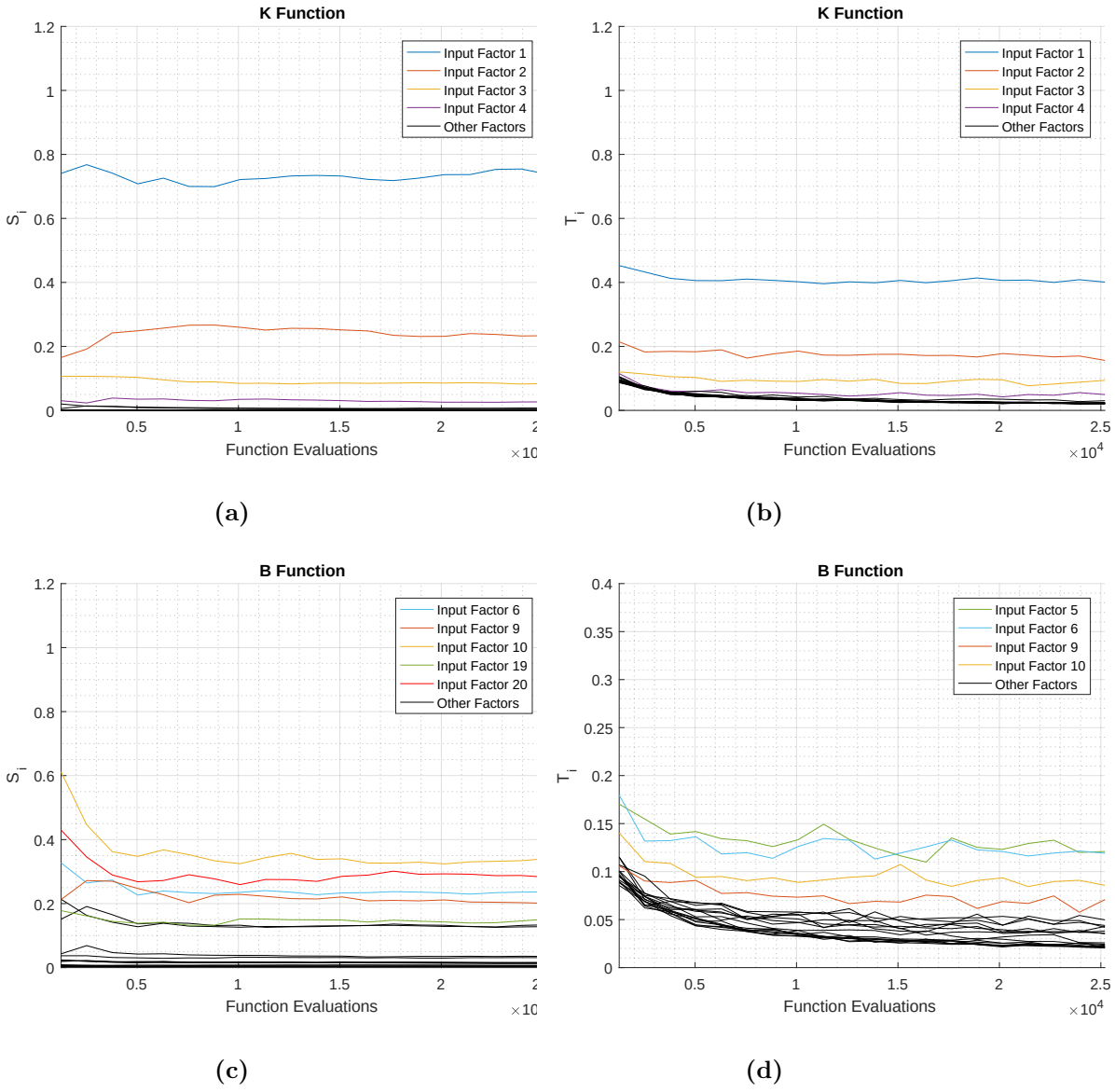

Figure 5.5: Covergence analysis for K Function (a,b) and B Function (c,d). Comparison of distribution-based T_i and Sobol S_i indices.(a,c): VBSA (b,d): distribution-based

factor importance X_1 over X_2, as it is shown in [48]. A convergence analysis in VBSA is conducted by increasing the sample size from 400 to 8000 by steps of 400, leading to a total of 24000 model evaluations in the last case. Distribution-based convergence analysis is carried out in a similar way with 10 conditioning points.

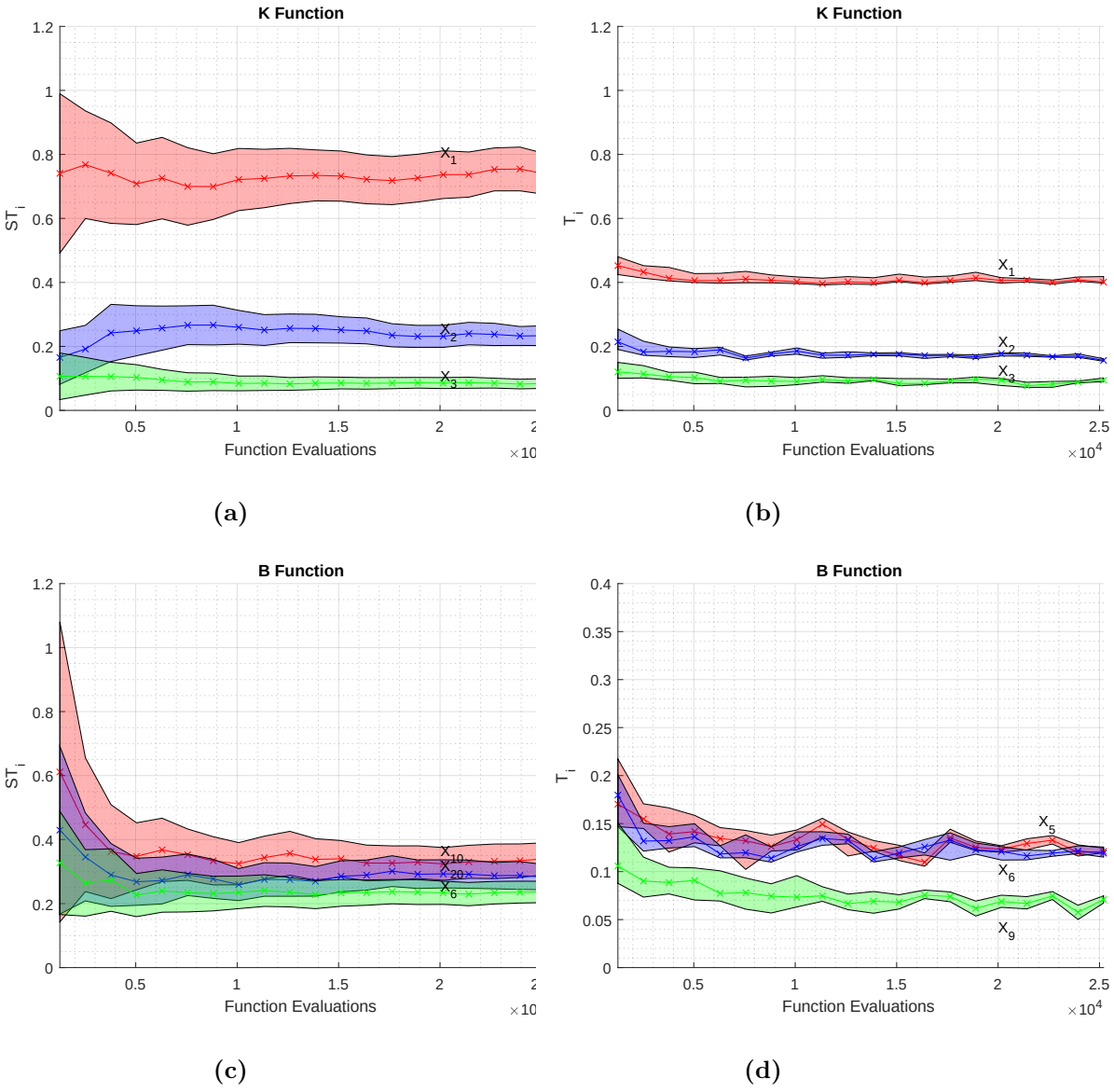

Figure 5.6: Covergence analysis for K Function (a,b) and B Function (c,d) for its three main inputs. Comparison of distribution-based T_i and Sobol S_{Ti} indices.(a,c): VBSA (b,d): distribution-based

Discussion:

From the results it is clear that the distribution-based method has an inherent high level of noise. A dummy variable X_d is considered to assess the level of noise for both

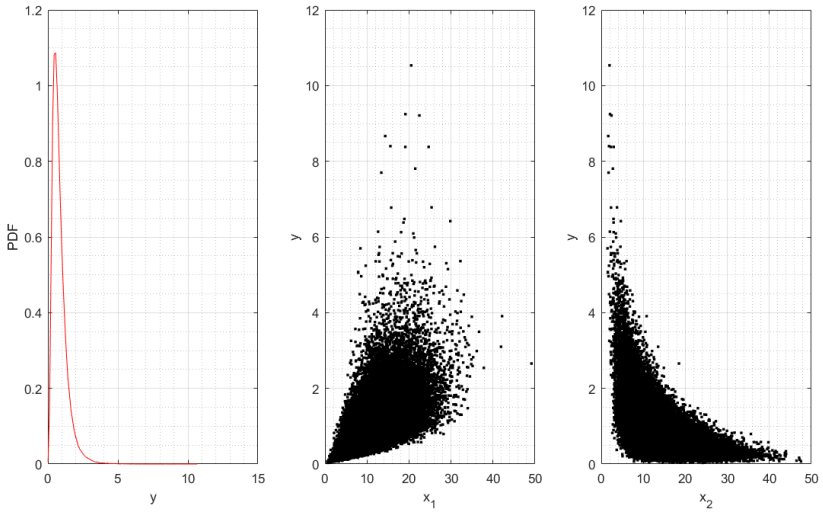

Figure 5.7: Empirical PDF of Function 6 and associated scatter plots with 100000 samples

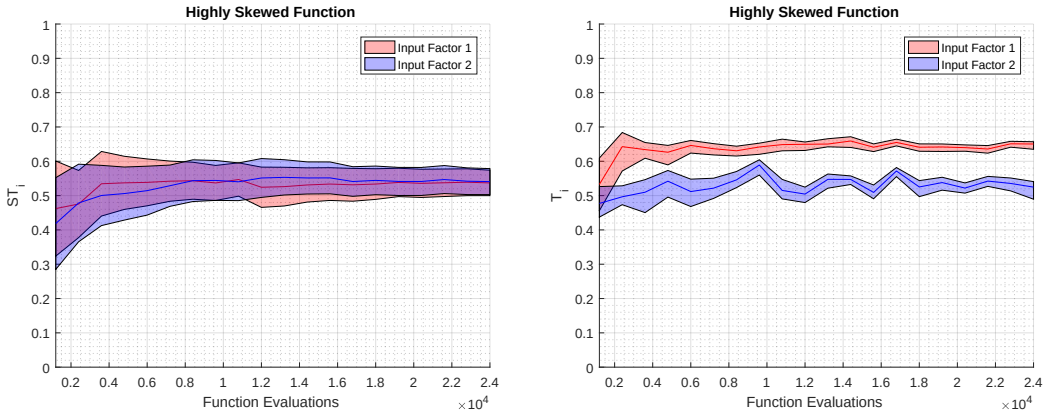

(a) **(b)**

Figure 5.8: Covergence analysis of PAWN T_i and Sobol S_{Ti} indices for a highly-skewed function. (a): VBSA (b): distribution-based

methods. When assuming a dummy variable for the VBSA method, matrix A and A_B differ in column B. If column B contains a dummy variable, then, when evaluating the response of the model y_A, this will be equal to y_{A_B}, resulting in a nil contribution to the variance, as shown in Equation 5.31. Therefore there is no inherent level of noise associated with the variance-based method.

$$\mathbf{E}_{\mathbf{X}_{\sim \mathbf{i}}}(\mathbf{V}_{X_i}([Y|X_{\sim i}]) = \frac{1}{2N}\sum_{j=1}^{N}[y({a_1}^{(j)}, {a_2}^{(j)}, ..., {a_k}^{(j)}) - y({a_1}^{(j)}, {a_2}^{(j)}, ..., {b_i}^{(j)}, ..., {a_k}^{(j)})]^2 \tag{5.31}$$

On the other hand, the distribution-based's difference between the UCDF and CCDF provides a metric as to how important an input is. Even if the two CDFs were the same - under the assumption of a dummy variable - the fact that the variable must be conditioned results into a level of noise. However, since we expect the input samples to be uniformly spread in the given dataset we may also expect the size of the conditional sample to be approximately equal to N/n. This means that the user is able to increase the resolution of the conditional sample at the expense of a higher computational cost by controlling both N and n. This rationale is tested on the Ishigami-Homma function. The level of noise is measured by the mean of the KS statistic, which is in turn based on the maximum distance of several conditioning points; this is displayed in Equation 5.32.

$$\widehat{T_{dummy}} = mean_{1,2,...,n} max|\widehat{F_y(y)} - \widehat{F_{y|x_i}(y)}| \tag{5.32}$$

Figure 5.9 shows the distribution-based indices for the three input factors of the Ishigami-Homma function. Each subplot report results for one input factor. Indices are approximated using an increasing sample size N and increasing number of conditioning intervals n. For each combination of (N,n), bootstrapping is used to estimate the 95% confidence interval (vertical line) and mean value (circle) of each distribution-based index. Dashed lines show the KS of the dummy parameter at each combination of (N,n). The number of conditioning points bears almost no effect as long as n is greater than 5; this figure has been reproduced from the work of [71], changing the Ishigami-Homma parameters as defined in the test function.

Furthermore, the computational complexity of estimating the model runs for the Sobol and distribution-based methods is displayed in Equation 5.33 and 5.34, where N is the

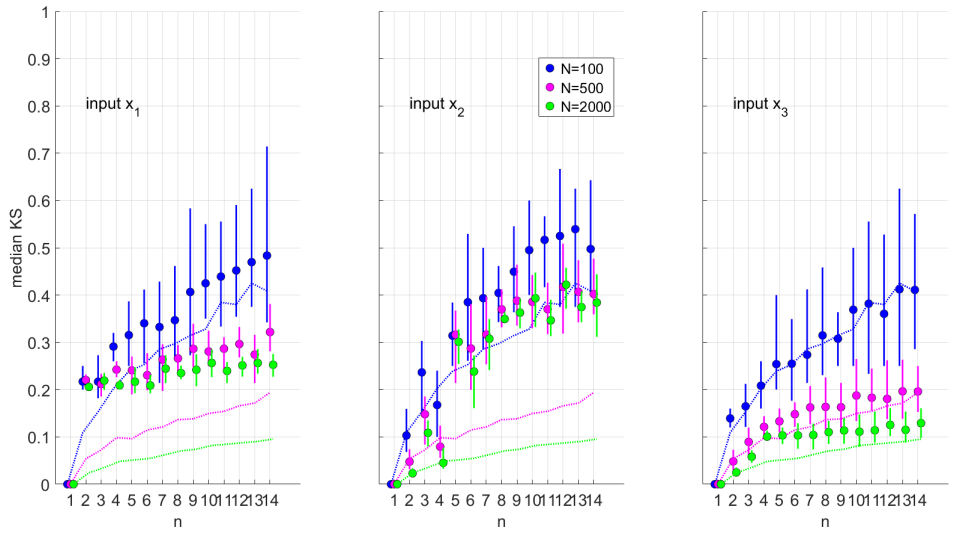

Figure 5.9: Assessing the level of noise when applying the PAWN distribution-based method to the Ishigami-Homma test function; the level of noise is displayed as a function of conditioning points n and number of samples N

number of samples and k is the number of model inputs. The number of conditioning points n for the distribution-based method does not appear in the equations below as it does not play a role in the computational complexity of the model runs. The same number of samples is used to estimate both global sensitivity indices.

$$F_{eval} = N * (k + 1) \tag{5.33}$$

$$F_{eval} = N \tag{5.34}$$

Given that the aim of this Chapter is to allow for a fair benchmark between the two methods, the total number of model evaluations has been kept the same in all the cases. One of the main advantages of the distribution-based method is that it does not require tailored evaluations of the model; in other words, given an input-output sample is possible to determine the T_i coefficients.

5.6 Conclusions

Global sensitivity analyses such as the Sobol or variance-based and distribution-based methods are widely adopted by the research community in order to identify key input drivers. However, in order for the results to be reproducible all parameters used in either method need to be provided. In addition, bootstrapping should be used to assess the confidence intervals and, where the computational complexity of the problem allows for it, a convergence analysis should be conducted. Given a set of model evaluations, the distribution-based method can be applied at no extra cost, adding value to the global sensitivity analysis and complementing the variance-based method. This Chapter's benchmarks establish a framework on how methods should be compared against each other. It also shows that while the distribution-based method can be used as a complementary approach to the variance-based, as it has the potential to characterise those probability functions that are highly-skewed or multi-modal, it fails to rank different inputs when these have different order of magnitude in their contribution of the response. This has been documented by using well-established test functions, whose analytical variances are known.

5.7 Future work

Future work will focus on adding the CDF-based measure following the ideas of Gamboa, Klein and Lagnoux (2018): "Sensitivity analysis based on Cramér–von Mises distance", which augments the Sobol' method with a CDF-based indicator [124]. Gamboa et al. investigated in 2018 the generalisation of the so-called Sobol indices to higher moments, where its index appears to be more general than Sobol as it takes into consideration the whole distribution and not the second moment.

5.8 Appendix

Analytical variances for the Ishigami-Homma function can be found in [127], whereas analytical variances for the K, B and G* functions are given in the work of [112]. This appendix includes the analytical variances for the highly-skewed test function, where

$x_1 \sim \chi^2(d_1)$ and $x_2 \sim \chi^2(d_2)$ follow chi-square distributions with d_1 and d_2 degrees of freedom.

$$y = \frac{x_1}{x_2}$$

Then, if we assume that U_1 is a chi-square distribution with d_1 degrees of freedom, U_2 is a chi-square distribution with d_2 degrees of freedom, and that U_1 and U_2 are independent. The distribution of

$$Y = \frac{U_1/d_1}{U_2/d_2}$$

is F-distributed with d_1 degrees of freedom in the numerator and d_2 degrees of freedom in the denominator. The total variance can be calculated as:

$$V(Y) = \frac{2d_2^2 \cdot (d_1 + d_2 - 2)}{d_1 \cdot (d_2 - 2)^2(d_2 - 4)} \; if \; d_2 > 4$$

Using the independence property between U_1 and U_2, the moment generating function of the chi-square distribution as well as some of the properties of the gamma function below:

$$E[U_2^{-1}] = \frac{1}{d_2 - 2}$$

$$E[X^k] = 2^k \frac{\Gamma(n/2 + k)}{\Gamma(n/2)}$$

$$\Gamma(n) = (n-1)\Gamma(n-1)$$

Total sensitivity indices S_{Ti} can be calculated as the sum of first order indices S_i together with the interactions between the two variables:

$$S_{T1} = S_1 + S_{12} = \frac{d_2 - 4}{d_1 + d_2 - 2} + \frac{2}{d_1 + d_2 - 2} = \frac{d_2 - 2}{d_1 + d_2 - 2}$$

$$S_{T2} = S_2 + S_{12} = \frac{d_1}{d_1 + d_2 - 2} + \frac{2}{d_1 + d_2 - 2} = \frac{d_1 + 2}{d_1 + d_2 - 2}$$

Chapter 6

Global Sensitivity Analysis for Offshore Wind Cost Modelling

Offshore wind costs are rapidly falling and therefore there is a need to better understand the key drivers behind these costs reductions. New environmental regulations, economic policies, technological advancements and financing structures have resulted in a set of relationships that need to be considered in order to define risks and profitability for the next generation of offshore wind farms. Simple cost models are no longer suitable to accurately represent these relationships and hence, an advanced stochastic decision-making tool for offshore wind cost modelling has been presented in Chapter 3, integrating site characteristics, technology specificities and financial modelling expertise. State-of-the-art global sensitivity analysis methods are applied to the cost modelling tool for different types of offshore wind farms, ranking the contribution of around hundred fifty parameters influencing cost and uncertainty in their design. The contribution of this Chapter will i)improve the understanding of key parameters when building a financial model for an offshore wind farm ii) guide additional efforts towards reducing the uncertainty of those key parameters to drive the financial costs down.

The aim of the current Chapter is to use the advanced stochastic cost modelling tool of Chapter 3 to investigate the most relevant parameters influencing cost and uncertainty in the design of offshore wind farms.

6.1 Case Study

A key metric for the life-cycle costs of an offshore wind project is the LCOE, defined as the discounted sum of the cash flow expenditures divided by the discounted sum of electricity production over the life span of the project. In order to calculate the LCOE, DEVEX, CAPEX, OPEX as well as DECEX need to be assessed. These costs are highly influenced by the physical characteristics of the wind farm, including but not limited to the water depth, distance from shore, wind speed and seabed conditions. Throughout the case study we consider the LCOE as the metric of interest. Therefore, we are interested in evaluating how different techno-economic model inputs affect the LCOE.

The purpose of the case study is to identify the main parameters for the development of an offshore wind farm, once an area has been awarded to the developer. For this reason, two theoretical offshore wind farms have been considered. Given that the average size of European commercial offshore wind farms commissioned in the year 2017 is 500MW[14]; the same size is chosen as a reference in our case study. The case study is based on commercial offshore wind farms with the following characteristics: site Type A is representative of UK round 2, whereas site Type B is similar to the Scottish Territorial Water and UK Round 3 sites. We have assumed that there is a trade-off between how close the farm is from shore, its water depth and the wind resource available. On the one hand, site Type A considers monopiles as the most cost-effective foundation, assuming that the seabed soil conditions are simple and drilling operations are kept to a minimum. On the other hand, Site Type B considers jackets as the most cost-effective foundation, assuming that seabed soil conditions are complex. We also assume, for the sake of simplicity, that the export cable length, construction and operational port distances are equal to the distance from shore. Another assumption is that both offshore wind projects use project finance. Both sites are to be assessed with a generic 8.3 MW wind turbine with a rotor diameter of 164m. The project specifications for those generic offshore wind farms are shown in Table 6.1 and based on a report from The Crown Estate [128].

Parameter	Site Type A	Site Type B
Water Depth [m]	25	45
Distance from shore [km]	25	35
Wind Speed @ 100m [m/s]	9	9.5
Foundation Type	Monopile	Jacket
Electrical Infrastructure	HVAC	HVAC
Wind Turbine Type	164-8.3 MW	164-8.3 MW

Table 6.1: Site Type A and B

6.2 Results

First stage - Factor Fixing

With the objective of screening out irrelevant inputs, the variance-based method (at low sample size) is applied to approximately 150 model inputs; this is described in Section 3 as the first stage GSA. A high performance computing cluster at the University of Edinburgh is used throughout the analysis to compute the total indices with 300 000 model evaluations. The same process is employed for both Type A and Type B offshore wind farms, with the only difference that Type A has 149 uncertain parameters whereas Type B has 150. The main goal of this analysis is to identify the key variables driving the response of the model as well as simplify model complexity.

Figure 6.1 shows the total contribution of factor X_i to the LCOE variation, in descending order of importance. Total sensitivity indices ST_i (small circles in blue) are estimated via Monte Carlo method (by means of the Sobol low-discrepancy sequence) for input factors X_i i = 1,...,149 for Type A (150 for Type B). 95 % confidence intervals (vertical dashed lines in blue) are estimated by bootstrapping 1000 replicas. Figure 6.1 emphasises that the cost modelling tool follows a very asymmetric distribution of importance, with few inputs accounting for most of the output uncertainty and most inputs playing little or no role. Whereas for Type A, the first five inputs add up to 98% of ST_i(whereas the rest to 1%) and the measured (P50) annual mean wind speed results in 91% of ST_i, for Type B, the first five add up to 100% of the ST_i (whereas the rest to 3%) and the measured (P50) annual mean wind speed results in 91% of ST_i. These

first five inputs are described later in the Chapter. It is worth keeping in mind that the sum of separate ST_i contributions does not typically add up to 100%, as this would only be the case for additive models - models that have no interactions between inputs. A threshold ST_i of 0.02% was established to select the relevant inputs for the second global sensitivity analysis phase: a benchmark between the PAWN distribution-based method and the variance-based method. The threshold was chosen based on a trade-off between high values running the risk of missing important inputs and low values potentially not being able to reduce the complexity of the model to a suitable level. As a result, 20 model inputs were selected for Type A and 22 for Type B. Figure 6.1 does not show the contribution of the first factor, the measured (P50) annual mean wind speed, given that it is two orders of magnitude higher than the rest and would difficult its interpretation.

Second stage - Factor Prioritisation

In order to enable a fair comparison between the PAWN distribution-based method and the variance-based method, the same number of model evaluations is considered; this is considered as the second stage of the GSA. The benchmark is carried out by taking the PAWN distribution-based method with 20 conditioning points, against the variance-based with the selected parameters from the previous analysis, resulting into approximately 300 000 model evaluations each.

The top chart in Figure 6.2 displays the total contribution of the LCOE variation due to factor X_i in ascending order of importance for the variance-based method. Total sensitivity indices ST_i (small circles in blue) are estimated via Monte Carlo method (by means of the Sobol low-discrepancy sequence) for input factors X_i i = 1,...,20. 95% confidence intervals (vertical dashed lines in blue) are estimated by bootstrapping 1000 replicas. The bottom chart in Figure 6.2 displays the total contribution of the LCOE variation due to factor X_i in ascending order of importance for the PAWN distribution-based method. Total Kolmogorov Smirnov (KS) statistics T_i (small circles in blue) are estimated via random Monte Carlo sampling. 95% confidence intervals (vertical dashed lines in blue) are estimated by bootstrapping 1000 replicas. The level of noise

for the PAWN distribution-based method (vertical dashed lines in red) is calculated by the introduction of a dummy variable. This level of noise is bootstrapped 1000 times and results into the upper and lower horizontal dashed lines in red. This means that, if the T_i was below the upper bound, we would not be able to say if this is due to the importance of the input or the level of noise of the method. The same process is repeated for Type B offshore wind farm for the 22 selected inputs and displayed in Figure 6.3.

The bottom 5 parameters in Figure 6.2 and 6.3 represent the items that contribute the most to the variability of the LCOE, and therefore what the decision maker should focus on. The reason for the difference between the variance- and distribution-based methods is explained in Chapter 5. A side-by-side comparison shows that the top 5 parameters for Type A are ranked the same for both the variance-based and PAWN distribution-based methods; these are the measured (P50) annual mean wind speed, the target equity rate of return, the default cost for generic turbine, the fraction of position requiring drilling, the minimum debt service coverage ratio and the additional time when drilling is required. This is similar for Type B, where the difference between the variance-based and PAWN distribution-based methods is reflected by swapping the fifth and 6th parameter - the additional time when drilling is required for the average installation duration for pinpiles. Further details for each of them are given below.

- Estimated (P50) annual mean wind speed:

  It is the mean wind speed that is expected to be exceeded in 50% of the estimates. It is worth noticing that this is the median mean wind speed estimate since half of the estimates are expected to be below this value and the other half are predicted to surpass it. Further information on the estimated annual mean wind speed can be found in [129] or Chapter 3.

- MARR:

  MARR is the minimum acceptable rate of return the company is willing to accept before starting a project, given its risk and opportunity cost of forgoing projects. MARR is typically defined by the company and imposed to be, at least, the IRR

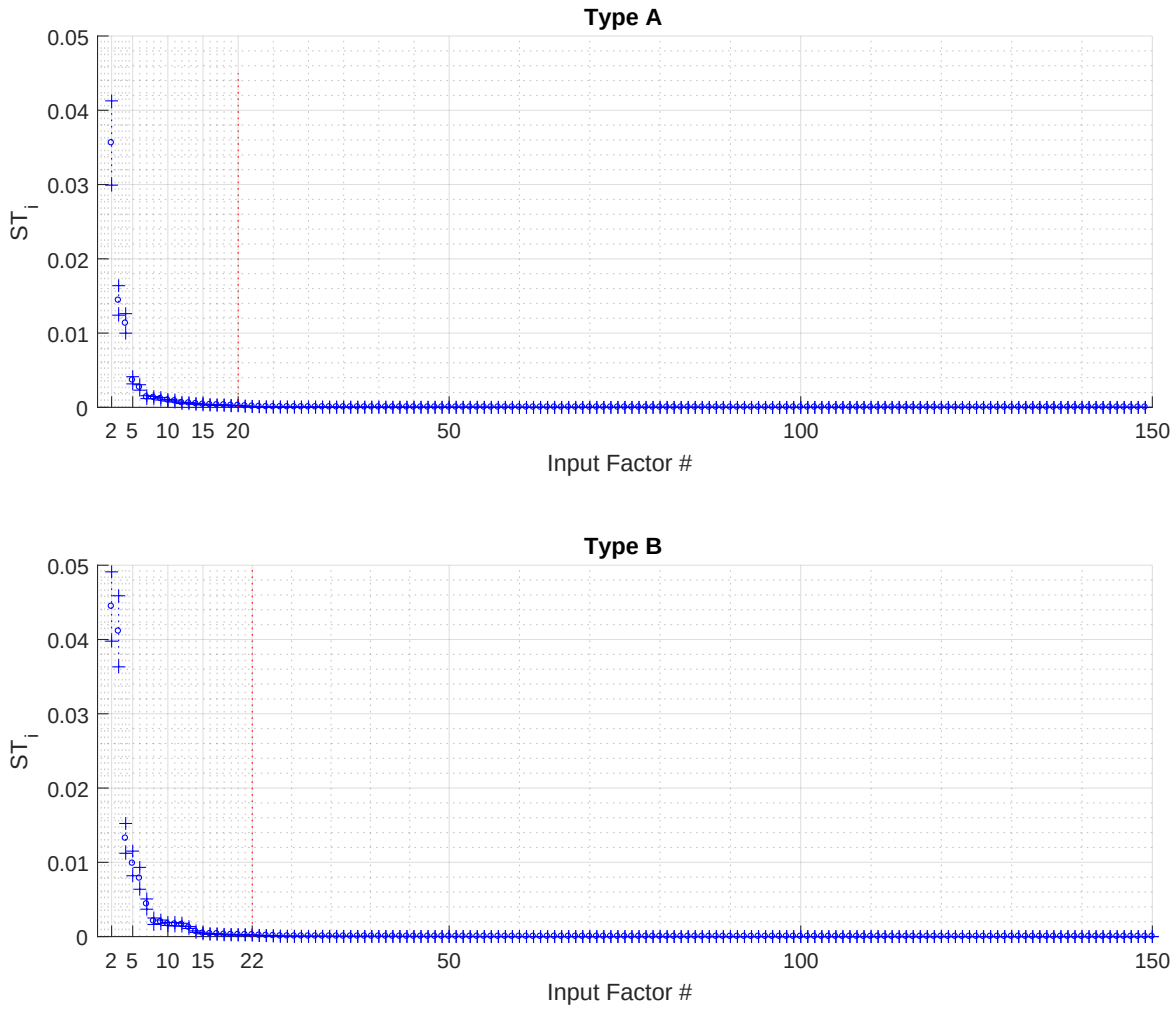

Figure 6.1: First stage global sensitivity analysis applied to OWCAT for Type A and B offshore wind farms. The graph does not show the contribution of the first factor, the measured (P50) annual mean wind speed, given that it is two orders of magnitude higher than the rest and would difficult its interpretation.

of the project. The cost modelling tool imposes a MARR to work out the LCOE. Further information on the financial modelling can be found in the "Formation of the financial module" section of [129] or Chapter 3.

- Default costs for generic wind turbine:

  Generic offshore wind turbine costs expressed as units of currency per kW.

- Fraction of position requiring drilling:

  This concerns the foundation installation part of the cost modelling tool. Foundations can be either driven or drilled depending on the soil conditions. A distinction needs to be made between Type A and Type B offshore wind farm. Whereas Type A is impacted by the use of monopiles which are highly sensitive to soil conditions, Type B uses jackets which are typically less sensitive.

- Minimum debt service coverage ratio:

  The debt service coverage ratio is defined as the cash flow available for debt service divided by the debt service. This metric is typically used in private infrastructure project debt to decide if the project generates enough cash to repay its obligation.

- Additional time when drilling is required:

  The installation time of the monopiles or pinpiles depends upon whether or not drilling is required. The model captures this feature by increasing the average installation time by an additional duration. Whereas this parameter models the additional time, the fraction of position requiring drilling accounts for the bathymetry of the offshore wind farm.

6.3 Conclusions

Global sensitivity analysis for offshore wind cost modelling provides a methodological framework to unlock further cost reductions. The methodological framework allows users to choose global sensitivity analysis techniques for offshore wind techno-economic models. A strategy to interrogate the model by means of the latest global sensitivity analysis techniques has been developed and applied to the cost modelling tool.

The results of the global sensitivity analysis highlight the importance of the mean wind speed uncertainty in the design of offshore wind farms. This piece of work was conducted in tandem with another research paper title “The effect of mean wind speed uncertainty on project finance debt sizing for project finance offshore wind farms” [129]. As it has been shown, the mean wind speed uncertainty and debt sizing parameters are

key contributors to the LCOE. Therefore this Chapter reinforces the importance of looking at both the mean wind speed uncertainty and debt sizing when project finance is considered. The results of the global sensitivity analysis also have implications on the research paper "How does risk aversion shape overplanting in the design of offshore wind farms?" [130], which ties in with how the optimal overplanting was modelled.

The following observations are drawn from the results:

- The cost modelling tool follows a very asymmetric distribution of importance, with few inputs accounting for most of the LCOE output uncertainty and most inputs playing little or no role.
- Monopile foundations are more sensitive to water depth than jackets. However, jacket offshore wind farms are very sensitive to pinpile installation times, especially when drilling is required. Even though it is well understood that wind speed and financing conditions are key drivers of offshore wind costs, other factors like the fraction of foundations requiring drilling are typically overlooked. This paper highlights the importance of the percentage of foundations that require drilling when assessing the financial viability of offshore wind farms.
- Top 6 parameters to consider when building an offshore wind investment business case are: the measured (P50) annual mean wind speed, the target equity rate of return, the default cost for generic turbine, the fraction of position requiring drilling, the minimum debt service coverage ratio and the additional time when drilling is required.

Conventional cost-based models do not have the stochastic capabilities required to conduct this analysis, and therefore, it is believed that this study will be of interest to developers, investors and policy-makers alike seeking to understand which techno-economic parameters are key when building offshore wind investment models.

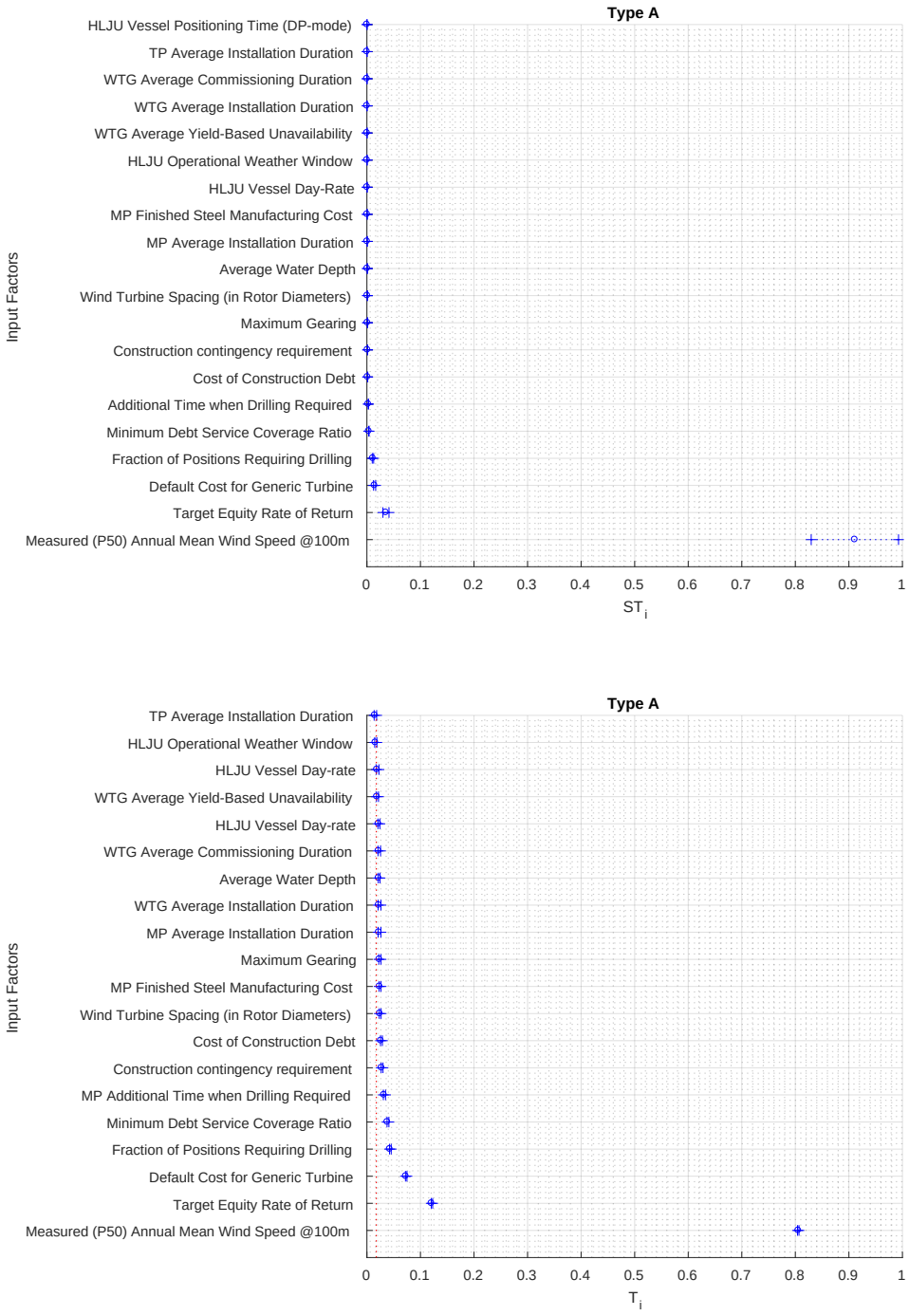

Figure 6.2: Second stage global sensitivity analysis applied to OWCAT for Type A offshore wind farm. (a)top chart: variance-based method. (b)bottom chart: PAWN distribution-based method.

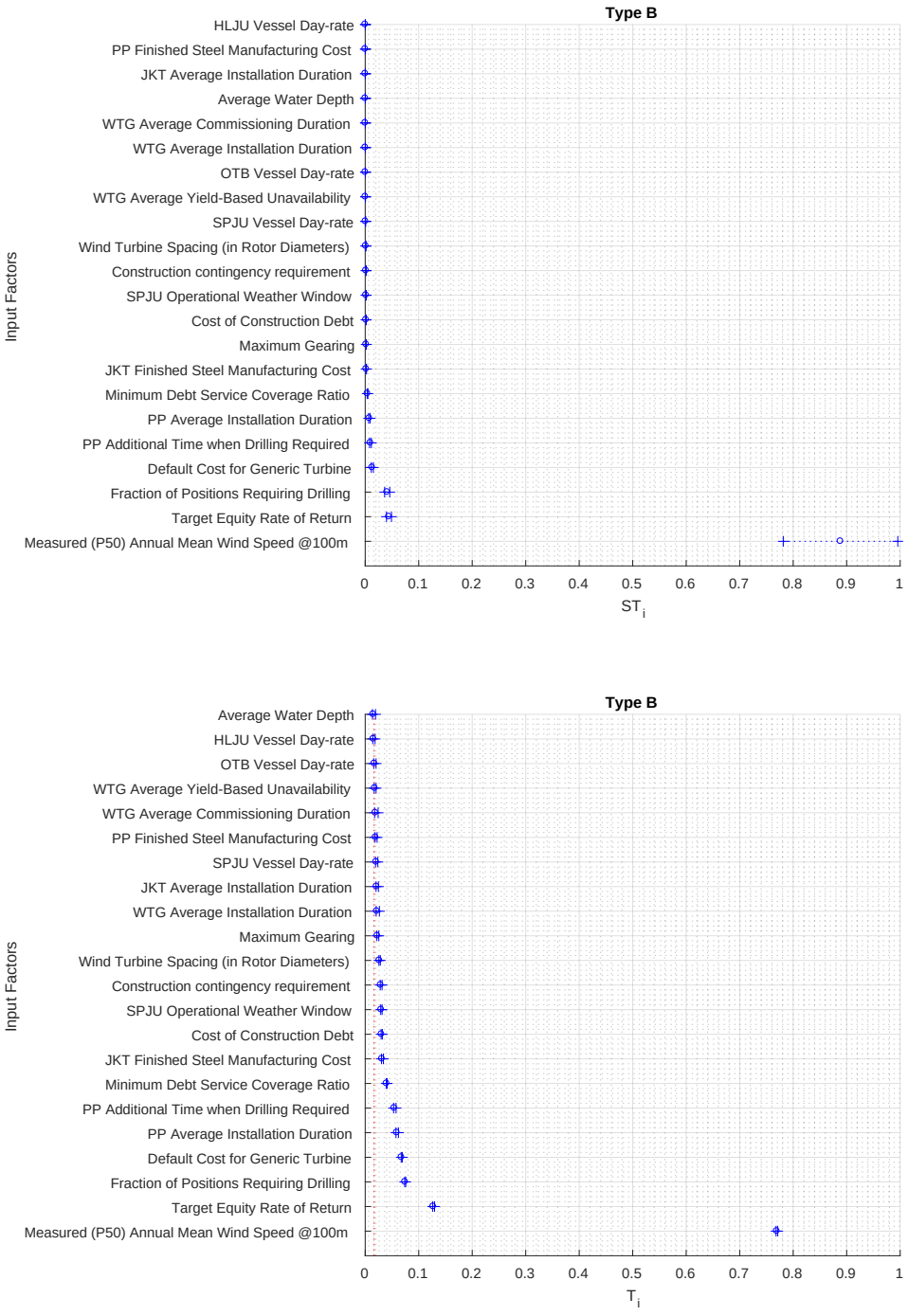

Figure 6.3: Second stage global sensitivity analysis applied to OWCAT for Type B offshore wind farm. (a)top chart: variance-based method. (b)bottom chart: PAWN distribution-based method.

Part III

Applications

Chapter 7

Mean Wind Speed Uncertainty on Project Finance Debt Sizing for Offshore Wind Farms

Financing costs for offshore projects depend, among many other variables, on the quality of mean wind speed predictions. Financial institutions determine the amount of debt that can be reasonably supported by the project, based on probabilistic cash flow metrics derived from estimated mean wind speeds. Within the offshore wind industry, it is widely believed that longer wind resource campaigns or more precise wind measurement devices that decrease mean wind speed uncertainty lead to lower LCOE values. This Chapter shows that this is not always true, while a decrease in mean wind speed uncertainty may result in better financing conditions, it typically requires higher development expenditure. We take advantage of the theoretical cost modelling framework presented in Chapter 3, which includes detailed project financing constraints, and then apply this to an industrial case study to analyse project financing of different types of offshore wind farms. We show that developers need to find the right balance between a decrease in financing costs and an increase in development expenditure. For projects limited by the maximum gearing or with an unfavourable trade-off between the development expenditure and the increased P90 annual energy production, more precise resource estimation can result in higher LCOE values.

7.1 Introduction

The importance of project finance for renewable energy projects has been highlighted in [131]. It is understood that project finance could be instrumental in increasing the availability of capital for a successful energy transition, of which offshore wind projects could benefit from. Large-scale offshore wind is often developed through stand-alone project companies, owned by the project investors. A project company, also referred to as a Special Purpose Vehicle (SPV), has its own revenues and balance sheet and therefore the ability to raise funding on its own merits. An SPV can raise two discrete categories of funding: equity and debt. In this Chapter, project finance, or non-recursive financing, is considered for the development of offshore wind farms. As the offshore wind industry grows and more banks are involved in non-recourse financing for offshore wind farms [132, 133, 14], a better understanding of how wind farms are financed and what the banks' requirements are, is needed. The financial terms offered by the lenders and the ability of the offshore wind farm to meet its financial obligations once operational depend, among many other variables, on uncertain wind-driven revenues. Given the fact that wind power varies with the cube of the wind speed, accurately and precisely determining the wind speed is of utmost importance for both developers and their bankers during the project's planning stage.

Consider a developer that wants to raise money from a bank or another financial institution in order to build an offshore wind farm. If all goes well and the project succeeds, the bank will have the loan repaid with interest. If the project exceeds its performance and generates more revenues than expected, the bank does not take any benefit from additional production - it has limited upside risk. On the contrary, if the project underperforms then the bank can lose up to the full value of the loan - it has full downside risk. Given that the bank has a limited upside but is exposed to a larger downside, it usually puts in place several mitigation measures to control the project risks, one of which is a comprehensive analysis of the wind resource assessment uncertainty. This is typically carried out before the FID and it requires a sound understanding of the uncertainty of the wind speed and energy losses in order to estimate the potential size of the debt funding that can be reasonably supported by the cash flows of the project.

Generally speaking, if the bank is satisfied with the level of confidence with which the yield has been evaluated, it might regard the value as a low uncertainty estimate and provide access to higher gearings, i.e. a higher proportion of finance that is provided by debt relative to the finance provided by equity. Since the cost of debt is cheaper than the cost of equity, developers always try to maximize the share of debt. Developers may therefore need to find the right balance between an increase in the development expenditure associated with better wind speed predictions and a decrease in the financing costs to minimise their LCOE.

The effects of mean wind speed uncertainty in project finance for offshore wind farms were first investigated in the work of Schreider [134]. A high-level study was conducted to select the optimal contract strategy for investing in an offshore wind project. Even though the study slightly touched upon mean wind speed uncertainty by considering a downside scenario with P84 instead of the P50 yield in one of the business cases, the study did not go further; it can be considered as a simple downside scenario analysis. However, wind risk has been identified as one of the fundamental pieces of technical due diligence for project finance offshore wind farms [135]. In addition, offshore wind research has devoted considerable efforts to characterise the uncertainty associated with the annual energy production, given by the inherent uncertainty in the resource as shown in [136, 137, 138] and the uncertainty in the technology [139].

Furthermore, offshore wind techno-economic models have been developed to offer a basis for objective communication and decision-making, allowing for a greater number of cases to be analysed and when considering new ideas, offering the option to assess the economic feasibility and potential. Examples of those can be found in [140, 13, 35, 141]. However, given the multidisciplinary nature of techno-economic modelling activities, studies tend to be either very detailed in the wind resource assessment part while ignoring financial valuation principles or they make use of sound financial models that do not take into consideration fundamental principles of wind resource assessment.

Thus, there is a research gap in the literature when it comes to bringing together the

wind resource assessment uncertainty and bank requirements, which have a direct impact on project finance costs. No previous literature has attempted to explain how a reduction in mean wind speed uncertainty can be translated to both an increase in the development expenditure and a reduction in the cost of financing. It is the trade-off between these two ingredients that determines their aggregated contribution to LCOE. Moreover, no previous project finance model has been published in the literature where the relationship between the P50 and P90 estimated mean wind speed is explained. This lack of analysis is probably due to the limited access to detailed industrial cost models, combining enough technical and financial expertise to be able to carry out this study.

When developing an offshore wind farm a trade-off between the wind resource assessment uncertainty and the development expenditure has to be made. That is to say, the developer has to choose a commercial sensing device (e.g. meteorological mast or FLIDAR) to deploy in order to characterize the wind resource in a given zone. The choice of one or another device determines the magnitude of the DEVEX and the uncertainty in the wind speed measurement. Within the offshore wind industry, it is widely believed that longer wind resource campaigns or more precise wind measurement devices that decrease mean wind speed uncertainty lead to lower LCOE values. But is this always the case? In other words, does the deployment of additional advanced sensing technology, which presumably reduces wind speed uncertainty, compensate for the incurred development expenditure?

The current Chapter is a first attempt to answer these questions, and to include detailed project finance constraints in wind farm planning decisions. Our focus lies on quantifying the impact of mean wind speed estimated uncertainty reduction on the LCOE of offshore wind farms. Naturally, there are many other long-term uncertainties that influence the operational, economical and financial performance of the farm, but, since wind speeds are such a crucial determinant of wind farm performance, we will leave other uncertainties aside in our quantitative analysis; however, we will briefly describe and, where possible, quantify them before moving on. Throughout, we will also assume

that the developer has a good track record of projects and that experienced contractors have been appointed; if this is not the case, banks may impose additional requirements beyond the scope of this Chapter before taking on any investment risk.

The contribution of this Chapter is the development of a novel theoretical cost modelling framework which includes, detailed considerations of financing requirements that until now have been usually ignored in the offshore wind planning models. The methodology presented here can be applied to any existing standard corporate finance cost model to account for project finance arrangements. At the same time, this cost modelling framework allows policy-makers and developers alike to assess the trade-off between DEVEX and the estimated wind speed uncertainty, leading to more informed decisions that have the potential to drive down the cost of energy.

The rest of this Chapter is organised as follows: Section 7.2 introduces the widely used concepts of P50, P90 and some fundamentals of project finance. Chapter 3 Section 3.1 described the offshore wind cost modelling tool and provided a high-level overview of its inputs, outputs and the interplay between them. Chapter 3 Section 3.9.4 described the formation of the financial module within the tool, which is a key ingredient to understand and quantify the effects of the estimated mean wind speed uncertainty in obtaining better financing conditions. Following this, engineering techniques and financial methods are brought together to understand the implications of the mean wind speed uncertainty reduction in the LCOE, as shown in Section 7.3. Finally, the findings of the Chapter are exemplified by an industrial case study throughout Section 7.4.

7.2 Project Finance for Offshore Wind Farms

The profits of an offshore wind project are wind-driven. Given the uncertain nature of the wind, developers use probabilistic metrics to characterise the wind resource at a given site; the mean wind speed is uncertain and its associated uncertainty is assumed to be normal. AEP_{p50} is associated with a P50 estimated mean wind speed $\overline{v_{P50}}$,

meaning that this is the mean wind speed that is expected to be exceeded in 50% of the estimates. It is important to highlight that this is the estimated mean wind speed and not the measured mean wind speed, which would follow a different probability distribution function such as Rayleigh or Weibull. To put it in other words, this is the median mean wind speed estimate since half of the estimates are expected to be below this value and the other half are predicted to be above it. Although this metric is typically considered from a developer's point of view when doing corporate finance, banks prefer a rather conservative approach; reasons for this are explained in Section 8.1. Thus, banks use the AEP_{p90}, which is the AEP associated with an estimated mean wind speed that is expected to be exceeded in 90% of the estimates $\overline{v_{P90}}$. The mean wind speed estimated uncertainty is assumed to be characterized by a normal probability distribution, as it is shown in the following relationship 7.1:

$$\overline{v_{PX}} = \overline{v_{P50}} - \sqrt{2} \cdot \sigma \cdot erf^{-1}\left[1 - 2 \cdot F_X\right] \forall X \in [0, 100] \tag{7.1}$$

Where σ is the given level of uncertainty expressed as a percentage of the wind speed representing one standard deviation and X is the level of exceedance requested by the bank. In particular, when looking at a level of exceedance of 90% or P90, Equation 7.1 results in:

$$\overline{v_{P90}} = \overline{v_{P50}} - 1.2816\sigma \tag{7.2}$$

Figure 7.1 shows the relationship between a $\overline{v_{P50}}$ of 9 m/s and its associated $\overline{v_{P90}}$ for a given σ of 4%, 6%, and 8%. Reducing the uncertainty increases the $\overline{v_{P90}}$ value as well as the AEP_{p90}.

The AEP uncertainty, represented by its probability distribution function, is determined by propagating the mean wind speed estimated uncertainty together with the uncertainty in the energy factors. However, given the scope of the Chapter, the energy factors have been held constant throughout the study and considered as known techno-economic assumptions (for instance, X% availability, Y% wake effect losses, Z% electrical losses). This means that the normality hypotheses assumed for the wind speed

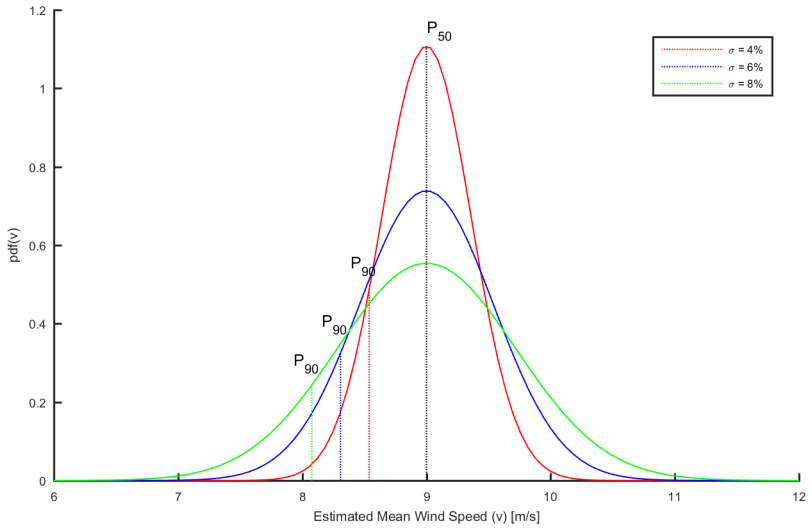

Figure 7.1: Relationship between P50 and P90 estimated mean wind speeds for different uncertainties

uncertainty are not applied in the energy factors. In this way, the uncertainty is propagated from the mean wind speed to the AEP based on these known techno-economic assumptions.

Debt sizing determines the maximum amount of project finance debt that an offshore wind farm can sustain based on the banks' requirements. Project lenders usually determine the borrowing capacity on the basis of debt service ratios and covenants. Covenants are restrictions that specify certain limitations, such as the size and use of the loan. Financial institutions have to have an idea of the amount of debt that can be reasonably supported by the project and typically base their limitation on probabilistic metrics such as the P50 and P90 mean wind speed. That is the reason why uncertainty plays a key role in determining the amount of debt.

In project finance, the most common debt service ratios are the Debt Service Coverage Ratio and the maximum gearing. While the gearing is expressed as a percentage of the total project debt the owners are allowed to take on, the DSCR is defined as the Cash Flow Available for Debt Service divided by the debt service (which is calculated as the

principal $P_{(t)}$ plus interest $I_{(t)}$) for any given period t. DSCR metrics are typically used in private infrastructure project debt [142], in particular in offshore wind projects [143]. Financial institutions might then decide upon the lower debt size resulting out of the two debt-sizing techniques [144]. They also determine what CFDAS is its mean wind speed estimate based on; typically a P50 or P90 mean wind speed. In this Chapter it is assumed that CFDAS is based on P90 cash flows, that is to say, cash flows based on a P90 mean wind speed.

The notion of deriving the debt repayments together with the debt size in order to meet a single or multiple DSCR ratios is known as debt sculpting. When sculpting debt, principal repayments are being manipulated so that the total debt service matches the CFDAS for any given period. As a consequence, the DSCR follows the desired target profile. By increasing the DSCR target, debt repayments are reduced in each period, but the last. As debt repayment are reduced, the span of time needed to fully repay the debt increases, which looks appealing from the sponsor point of view. On the other hand, lower DSCR targets increase repayments, resulting in the debt being repaid earlier. The limiting DSCR is given by the bank in conjunction with a constraint in the maximum gearing, since the debt has to be repaid within the debt tenor. When assuming a constant DSCR target, the following Equation 7.3 holds for every cash flow period t:

$$DSCR = \frac{CFADS_{(t)}}{P_{(t)} + I_{(t)}} \ \forall t \tag{7.3}$$

From Equation 7.3, it is seen that, if this is true for every time period, the sum of the cash flows follows the relationship displayed in Equation 7.4, where k is the number of cash flow periods. Thus, by limiting the amount of gearing that a project can take on, a new DSCR is obtained, shown in Equation 7.5.

$$DSCR = \frac{\sum_{t=1}^{k} CFADS_{(t)}}{\sum_{t=1}^{k} P_{(t)} + \sum_{t=1}^{k} I_{(t)}} \tag{7.4}$$

$$DSCR = \frac{\sum_{t=1}^{k} CFADS_{(t)}}{gearing \cdot debtservice} \tag{7.5}$$

This means that the minimum DSCR target used in the financial calculation should be the minimum of the one imposed by the bank, which we define as $DSCR_1$, and the one calculated based on Equation 7.5, which we define as $DSCR_2$. Therefore, the resulting DSCR of a project is displayed in Equation 7.6.

$$DSCR = min(DSCR_1, DSCR_2) \tag{7.6}$$

If $DSCR_2$ is higher than $DSCR_1$, the debt cannot be repaid before maturity; that is why the minimum of the two DSCRs is used in the financial calculation. For a developer, the lower the DSCR, the better the offshore wind investment is, as the DSCR measures how many times the cash flows after debt service can repay the scheduled debt service.

The approach taken so far consisted of explaining how a limitation in the maximum gearing is reflected into the DSCR in order to be able to take the most restrictive covenant based on a DSCR criteria. This can also be done based on a gearing criteria. A maximum gearing is given by the bank, so we can now find an equivalent gearing given by a DSCR condition, following the same rationale explained in Equation 7.5. This relationship is shown in Equation 7.7.

$$gearing = \frac{\sum_{t=1}^{k} CFADS_{(t)}}{DSCR \cdot debtservice} \tag{7.7}$$

As a consequence, if we define the maximum gearing imposed by the bank as $gearing_1$ and the maximum gearing given a DSCR condition based on Equation 7.7 as $gearing_2$, the resulting gearing for a project is obtained from the most restrictive covenant, shown in Equation 7.8.

$$gearing = min(gearing_1, gearing_2) \tag{7.8}$$

In addition, bank requirements for different types of infrastructure asset classes such as offshore wind projects evolve with time. It is well understood that the risks involved when building, commissioning and operating an offshore wind project are reflected in the cost of capital. In this regard, the offshore industry has entered a maturation phase and a strong group of actors has emerged. These range from developers to independent power producers, from institutional banks to commercial banks, from suppliers of wind turbines to cables. Over the last few years, this strong group of actors has acquired experience and knowledge about what it takes to bring a project to commissioning or to deal with the marine construction risk. All of this supported by a strong track record of projects being delivered on time and on budget. As these risks are being better understood by the financial institutions and there is a strong track record of successful projects, the bank requirements are being reduced. This maturation phase of the sector is reflected in better financing conditions as shown in Table 7.1.

Period	Gearing	Maturity post-completion	Pricing in basis points (bps)
2006-2007	60:40	10-15 years	150-200 bps
2009-2011	65:35	10-15 years	300 bps
2012-2013	70:30	10-15 years	300-375 bps
2014-2015	70:30	10-15 years	200-250 bps
2016-2017	75:25	15-17 years	150-225 bps

Table 7.1: Typical project finance conditions for offshore wind farms from 2006 to 2017 [145]

Typical DSCR constraints are now 1.50 with P50 and 1.30 with P90. This arises from the fact that financial institutions see no or very limited price risk on the revenue side, a net availability in the 92-95% range, conservative operation and maintenance cost assumptions and a full insurance package included [146].

The modelling approach and the formation of the financial model has been described in Chapter 3.

7.3 Relationship between Mean Wind Speed Estimated Uncertainty and Debt Sculpting

This section builds on Section 3.9.4 to derive some theoretical relationships between the mean wind speed estimated uncertainty and the debt sculpting, which gives rise to the curves depicted in Figure 7.2. Figure 7.2 is used as a reference figure for this section. Let us put aside the red lines for the moment. The top right chart shows the relationship between the DEVEX and the uncertainty in the mean wind speed. Longer wind campaigns and the use of more precise sensing devices allow for a reduction in uncertainty; however, this comes at a cost. A met mast is much more expensive than a Floating LIDAR (FLIDAR), which in turn is much more expensive than mesoscale modelling. However, mesoscale modelling is much less precise than a FLIDAR, which itself is less precise than a met mast. In general, higher development expenditure results in a decrease in uncertainty. Also, in general, uncertainty is dependent on the quality of the resulting data and the successfulness of the campaign. However, for the sake of simplicity, it is assumed that all campaigns are equally successful, with high availability of data.

The top left chart shows the theoretical relationship between the AEP_{P90} and the uncertainty in mean wind speeds. As the uncertainty decreases, the v_{P90} and the AEP_{P90} increases. This relationship is a direct consequence of what has been displayed in Figure 7.1, where a smaller σ would give higher values of v_{P90}. It is worth keeping in mind that all the other factors affecting the AEP have been kept constant here.

Two constraints imposed by banks are applied: the maximum gearing and the DSCR. For further details and description of these terms, see Section 7.2. Consider an offshore wind project for which the binding constraint on debt sizing is the DSCR. As we have seen in the previous section, a limitation on the DSCR can be translated into a limitation on the gearing. If the gearing obtained by the DSCR is lower than the maximum gearing allowed by the bank, this means that extra money could be lent if the CFADS increased. The CFADS is directly related to the wind speed uncertainty as the revenue

stream calculated by the banks is based on a AEP_{P90}. Consequently, when the mean wind speed estimated uncertainty is reduced, a higher CFADS becomes available, and this in turn increases the gearing. The bottom left chart shows the relationship between gearing and uncertainty in the estimated mean wind speed. As can be seen in the same chart, the project reaches a point where a further reduction in uncertainty does not give rise to a higher gearing - this uncertainty threshold is defined as U^*. Reaching U^* means that the maximum gearing has been met.

The bottom right chart combines the rest of the charts to calculate the LCOE as a function of the mean wind speed uncertainty. This chart can be divided into two regions. The first region has values of uncertainty higher than U^*. In this case, a higher development expenditure gives rise to a reduction in uncertainty, which increases the AEP_{P90}. That means that a higher gearing can be obtained, decreasing the LCOE. In the second region, to the left of U^*, higher development expenditures also lead to higher AEP_{P90}. However, in this case, since the project is limited by the maximum gearing, no extra gearing is reached. As we reduce the uncertainty further there is an increase in the development expenditure but this does not lead to more favourable financial conditions. The LCOE therefore increases as mean wind speed uncertainty is reduced.

In the above, U^* is the optimal level of uncertainty. However, for some projects, it may be optimal to choose a higher level of uncertainty, depending on how sensitive variations or incremental costs and aep values are to uncertainty. As an example, consider the red lines in Figure 7.2. These exemplify a project not limited by the maximum gearing. For this project, an increase in the DEVEX still leads to an increase in the AEP_{P90}. As a result better financing conditions are reached. But despite this, the LCOE reaches an optimal before the maximum gearing is obtained. The reason for this may be, for instance, that the increase in DEVEX is not compensated by the estimated resource.

In this case, $U_2^* > U^*$ is the optimal amount of uncertainty. In general, whatever the characteristics of the sensitivities of DEVEX and financing costs to uncertainty, it is never optimal to reduce uncertainty below U^*. This conventional wisdom that better

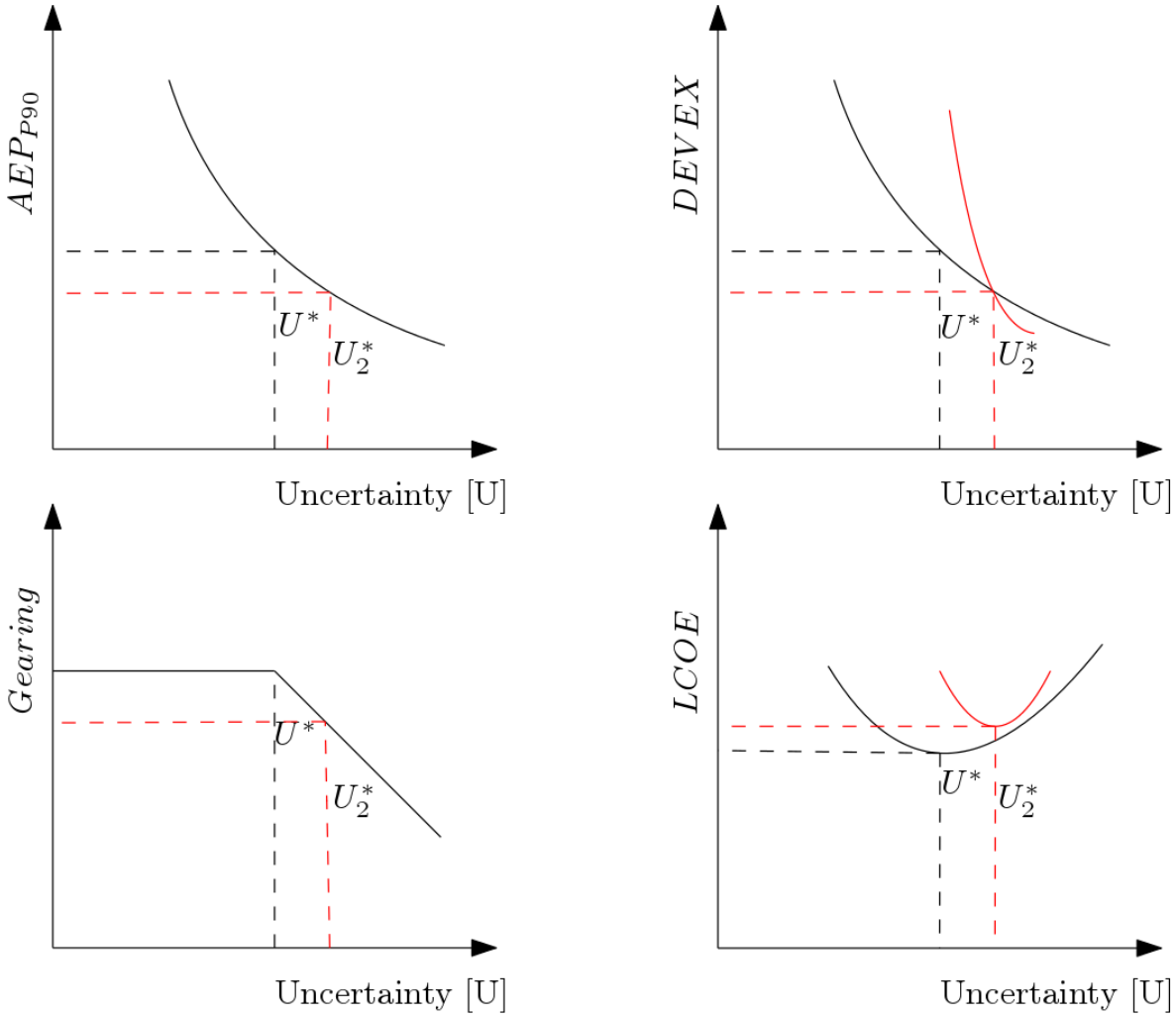

Figure 7.2: Theoretical AEP_{P90}, DEVEX, Gearing and LCOE curves for different values of mean wind speed uncertainty, all the other factors being equal.

mean wind speed predictions are always worth the increased development expenditure is not true. The next section considers cost modelling for real offshore wind farm projects, where these relationships in Figure 7.2 are investigated.

7.4 Case Study

The case study consists on selecting the sensing device that minimises the LCOE, which is a real-world problem faced by developers in the offshore wind industry. The average size of European commercial offshore wind farms commissioned in the year 2017 is 500 MW [132]; we therefore chose the same size as a reference in our case study. The case study is based on three commercial offshore wind farms with the following characteristics: Project A represents our reference offshore wind farm, which is representative of UK round 2 offshore wind projects. Project B represents an offshore wind farm located near the coast, meaning that only a relatively small amount of CAPEX is required to develop the project. However, it is assumed that the site has a poorer wind resource. Finally, Project C represents an offshore wind farm located very far from shore. Project C has a high CAPEX, but it also has access to higher wind resource than previous A and B projects. To some extent, Project C is representative of German offshore wind farms. All projects are assessed with a generic 8.3 MW wind turbine with a rotor diameter of 164 m. In reality, different turbine models would be used for different conditions, changing the turbine CAPEX even for the same installed capacity. However, for the sake of this analysis, we've assumed the same turbine model. We also assume, for the sake of simplicity, that the export cable length, construction and operational port distances are equal to the distance from shore. Whereas Project A and B wind turbines are commissioned atop monopile foundations, project C uses jackets due to water depth requirements. The project specifications of the offshore wind farms are shown in Table 7.2.

The modelling approach to offshore wind cost analysis presented in this Chapter is based around OWCAT developed at the EDF Energy R&D UK Centre. Further information on the tool can be found in Chapter 3 (overview in Section 3.1) as well as [72]. The only parameters that are modified within the tool are the development expenditure and the

Parameter	Project A	Project B	Project C
Water Depth [m]	25	15	40
Distance from shore [km]	25	15	100
Wind Speed @ 100m [m/s]	9	8	10
Foundation Type	Monopile	Monopile	Jacket
Electrical Infrastructure	hvac	hvac	hvac
Wind Turbine Type	164-8.3 MW	164-8.3 MW	164-8.3 MW
CAPEX [2015/kW]	2600	2500	3300
opex [2015/kW/yr]	85	80	100

Table 7.2: Project A, B and C specifications

uncertainty in the estimated mean wind speed (apart from the site specifications for the different cases). All other uncertain parameters such as the availability of the offshore wind farm, wake losses, are assumed to be the same in all three cases. We also assume that the availability of the offshore wind farm does not depend on the distance from shore, and therefore, that the technical performance of project A, B and C is similar.

In order to reflect the recent changes in financing conditions displayed in Table 7.1, we consider two scenarios. The first scenario assumes a gearing representative of the period between 2014 and 2015 (70:30). A second scenario is representative of more recent gearings (75:25).

The aim of the current Chapter is to reflect the changes of the mean wind speed estimated uncertainty in the LCOE, and not to analyse detailed site-specific uncertainties. In consequence, the emphasis has been placed on the choice of measurement devices, which developers face once a site has been selected. Individual devices are assumed to be deployed in the centre of the offshore wind farm so as to avoid comparisons that

favour horizontal extrapolations above others. In this case study, the developer considers the following available options to assess the wind speed of projects A, B and C. A Hub Height Met Mast (HHMM), a Below Hub Height Met Mast (BHHMM) that has a shorter mast than HHMM, a HAFLIDAR, a LAFLIDAR and Mesoscale modelling are assumed. Mesoscale modelling is considered as a service provided to the developer. Table 7.3 shows the respective costs of these methods. The difference between HHMM and BHHMM is the cost of having a taller mast, which allows wind speeds to be measured closer to hub height. The difference between HAFLIDAR and LAFLIDAR is their degree of precision. The developer may opt for a cheaper and less precise device or for a more expensive and precise one.

Cost [£m 2017]	**HHMM**	**bHHMM**	**HAFLIDAR**	**LAFLIDAR**	**Mesoscale**
DEVEX	10	9	1.2	1	0.15

Table 7.3: Development expenditure for the different wind measurement campaigns

These cost estimates have been derived from [147] [148] [149][150][151] as well as from discussion with experts in the field of wind resource assessment. If bigger offshore wind farms were to be analysed, then economies of scale in the cost of the devices should be considered as reflected in [152].

In order to represent current technology trends, and given that the first offshore wind project to be built using the AEP_{P90} on wind resource data from a Floating LIDAR was Burbo Bank Extension in the UK, in 2014 [153], two different types of Floating LIDAR are considered in this study. According to the Carbon Trust Offshore Wind Accelerator [151], a pre-commercial LIDAR has an indicative measurement uncertainty range between 4 to 7%, whereas a commercial one can achieve a range between 2 to 4%. The Floating LIDAR industry has benefited from research and development programmes and has reached the commercialisation stage [154][155] [150]. This is the reason why two commercial LIDARs are considered. More recently, it was announced that AXYS FLIDAR met the commercialisation stage of the Carbon Trust Offshore Wind Accelerator [156], meaning that uncertainties between 3 and 4% in instrument accuracy for a

Floating LIDAR is a sensible choice according to the current state of technology.

A section on the classification and description of wind speed uncertainties is out of the scope of this research Chapter, however wind speed uncertainties have been estimated based on the classification provided by DNV GL [157] [136] and [150] as well as discussions with industry experts. Those values are displayed in Table 7.4. The different site-specific uncertainties for A, B and C are shown in Table 7.5 and are independent of the device. Table 7.6 shows the devices ordered in terms of total precision, HHMM is the most precise one (4.25%) and Mesoscale the less precise (10.84%). All uncertainties are expressed as a percentage of the standard deviation of the mean wind speed and are combined by assuming they are independent and normally-distributed.

The relationship between cost and mean wind speed estimated uncertainty for the different campaigns is given in Figure 7.3. It is shown that this relationship follows a negative concave trend hypothesised in Section 7.3 on the top right of Figure 7.2.

Uncertainty [%]	**HHMM**	**bHHMM**	**HAFLIDAR**	**LAFLIDAR**	**Mesoscale**
Instrument Accuracy	2	2	3	4	10
Measurement Interference	1.5	1.5	0.5	0.5	0
Data Quality & Metadata	1	1	1	1	0
Vertical Extrapolation	0	1	0	0	3
Horizontal Extrapolation	1.5	1.5	1	1	0
Total Wind Speed Measurement	3.08	3.24	3.35	4.27	10.44

Table 7.4: Breakdown of the device-specific uncertainties for the different measurement campaigns, based on DNV GL [158], [136] and [150]

In addition, two scenarios are assumed with different gearing regimes, that reflect a reduction on the perceived risk from financial institutions when investing in offshore wind.

Description for A, B and C Projects	Uncertainty [%]
Representativeness of Data Period	1.5
Consistency & Quality of Reference Data	1
Correlation	0.5
On-site data	0.5
Wind Frequency Distribution - Past	0.5
Wind Frequency Distribution - Future	0.5
iav of the Wind - Future	1.5
Climate Change	1.5
Total Site	2.92

Table 7.5: Breakdown of the site-specific uncertainties for the different measurement campaigns [158]

Uncertainty [%]	HHMM	bHHMM	HAFLIDAR	LAFLIDAR	Mesoscale
Total Wind Speed	4.25	4.36	4.45	5.17	10.84

Table 7.6: Breakdown of the total uncertainties for the different measurement campaigns

7.4.1 Scenario 1: Maximum gearing of 0.70

Figure 7.4 shows the first set of results, assuming 0.70 maximum gearing. All charts show the relationship between the uncertainty in the estimated mean wind speed (on the horizontal axis), the gearing (the right vertical axis) and the LCOE (the left vertical axis) for all three projects. The continuous black line depicts the gearing for different levels of uncertainty, whereas the dashed red line highlights the lowest LCOE that can be achieved in each project.

Starting off with the Mesoscale Modelling campaign on the right in all three projects,

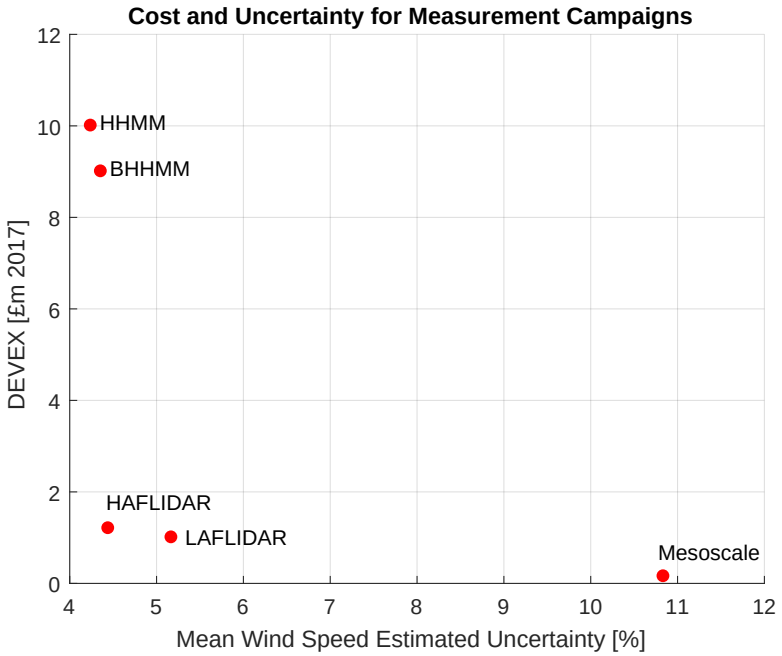

Figure 7.3: Relationship between DEVEX and Wind Speed Measurement Uncertainty for Different Wind Measurement Campaigns

none of the projects are limited by the gearing and hence a further reduction in uncertainty may lead to a reduction in financing costs that more than compensates the higher development expenditure. In all projects, using LAFLIDARs allows the developer to reach the point where projects become limited by the gearing. Although HAFLIDARs are more precise than LAFLIDAR, they are not the optimal choice, since the further reduction in uncertainty they achieve do not decrease financing costs, while they do increase development expenditure.

In all cases, the optimal device is the LAFLIDAR. A slightly higher LCOE is obtained by using a HAFLIDAR. The slopes of maximum gearing are affected by the type of offshore wind farm. Higher wind resource results in flatter slopes for the maximum gearing, whereas poor wind results in steeper slopes. Project B has a lower CAPEX and lower wind resource than the other projects. For this reason, the maximum gearing of the project is achieved with a lower uncertainty, since the effect of improving financing conditions by reducing the uncertainty is weaker. Project C, with high CAPEX

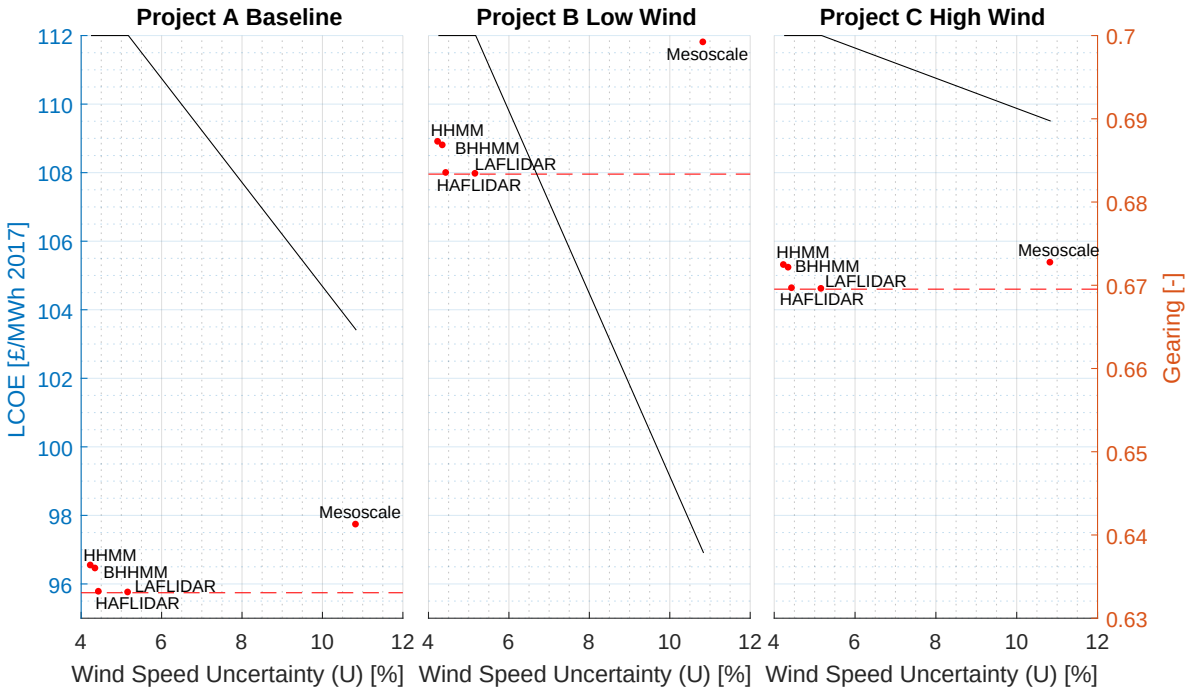

Figure 7.4: Project A, B and C relationship between Uncertainty, Gearing and LCOE for a maximum gearing of 0.70

and a high wind resources, achieves maximum gearing at a higher uncertainty, since the effect of improving the financing conditions by reducing the uncertainty is stronger – for the same level of uncertainty, a higher level of production can be obtained.

7.4.2 Scenario 2: Maximum gearing of 0.75

Figure 7.5 shows the results of a similar exercise, but with a more recent gearing of 0.75. As above, all charts show the relationship between the uncertainty in the estimated mean wind speed (on the horizontal axis), the gearing (the right vertical axis) and the LCOE (the left vertical axis) for all three projects. The continuous black line depicts the gearing for different levels of uncertainty, whereas the dashed red line highlights the lowest LCOE that can be achieved in each project.

The main difference with the previous results is that the point where project A becomes

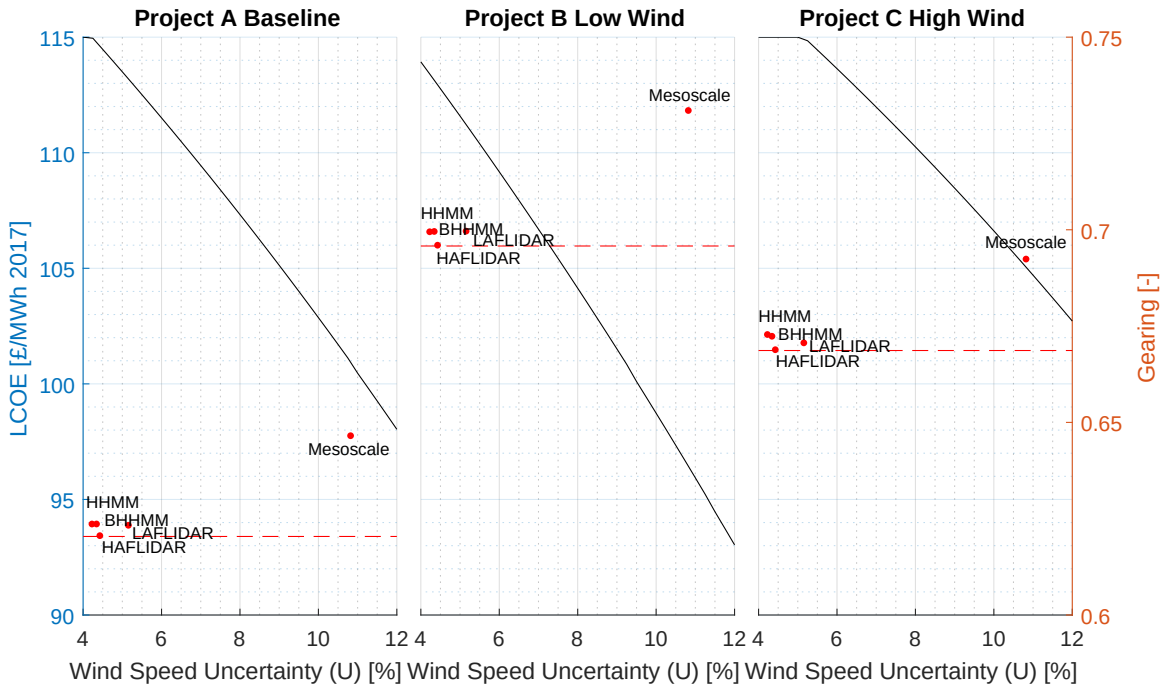

Figure 7.5: Project A, B and C relationship between Uncertainty, Gearing and LCOE for a maximum gearing of 0.75

limited by the gearing has moved from the LAFLIDAR to the BHHMM. However, given the unfavourable trade-off between uncertainty and DEVEX, the HAFLIDAR is the optimal choice - more precise resource estimation is not worth the high costs associated with a BHHMM. . Project B, characterized by a poor wind resource, also does not reach maximum gearing, with the HAFLIDAR being LCOE optimal. In both cases, this happens because of the steep slope of the trade-off between DEVEX and uncertainty as displayed in Figure 7.3. If the developer wants to slightly reduce the uncertainty from HAFLIDAR, a very large increase in DEVEX is incurred. In Project C the maximum gearing of the project is achieved with a higher uncertainty, since the effect of improving the financing conditions by reducing the uncertainty is stronger, and therefore the project also reaches its minimum LCOE with a HAFLIDAR.

7.5 Conclusions

We have shown that offshore wind projects can be categorised into two different types, based on project finance conditions. The first type is limited by the DSCR, whereas the second is limited by the maximum gearing offered by the bank. For projects limited by the maximum gearing the costs of decreasing mean wind speed uncertainty only increase the LCOE, whereas for projects limited by the DSCR the effect of decreasing the LCOE depends on the trade-off between the DEVEX and the mean wind speed estimated uncertainty. This is represented in Figure 7.3 and more theoretically on the top right of Figure 7.2. This means that it is never optimal to reduce uncertainty as far as possible, as it is commonly believed in the industry.

In a realistic case study, based on validated industrial data, we have further explored this effect. Interestingly, this case study suggests that it is not optimal to use met masts to obtain the most reliable mean wind speed estimates. Commercial LIDARs are optimal in all cases, highlighting the maturation phase of this technology. Differences between different offshore wind farms specifications are reflected in the slope of the gearing and the point at which maximum gearings are reached. High wind resource offshore wind farms will have higher gearings than other average-wind farms for the same level of uncertainty. Conversely, poor wind resource offshore wind farms may not reach the gearing limit or reach it for smaller levels of uncertainty than average-wind farms.

In addition, the maximum gearing has a big effect on the financial conditions and on optimal wind speed estimation techniques. As we have seen, the maximum gearing is increasing, as banks are becoming more familiar with offshore wind projects. This means that additional measurements become more valuable. In our case study, the optimal device for a maximum gearing of 0.75 is the more precise and expensive HAFLIDAR, whereas for a gearing of 0.70 it is the cheaper and less precise LAFLIDAR. This illustrates that a detailed understanding of project finance constraints is necessary to optimally plan and execute offshore wind projects.

This Chapter has presented the development of a novel theoretical cost modelling framework which includes detailed considerations of financing requirements that until now have been usually ignored in the offshore wind planning models. The methodology presented here links these financing requirements such as the DSCR and the maximum gearing to the cash flow metrics, while considering the development expenditure incurred in choosing a wind speed measurement device and its mean wind speed estimated uncertainty represented by the P50 and P90 metrics. This methodology can be applied to any existing standard corporate finance cost model to account for project finance arrangements. At the same time, this cost modelling framework allows policymakers and developers alike to assess the trade-off between DEVEX and the estimated wind speed uncertainty, leading to more informed decision that have the potential to drive down the cost of energy.

It has been assumed in this study that the DSCR metric is based on P90 cash flows. However, in reality, projects might be evaluated against two DSCRs metrics based on P50 and P90 cash flows; this imposes an additional constraint. Further work should include the ability to incorporate these two constraints as well as a description of the different uncertainties that characterise the mean wind speed and energy factors. In addition, the sensitivity of these conclusions should be tested when using different sets of industrial data.

Chapter 8

Overplanting Offshore Wind Farms

To date the connection of offshore wind farms is subjected to a Maximum Export Capacity (MEC) set in their connection agreement with the Transmission System Operator (TSO). Generators can export up to their contracted MEC, with any additional generation curtailed by the TSO. However, the share of time an offshore wind farm is generating at its MEC tends to be low. Overplanting the offshore wind farm by installing a higher wind farm capacity compared to the fixed electrical infrastructure can result in better overall economics, but because wind speeds and wind farm component availabilities are uncertain, there are trade-offs between the probability of additional revenue produced by capturing more wind and higher capital costs of over-installation of turbines. Nevertheless, there is enough evidence to suggest that overplanting can lead to further cost reductions in the maturing offshore wind sector. The percentage of time an offshore wind farm operates at its MEC is an indication of the extent to which the asset can profit from higher transmission utilisation rates. This Chapter provides a framework to assess overplanting when developers, policy-makers or regulatory bodies are confronted with trade-offs between cost and uncertainty. The Chapter sheds light onto which sites and technology-specific factors make overplanting a viable option. Finally, the findings of the Chapter are exemplified by an industrial case study where several offshore wind farms configurations are analysed.

8.1 Introduction

The connection of offshore wind farms is subjected to a maximum export capacity (MEC) set in their connection agreement with the Transmission System Operator (TSO). Generators can export up to their contracted MEC, with any additional generation curtailed by the TSO. For this reason, it has been common practice to size the capacity of offshore wind farms to its MEC, even though the majority of the time they are not generating at full power. Little thought has been put into designing offshore wind farms which optimise its farm capacity in regard to the fixed electrical connection capacity. In this Chapter, overplanting is defined as the process of installing additional wind farm capacity compared to its MEC.

In 2008, while planning the UK Offshore Wind Round 3, it came to the attention of National Grid that installing a higher installed generating capacity than the connection capacity could result in better overall economics for the development of offshore wind farms despite power being constrained at generations peaks [159]. In that report, a high level study was undertaken in Appendix 1 where 12% overplanting was suggested as an optimal setup, which meant that 1200 MW of offshore wind should be built for 1000 MW of grid connection. The report also looked at the sensitivity of ratio of connection costs to installed wind turbine costs, average wind speed and wind turbine availability. The findings of the study showed that (i) as the cost ratio increases there's an asymptotic trend for the optimum size of the wind farm towards 111%, (ii) as the average wind speed increases there is little change in the optimum size, but if the mean wind speed is less than 9 m/s then the optimum size increases in order to maximise the utilisation of the available capacity and (iii) as the percentage of the wind turbine availability decreases, the installed capacity needs to increase to maximise the utilisation of the available capacity. Although this was a high level study and some of the assumptions are a bit conservative at the current state of the offshore wind sector, it opened up further points for analysis.

In 2011, The Irish Commission for Energy Regulation (CER) published a report where generators were allowed to overplant their onshore wind farm capacity up to 5%, value

driven by wind farm cabling and transformer losses which would compensate for losses on the generator's side of the grid connection and would allow the developer to export up to its MEC at the connection point [160]. In 2014, CER decided to update the earlier decision in light of potential economic benefits by increasing overplanting to 20% [161].

In 2012, Forewind looked at overplanting by factoring a number of variables: different turbine types, export and inter-array cable losses, wake losses, grid connection downtime and the total cost for wind turbines, including construction, operation and maintenance [162]. In this study it was also shown that adding more wind turbines improves the economics of the project, however further conclusions could not be drawn given the dependence of many site and technology-specific variables. Similar studies have mentioned the economic benefits of overplanting [163].

A clear example of overplanting in the offshore wind industry is given in the Netherlands for the Wind Farm Zone Borssele. The wind farm is divided into 5 sites. Site I, II and IV can accommodate 350 MW plus 30 MW of overplanting, whereas Site III can accommodate 330 MW plus 30 MW of overplanting. This is around 9 % of overplanting for both cases. TenneT, the Dutch TSO, contemplated the option of dynamic loading of the export cables. Namely, in case that Site I, II and IV was producing at full power, which would see a load of 380 MW being transferred through one of the export cables, this electricity could be handled by the cable and sent to the grid [164]. However, the capacity in excess of 350 MW is not always guaranteed by TenneT, but it is subjected to some constraints linked to the final soil resistivity values, temperature of the cable, final design of the cable system and voltage level of the system.

More recently, some authors have attempted to model overplanting for onshore and offshore wind farms [165, 166]. However, the models utilised in assessing overplanting did not capture the complex relationships between offshore wind engineering variables and financing constraints. Whereas the work of McInerney et al [165] sought to emphasize the benefits of overplanting from the economical point of view, it didn't consider technical variables. Conversely, the work of Wolter et al [166] placed more weight on the technical variables but left aside important financing constraints. Nevertheless, there

is enough evidence to suggest that overplanting can lead to further cost reductions in the maturing offshore wind sector. However, a tailored techno-economic model that integrates site characteristics, technology specificities and financing constraints is needed to demonstrate the benefits of overplanting. Furthermore, this techno-economic model should be grounded in the framework of uncertainty quantification, where its model inputs are represented by probability distribution functions.

The contribution of the current Chapter is to provide a framework to assess overplanting under uncertainty in the design of offshore wind farms; allowing developers and regulatory bodies to identify pareto-optimal trade-offs between cost and uncertainty when deploying additional turbines for a given electrical infrastructure. The rest of this Chapter is structured as follows: Section 8.2 explains the main factors driving overplanting. Section 8.3 and 8.4 describes the detailed modelling of overplanting and its main assumptions. Section 8.5 benchmarks the current model against previous studies on overplanting. Section 8.6 applies the modelling techniques to different wind farm configurations. Finally, conclusions are drawn in Section 8.7.

8.2 Factors Affecting Overplanting

Overplanting is mainly driven by the following factors:

- Ratio of wind turbine expenditure to electrical infrastructure: higher costs of installing an additional turbine for a given electrical infrastructure makes it more difficult for developers to consider this option.

- Wind speed distribution: it describes the variation of wind speeds for a given site. Sites with low mean wind speed mean that the share of time generating at its MEC is low and so is the amount of curtailment; this encourages developers to increase the installation of additional capacity. On the contrary, sites with high mean wind speed mean that the share of time generating at its MEC is high and so is the amount of curtailment; this doesn't favour the installation of additional capacity.

- Wind turbine and inter-array availability: it is defined as the amount of time that the turbine/cable is able to operate over a certain period of time divided by the total time in that period. Farms with high availability values mean that more turbines/cables are operational at a given point in time and therefore it is expected a higher share of curtailment when overplanting. Likewise, low availabilities result in less amount of curtailment and favour overplanting.

- Wake effect: they reduce the wind speed downstream a generating wind turbine. At high wind speeds the farm is able to produce at rated power. However, wake effects need to be taken into consideration for low wind speeds, which is the amount of generation that is not constrained.

- Electrical losses: they take place in transformers, collection wiring, substation and cables. Higher losses will encourage developers to overplant to be able to generate at MEC at the connection point.

- Degradation factor: wind turbine blades are subjected to environmental conditions that result in blade degradation over time, which directly reduces energy production and encourages overplanting.

8.3 Modelling of Overplanting

In order to determine the optimal size of an offshore wind farm relative to the electrical infrastructure it is important to capture the elements described in Section 8.2 within the modelling process. Two types of modelling are considered. Modelling Type 1 is based on constraining individual power curves as a function of the number of turbines and its MEC. As the number of additional turbines to the given MEC increases, the power that can be generated per turbine is reduced due to the electrical constraint of the connection capacity, as shown in Figure 8.1. In addition, wind turbine and inter-array cable availabilities are assumed to be fixed, following the work of National Grid [159]. Modelling Type 2 takes advantage of the stochastic capabilities of the cost modelling tool and propagates the uncertainties of the wind speed and availabilities to the power output via Monte Carlo simulation. Then, the resulting aggregated power transferred

to the grid is obtained by constraining all those ocurrences that are higher than the MEC, as shown in Figure 8.2.

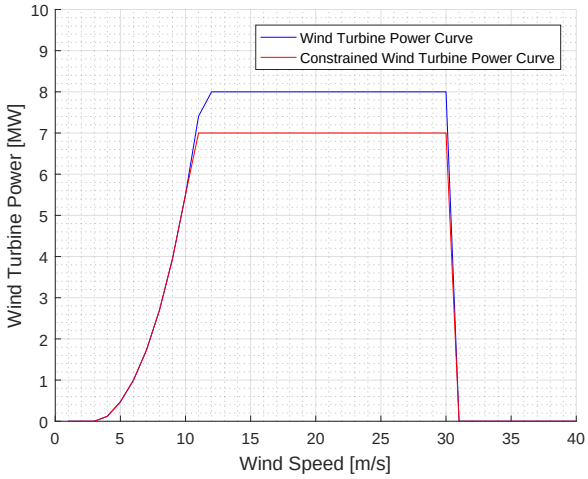

Figure 8.1: 8MW wind turbine constrained to 7MW due to overplanting in Modelling Type 1.

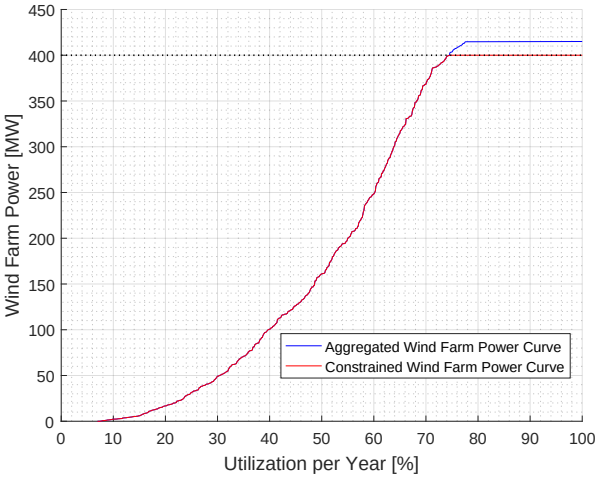

Figure 8.2: 52 8MW wind turbines constrained to a MEC of 400 MW in Modelling Type 2.

The philosophy of modelling the wake effects lies on decreasing the energy available in the wind so that the total losses are equal to the known wake effects calculated through standard commercial tools f_{wake}. Since it is assumed that each turbine produces the same energy over the lifetime of the farm, wake effects are obtained at wind farm level and not at individual turbines. The power output $P(v)$ produced by a single turbine is modelled by a theoretical power curve, which is a function of the rated power P_{rated}, cut-in speed v_{cut-in}, cut-off speed $v_{cut-off}$, turbine efficiency C_{eff}, the air density ρ_{air}, parameter α, wind speed v and the rotor diameter D, according to Equation 8.1.

The cut-in speed is defined as the speed at which the turbine begins to rotate, when applying sufficient torque on the rotor to generate power. At the other side of the curve, when the speed increases beyond a given threshold or cut-off speed, putting the integrity of the rotor at risk, the braking system is employed to bring the rotor to a standstill. Both situations result in a nil amount of power being produced. Otherwise, when the wind speed is found between the cut-in and cut-off speed, then the production is governed by Equation 8.1. It is worth noting that, whereas the Betz limit is a

theoretical maximum of the wind energy that can be extracted, the turbine efficiency has been considered as the efficiency of the wind turbine generator. From Equation 8.1 it is also possible to make a distinction between the energy available in the wind and the energy produced by a wind turbine generator, which is a preliminary step to model the wake effects in the cost modelling tool. We've assumed a parameter $\alpha = 1$, the challenge is now to work out α so that the total losses are equal to the known wake effects calculated through standard commercial tools f_{wake}. Wake losses are obtained by fitting a statistical model to results from OpenWind simulations; details as to how this model has been constructed can be found in Chapter 3. As overplanting means installing more turbines in a given constrained area, inter-turbine distances will vary and therefore this will result in a change in wake losses - this is accounted for in the modelling. In order to solve this problem and obtain alpha, an iterative method is conducted and displayed in the flowchart of Figure 8.3.

$$P(v) = min\left(P_{rated}, \alpha\frac{1}{2}\cdot C_{eff}\frac{16}{27}\cdot\pi\rho_{air}\frac{D^2}{2}\left(v^3 - v_{cut-in}^3\right)\right)\forall v \in (v_{cut-in}, v_{cut-off}) \tag{8.1}$$

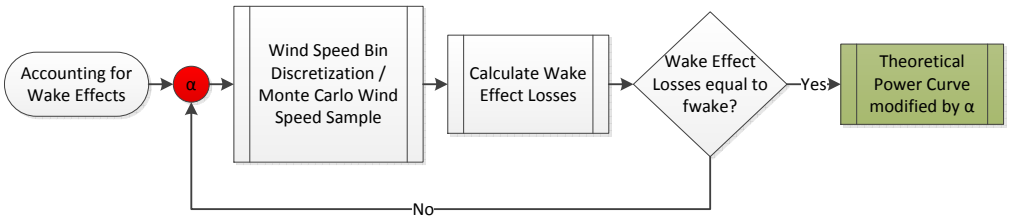

Figure 8.3: Wake Effects Flowchart

Figure 8.4 shows a wind speed distribution associated with a given site. Figure 8.5 displays the theoretical wind turbine power curve for different alpha coefficients. An alpha coefficient of 1 means that there are no wake effects, while decreasing values imply higher wake effects. Figure 8.6 shows the aggregated power curve distribution for a 400 MW farm and alpha coefficients. Figure 8.7 shows the losses incurred for each alpha parameter. Once alpha has been determined, it is fixed for the rest of the calculations.

On another note, availability is defined in this Chapter as the amount of time that a component is able to operate over a certain period, divided by the amount of the time in the period. Whereas a constant wind turbine availability rate is assumed for Modelling Type 1, its stochastic counterpart, Modelling Type 2, uses a binomial distribution to represent the number of wind turbines and inter-array cables available for energy production at a given point in time. Figure 8.8 displays the cumulative distribution functions of the number of wind turbines available for energy production for given wind turbine availability rates. It becomes apparent that higher availability rates lead to a higher share of time where the same number of wind turbines are available. Modelling Type 1 assumes the expected value of the number of wind turbines available for energy production. However, overplanting means that we need to be careful on how to determine the share of time the electrical connection is constrained.

Adding additional turbines to a fixed electrical infrastructure and assuming constant availability rates could lead to an overestimation of the annual energy production. Firstly, there are times where the power produced by the number of available wind turbines is higher than the MEC, resulting in some curtailment by the TSO. Secondly, there are also times where the power flowing through the connection point is less than the MEC, meaning that fewer wind turbines are available for production than its expected number. Figure 8.9 shows the difference between considering a fixed wind turbine and inter-array cable availability rates and modelling its stochastic counterparts; this is to say Modelling Type 1 is compared against Modelling Type 2. Even though it is possible for a developer to optimise an offshore wind farm so that its aggregated power curve matches the MEC at its expected value, the full information on the stochastic behaviour should also be considered. Modelling Type 1 leads to the aggregated power curve in blue, whereas the one in red represents Modelling Type 2. In order to avoid an overestimation of the energy production, Modelling Type 2 is considered for the rest of the Chapter despite requiring a higher computational cost. Electrical losses are modelled as a function of the power factor, which is the ratio between the real and reactive power, the cross section of the cables, the operating voltage and efficiencies of the system. The degradation factor is modelled by as a coefficient which decreases the energy production as the asset ages based on the work of Staffell [75].

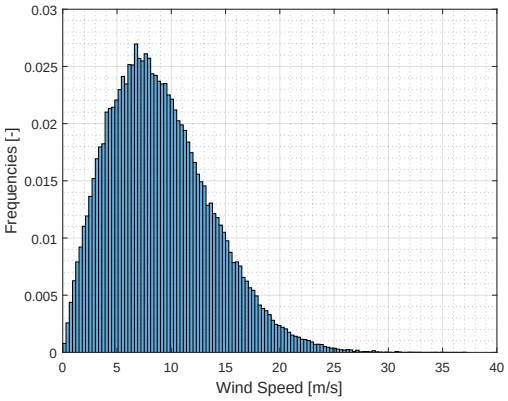

Figure 8.4: Wind speed represented by a Rayleigh distribution associated with a mean wind speed of 9 m/s.

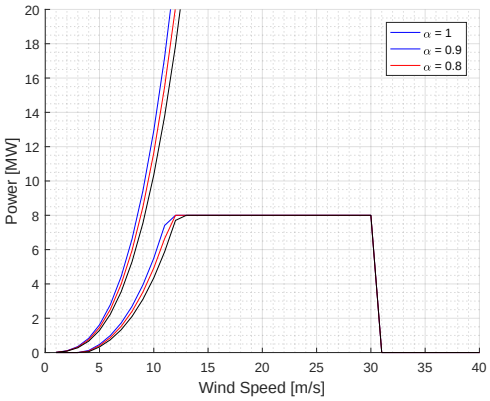

Figure 8.5: Theoretical energy available in the wind and theoretical turbine power curve for different alpha coefficients and wind speeds.

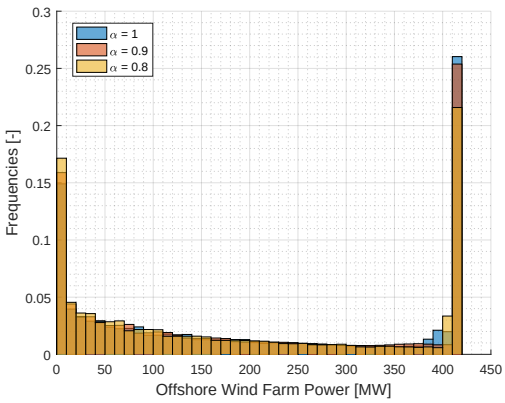

Figure 8.6: Wind power output distribution for different alpha coefficients.

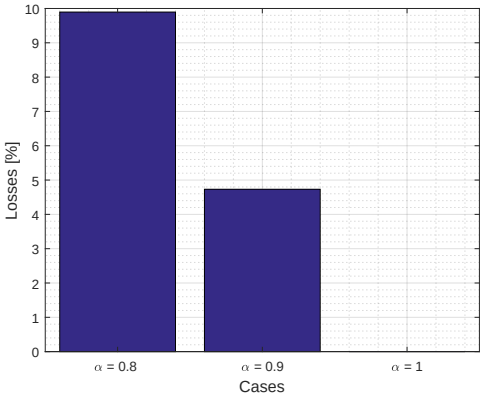

Figure 8.7: Incurred losses for different alpha coefficients.

8.4 Modelling Risk Aversion

Risk aversion is modelled by risk metrics originated in the financial mathematics literature such as the Value at Risk (VaR) and Conditional Value at Risk (CVaR). The $\mathbf{VaR}_\alpha$ gives the probability α that a certain outcome is worse than a given threshold. Typically the probability α represents the confidence level and $\mathbf{VaR}_\alpha$ is regarded as the maximum value that will not be exceeded at this given confidence level. Building on $\mathbf{VaR}_\alpha$, $\mathbf{CVaR}_\alpha$ gives the expected outcome given that the value is worse than $\mathbf{VaR}_\alpha$.

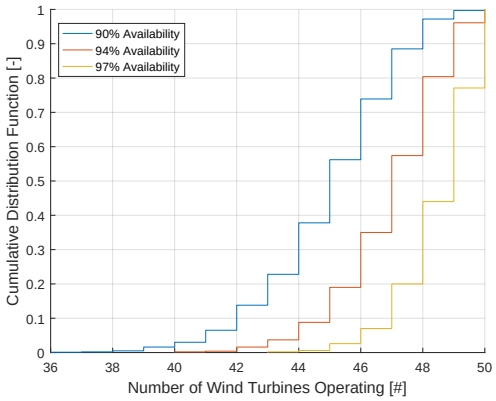

Figure 8.8: Binomial Cumulative Distribution Function of 50 WTG farm for given WTG availability rates.

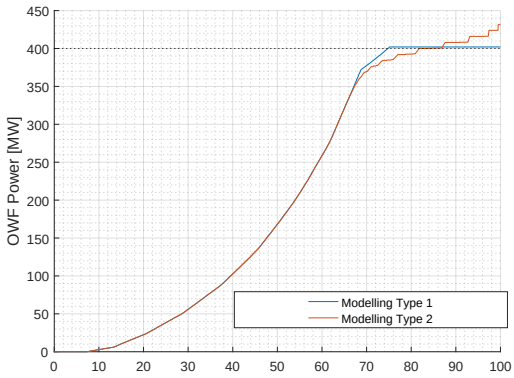

Figure 8.9: Modelling Type 1 against Modelling Type 2; limitations of considering fixed availability rates.

The concept was first introduced in Rockafellar [113] and further developed by him in [114]. The mathematical formulation for $\mathbf{VaR}_\alpha$ and $\mathbf{CVaR}_\alpha$ for continuous functions is given in Equation 8.2 and 8.3, respectively.

$$\mathbf{VaR}_\alpha(LCOE) = min\left(c : P(LCOE \leq c) \geq \alpha\right). \tag{8.2}$$

$$\mathbf{CVaR}_\alpha[LCOE] = \mathbf{E}[LCOE|LCOE \geq \mathbf{VaR}_\alpha(LCOE)] \tag{8.3}$$

Where LCOE is the Levelised Cost of Energy, $P(LCOE \leq c)$ is the probability of the LCOE being less or equal than c and $\mathbf{E}$ is the mathematical expectation operator. One of the main shortcomings of the $\mathbf{VaR}_\alpha$ is that it provides no information on the extent to which values might materialise beyond the threshold amount indicated by the $\mathbf{VaR}_\alpha$ itself, whereas $\mathbf{CVaR}_\alpha$ does. In addition, $\mathbf{CVaR}_\alpha$ has superior mathematical properties since this measure is coherent in the sense of Artzner [115]. For this reason, we've selected $\mathbf{CVaR}_\alpha$ as the preferred financial risk metric. In this approach risk aversion is modelled as a weighted average λ of the **Median** and $\mathbf{CVaR}_\alpha$ of the LCOE values. Parameter λ can be varied from 0 (in a risk neutrality setting) to 1 (extreme risk aversion), based on the work of Munoz [116] and displayed in Equation 8.4.

$$\boldsymbol{\rho}_\alpha[\lambda, LCOE] = \lambda\mathbf{CVaR}_\alpha[LCOE] + (1-\lambda)\mathbf{Median}[LCOE] \tag{8.4}$$

8.5 Benchmark against National Grid

National Grid conducted a high level study on the optimal amount of overplanting for the UK Round 3 offshore wind farms [159]. The findings of the study suggested a 12% overplanting. However these findings are based on the following parameters: 5MW wind turbine, 90% wind turbine availability, 1.1GW of total capacity and an average wind speed of 9 m/s, which meant that 1200 MW of offshore wind should be built for 1000 MW of grid connection. Assuming the same base parameters, Figure 8.10 and 8.11 were obtained using our cost modelling tool. Figure 8.10 shows the difference between the unconstrained and constrained yield as a function of overplanting; the amount of constraint is minimum up to 8% overplanting, where the two lines start to diverge. This point is also reflected in Figure 8.11, suggesting that additional energy produced by the over installation of turbines doesn't outweigh its wind turbine expenditure; a 9% overplanting is considered optimal for this farm. Although the cost modelling tool provides similar levels of overplanting as National Grid, some of the assumptions are a bit conservative in the current state of the offshore wind sector. For example, the rated capacity of wind turbines has almost double since 2010, moving from 5MW to 10MW wind turbines. Moreover, wind turbine availability rates have also increased from 90 to 95% or above. This suggests that past studies on overplanting based on these assumptions need to be revisited.

8.6 Case Study

Several offshore wind farm configurations are analysed in terms of their suitability to overplanting; their project specifications are shown in Table 8.1. It is assumed, for the sake of simplicity, that the export cable length, construction and operational port distances are equal to the distance from shore. The MEC is 400MW, 1GW and 2GW and offshore wind farm capacities are varied from 0% to 14% in overplanting. The estimated mean wind speed is represented by a normal distribution with mean (μ) and

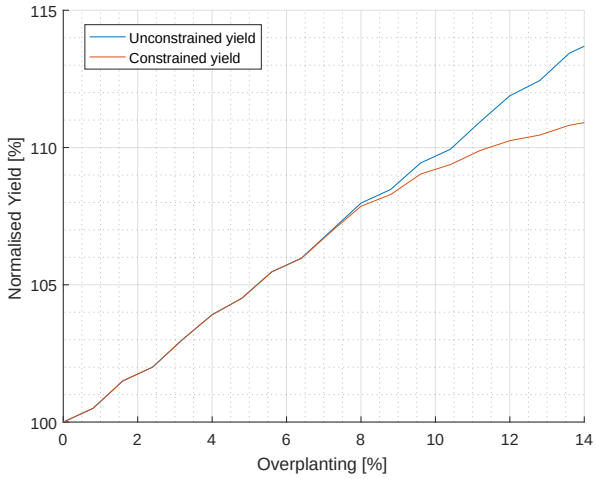

Figure 8.10: Unconstrained versus constrained normalised yield as a function of overplanting.

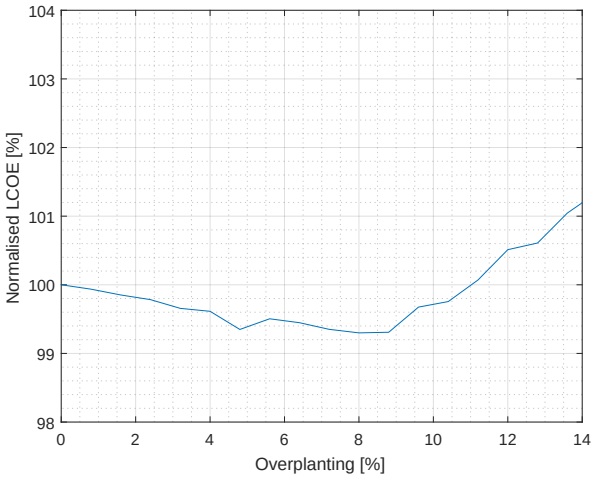

Figure 8.11: Reference case LCOE values for National Grid as a function of overplanting

standard deviation (σ) as $\mathcal{N}(\mu, \sigma^2)$[1]. Likewise, availabilities are represented by uniform distributions with lower(a) and upper(b) bounds as $\mathcal{U}(a, b)$.

The reference case is calculated through a Monte Carlo simulation with input parameters from Table 8.1 (without uncertainties). Figure 8.12 shows the difference between the unconstrained and constrained yield as a function of overplanting; the amount of constraint is minimum up to 2% overplanting, where the two lines start to diverge. This point is also reflected in Figure 8.13, suggesting that additional energy produced by the over installation of turbines doesn't outweigh its wind turbine expenditure; a 2% overplanting is considered optimal for this farm. This is considerably lower compared to National Grid. As shown in Borras [170], several technology-specific factors were investigated in terms of its suitability to overplanting: wind speed, wake effects and wind turbine and inter-array cable availability. It was shown that the most sensitive parameter to overplanting is the wind turbine availability, which has been fixed to 95% for the local sensitivity in this study. The purpose of this Chapter is to expand this study to examine parameters such as wind farm capacity, wind turbine size, average water depth and average distance from shore, in order to provide some insight on how

[1] 0.1 m/s is a representative value combined from independent uncertainties, individually determined by normal distributions as seen in [167, 168, 169]

Table 8.1: Offshore wind farm project specifications.

Characteristic	Value	Uncertainty
Water Depth [m]	25	None
Distance from shore [km]	25	None
Mean Wind Speed @ 100m [m/s]	9	$\mathcal{N}(9, 0.1^2)$
Wind Turbine Availability [%]	95	$\mathcal{U}(90, 97)$
Inter-Array Cable Availability [%]	99	$\mathcal{U}(97, 99)$
Foundation Type [-]	Monopile	None
Electrical Infrastructure [-]	HVAC	None
Wind Turbine Type [-]	164-8 MW	None
Wake effect [%]	10	None
Degradation Factor [%]	0.05	None

overplanting is influenced by larger turbines and sites located further from shore. In order to do so, the following number of combinatorial configurations (81), displayed in Table 8.2, have been examined.

Table 8.2: Wind farm configurations.

OWF Capacity[MW]	WTG Size[MW]	Distance Shore[km]	Water Depth[m]
400	4	25	25
1000	8	50	40
2000	12	75	60

Figure 8.14 shows the optimal amount of overplanting as a function of the wind farm

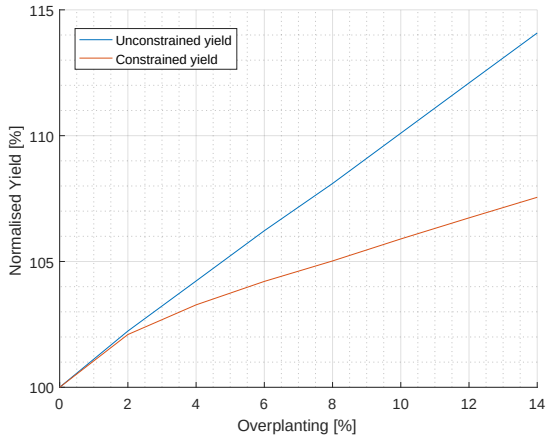

Figure 8.12: Unconstrained versus constrained normalised yield as a function of overplanting.

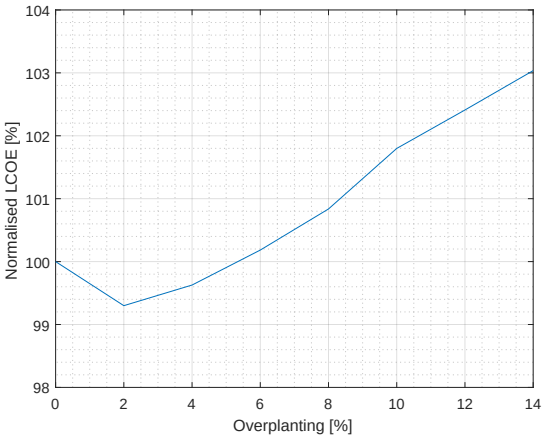

Figure 8.13: Reference case LCOE values as a function of overplanting.

total capacity and distance from shore. For a 25km distance from shore, overplanting the farm results in overall economic benefits. As the wind farm size increases so does the optimal amount of overplanting, moving from 2% to 4%. On the contrary, for 50 and 75km distance from shore, the optimal amount of overplanting remains at %2 for 400 MW while higher capacities lead to a negative overplanting effect; to the extent that for a 75km from distance any amount of overplanting results in a negative effect. For a given site, the further from shore, the higher the installation costs of wind turbines are. Given that the wind resource remains constant for all cases (at 9m/s mean wind speed), increasing the distance from shore, reduces the amount of optimal overplanting. In addition, the increase in wind farm size acts as a catalyst, increasing the effects of overplanting - derived from its economies of scale. What we can observe from Figures 8.10, 8.11, 8.12 and 8.13 is that the LCOE minimum occurs approximately when curtailment starts to become an issue. Therefore, this analysis suggests that the optimal is purely a function of the wind speed distribution compared to the turbine power curve (and the modelling of the wake losses). In order to generalise this conclusion however, the sensitivity of the offshore wind farm configuration to the LCOE minimum should be investigated. Figure 8.15 takes advantage of the same data as Figure 8.14; however these are display holding wind farm capacity constant for every subplot. It is important

to notice that the blue line in the top graph of Figure 8.15 is the same as the red line in the top graph of Figure 8.14. Figure 8.16 shows the optimal amount of overplanting as a function of the number of wind turbines for several wind farm sizes. Although the amount of overplanting changes depending on the size of the wind turbines, this effect is reduced as the the size of the farm grows. Figure 8.17 shows the optimal amount of overplanting as a function of the water depth and distance from shore in a 400 MW farm, whereas Figure 8.18 represents the same data but for a 2000 MW farm. Both figures suggest that the water depth has a neglegible effect on the optimal amount of overplanting. Figure 8.14 et seq, would require to estimate its uncertainty distributions in future work.

The probability distribution function of the LCOE is obtained by 20,000 model evaluations of an outer Monte Carlo loop with parameters displayed in Table 8.1. It is worth bearing in mind that, for each model evaluation, an inner Monte Carlo simulation propagates the wind speed and availabilities with another 10,000 model evaluations within the Annual Energy Production module; this process is repeated for several degrees of overplanting. The risk metrics given by the expression $\lambda \mathbf{CVaR}_{\alpha=0.05}[LCOE] + (1 - \lambda)\mathbf{Median}[LCOE]$ are normalised with respect to the values obtained when no overplanting is applied, as displayed in Figure 8.19. Overplanting the farm from 2% to 8% results in risk metrics (in a risk neutrality setting) that improve the economics of the farm. However, the optimal design is found at 4% of overplanting regardless of the risk appetite. Figure 8.20 includes the case when a 0.05 m/s mean wind speed uncertainty is given - the optimal amount of overplanting remains constant.

8.7 Conclusions

This Chapter has presented the development of a novel framework to assess overplanting in the design of offshore wind farms when the underlying variables, such as the wind speed and availability rates, among others, are uncertain. Two types of modelling have been compared, taking into consideration the estimated mean wind speed, wind speed distribution, availability rates, electrical losses, wake effects and a degradation factor. Although Modelling Type 1 is easier to implement than Modelling Type 2, it can lead

to an overestimation of the annual energy production. Modelling Type 2 addresses this problem via an inner Monte Carlo simulation despite requiring higher computational costs by assessing the percentage of time the MEC is constrained, and it has therefore been the preferred method for this Chapter. The role of the computational speed is limited given that these investment decisions are made once every few years and the current state of technology allows for access to high-performing computing clusters at reasonable costs. As seen by a benchmark with National Grid, as the wind turbine availability increases, overplanting becomes less valuable. This suggests that previous studies on overplanting, which were based on low wind turbine availabilities rates from UK Round 1 offshore wind farms (in the order of 90%), need to be revisited.

A local sensitivity analysis has revealed that wind turbine availability (key driver), wind farm capacities, turbine sizes and distances from shore are sensitive parameters to overplanting, whereas the estimated mean wind speed, wake effects and inter-array cable availability play a secondary role. For a given site, wind farm sizes act as a catalyst for overplanting - increasing the positive or negative effects depending on the wind farm configuration. In addition, bigger wind turbine sizes reduce the effect of overplanting. Finally, the further the distance from shore, the higher installation costs of the wind turbines are and when holding wind resource constant, it reduces the amount of optimal overplanting. As a consequence, it is expected that sites located further from shore, with bigger wind turbines and fewer units for a given wind farm capacity will most likely have small benefits from overplanting.

Without considering the uncertainties in the different parameters represented by the outer Monte Carlo loop, it appears that the optimal amount of overplanting is 2% for our reference offshore wind farm. Generally speaking, the role of determining the optimal setup comes down to the risk appetite of the developer, which in this case is represented by a linear combination of the risk aversion and risk neutrality setting, governed by the λ parameter. However, when conducting the double loop Monte Carlo simulation, the optimal setup is found at 4% regardless of the risk appetite considered. Furthermore, overplanting the farm by any value from 2% to 8% gives a better result

than with no overplanting for a risk neutral setting, meaning that overplanting can be used as a hedging instrument. Sensitivities on wind speed uncertainty do not change the optimal amount of overplanting. Future work will take advantage of the framework developed in this Chapter to quantify how risk aversion influences the investment decision for the local sensitivity analysis carried out in this study. On another note, the degradation factor has been taken into account after the constraint in the modelling, but we would expect greater amounts of overplanting if this was taken before the constraint.

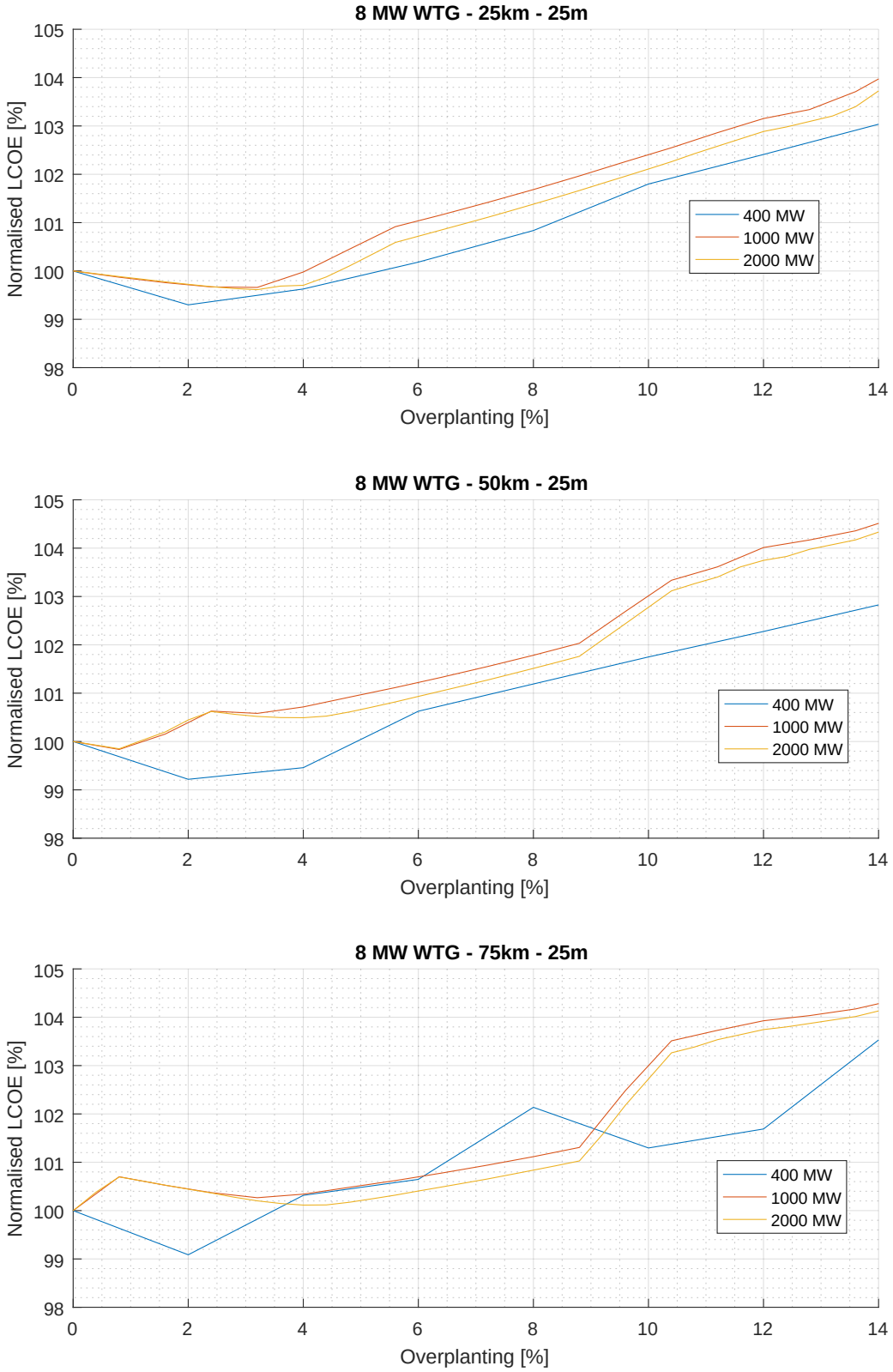

Figure 8.14: Influence of wind farm capacity and distance from shore to the optimal amount of overplanting.

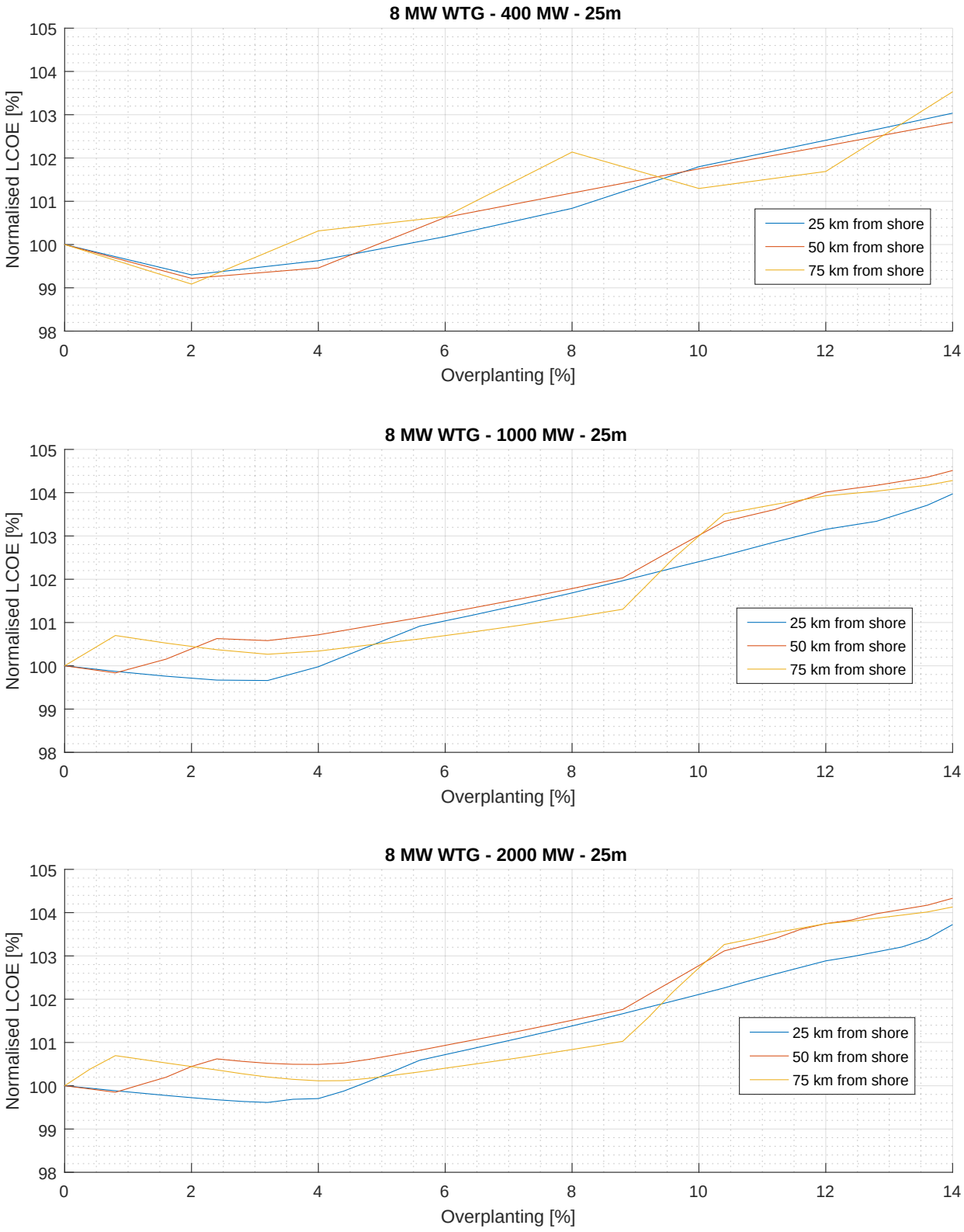

Figure 8.15: Influence of wind farm capacity and distance from shore to the optimal amount of overplanting.

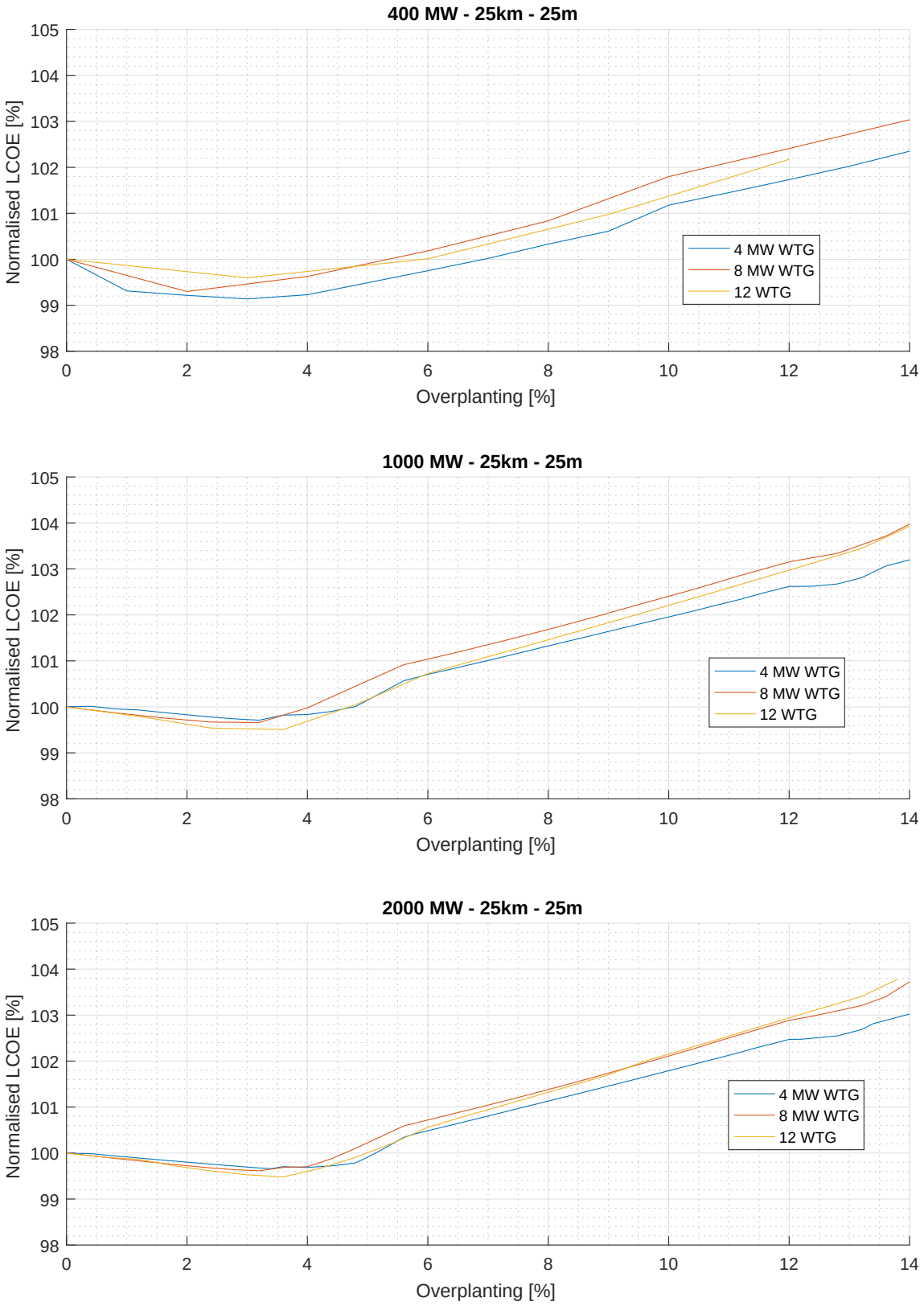

Figure 8.16: Influence of wind turbine size to the optimal amount of overplanting.

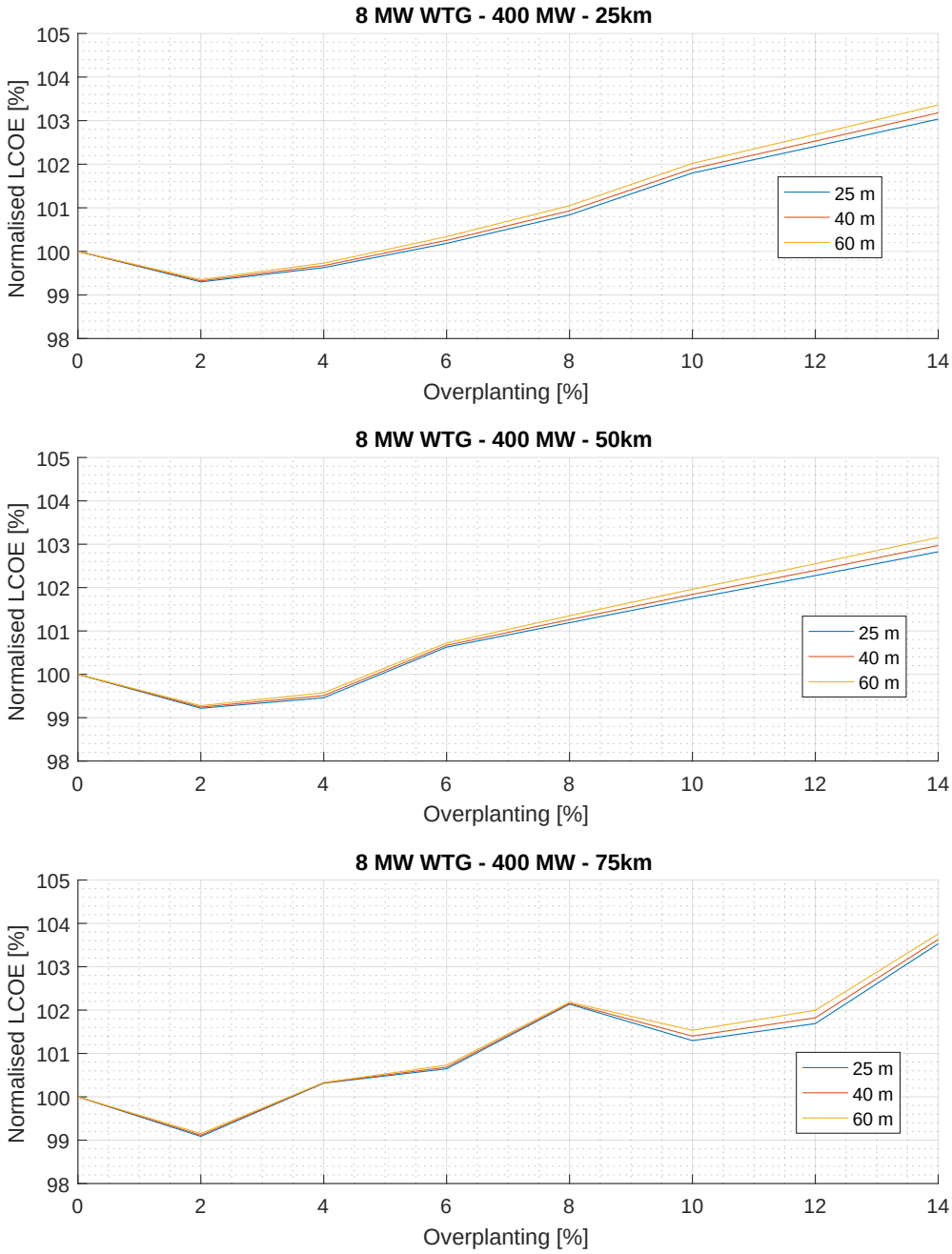

Figure 8.17: Influence of water depth to the optimal amount of overplanting in 400 MW farm.

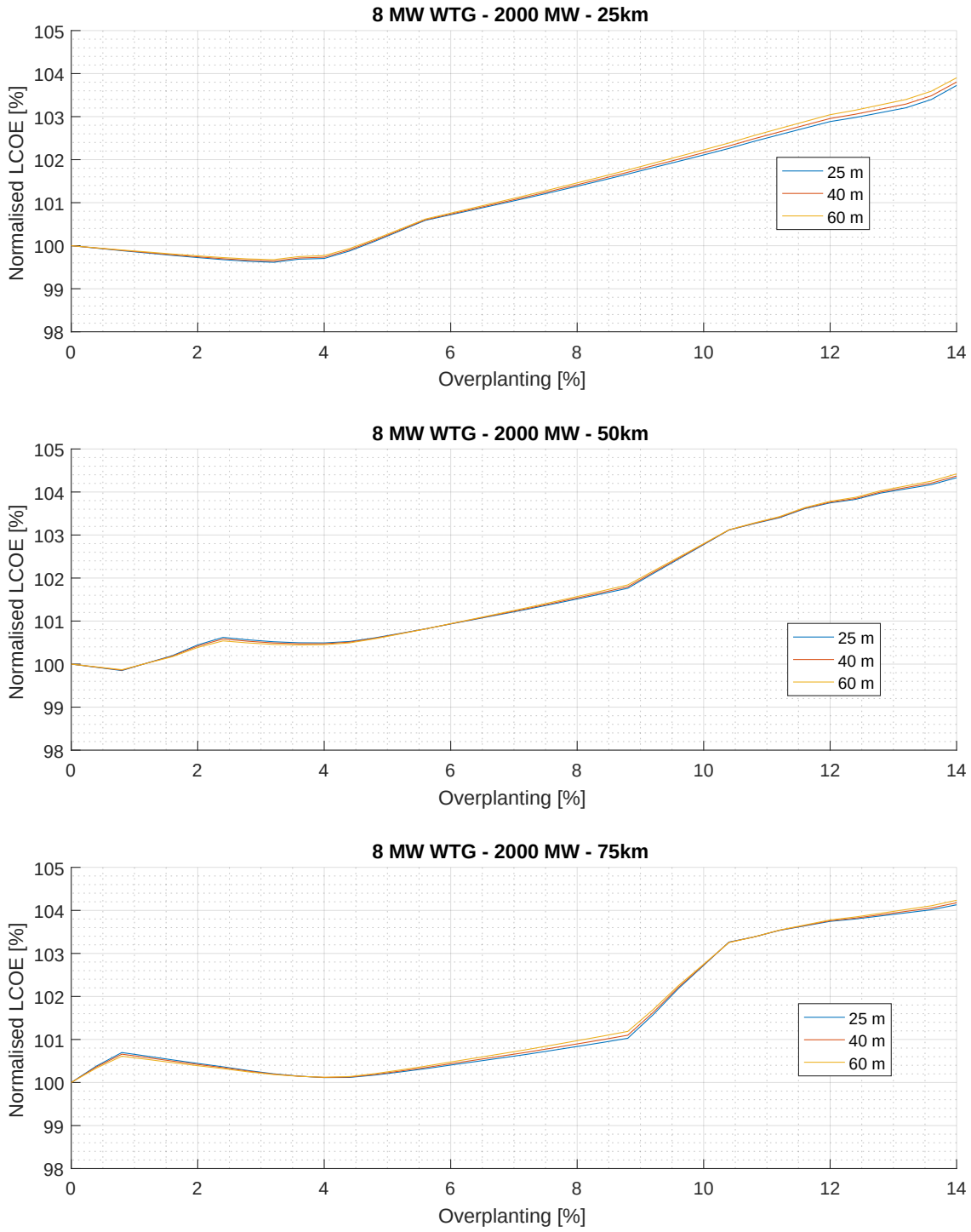

Figure 8.18: Influence of water depth to the optimal amount of overplanting in 2000 MW farm.

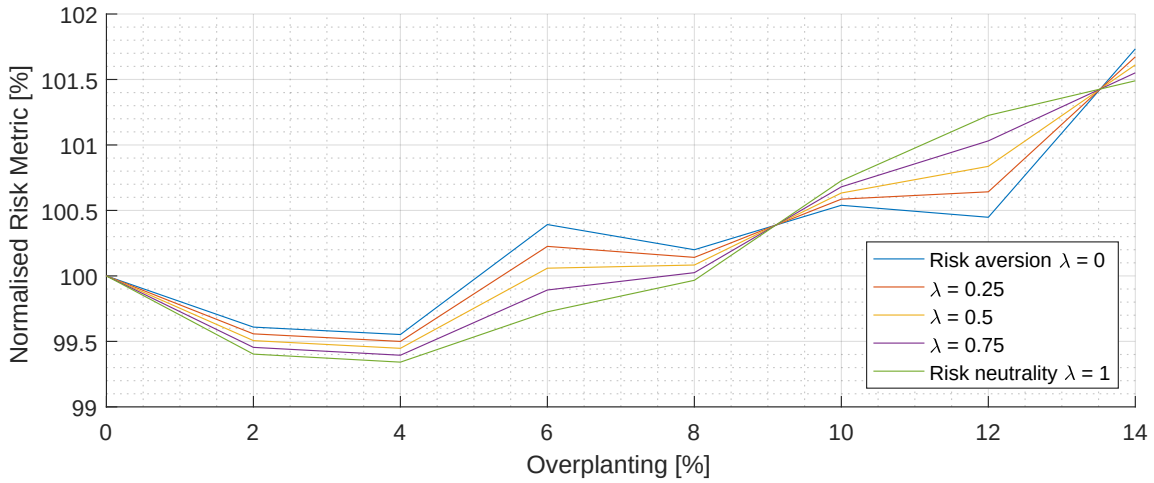

Figure 8.19: Risk aversion represented by $\boldsymbol{\rho}_{\alpha}[\lambda, overplanting]$ - 0.1 m/s mean wind speed uncertainty.

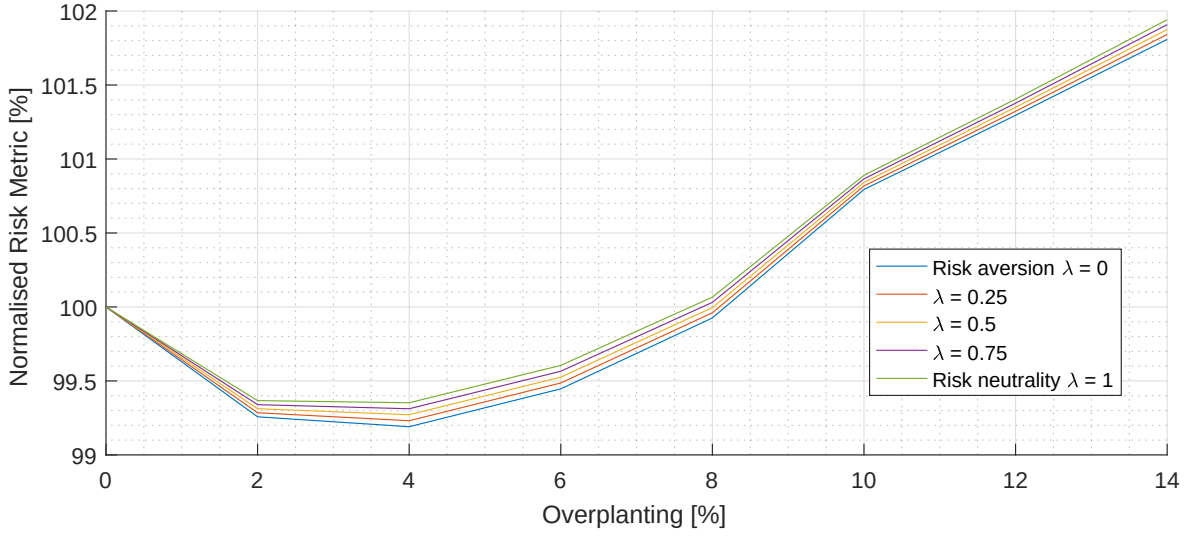

Figure 8.20: Risk aversion represented by $\boldsymbol{\rho}_{\alpha}[\lambda, overplanting]$ - 0.05 m/s mean wind speed uncertainty.

Part IV

Concluding Remarks

Chapter 9

Conclusions and Recommendations

This section draws on individual chapters throughout the thesis to provide a set of conclusions and recommendations for academia, industry and policy.

9.1 Conclusions

Offshore wind is expected to form the backbone of the UK low carbon electricity supply as a result of an unprecedented cost reduction trajectory. The principal goal of the Engineering Doctorate has been to develop new methodologies to optimise the design of large-scale offshore wind projects subject to uncertainty, simultaneously considering cost and risk aspects. This thesis has described the methodology of an industrial cost modelling tool to evaluate the financial performance of offshore wind assets, as well as the development, validation and deployment of a framework for quantitative uncertainty management with several applications relevant to the offshore wind industry. This section draws on individual chapters throughout the thesis to provide a set of conclusions and recommendations for academia, industry and policy. Building a cost modelling tool for offshore wind projects is a multidisciplinary undertaking as it requires expertise from project development, consenting, wind resource assessment, procurement, marine operations, foundation and geotechnical engineering, operation and maintenance, electrical infrastructure and finance. In addition, cost modelling is

not an exact science as it calls for subjective expert judgement when projects are at the early stages of development. Therefore, by building an overarching stochastic framework around the cost modelling tool, we are able to improve the project performance and further optimise the design of offshore wind farms. This process was carried out in two phases.

The first phase consisted in the development of a framework for quantitative uncertainty management, which includes uncertainty quantification, uncertainty propagation and global sensitivity analysis. A global sensitivity analysis toolbox was built to benchmark existing methods for a set of well-known test functions with the purpose of validating its tools and methods before applying them to the cost modelling tool. In this phase, a framework from which to choose global sensitivity analysis techniques was provided. In particular, it was shown that the PAWN distribution-based method can be used as a complementary approach to the variance-based method, especially in those cases when dealing with highly-skewed or multi-modal distributions. In addition, given a set of model evaluations, the PAWN distribution-based method can be applied at no extra cost (from the original set) as there is no need to tailor the design of experiments. However, the PAWN distribution-based method fails to rank different inputs that have different orders of magnitude in their contribution of the response. Therefore, it is important to complement any standard variance-based global sensitivity analysis with a moment independent technique, to avoid giving decision makers a false sense of security, whereby attempting to fix or reduce some of the input uncertainty might result in higher variability of the output. This comparison demonstrated the application of these two methods and provided new insights across the applied mathematics community. The first phase also shed some light on the first part of the research question regarding the use of quantitative uncertainty management techniques for offshore wind techno-economic models.

The second phase was the deployment of the framework to the cost modelling tool. The results of the global sensitivity analysis applied to the cost modelling tool showed key techno-economic parameters when building offshore wind investment models; few

inputs accounted for most of the LCOE uncertainty while most inputs played little or no role. The top 6 parameters to consider when building an offshore wind investment business case are: the measured (P50) annual mean wind speed, the target equity rate of return, the default cost for generic turbine, the fraction of position requiring drilling, the minimum debt service coverage ratio (if project finance is considered) and the additional time when drilling is required. During this work we indirectly captured the overriding factor to falling costs - larger turbine sizes. Larger turbines sweep a larger area and have access to higher, more consistent winds at higher altitude, increasing their yield and capacity factors. Larger turbines not only increase yield but also reduce offshore wind CAPEX and OPEX, with key impacts seen on balance of plant and installation costs due to the reduced number of units. This, combined with smaller technical developments in turbine design, manufacture and installation and maintenance, has led to significant LCOE reductions. The second phase addressed the second part of the research question regarding the identification of key drivers in building complex offshore wind investment models.

The outcome of the global sensitivity analysis for offshore wind investments restated the importance of the wind speed uncertainty in the design of offshore wind farms. This led to two independent research questions where the previous quantitative uncertainty framework was utilised. On the one hand we showed that there is a relationship between the wind speed uncertainty and access to better financing conditions for project finance offshore wind farms. Whereas some projects might be limited by the debt service coverage ratio, others might be limited by the gearing. When the project is limited by the gearing, attempting to reduce the wind speed uncertainty only leads to higher LCOEs, whereas for projects limited by the debt service coverage ratio it depends on the trade-off between the increase development expenditure and how much uncertainty reduction in the estimated mean wind speed is obtained. This confirms that it is never optimal to reduce the uncertainty as far as possible, as it is commonly believed in the industry. On the other hand, this thesis also provided a framework to assess overplanting in the design of offshore wind farms. Overplanting wind farms by installing higher rated capacities compared to the fixed electrical infrastructure can result in better overall

economics despite power output being curtailed at generations' peaks. However, it has been shown that the further the distance from shore, the higher the installation costs for the wind turbines are and for the same wind resource, it reduces the amount of optimal overplanting. As a consequence, it is expected that sites located further from shore, with bigger wind turbines and fewer units will most likely have small benefits from overplanting. Nevertheless, overplanting can be used as a hedging instrument when designing offshore wind projects. After refreshing the conclusions and interactions from individual chapters, general conclusions and recommendations for academia, industry and policy are given below.

9.1.1 Academia

Three general recommendations have been drawn from this work. First, techno-economic models should be built with considerations about the uncertainty of their inputs from the very beginning. Most model users decide to include uncertainty analysis too late in the development process. However, this should be dealt with when defining the model purpose. An example of this is the cost modelling tool in this work. Should uncertainty analysis been accounted for from the very beginning, we would not have needed to change the entire software architecture at later stages. Second, global sensitivity analysis should be used instead of local, provided the model allows for it. Global sensitivity analysis explores the full domain of input parameters rather than investigating the behaviour of the model at a particular configuration, providing greater insight on the model response. Finally, variance-based global sensitivity analysis should be complemented with moment independent methods. Variance-based methods are not always a good proxy for uncertainty and might give decision makers a false sense of security, whereby attempting to reduce some of the input uncertainty might result in higher variability of the output due to interactions of the model.

9.1.2 Industry

Industry should employ more time, resources and skills in developing advanced analytical tools that can handle uncertainty analysis. The application of this quantitative uncertainty framework to offshore wind cost modelling has equipped management with a method to arrive at optimal solutions to complex decision-making problems. For example, it has provided a competitive advantage when performing uncertainty analysis in comparative evaluation of multiple sites, detailed evaluation of specific project layouts and sensitivity studies on both design/technology choices and cost variations. Building advance analytics tools that can handle uncertainty analysis is expensive and time-consuming, however they have proven invaluable to support investment decisions. Examples of those are explained in Chapter 7 and 8.

9.1.3 Policy

More broadly, policy-makers should engage with industry and academia to build real-world techno-economic models for different renewable energy technologies, accompanied by an overarching stochastic framework. This methodology would allow policy-makers to carry out uncertainty quantification and propagation as well as global sensitivity analysis, with the aim of identifying key cost and risk drivers. By doing so, they could improve communication, be more transparent and drive the right discussions with industry. Policy makers could then use this results to set strategic goals. For example, targeting those drivers that lead to higher cost reductions will make a positive difference for all energy consumers. Finally, policy-makers could disseminate the evidence provided by those models and align industry participants with these strategic goals by means of appropriate policy levers.

9.2 Industrial Impact

In addition to the contribution to knowledge, this thesis has provided a range of commercial benefits to the sponsoring company, EDF Energy R&D UK Centre. Firstly,

the cost modelling tool has been adapted to account for current technology choices and market trends. This not only required up-to-date information about the offshore wind industry but it also challenged fundamental modelling assumptions. As the global offshore wind market continued to grow rapidly, new technology, revenue support schemes and financing structures needed to be built into the model. Therefore, the tool was constantly evolving in light of new cost data being released, developments in technology and changes in policy, as well as state-of-the-art modelling techniques. The company also benefited from an extensive validation of the modelling assumptions. Given the multidisciplinary nature of cost modelling, this extensive validation required collaboration with numerous teams across several group locations in both the United Kingdom and France. The results of the validation phase increased stakeholders' confidence in the offshore wind cost modelling capabilities of the EDF Energy R&D UK Centre. Over the course of this Engineering Doctorate, the tool was applied to a wide range of projects to support its investment decisions (corporate and project finance), from innovative projects such as the Blyth offshore demonstrator to utility-scale projects such as the Dunkirk offshore wind farm. Additional work was conducted with the tool to gain further insight into:

- The impact of larger turbine sizes on the group's offshore wind investments
- Prospective analysis and weighting up different scenarios for offshore wind projects
- Tailored techno-economic modelling for large-scale offshore wind projects
- High-level cost modelling for offshore wind supply curves
- The future cost of offshore wind pathways

Secondly, the stochastic methods and tools developed through this research significantly enhanced EDF Energy R&D UK Centre cost modelling capabilities. It enabled the Centre to expand internal discussions from simple scenario analysis to more advanced considerations of risk and uncertainty. The stochastic module, which meant building a new software architecture around it, was developed with the aim to be flexible and modular, allowing the user to switch from single to stochastic runs. Furthermore, the stochastic module allows to perform state-of-the-art global sensitivity analysis

using a high performance computing cluster in order to assess the cost and risks of offshore wind projects. This is a unique capability that provides the Centre with a competitive advantage when performing uncertainty analysis. The results of these stochastic methods and tools informed senior management about:

- Key techno-economic parameters driving the costs and risks of offshore wind projects
- The effects of mean wind speed uncertainty on project finance debt sizing for offshore wind farms
- How risk aversion shapes overplanting in the design of offshore wind farms

Besides the sponsoring company, other players in the offshore wind sector have benefited from the different publications and insights provided over the course of this research.

9.3 Limitations and Further Work

A number of limitations has been found throughout this thesis and listed below:

Further case studies or offshore wind farm configurations

This thesis has focused on the methodology of an industrial cost modelling tool as well as the development, validation and implementation of a framework for quantitative uncertainty management with a several applications relevant to the offshore wind industry. Further work will need to explore the application of this framework to additional offshore wind farm configurations in order to understand key techno-economic parameters when building offshore wind investment cases. For example, additional configurations will need to be considered in light of the latest technological developments for the global sensitivity analysis, the effects of the mean wind speed uncertainty on project finance debt sizing and the overplanting chapters.

Updating modelling assumptions

The cost modelling tool has been conceived for offshore wind projects at early stages of development with high degree of uncertainty surrounding their assumptions. The

model is particularly useful to challenge existing assumptions and objectively assess the feasibility of a high number of scenarios, rather than to validate or verify them. Although the model has been benchmarked against existing offshore wind project costs, it is almost impossible to carry out an extended cost data validation phase due to limited cost data available and the stage of the offshore wind sector. A particular set of assumptions used to model an offshore wind project might change when the project starts construction as there are always discrepancies between modelling and reality. This is exacerbated by the speed at which innovation and development occur in such a dynamic industry. Therefore, it is vital to keep the model up to date.

Another important feature of the model is its granularity. Cost models tend to follow either a bottom up or a top down approach in order to work out aggregated costs. This cost modelling tool uses a combination of these two approaches based on the nature of the data and information available to the model user.

Updating input data

Data is a sensitive topic, especially when it comes to cost data. Although we have had access to extensive resources from internal procurement teams as well as publicly available information, purchasing external cost databases has not been an option as they come with expensive price tags. As new sources of publicly available data are released, these will need to be incorporated into the model.

Wholesale electricity price risk

Although we have been predominantly interested in the LCOE, and therefore we haven't dealt with wholesale electricity prices, it would be interesting to look at the profitability of merchant offshore wind projects. Even though current revenue support mechanisms, such as the contract for difference, remove most of the wholesale market exposure to generators, this situation might change in the future. The current model could be complemented with wholesale market price modelling to assess the financial viability of offshore wind farms exposed to wholesale electricity market prices. As renewables become mainstream, it is expected that they will develop merchant risk management

techniques.

Uncertainty quantification

The quantification of the uncertainty bounds of the model inputs is key to uncertainty analysis. In the absence of appropriate data to quantify these uncertainty bounds, expert judgment is used. This was the case for the global sensitivity analysis used in this thesis. However, further work should look at quantifying the different uncertainty bounds of the model inputs by using expert elicitation methods in conjunction with data. Uncertainty quantification should be considered as important as uncertainty propagation. A small cost item with extreme uncertainty might appear more prominent in the global sensitivity analysis than a large cost item with negligible uncertainty. This means that regardless of the contribution of the variable of interest to the LCOE, the definition of the uncertainty bounds around the input parameters has a big impact on the ranking of the parameters.

Independence – no correlations

Although Monte Carlo analysis is able to propagate fully or partially correlated input variables, we have assumed independence among input variables; separate probability distribution functions are used instead of a joint probability distribution function, for which no data and expertise in the offshore wind industry exists. However, it would be interesting to explore how key techno-economic parameters would affect the ranking of importance for the LCOE metric when correlations are taken into consideration.

Additional global sensitivity analysis methods

In the development of the quantitative uncertainty framework, and in particular, the global sensitivity analysis part, two separate modules addressing the variance-based and PAWN distribution-based method have been constructed, validated and then implemented into the commercial cost modelling tool. However, the search for global sensitivity analysis methods, that study how the different sources of uncertainty in the model output can be apportioned to the different sources of uncertainty in model inputs,

continues. Therefore, we have identified an additional method that could be benchmarked against well-known test functions and applied to the cost modelling tool. This new method is based on the cumulative distribution function-based indicator following the ideas of Gamboa, Klein and Lagnoux. This indicator is regarded as the generalisation of the so-called variance-based or Sobol indices to higher moments, where its index appears to be more general than Sobol as it takes into consideration the whole distribution and not only the second moment.

Computational power

The use of a high performance computing cluster and a parallel computing architecture allows the user to take advantage of huge amounts of computational power. Therefore, further resources could be employed to characterise not only total sensitivity indices but also high-order interactions among input variables.

Additional insight into overplanting

Given the discussion about CVaR in Chapter 8, further work should address the creation of an efficient frontier that displays both the CVaR and the expected LCOE for various degrees of risk aversion. Also, a comparison with the real options literature could be made because overplanting can be thought of as creating an option to be exploited in the future.

This thesis has focused on developing new methodologies to optimise the design of large-scale offshore wind projects subject to uncertainty, simultaneously considering cost and risk aspects. This framework, if applied early on in the development of the project, can unlock further cost reductions and link the design of offshore wind farms to extensive financial valuation techniques. Further work should therefore look at improving the existing methodology and extend its applications.

Bibliography

[1] Parliament of the United Kingdom. *Climate Change Act 2008*. Tech. rep. 2008, pp. 1–103. DOI: 10.1136/bmj.39469.569815.47. URL: http://www.legislation.gov.uk/ukpga/2008/27/pdfs/ukpga{_}20080027{_}en.pdf.

[2] Intergovernmental Panel on Climate Change. *Global warming of 1.5 degrees C - An IPCC Special Report*. Tech. rep. 2018, pp. 1–32. DOI: 10.1017/CBO9781107415324. arXiv: arXiv:1011.1669v3. URL: https://www.ipcc.ch/site/assets/uploads/sites/2/2018/07/SR15{_}SPM{_}High{_}Res.pdf.

[3] Siemens. *Offshore wind power projects*. Tech. rep. 2011, pp. 1–8. URL: www.siemens.com/energy.

[4] International Energy Association - Renewable Energy Technology Deployment. *Comparative Analysis of International Offshore Wind Energy Development*. Tech. rep. March. 2017. URL: http://iea-retd.org.

[5] David Flood. *Round 3 offshore wind farms UK Future Energy Scenarios seminar 2012*. 2012.

[6] ReNEWS. *'Late spring' launch for 7GW UK offshore wind Round 4*. 2019.

[7] Ofgem. *RO closure*. 2017. DOI: .1037//0033-2909.I26.1.78. URL: https://www.ofgem.gov.uk/environmental-programmes/ro/about-ro/ro-closure.

[8] UK Department of Energy & Climate Change. *Electricity market reform: policy overview*. Tech. rep. November. 2012, pp. 1–48. DOI: 10.1109/CONECCT.2013.6469293. URL: https://www.gov.uk/.../7090-electricity-market-reform-policy-overview-.

[9] Department for Energy and Climate. *Planning our electric future: a White Paper for secure, affordable and low-carbon electricity*. Tech. rep., pp. 1–142. DOI: 10.1016/S0264-410X(12)01439-9. URL: http://www.decc.gov.uk/en/content/cms/legislation/white{_}papers/emr{_}wp{_}2011/emr{_}wp{_}2011.aspx{\%}5Cnhttp://linkinghub.elsevier.com/retrieve/pii/S0264410X12014399.

[10] National Audit Office. *Early contracts for renewable electricity*. 2014. URL: https://publications.parliament.uk/pa/cm201415/cmselect/cmpubacc/454/454.pdf.

[11] UK Department of Business Energy and Industrial Strategy. "Contracts for Difference Allocation Framework for the second Allocation Round". In: March (2017). ISSN: 2045-4015 2045-4015. DOI: 10.1186/s13584-016-0084-5. URL: https://www.gov.uk/government/uploads/system/uploads/attachment{_}data/file/601120/Allocation{_}Framework{_}for{_}the{_}second{_}Allocation{_}Round.pdf.

[12] UK Department of Business Energy and Industrial Strategy. *CONTRACTS FOR Methodology used to set Administrative Strike Prices for CfD Allocation Round 3*. Tech. rep. December. 2018. URL: https://assets.publishing.service.gov.uk/government/uploads/system/uploads/attachment{_}data/file/765690/Admin{_}Strike{_}Prices{_}Methodology{_}AR3.pdf.

[13] BVG associates. *Future renewable energy costs: offshore wind: 57 technology innovations that will have greater impact on reducing the cost of electricity from European offshore wind farms*. Tech. rep. 2017, p. 80.

[14] Wind Europe. *Offshore wind in Europe: key trends and statistics 2018*. Tech. rep. 2018, pp. 1–37. DOI: 10.1016/S1471-0846(02)80021-X.

[15] UK Department of Energy and Climate Change (DECC). *Offshore Wind Cost Reduction Task Force Report*. Tech. rep. June. 2012, p. 44. URL: https://www.gov.uk/government/uploads/system/uploads/attachment{_}data/file/66776/5584-offshore-wind-cost-reduction-task-force-report.pdf.

[16] Shell. *Blauwwind Consortium reaches Financial Close on Borssele III/IV*. 2018. URL: https://www.shell.co.uk/media/2018-media-releases/blauwwind-consortium-reaches-financial-close-on-borssele-iii-iv.html{\%}0A.

[17] David Weston. *Vattenfall wins Kriegers Flak with €49.9/MWh bid*. 2016. DOI: 10.1111/cjag.12228. arXiv: arXiv:1011.1669v3. (Visited on 08/19/2020).

[18] Dominik Huebler, Daniel Radov, and Lorenz Wieshammer. *Method or Madness: Insights from Germany's Record-Breaking Offshore Wind Auction and Its Implications for Future Auctions Key Points*. Tech. rep. May. 2017. URL: http://www.nera.com/content/dam/nera/publications/2017/PUB{_}Offshore{_}EMI{_}A4{_}0417.pdf.

[19] UK Department of Business Energy and Industrial Strategy. *Contracts for Difference Second Allocation Round Results*. 2017. URL: https://www.gov.uk/government/uploads/system/uploads/attachment{_}data/file/643560/CFD{_}allocation{_}round{_}2{_}outcome{_}FINAL.pdf.

[20] UK Department of Energy and Climate Change (DECC). *CFD Auction Allocation Round One*. 2014. URL: http://e-journal.uajy.ac.id/14649/1/JURNAL.pdf.

[21] UK Department of Business Energy and Industrial Strategy. *Contracts for Difference Allocation Round 3 Results*. Tech. rep. September. 2019. URL: https://assets.publishing.service.gov.uk/government/uploads/system/uploads/attachment{_}data/file/838914/cfd-ar3-results-corrected-111019.pdf{\%}0A.

[22] ReNEWS. *UK commits to rolling CfD rounds*. 2018. URL: http://renews.biz/111908/uk-commits-to-rolling-cfd-rounds/.

[23] National Grid. "Future Energy Scenarios 2019". In: *Future Energy Scenarios* July (2019), p. 162.

[24] ARPA-E Tech-to-Market. *Introduction to Cost Modeling, Template Overview for Performers*. 2014. URL: https://arpa-e.energy.gov/sites/default/files/documents/files/CostModeling{\%}26TemplateIntro20140210.pdf.

[25] Deniz Ozkan. "Financial Analysis and Cost Optimization of Offshore Wind Energy under Uncertainty and in Deregulated Power Markets". PhD thesis. 2011.

[26] S. A. Herman. *Probabilistic Cost Model for analysis of offshore wind energy costs and potential*. Tech. rep. May. 2002, p. 47. URL: http://www.ecn.nl/docs/library/report/2002/i02007.pdf.

[27] M B Zaaijer et al. *How To Benefit From Cost Modelling of Offshore Wind Farms?* Tech. rep. 2003.

[28] UK Department of Energy and Climate Change (DECC). *DECC Offshore Wind Programme Simple Levelised Cost of Energy Model shore Wind Programme velised Cost of Energy Model*. 2014.

[29] Anastasia Ioannou, Andrew Angus, and Feargal Brennan. "Stochastic Prediction of Offshore Wind Farm LCOE through an Integrated Cost Model". In: *Energy Procedia* 107.September 2016 (2017), pp. 383–389. ISSN: 18766102. DOI: 10.1016/j.egypro.2016.12.180.

[30] Mark J. Kaiser and Brian F. Snyder. *Offshore wind energy cost modeling-Installation and decommissioning*. 2012, 248 pp. ISBN: 9781608052851. DOI: 10.2174/97816080528511060101. URL: http://www.benthamdirect.org/pages/content.php?9781608052851.

[31] Mahmood Shafiee, Feargal Brennan, and Inés Armada Espinosa. "A parametric whole life cost model for offshore wind farms". In: *International Journal of Life Cycle Assessment* 21.7 (2016), pp. 961–975. ISSN: 16147502. DOI: 10.1007/s11367-016-1075-z. URL: http://dx.doi.org/10.1007/s11367-016-1075-z.

[32] Marita Balks and Jonathan Grasse. "Aggregierte Risiken für Offshore-Wind-Investitionen — eine Simulation". In: *Analysen und Berichte Klimapolitik* 96 (2016), pp. 842–848. ISSN: 0043-6275. DOI: 10.1007/s10273-016-2059-0. URL: http://link.springer.com/10.1007/s10273-016-2059-0.

[33] Anastasia Ioannou, Andrew Angus, and Feargal Brennan. "A lifecycle techno-economic model of offshore wind energy for different entry and exit instances". In: *Applied Energy* 221.March (2018), pp. 406–424. ISSN: 03062619. DOI: 10.

1016/j.apenergy.2018.03.143. URL: https://doi.org/10.1016/j.apenergy.2018.03.143.

[34] Anastasia Ioannou, Andrew Angus, and Feargal Brennan. "Stochastic financial appraisal of offshore wind farms". In: *Renewable Energy* 145 (2019), pp. 1176–1191. ISSN: 0960-1481. DOI: 10.1016/j.renene.2019.06.111. URL: https://doi.org/10.1016/j.renene.2019.06.111.

[35] Varvara Mytilinou and Athanasios J. Kolios. "Techno-economic optimisation of offshore wind farms based on life cycle cost analysis on the UK". In: *Renewable Energy* 132 (2019), pp. 439–454. ISSN: 18790682. DOI: 10.1016/j.renene.2018.07.146. URL: https://doi.org/10.1016/j.renene.2018.07.146.

[36] DNV GL. *VALUE CHAIN ASSESSMENT SERVICE The power of seeing the bigger picture*. 2014.

[37] Angel G. Gonzalez-Rodriguez. "Review of offshore wind farm cost components". In: *Energy for Sustainable Development* 37 (2017), pp. 10–19. ISSN: 23524669. DOI: 10.1016/j.esd.2016.12.001. URL: http://dx.doi.org/10.1016/j.esd.2016.12.001.

[38] BVG Associates, The Crown Estate, and ORE Catapult. *Guide to an offshore wind farm*. Tech. rep. January. 2019.

[39] Philipp Härtel and Til Kristian Vrana. "Estimation of investment model cost parameters for VSC HVDC transmission infrastructure". In: *Electric Power Systems Research* 160 (2018), pp. 99–108. ISSN: 03787796. DOI: 10.1016/j.epsr.2018.02.007. URL: http://dx.doi.org/10.1016/j.epsr.2017.06.008.

[40] Dan G Cacuci. *Sensitivity & Uncertainty Analysis, Volume I: Theory*. CHAPMAN & HALL/CRC A, 2003, p. 285. ISBN: 1584881151. DOI: 10.1201/9780203911396.ch10.

[41] Etienne de Rocquigny, Nicolas Devictor, and Stefano Tarantola. *Uncertainty in Industrial Practice: A Guide to Quantitative Uncertainty Management*. 2008, p. 364. ISBN: 0470770740. DOI: 10.1002/9780470770733. URL: https://books.google.com/books?id=qg8bqw6ByskC{\&}pgis=1.

[42] Federico Ferretti, Andrea Saltelli, and Stefano Tarantola. "Trends in sensitivity analysis practice in the last decade". In: *Science of the Total Environment* 568 (2016), pp. 666–670. ISSN: 18791026. DOI: 10.1016/j.scitotenv.2016.02.133. URL: http://dx.doi.org/10.1016/j.scitotenv.2016.02.133.

[43] Andrea Saltelli et al. *Global Sensitivity Analysis. The Primer*. 2008, pp. 237–275. ISBN: 9780470725184. DOI: 10.1002/9780470725184. arXiv: arXiv:1011.1669v3. URL: http://doi.wiley.com/10.1002/9780470725184.ch6{\%}5Cnhttp://doi.wiley.com/10.1002/9780470725184.

[44] John Norton. "An introduction to sensitivity assessment of simulation models". In: *Environmental Modelling and Software* 69 (2015), pp. 166–174. ISSN: 13648152. DOI: 10.1016/j.envsoft.2015.03.020. URL: http://dx.doi.org/10.1016/j.envsoft.2015.03.020.

[45] Francesca Pianosi, Fanny Sarrazin, and Thorsten Wagener. "A Matlab toolbox for Global Sensitivity Analysis". In: *Environmental Modelling and Software* 70 (2015), pp. 80–85. ISSN: 13648152. DOI: 10.1016/j.envsoft.2015.04.009. arXiv: NIHMS150003. URL: http://dx.doi.org/10.1016/j.envsoft.2015.04.009.

[46] Francesca Pianosi et al. "Sensitivity analysis of environmental models: A systematic review with practical workflow". In: *Environmental Modelling and Software* 79 (2016), pp. 214–232. ISSN: 13648152. DOI: 10.1016/j.envsoft.2016.02.008. arXiv: j.envsoft.2016.02.008 [10.1016]. URL: http://dx.doi.org/10.1016/j.envsoft.2016.02.008.

[47] Fanny Sarrazin, Francesca Pianosi, and Thorsten Wagener. "Global Sensitivity Analysis of environmental models: Convergence and validation". In: *Environmental Modelling and Software* 79 (2016), pp. 135–152. ISSN: 13648152. DOI: 10.1016/j.envsoft.2016.02.005. URL: http://dx.doi.org/10.1016/j.envsoft.2016.02.005.

[48] Francesca Pianosi and Thorsten Wagener. "A simple and efficient method for global sensitivity analysis based oncumulative distribution functions". In: *Environmental Modelling and Software* 67 (2015), pp. 1–11. ISSN: 13648152. DOI:

10.1016/j.envsoft.2015.01.004. URL: http://dx.doi.org/10.1016/j.envsoft.2015.01.004.

[49] Zhang Chun Tang et al. "Uncertainty analysis and global sensitivity analysis of techno-economic assessments for biodiesel production". In: *Bioresource Technology* 175 (2015), pp. 502–508. ISSN: 18732976. DOI: 10.1016/j.biortech.2014.10.162. URL: http://dx.doi.org/10.1016/j.biortech.2014.10.162.

[50] Clemens Hübler, Cristian Guillermo Gebhardt, and Raimund Rolfes. "Hierarchical four-step global sensitivity analysis of offshore wind turbines based on aeroelastic time domain simulations". In: *Renewable Energy* 111.May (2017), pp. 878–891. ISSN: 18790682. DOI: 10.1016/j.renene.2017.05.013.

[51] Rebecca Martin et al. "Sensitivity analysis of offshore wind farm operation and maintenance cost and availability". In: *Renewable Energy* 85 (2016), pp. 1226–1236. ISSN: 18790682. DOI: 10.1016/j.renene.2015.07.078. URL: http://dx.doi.org/10.1016/j.renene.2015.07.078.

[52] Francesca Campolongo, Andrea Saltelli, and Jessica Cariboni. "From screening to quantitative sensitivity analysis. A unified approach". In: *Computer Physics Communications* 182.4 (2011), pp. 978–988. ISSN: 00104655. DOI: 10.1016/j.cpc.2010.12.039. URL: http://dx.doi.org/10.1016/j.cpc.2010.12.039.

[53] Esteve Borràs Mora, James Spelling, and Adriaan H. van der Weijde. "Benchmarking the PAWN distribution-based method against the variance-based method in global sensitivity analysis: Empirical results". In: *Environmental Modelling and Software* 122.October (2019). ISSN: 13648152. DOI: 10.1016/j.envsoft.2019.104556.

[54] Emanuele Borgonovo and Elmar Plischke. "Sensitivity analysis: A review of recent advances". In: *European Journal of Operational Research* 248.3 (2016), pp. 869–887. ISSN: 03772217. DOI: 10.1016/j.ejor.2015.06.032. URL: http://dx.doi.org/10.1016/j.ejor.2015.06.032.

[55] Bertrand Iooss and Paul Lemaître. "A Review on Global Sensitivity Analysis Methods". In: (2015), pp. 101–122. ISSN: 1387666X. DOI: 10.1007/978-1-4899-

7547-8_5. arXiv: 1404.2405. URL: http://link.springer.com/10.1007/978-1-4899-7547-8{_}5.

[56] M D Morris. "Factorial plans for preliminary computational experiments". In: *Technometrics* 33.2 (1991), pp. 161–174.

[57] Andrea Saltelli et al. *Sensitivity analysis practice: A guide to scientific models.* 2004. ISBN: 0951-8320. DOI: 10.1016/j.ress.2005.11.014.

[58] Francesca Campolongo, Jessica Cariboni, and Andrea Saltelli. "An effective screening design for sensitivity analysis of large models". In: *Environmental Modelling and Software* 22.10 (2007), pp. 1509–1518. ISSN: 13648152. DOI: 10.1016/j.envsoft.2006.10.004.

[59] Francesca Campolongo and Jessica Cariboni. "Sensitivity analysis: how to detect important factors in large models". In: *European Commission, Joint Research Centre, Ispra (VA), Italy* (2007). URL: http://scholar.google.com/scholar?hl=en{\&}btnG=Search{\&}q=intitle:Sensitivity+analysis+:+how+to+detect+important+factors+in+large+models{\#}0.

[60] R. I. Cukier, H. B. Levine, and K. E. Shuler. "Nonlinear sensitivity analysis of multiparameter model systems". In: *Journal of Computational Physics* 26 (1978), pp. 1–42. ISSN: 00223654. DOI: 10.1021/j100540a010.

[61] Andrea Saltelli and Ricardo Bolado. "An alternative way to compute Fourier amplitude sensitivity test (FAST)". In: *Computational Statistics and Data Analysis* 26.4 (1998), pp. 445–460. ISSN: 01679473. DOI: 10.1016/S0167-9473(97)00043-1.

[62] A. Saltelli, S. Tarantola, and K. P.S. Chan. "A quantitative model-independent method for global sensitivity analysis of model output". In: *Technometrics* 41.1 (1999), pp. 39–56. ISSN: 15372723. DOI: 10.1080/00401706.1999.10485594.

[63] T Homma and Andrea Saltelli. "Importance measures in global sensitivity analysis of nonlinear models". In: *Reliability Engineering & System Safety* 52 (1996), pp. 1–17. ISSN: 09518320. DOI: 10.1016/0951-8320(96)00002-6. URL: http://www.sciencedirect.com/science/article/pii/0951832096000026.

[64] I M Sobol. “Sensitivity analysis for nonlinear mathematical models”. In: *Math. Model. Computer.Exp* 1.4 (1993), pp. 407–414. ISSN: 0234-0879. DOI: 10.18287/0134-2452-2015-39-4-459-461.. arXiv: arXiv:1305.4373v1. URL: http://max2.ese.u-psud.fr/epc/conservation/MODE/SobolOriginalPaper.pdf{\%}0Ahttp://www.mathnet.ru/eng/mm2320.

[65] Andrea Saltelli. “Making best use of model valuations to compute sensitivity indices”. In: *Computer Physics Communications* 145 (2002), pp. 280–297. DOI: 10.1016/S0010-4655(02)00280-1.

[66] I. M. Sobol. “Theorems and examples on high dimensional model representation”. In: *Reliability Engineering & System Safety* 79.2 (2003), pp. 187–193. ISSN: 09518320. DOI: 10.1016/S0951-8320(02)00229-6. URL: http://www.sciencedirect.com/science/article/pii/S0951832002002296.

[67] Michiel J.W. Jansen. “Analysis of variance designs for model output”. In: *Computer Physics Communications* 117.1 (1999), pp. 35–43. ISSN: 00104655. DOI: 10.1016/S0010-4655(98)00154-4.

[68] Huibin Liu, Wei Chen, and Agus Sudjianto. “Relative Entropy Based Method for Probabilistic Sensitivity Analysis in Engineering Design”. In: *Journal of Mechanical Design* 128.2 (2006), p. 326. ISSN: 10500472. DOI: 10.1115/1.2159025. URL: http://mechanicaldesign.asmedigitalcollection.asme.org/article.aspx?articleid=1448867.

[69] Emanuele Borgonovo, William Castaings, and Stefano Tarantola. “Moment Independent Importance Measures: New Results and Analytical Test Cases”. In: *Risk Analysis* 31.3 (2011), pp. 404–428. ISSN: 02724332. DOI: 10.1111/j.1539-6924.2010.01519.x.

[70] Farkhondeh Khorashadi Zadesh. “Comparison of variance-based and moment-independent global SA approached by the application of SWAT model”. In: *Environmental Modelling and Software* 91 (2017), pp. 210–222.

[71] Francesca Pianosi and Thorsten Wagener. “Distribution-based sensitivity analysis from a generic input-output sample”. In: *Environmental Modelling and Software* 108.August 2018 (2018), pp. 197–207. ISSN: 13648152. DOI: 10.1016/j.

envsoft.2018.07.019. URL: https://doi.org/10.1016/j.envsoft.2018.07.019.

[72] Esteve Borras Mora. "Transition from Deterministic to Stochastic Cost Models for Offshore Wind Farms". In: *Offshore Wind Energy Conference*. June. 2017.

[73] The Crown Estate. *A Guide to an Offshore Wind Farm*. Tech. rep. 2010, pp. 1–70. URL: http://www.thecrownestate.co.uk/guide{_}to{_}offshore{_}windfarm.pdf.

[74] Gavin Towler and Ray Sinnott. "Capital Cost Estimating". In: *Chemical Engineering Design*. 1975. 2013. Chap. 7, pp. 307–354. ISBN: 978-0-08-096659-5. DOI: 10.1016/B978-0-08-096659-5.00007-9. URL: http://linkinghub.elsevier.com/retrieve/pii/B9780080966595000079.

[75] Iain Staffell and Richard Green. "How does wind farm performance decline with age ?" In: *Renewable Energy* 66 (2014), pp. 775–786. ISSN: 0960-1481. DOI: 10.1016/j.renene.2013.10.041. URL: http://dx.doi.org/10.1016/j.renene.2013.10.041.

[76] EnergyNumbers. *UK offshore wind capacity factors*. 2019. URL: http://energynumbers.info/uk-offshore-wind-capacity-factors.

[77] IRENA. "Offshore innovation widens renewable energy options: Opportunities, challenges and the vital role of international co-operation to spur the global energy transformation". In: *Irena* (2018). URL: https://www.irena.org/-/media/Files/IRENA/Agency/Publication/2018/Sep/IRENA{_}offshore{_}wind{_}brief{_}G7{_}2018.pdf.

[78] Tobias Wiesenthal et al. *Technology Learning Curves for Energy Policy Support*. 2012, p. 36. ISBN: 9789279256769. DOI: 10.2790/59345.

[79] J. Bard and F. Thalemann. *Offshore Infrastructure : Ports and Vessels*. Tech. rep. 2011.

[80] Ramboll. *150 Monopiles in the North Sea push offshore wind into deeper waters*. 2016. URL: https://uk.ramboll.com/projects/re/150-monopiles-in-the-north-sea-push-offshore-wind-into-deeper-waters.

[81] OffshoreWind.biz. *Bladt Industries: Uniform Jacket Foundation Design Would Save Money (Interview)*. URL: https://www.offshorewind.biz/2016/10/31/bladt-industries-uniform-jacket-foundation-design-would-save-money-interview/.

[82] DONG Energy. *A view on steel demand for offshore wind power*. Tech. rep. 2013.

[83] Salzgitterag. *Mass Production of Offshore-Wind-Jackets requires new Industrial Solutions*. Tech. rep. 2014.

[84] Kirsty Shearer. "Assessment of cumulative impacts in offshore wind developments". PhD thesis. 2013.

[85] Ballast Nedam. *Optimal integrated combination of foundation concept and installation method*. Tech. rep. 2009.

[86] Civil Engineering and Development Department. The Government of the Hong Kong Special Administrative Region. *Appendix c determination of size of armour*. URL: https://www.cedd.gov.hk/filemanager/eng/content{_}101/p4{_}c.pdf.

[87] P. Gardner, L. M. Craig, and G.J. Smith. "Electrical Systems for Offshore Wind Farms". In: (). ISSN: 2193-1801.

[88] EDF Energy. *NAVITUS BAY OFFSHORE WIND PARK*. Tech. rep. Unpublished Internal Document, EDF Energy R&D UK Centre, 2015.

[89] James Spelling. *Offshore Wind Structures: Simplified Mass Correlations*. Tech. rep. January. 2016, pp. 1–31. DOI: 10.1007/978-3-642-25850-3_25.

[90] James Spelling. *Electrical Cost Functions Excel File*. Tech. rep. 2016.

[91] Ofgem. "Report on the Recommendations Arising from Additional Cost Benefit Analyses". In: (2008). URL: https://www.ofgem.gov.uk/publications-and-updates/report-recommendations-arising-additional-cost-benefit-analyses.

[92] Bela H Buck and Richard Langan. *Aquaculture Perspective of Multi-Use Sites in the Open Ocean*. 2017. ISBN: 9783319511573. DOI: 10.1007/978-3-319-51159-7.

[93] Mainstream Renewable Power. *Offshore O&M Costs Estimates*. Tech. rep. 2009, pp. 1–18.

[94] The Crown Estate. *A guide to UK offshore wind operations and maintenance*. Tech. rep. 2013, p. 42.

[95] Mainstream Renewable Power. *First, Second and Third Line Event Synergies, 1GW versus 500MW*. Tech. rep. 2009, pp. 1–6.

[96] Rebecca Martin. "Sensitivity Analysis of Offshore Wind Farm Availability and Operations & Maintenance Costs Subject to Uncertain Input Factors". PhD thesis. 2015.

[97] Helene Seyr and Michael Muskulus. "Decision Support Models for Operations and Maintenance for Offshore Wind Farms: A Review". In: *Applied Sciences* 9.2 (2019), p. 278. DOI: 10.3390/app9020278.

[98] National Grid. *Transmission Network Use of System (TNUoS) charges*. 2019. URL: https://www.nationalgrideso.com/charging/transmission-network-use-system-tnuos-charges.

[99] National Grid. *Balancing Services Use of System (BSUoS) charges*. 2019. URL: https://www.nationalgrideso.com/charging/balancing-services-use-system-bsuos-charges.

[100] In3 Finance. *What's the difference between Venture Finance and Project Finance?* URL: http://www.in3finance.com/project-vs-venture-finance-for-startups/{\%}0A.

[101] UK Department of Business Energy and Industrial Strategy. *Cost Estimation and Liabilities in Decommissioning Offshore Wind Installations Public Report*. Tech. rep. 2018, p. 39. URL: www.arup.com.

[102] Frank H Knight. *Risk Uncertainty and Profit Knight*. Vol. 36. 4. 1921, p. 682. DOI: 10.2307/1884757. URL: http://www.jstor.org/stable/1884757?origin=crossref.

[103] L Savage. *The foundations of statistics*. 1954, p. 352. URL: http://portal.acm.org/citation.cfm?id=85307{\%}5Cnpapers2://publication/uuid/F4932434-028B-4F64-82CA-B366640DD43D.

[104] Daniel Ellsberg. "Risk , Ambiguity, and the Savage Axioms". In: *The Quarterly Journal of Economics* 75.4 (1961), pp. 643–669.

[105] Alberto Pasanisi. "An Industrial Viewpoint on Uncertainty Quantification in Simulation : Stakes , Methods , Tools , Examples". In: *Conference on Uncertainty Quantification in Scientific Computing*. 2011.

[106] Othmane El Mountassir and Strang-Moran Charlotte. *Offshore Wind Subsea Power Cables. Installation, Operation and Market Trends*. Tech. rep. September 2018. CATAPULT Offshore Renewable Energy, 2018, pp. 1–6.

[107] Low Carbon Contracts Company. *Contracts for Difference (CFD) Booklet 2016 / 17 : Overview of the CFD mechanism and Delivery Partners*. Tech. rep. 2016.

[108] Nadine Gatzert and Thomas Kosub. "Risks and risk management of renewable energy projects : The case of onshore and offshore wind parks". In: *Renewable and Sustainable Energy Reviews* 60 (2016), pp. 982–998. ISSN: 1364-0321. DOI: 10.1016/j.rser.2016.01.103. URL: http://dx.doi.org/10.1016/j.rser.2016.01.103.

[109] The University of Edinburgh Research Services. *Introduction to Eddie*. Tech. rep. 2018.

[110] I.M Sobol, Yu Turchaninov, and B.V Leviatan. "Quasi Random Sequence Generator". In: *Keldysh Institute of Applied Mathematics, Russian Accademy of Sciences, Moscow* (1992).

[111] Paul Bratley. "Implementation and Tests of Low-Discrepancy Sequences". In: *ACM Transactions on Modeling and Computer Simulation* 2.3 (1992), pp. 195–213.

[112] Andrea Saltelli et al. "Variance based sensitivity analysis of model output. Design and estimator for the total sensitivity index". In: *Computer Physics Communications* 181.2 (2010), pp. 259–270. ISSN: 00104655. DOI: 10.1016/j.cpc.2009.09.018. URL: http://dx.doi.org/10.1016/j.cpc.2009.09.018.

[113] R. Tyrrell Rockafellar and Stanislav Uryasev. "Optimization of conditional value-at-risk". In: *The Journal of Risk* 2.3 (2000), pp. 21–41. ISSN: 14651211. DOI: 10.21314/JOR.2000.038. arXiv: arXiv:1011.1669v3. URL: http://www.risk.net/journal-of-risk/technical-paper/2161159/optimization-conditional-value-risk.

[114] R Tyrrell Rockafellar and Stanislav Uryasev. "Conditional value-at-risk for general loss distributions". In: *Journal of Banking & Finance* 26 (2002), pp. 1443–1471.

[115] Philippe Artzner et al. "Coherent measures of risk". In: *Mathematical Finance* 9.3 (1999), pp. 203–228. ISSN: 09601627. DOI: 10.1111/1467-9965.00068.

[116] Francisco D Munoz et al. "Does risk aversion affect transmission and generation planning ? A Western North America case study". In: *Energy Economics* 64 (2017), pp. 213–225. ISSN: 0140-9883. DOI: 10.1016/j.eneco.2017.03.025. URL: http://dx.doi.org/10.1016/j.eneco.2017.03.025.

[117] Tom Carsey et al. *Monte Carlo Simulation and Resampling*. Tech. rep. 2011.

[118] Efron Bradley. "Bootstrap Methods: Another Look at the Jackknife". In: *The Annals of Statistics* 7.1 (1979), pp. 1–26. DOI: doi:10.1214/aos/1176344552. URL: http://www.ncbi.nlm.nih.gov/entrez/query.fcgi?db=pubmed{\&}cmd=Retrieve{\&}dopt=AbstractPlus{\&}list{_}uids=MR1429931.

[119] E de Rocquigny, N Devictor, and S Tarantola. *Uncertainty in industrial practice: a guide to quantitative uncertainty management*. 2008, p. 364. ISBN: 0470770740. DOI: 10.1002/9780470770733.

[120] Emanuele Borgonovo. "A new uncertainty importance measure". In: *Reliability Engineering & System Safety* 92 (2007), pp. 771–784. DOI: 10.1016/j.ress.2006.04.015.

[121] Manel Baucells and Emanuele Borgonovo. "Invariant Probabilistic Sensitivity Analysis". In: *Management Science* 59 (2013), pp. 2536–2549.

[122] Elmar Plischke, Emanuele Borgonovo, and Curtis L Smith. "Global sensitivity measures from given data". In: *European Journal of Operational Research* 226.3 (2013), pp. 536–550. ISSN: 0377-2217. DOI: 10.1016/j.ejor.2012.11.047. URL: http://dx.doi.org/10.1016/j.ejor.2012.11.047.

[123] Mario Holl et al. "Sensitivity analysis of a techno-economic optimal wind-energy converter". In: *International Conference On Next Generation Wind Energy (ICNGWE)*. i. 2016, pp. 1–24.

[124] Fabrice Gamboa et al. "Sensitivity analysis based on Cramer von Mises distance e". In: *SIAM/ASA Journal on Uncertainty Quantification* 6 (2018), pp. 522–548.

[125] Bruno Sudret. "Uncertainty propagation and sensitivity analysis in mechanical models Contributions to structural and stochastic spectral methods". PhD thesis. Universite BLAISE PASCAL - Clermont II, 2007, p. 252.

[126] T Ishigami and T Homma. *An Importance Quantification Technique in Uncertainty Analysis for Computer Models*. Tech. rep. Japan Atomic Energy Research Institute, 1990, pp. 398–403.

[127] Jean-Marc Baudin, Michael; Matinez. *Introduction to Sensitivity Analysis with NISP*. Tech. rep. January. 2013, p. 73. URL: file:///C:/Users/MAS/Downloads/nisp{_}introsensal{_}v0.5.pdf{\%}0Ahttp://forge.scilab.org/index.php/p/nisp/downloads/get/nisp{_}introsensal{_}-{_}v0.4.pdf.

[128] The Crown Estate. *Offshore wind cost reduction-Pathways study*. Tech. rep. 2012, 88 pp. URL: http://www.thecrownestate.co.uk/media/5462/ei-offshore-wind-operational-report-2015.pdf.

[129] Esteve Borràs Mora et al. "The effects of mean wind speed uncertainty on project finance debt sizing for offshore wind farms". In: *Applied Energy* 252.June (2019). ISSN: 03062619. DOI: 10.1016/j.apenergy.2019.113419.

[130] Esteve Borras Mora. "How does risk aversion shape overplanting in the design of offshore wind farms ?" In: *Journal of Physics: Conference Series* (2019). DOI: 10.1088/1742-6596/1356/1/012026.

[131] Bjarne Steffen. "The importance of project finance for renewable energy projects". In: *Energy Economics* 69 (2018), pp. 280–294. ISSN: 0140-9883. DOI: 10.1016/j.eneco.2017.11.006. URL: https://doi.org/10.1016/j.eneco.2017.11.006.

[132] Wind Europe. *Financing and investment trends: The European wind industry in 2017*. Tech. rep. 2018, p. 32. DOI: 10.1080/00218460701751855. URL: https://windeurope.org/wp-content/uploads/files/about-wind/reports/Financing-and-Investment-Trends-2017.pdf.

[133] IEA - RETD Renewable Energy Technology Deployment. *Gusts of change: How effective policy is catalysing a booming offshore wind sector*. Tech. rep. March. 2017.

[134] Achim Schreider and Mirko Sedlacek. "Project Financing Offshore Wind Farms: Risk Analysis for a Structured Finance". In: *European Offshore WInd 2009 Conference*. Stockholm, 2009, pp. 1–10.

[135] David Wadham. *Financig Offshore Wind: Plain sailing?* Tech. rep. 20. 2018.

[136] D Foussekis et al. "Uncertainty estimations for offshore wind resource assessment and power verification". In: *EERA DeepWInd 18*. Trondheim, 2018.

[137] Angeliki Loukatou et al. "Stochastic wind speed modelling for estimation of expected wind power output". In: *Applied Energy* 228.May (2018), pp. 1328–1340. ISSN: 03062619. DOI: 10.1016/j.apenergy.2018.06.117. URL: https://doi.org/10.1016/j.apenergy.2018.06.117.

[138] Anthony Crockford et al. *Estimated uncertainty for various wind measurement strategies including floating LiDAR at the Hollandse Kust Zuid offshore wind farm zone*. Tech. rep. 2016.

[139] Jie Yan et al. "Uncertainty estimation for wind energy conversion by probabilistic wind turbine power curve modelling". In: *Applied Energy* 239.September 2018 (2019), pp. 1356–1370. ISSN: 03062619. DOI: 10.1016/j.apenergy.2019.01.180.

[140] Gavin Smart. *Offshore Wind Cost Reduction: Recent and future trends in the UK and Europe*. Tech. rep. November. 2016, pp. 1–10.

[141] Anastasia Ioannou, Andrew Angus, and Feargal Brennan. "A lifecycle techno-economic model of offshore wind energy for different entry and exit instances". In: *Applied Energy* 221.November 2017 (2018), pp. 406–424. ISSN: 03062619. DOI: 10.1016/j.apenergy.2018.03.143. URL: https://doi.org/10.1016/j.apenergy.2018.03.143.

[142] EDHEC Infrastructure Institute-Singapore. *Cash Flow Dynamics of Private infrastructure Project Debt*. Tech. rep. March. 2016, pp. 1–108.

[143] Green Giraffe. *Project finance for German offshore wind*. Tech. rep. February. 2017.

[144] Edward Bodmer. "Debt Sculpting in a Project Finance Model". In: *Corporate and Project Finance Modeling. Theory and Practice*. 2015. Chap. 41, pp. 515–537. ISBN: 9781118854365. DOI: 10.1002/9781118957394. URL: https://drive.google.com/open?id=0B544TwTVwnWkN2Z1Sm9YZHZxSG8.

[145] Green Giraffe. *Offshore wind finance – evolution and outlook*. Tech. rep. September. 2017.

[146] Green Giraffe. *Introduction to wind project finance*. Tech. rep. March. 2017.

[147] Peter Clive et al. *Offshore Power Curve Tests for Onshore Costs : A Real World Case Study*. Tech. rep. 2014, pp. 1–9. DOI: 10.1177/1066480709355039.

[148] BVG Associates. *Value breakdown for the offshore wind sector*. Tech. rep. February. 2010, pp. 1–20. URL: https://www.gov.uk/government/uploads/system/uploads/attachment{_}data/file/48171/2806-value-breakdown-offshore-wind-sector.pdf.

[149] G.A.Cool. "Floating LiDAR technology: Oceanographic parameters influencing accuracy of wind vector reconstruction". PhD thesis. 2016.

[150] Hugo Herrmann et al. "Floating LiDAR Uncertainty Assessment Wind Europe – Resource Assessment March 2017". In: March. 2017.

[151] Carbon Trust. *Carbon Trust Offshore Wind Accelerator Program*. Tech. rep. 2017. URL: https://www.carbontrust.com/offshore-wind/owa/.

[152] Electricity Market Reform. "Supply Chain Plan Consultation". In: November (2013).

[153] Offshorewindbiz. *Burbo Bank Extension First FLiDAR-Calculated OWF to Be Built*. 2015. URL: https://www.offshorewind.biz/2015/04/24/burbo-bank-extension-first-flidar-calculated-owf-to-be-built/.

[154] J. Gottschall et al. "Results and conclusions of a floating-lidar offshore test". In: *Energy Procedia* 53.C (2014), pp. 156–161. ISSN: 18766102. DOI: 10.1016/j.egypro.2014.07.224. URL: http://dx.doi.org/10.1016/j.egypro.2014.07.224.

[155] Julia Gottschall et al. "Floating lidar as an advanced offshore wind speed measurement technique: current technology status and gap analysis in regard to full maturity". In: *Wiley Interdisciplinary Reviews: Energy and Environment* 6.5 (2017). ISSN: 2041840X. DOI: 10.1002/wene.250.

[156] Offshorewindbiz. *Axys FLIDAR Reaches Stage 3 on Carbon Trust Roadmap*. 2018. URL: https://www.offshorewind.biz/2017/06/06/axys-flidar-reaches-stage-3-on-carbon-trust-roadmap/.

[157] DNV KEMA ENERGY & SUSTAINABILITY. *Framework for the Categorisation of Losses and Uncertainty for Wind Energy Assessments*. Tech. rep. 2013. URL: http://www.sgurrenergy.com/wp-content/uploads/2013/02/Loss-and-Uncertainty-Definitions-Report-05Feb2013.pdf.

[158] DNV GL. *Study on UK Offshore Wind Variability*. Tech. rep. L2C124303-UKBR-R-01, Issue B. 2016.

[159] National Grid. *Round 3 Offshore Wind Farm Connection Study*. Tech. rep. 2008.

[160] Brid ODonovan. *Connection Offer Policy & Process (COPP)*. Tech. rep. Commission for Energy Regulation, 2011.

[161] Nigel Morris. *Decision on Installed Capacity Cap Installed Capacity Cap*. Tech. rep. Commission for Energy Regulation, 2014.

[162] Forewind. *Environmental Statement Chapter 6 Appendix B Offshore Project Boundary Selection Report*. Tech. rep. March. 2014.

[163] Limited SMart Wind. "Hornsea Offshore Wind Farm - Project Two". In: 5.January (2015), p. 19.

[164] TenneT Team. *POSITION PAPER Overplanting*. Tech. rep. TenneT, 2015, pp. 1–7. URL: https://www.tennet.eu/fileadmin/user{_}upload/Our{_}Grid/Offshore{_}Netherlands/Consultatie{_}proces{_}net{_}op{_}zee/Technical{_}Topics/50{_}ONL{_}15-083-T11{_}Overplanting{_}PP{_}v2.pdf.

[165] Celine Mcinerney and Derek W Bunn. "Optimal over installation of wind generation facilities". In: *Energy Economics* 61 (2017), pp. 87–96. ISSN: 0140-9883. DOI: 10.1016/j.eneco.2016.10.022. URL: http://dx.doi.org/10.1016/j.eneco.2016.10.022.

[166] C Wolter et al. "Overplanting in Offshore Wind Power Plants in Different Regulatory Regimes". In: *15th Wind Integration Workshop* 49.0 (2016), pp. 0–4. DOI: 10.1146/annurev.matsci.35.100303.110641.

[167] Pramod Jain. *Wind Resource Assessment : A Key Step in Wind Projects Green Energy Financing Workshop Asia Clean Energy Forum*. 2017.

[168] Brian Gribben, Mark Joyce, and Frazer-Nash Consultancy. *Uncertainty analysis to support asset procurement decisions in offshore wind*. Tech. rep. 2011.

[169] Matthew Huaiquan Zhang. "Wind Park Production Estimate". In: *Wind Resource Assessment and Micro-sitting*. 2015. Chap. 7, pp. 143–167.

[170] Esteve Borras Mora. "How does risk aversion shape overplanting in the design of offshore wind farms ?" In: *Journal of Physics: Conference Series* (2019).

Chapter 10

Appendices

Offshore Wind Energy 2017
6-8 June 2017, London, United Kingdom

Transition from Deterministic to Stochastic Cost Models for Offshore Wind Farms

Esteve Borràs Mora[1,2*] , James Spelling[2], Harry van der Weijde[3]

[1] Industrial Doctoral Centre for Offshore Renewable Energy (IDCORE), The University of Edinburgh, Edinburgh, EH9 3JL, UK
[2] EDF Energy R&D UK Centre, Interchange, 81-85 Station Road, Croydon, CR0 2AJ, UK
[3] University of Edinburgh, Institute for Energy Systems, School of Engineering, King's Buildings, Edinburgh, EH9 3JL, UK

Abstract

Offshore wind cost modelling seeks to understand and quantify how different project specifications, technology choices and market trends contribute to the overall project finances. Better understanding of costs leads to more informed business decisions in the industry that will help shorten the gap between origination and financing. In order to carry out such tasks, project developers, investors and bankers need to get a better understanding of the risks that they are faced with: Will the wind blow as predicted? Will the export cable have the stated availability? Will construction and commissioning be completed on time without any major overruns? Will the O&M strategy be performed as described? Often, scenario analysis has been used in order to address these uncertainties, by means of best, worst and most likely scenarios, and the differences between the key output metrics used as a measure of risk by decision makers. However, in general, such analyses are not rigorous and differ substantially from the risk measures used in the financial world. Establishing a probabilistic framework helps to better quantify these risks, identify how they impact the costs and allow engineers and investors to "talk the same language" about common risk measures. The probabilistic framework developed in this paper will be of interest to offshore wind farm developers and investors for early-stage decision-making under uncertainty.

Keywords: Offshore wind cost modelling, Stochastic models, Decision-making processes under uncertainty

*Corresponding author.
Email: E.Borras-Mora@ed.ac.uk.
Tel: +44 (0)2089 352 858

1 Introduction

By the end of 2016, the European offshore wind market had installed a cumulative total capacity of more than 12MW. Within Europe, the UK is the market leader for offshore wind, responsible for 41% of the total number of all grid-connected turbines [1]. To sustain this leading position in the market, a Levelised Cost of Energy Cost (LCOE) target of £100 per megawatt hour (MWh) was set jointly by the UK government and industry in 2012 [2], which was expected to be met by 2020. However, four years ahead of schedule, wind farms taking investment decisions (FIDs) in 2015/2016 were already achieving prices lower than this target. Record-low contracts for offshore wind farms were awarded to Borsselle 3 and 4 offshore wind project in the Netherlands at 54.5€/MWh in July 2016 and Kriegers Flak in Denmark at 49.9€/MWh in November 2016. More recently, competitive tenders in Germany resulted in bid prices of 0€/MWh in April 2017. Although those bids cannot be compared directly with UK prices, since they do not bear the cost of the electrical transmission system, the bid levels were lower than expected. In addition, the transition to central auctioning systems has pushed developers to make predictions further into the future, increasing the level of uncertainty in their estimates and challenging the way offshore wind cost modelling had previously been addressed. As a result, the aim of this paper is to present a constantly evolving tool capable to cope with quantitative uncertainty management in the burgeoning offshore wind industry.

The paper starts with a presentation of the tool used for offshore wind cost analysis, where the reader is taken through the different stages of the calculation process in Section 2. Then the capital cost estimation methodology is presented in Section 3. After this, Section 4 examines the transition from a deterministic to a stochastic cost model. A probabilistic framework is established to account for the different uncertainties which serve as inputs for the probabilistic cost model. Results comparing probabilistic analysis against scenario analysis for a case study are given in Section 5, followed by conclusions drawn in Section 6, given in conjunction with directions for future research.

2 Cost Modelling - OWCAT

The first studies on offshore wind costs models were based on projecting onshore data to offshore[3]. By doing so the models didn't account for specific offshore parameters and consequently, didn't represent the harsh environmental conditions that offshore wind farms operate in. Later, based on real offshore wind experience from developers, contractors and suppliers, new cost models were specifically created to explain interactions within the offshore industry. In parallel, sensitivity analysis and probabilistic models were developed to attempt to quantify the key cost drivers and uncertainties in their inputs [3], [4] and [5].

Since then, many new offshore wind cost models both commercial and academic have been developed in order to estimate the capital costs, operational expenditure and the LCOE. In 2012 the UK government published a simple Levelised Cost of Energy model to assess the impact of innovations for a given offshore wind farm [6]. Based on that model, a stochastic version was presented in [7] by means of the @RISK extension, where a sensitivity analysis was performed in order to identify the impact of the uncertain input parameters. Given the stochastic nature of the environmental conditions and multidisciplinary content of an offshore wind farm, many approaches have been followed to the development of cost models. Whereas cost modelling engineers tend to focus more on a detailed breakdown of the different offshore wind farm components, as shown in [8], investors typically take a high level perspective on technology and focus more on the risks associated to them, as has been shown in [9].

Despite these attempts to capture offshore wind technicalities, the introduction of new environmental regulations, economic policies, technological advancements and financing structures has resulted in a new set of relationships that need to be considered in order to define risks and profitability for the next generation of offshore wind farms. For these reasons, simple cost models are no longer suitable to accurately represent these relationships, when using them as decision-making tools. Instead, tailored techno-economic models should be developed having the best of both worlds - technology specificities and financial modelling expertise.

The modelling approach to offshore wind cost analysis presented in this paper is based around the Offshore Wind Cost Analysis Tool (OWCAT) developed at the EDF Energy R&D UK Centre. This cost modelling tool has been used in the past for comparative evaluation of multiple sites, detailed evaluation of specific project layouts and sensitivity studies on both design/technology choices and cost variations. The tool has been validated against cost data from the Navitus Bay and Courseulles-sur-Mer projects and shown to be accurate within ± 15% for these cases.

The model consists of three main modules: a wind farm design module, a cost calculation module and a financial module. The first stage of the module concerns the wind farm design. In order to evaluate the costs of the project, it is necessary to have information about the number and type of wind turbines, foundations, inter-array cabling and the export system. In other words, the wind farm itself must be modelled. Designing an offshore wind farm requires interaction between teams from different disciplines; for example, the wind turbine team will have to interact with the foundation team to make sure that the loads of the turbine are correctly passed onto the foundation, and the foundation team will need to make sure that the electrical connections are correctly secured within the foundation. As such, a cost model must capture the same interactions as are involved in the design process and cannot be a simple accumulation of models from separate disciplines.

The design outputs of the first module are fed as inputs into the second module, which calculates the costs of the different offshore wind farm components. The cost module can be divided into Development Expenditure (DEVEX), Capital Expenditure (CAPEX), Operational Expenditure (OPEX) and Decommissioning Expenditure (DECEX). DEVEX covers the costs of all the processes up to the financial close or placing firm orders to proceed with the construction. CAPEX calculates the supply and installation costs of the wind farm, including wind turbines, foundations, inter-array cables, offshore substations, export cables and onshore substations. Indirect costs such as Engineering, Procurement, and Construction Management (EPCM) costs and insurance are also included in the CAPEX breakdown. OPEX includes direct costs for the operation and maintenance of the wind farm, as well as transmission charges, insurance, taxes and royalties. DECEX accounts for the decommissioning of the wind turbines, foundations and offshore substations.

The cost outputs of the second module are passed into the third module, which accounts for the financial model of the wind farm project. The financial model takes into consideration the different cash flows throughout the life of the wind farm, as well as the financing structure put in place to supply the initial capital investment. Based on the resulting free cash flows and financing costs, the LCOE can be determined, together with other financial performance indicators.

Prior to the calculation of the design module, all input data need to be loaded into the tool. The OWCAT structure is shown in Figure 1. This information has been divided into:

- (i) Project Specifications
- (ii) Technical Specifications
- (iii) Economic Specifications
- (iv) Vessel Specifications
- (v) Structural Masses Database

(i) refers to the project offshore wind farm characteristics such as the capacity of the farm, the wind speed at a given referenced height, the average water depth, the soil conditions, the distance from shore, the wind turbine model, foundation type and export system specifications among others. Since no two projects will have the same characteristics, project specifications attempt to model each particular site.(ii) addresses the details of the offshore wind technology, representing wind turbine, foundation, inter-array cable, export system and grid parameters. For example, as far as the wind turbine is concerned, parameters such as the wind turbine availability, the installation vessel associated with the wind turbine, the average loading, installation and commissioning times are accounted for. In addition, a decommissioning factor is used for all offshore wind farm components to account for a reduction in time from the installation phase.(iii) concerns the reference year for real prices, the risk-free rate and

cost of debt, insurance and insurance premium tax rates, contingency requirements, corporation taxes, depreciation, seabed rent, exchange rates and inflation.(iv) involves the different vessel characteristics used in the installation and decommissioning of the offshore wind farms. As an example, heavy-lift jack-up vessel parameters would comprise the day rate, vessel transit speed, vessel positioning time, vessel mobilisation time, operational weather window and carrying capacities in regard to different components.(v) consists of the data used to establish the foundation mass correlations, which are the basis for the CAPEX estimation in the foundation procurement.

The final design contains not only the design of the offshore wind farm, where the foundations masses, inter-array and export system are sized, but also the procurement, vessel charter model and the Annual Energy Production (AEP) as displayed in Figure 1. Procurement stores all information concerning wind turbines, foundations and the electrical system, in terms of the type, number of elements and size (also length if required), giving rise to a procurement catalogue which forms the basis for the cost module. The vessel charter model is based on [10], whereas the AEPs is built upon industry's best practices assuming respectively either a logarithmic- or power-law wind profile in conjunction with a Rayleigh or Weibull probability distribution to model the wind speed. Wake losses and electrical losses are also accounted for in the AEP submodule.

As far as the financial module is concerned, the calculation itself entails not only one but twofold iterative processes. The external loop consists of determining the value of λ that makes Equation 1 equal to 0.

$$LCOE = \lambda | \sum_{t=1}^{n} \frac{FCF_t(t)}{(1+ROE)^t} = 0; \qquad (1)$$

Where FCF are the free cash flows, ROE is the desired return on equity and λ_0 is the intial guess obtained from a simplified financial model. This financial metric such as the LCOE is calculated as the constant inflation-linked real electricity price required to meet the desired ROE. Although the LCOE metric is described below, other financial metrics can also be computed using OWCAT.

The internal loop concerns the debt sizing or sculpting, which determines the maximum amount of project finance debt that the offshore wind farm can sustain based on the bank's requirements. Project lenders usually specify the borrowing capacity on the basis of debt service ratio and convenants. As such, parameters such as the Debt Service Coverage Ratio (DSCR), the maximum leverage and the Cash Flow Available for Debt Service (CFADS) have been considered. Whereas the leverage is expressed as a percentage of the total project debt the owners are allowed to take on, the DSCR is defined as the CFADS divided by the debt service (understanding the debt service as the sum of the principal and interest).

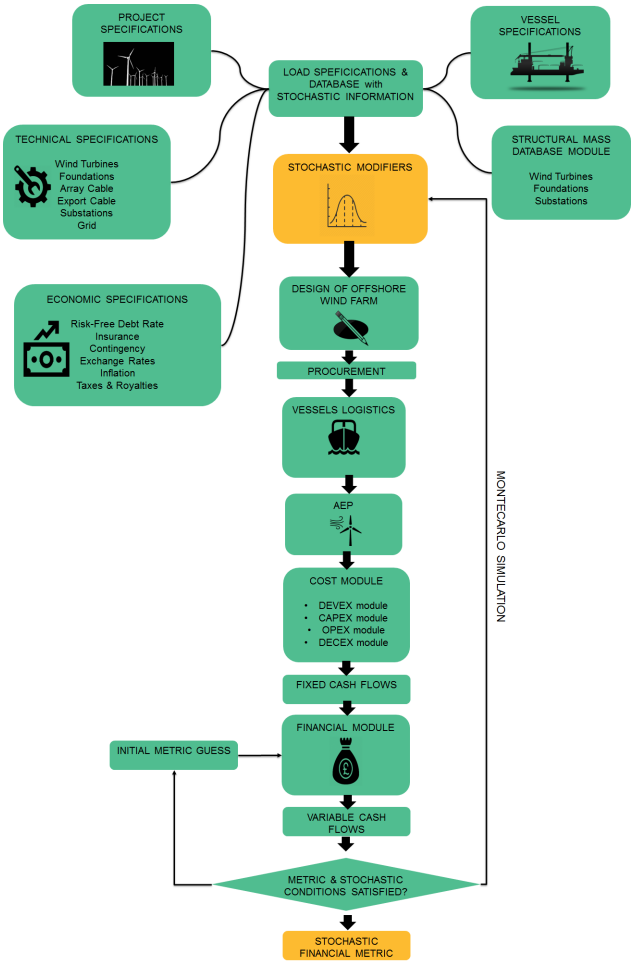

Figure 1: OWCAT structure

3 Estimation of the Capital Costs

Cost estimation is not an exact science, and therefore the level of detail of the cost estimate will depend on the stage the project is at and the amount of resources and effort to compute this estimate. It is worth noting that several associations have established cost estimation classes based on the end usage of the estimate. In the development stage of an offshore wind farm, the cost estimate is understood to belong to Class 3 ([11], [12]), aimed at budget, authorization or control with an expected or probable accuracy range from low: -10% to -20% to high: +10% to +30% .

The preparation method of the farm estimate is based on semi-detailed unit costs together with historical relationship factors included in OWCAT. As the project progresses the level of engineering detail will result in an increase in the accuracy of the cost estimate, as diplayed in Figure 2. However, it should be kept in mind that the tool has been developed and tailored for feasibility studies and no Class 1& 2 estimates should be considered.

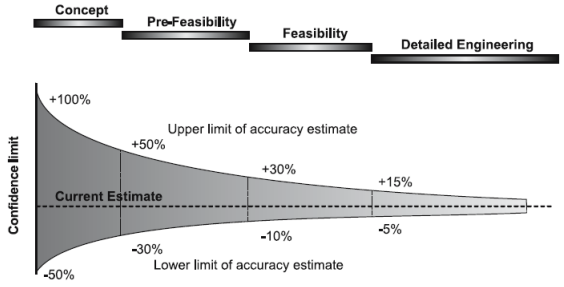

Figure 2: Increasing level of accuracy with the increased definition of the engineering design

Two main techniques are used for estimating capital costs: factored estimation techniques and unit cost techniques [12]. Whereas the unit cost techniques tend to be used when a bill of quantities is available, namely, when the design is at a defined stage, the factored estimation techniques are generally used in the earlier stages. As OWCAT has been tailored for the techno-economic analysis in the earlier stages of an offshore wind farm, a review of the factored estimation techniques is provided in support of the cost modelling functions. Limited availability of cost data in the offshore wind industry means that estimating the price of an item is usually based on historical similar items or publicly available cost data. As a result, there are different types of factoring to account for changes in time, size or capacity or even to estimate the cost of one item based on a factor of major equipment costs. Factoring the time (i): the ratio of an item's cost today to its cost in the past is defined as a cost index, provided those costs are given in the same currency. One of the most watched cost index is the Consumer Price Index (CPI) used as a measure of inflation, providing some insights on the speed at which prices fall or rise. Factoring the exchange rate (ii): As different offshore wind farm components may be supplied by European manufactures, the exchange rate needs to be factored in. Factoring the size (iii): A common standard power law cost function corrects for size or capacity differences, where the exponent n usually ranges from 0 to 1. Economies of scale exist if n is less than one. This means that the cost of the component increases less that the rate in capacity. Otherwise, exponent values greater than one translate into cost increases greater than the rate in capacity. As an example, the civil engineering costs C_{OnS} for the onshore substation (OnS) have been modelled using (iii) subjected to the capacity of OnS Cap_{OnS} and the reference costs C_{ref} for the OnS for a given reference capacity Cap_{ref}. This is displayed below in equation 2.

$$C_{OnS} = C_{ref}(\frac{Cap_{OnS}}{Cap_{ref}})^n \tag{2}$$

Where the exponent n is close to 0.67, and it has been usually referred to as the "rule of the two-thirds". Furthermore, a scaling exponent of 0.5 is typically used for indirect costs such as engineering, design and management activities [13]. OWCAT uses this exponent for all cost functions related to indirect costs, provided no data is available on how to scale them. For instance, the overhead costs for the onshore export cable consider a scaling coefficient of 0.5. If instead of factoring the size, the item's cost is based on a major equipment's cost, the Lang method can be used [12] and [13]. This method relates the total plant cost to the cost of the major equipment. Several refinements to this method exist that may allow for different categories of the farm to be estimated from the equipment costs. However, this approach has only been used for estimating the onshore substa-

tion installation costs.

As has been highlighted in Section 2, a cost estimate is typically based on quotations, curve fits, scaling rules, engineering models , guest estimates or expert input from a design process. Some methods that haven't mentioned before concern the foundations and electrical parts of the wind farm, for which an extensive internal cost data base has been built.

Foundations mass correlation

To be able to evaluate the cost of the foundations during the early stages of project development, a set of simple relationships relating main parameters to the mass of the foundations are needed. First of all, a foundation mass data base was created at EDF R&D UK Centre, where information regarding several parameters of the foundations was gathered. Then the foundation mass estimates are used to obtain the primary steel costs based on finished material costs. The generic form for all mass foundation correlations is given by equation 3.

$$M = C + A \cdot \prod_{i=1}^{N_p} X_i^{b_i} \tag{3}$$

This is based on the extended power law formulation recommended by [13]. The formulation give the mass M as a function of a constant C, a scale parameter A and a series of N_p influence parameters X, each of which is associated with an exponent b. With a view to determine the parameters of the correlations, least squares regression was used. This minimizes the sum of the squared residuals, being those the difference between the observed value $M_{j,ref}$ and the fitted value $M_{j,calc}$ provided by the model, as shown in equation 4.

$$S_{res} = \sum_{j=1}^{N_{ref}} \left(M_{j,calc} - M_{j,ref}\right)^2 \tag{4}$$

The influence parameters that were used to model the foundation mass correlation are based on the water depth (at which the foundation is to be installed), the wind turbine rotor diameter and the topside mass for the wind turbine foundations. When modelling foundations for the electrical substations, the additional following parameters: equivalent capacity and exporting voltage were used.

Electrical components correlation

Although no mass correlation was applied for estimating the cost of the electrical components, a similar approach was carried out to directly obtain the price. This time, the formulation gives the cost of the electrical component as a function of a fixed constant, a scale parameter and a series of influence parameters, each of which is also associated with an exponent. Those parameters differ among different electrical components and include the rated power of the electrical device, the capacity of the substation, the reactive power, the operational voltage and a dummy variable representing if the component is installed either onshore or offshore.

OWCAT cost data come from a variety of sources, based on unpublished internal EDF R&D UK Centre documents and data, publicly available data and discussions with different experts within the group. In any case, a review of offshore wind farm cost components can be found in [14].

4 Methodology

The transition from deterministic to stochastic models require an added level of complexity that can only be justified if three of the following basic features exist. Firstly a pre-existing model, which in this case represents the OWCAT, explained in Section 2. Secondly a variety of sources of uncertainty affecting the inputs of OWCAT. Finally, industrial stakes and decision-making circumstances motivating the uncertainty assessment. This three general features were given in the common framework for uncertainty management developed in the European Safety, Reliability & Data Association. Consequently, the formulation provided in this paper has been written in accordance with [15].

OWCAT can be considered as a numerical function linking inputs (uncertain $\underline{x}$ or fixed variables $\underline{d}$) to outputs $\underline{z}$ (from which decision criteria can be established). This can be formally defined in Equation 5.

$$\underline{x}, \underline{d} \Longrightarrow \underline{z} = G(\underline{x}, \underline{d}) \tag{5}$$

It is worth noting the difference between these two set of inputs. Whereas some inputs have un-

certainty associated to them, others may be fixed – as they will play another role in the model, those are represented with notation $\underline{d}$. This is the case when: (i) model inputs represent variables under full control: for example the number of pinpiles of a jacket foundation, (ii) the uncertainties affecting the model inputs are considered to be negligible (iii) the decision process conventionally fix some variables for comparative purposes and time constraints. However, it is important to bear in mind that a distinction between "uncertain" and "fix" variables usually involve an iterative process by means of sensitivity analyses of the model and it is not therefore the scope of this paper. The main goals of the QUA (Quantitative Uncertainty Assessment) in OWCAT are the three following categories, also usually found in practice. First of all, **Understand (U)** : to understand the influence or rank importance of uncertainties, focusing on the main key drivers. This will allow the model user to identify the key variables for cost and uncertainty in the different offshore wind farm components. Furthermore, at this stage this could mean that "uncertain" variables could be shifted to "fixed" variables and the other way round. Secondly, **Accredit(A)**: to benchmark the model with existing costs, simplify the number of variables that are not required and finally validate it according to the context and stage of the development process of the farm. Last but not least, **Select (S)**: to compare the different selected quantities of interest outputs to determine which combination of technology choices are optimal for a given site.

The uncertainty modelling can be conducted through a deterministic, probabilistic, extended probabilistic and non-probabilistic framework. Regardless of the framework chosen, the model should include as much information on the measure of uncertainty as possible. There have been many discussions around which the best framework is but no consensus has been reached [15]. From a practitioner's point of view a standard probabilistic setting has been considered, whereby probabilistic distributions are assigned to the components of the input $\underline{x}$. It has also been considered independence between uncertain input variables and hence separate probability distributions can be implemented instead of a joint probability distribution, for which no data and expertise in the offshore wind industry would exist. After that, computations are then made on the quantities of interest obtained from the resulting probabilistic distribution of the output random vector.

The methodology of quantitative uncertainty management is a staged process, which is represented in Figure 3. First, the specification of the problem needs to be considered. This is mathematically represented as the function G, or the deterministic function of the model OWCAT (Step A). After that, Step B consists of characterizing and quantifying the uncertain inputs modelled by probability distributions. Once this has been done, the propagation of uncertainty sources to the quantities of interest outputs can be carried out. As shown in Figure 3, Step C can be done in both directions: C representing the propagation of uncertainty sources to the outputs and C' representing the feedback from the output to the input variables probability distributions. Although this framework involves an interactive process from steps A to C' in order to distinguish which the key drivers are, this paper aims at introducing the tool (Step A) and get started with comments and a case study on Step B and C.

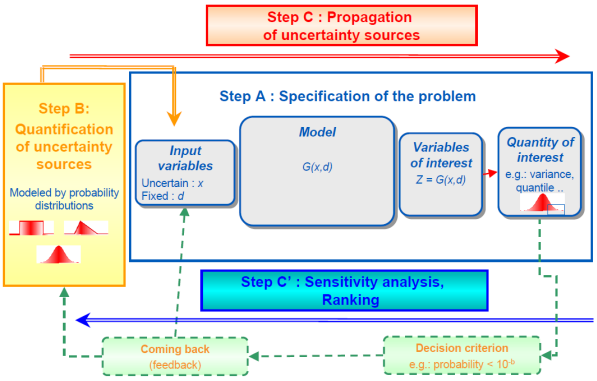

Figure 3: Uncertainty Management- The Global Methodology [16]

Practical considerations

OWCAT is MATLAB-based complex mathematical algorithm used to estimate the cost of the farm. Without limiting the generality of the foregoing, it can be assumed that the pre-existing deterministic model of OWCAT: G, considered to be the validated baseline model, is divided into N different Modules, as explained above in Section 2 and displayed on the left hand side of Figure 4. This Section describes the changes that had to be done to the initial model G to ease the implementation of the probabilistic framework from a prac-

tical point of view. The pre-existing model starts off by loading the input information into Module 1, together with structure Data 1, to perform the first set of operations. The following modules may also require additional information to perform the subroutines, namely Module j might require information from data structure Data j. After completion of Module N, an output is obtained. It is understood that this refers to any financial metric of interest such as the Levelised Cost of Energy (LCOE) or the Strike Price. In this context, given that the model is deterministic, the same input data would result into the same output if the model is run twice. Furthermore, data structures Data j $\forall j = 1, \ldots, k$ are in m-file format and were embedded inside the main core of the tool. These data structures are based on external Excel files, where cost data is stored. Each of those Excel files allows for the optimization of curve fittings based on cost data points. As a result, if new data was made available (for instance, new offshore wind costs released), a new set of calculations should be run again and the resulting cost modelling coefficients would need to be manually embedded into the code. This is time-consuming, hard to maintain and prone to making errors. Moreover, when implementing the stochastic version of the current tool, information would need to be stored within a main structure and be passed along through each of the modules. Each module would then need to have stochastic settings to control which variables need to be updated at each iteration, increasing the complexity of the stochasticity across the source code. A solution to this approach has focus on restructuring how the different data structures are loaded into the model. If instead of loading the data structures separately into each Modules, all data were loaded directly from the external Excel files into the stochastic module, stochastic settings would only need to be applied once. In addition, having all the information stored in Excel files, would provide model users an easy way to communicate those inputs and share them to confirm the validity of the estimates. For this reason, the approach on the right hand side of Figure 4 has been followed to apply the probabilistic framework, which takes advantage of the Montecarlo method to propagate the uncertainties (as per Step C).

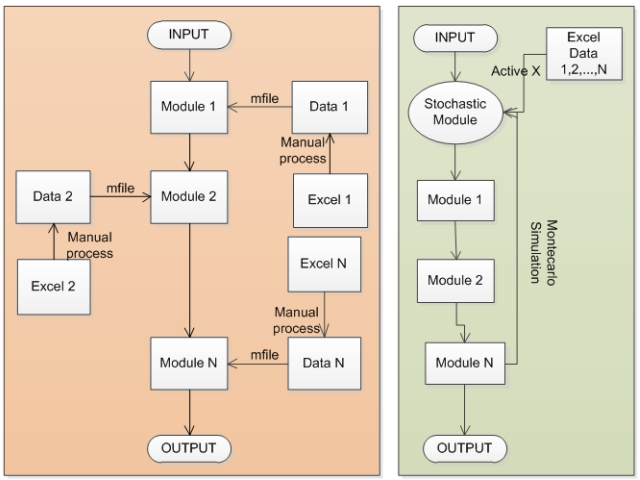

Figure 4: Deterministic (LHS) and Stochastic (RHS) Cost Model Flowcharts

Scenario analysis versus stochastic analysis

Risk analysis is conducted when assessing the feasibility of an offshore wind project by determining how often specified events may occur and the extent of their consequences. Two types of risk analyses are usually performed: qualitatively or quantitatively. Qualitatively risk analyses are typically based on experience or instinct and will therefore not be considered in this paper. On the other hand, quantitative risk analyses address the risks by assigning numerical values to them. Many organizations use the scenario analysis as a quantitative risk analysis, where a worst, best and most like scenario are chosen. The worst case scenario would choose the set of variables that would lead to the highest possible cost. Likewise, the same procedure is conducted for the best and most likely scenario, assigning values as "the best" and the "most likely", respectively. In order to show the difference between these two distinctive approaches, the new stochastic version of OWCAT is compared with the deterministic version on two different test cases for two degrees of uncertainty. Generic Offshore Wind Farm(OWF) A and B are described in Table 4, which were inspired from [17] and [18].

As a matter of initially testing the model, normal probability distributions have been assigned to over 200 inputs, considering the mean as the expected input and a relative standard deviation of $\pm 10\%$ and $\pm 20\%$. On the other hand, the best,

most likely and worst scenarios were obtained by running the deterministic version of the tool with 10-20% reduction (reduction ($\pm 10-20\%$ depending on the input), the expected value and a 10-20% increase ($\pm 10-20\%$ depending on the input), respectively.

OWF	A	B
Capacity [MW]	500	500
Water depth [m]	25	45
Soil Conditions [MW]	Simple	Complex
Distance from shore [km]	25	35
Wind speed [m/s]	9	9.5

Table 1: OWF Test Cases

5 Results

It is clear from Figure 5 and 6 that both the worst and best case scenario overestimate and underestimate the LCOE, respectively. Even when dealing with the expectation of the tails, also considered as the conditional probabilities or Conditional Value at Risk (CVaR) [19], the results show that risk metrics should be considered as a more realistic estimate. Worst and best case scenario do not provide much information as the joint probability of the combination of inputs is really low. In the same way as the best and worst case scenario do not need to be symmetric respect to the mean (due to the nonlinearities of the model), the propagation of the uncertainty distribution of the inputs into the LCOE do not necessarily lead to symmetrical distributions In this case, given that all the probability distributions are considered to be normal, the model shows some nonlinearities but still it behaves fairly symmetrical. Figure 7 shows how the shape of the distribution changes with uncertainty. Since most inputs were considered normally distributed, the LCOE relative to Deterministic LCOE values is expected to have similar behaviours for both A and B OWFs.

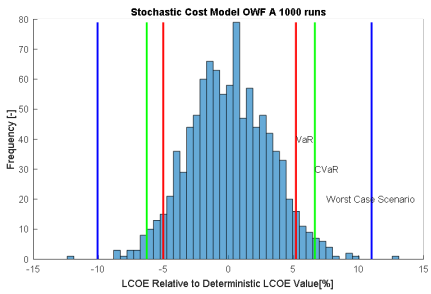

Figure 5: Stochastic Cost Model OWF A

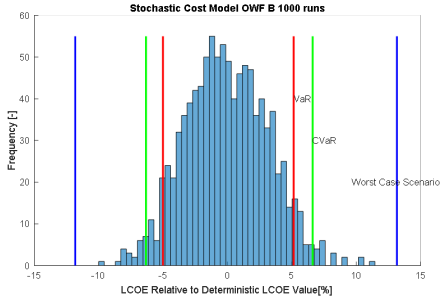

Figure 6: Stochastic Cost Model OWF B

6 Conclusion

Developers and investors alike should be aware of the complexity of offshore wind cost modelling and the importance of having an in-house software tool allowing quick reactions to market and technology trends. This, combined with new mathematical modules for advance decision-making processes such as the treatment of uncertainty will help the industry to make more informed business decisions and drive offshore wind costs down even further.

The enhanced capabilities of stochastic simulations allows for better judgement of the common risk metrics used in the financial industry: VaR and CVaR instead of the widely used and some times too conservative, scenario analysis. All this work has been done with the future aim of undertaking the different phases of the common uncertainty framework - Understand, Accredit and Select as explained in Section 4.

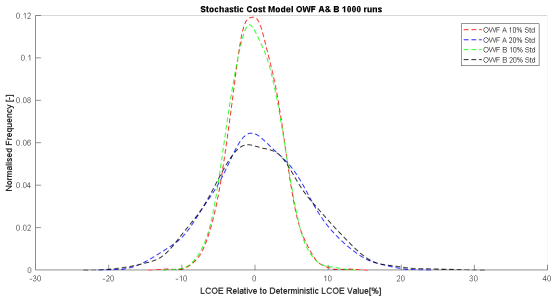

Figure 7: Stochastic Cost Model OWF A&B for 10% and 20% uncertainty estimates

Acknowledgements

I would like to thank the Energy Technology Institute and the Research Council Energy Programme for funding this research as part of the IDCORE programme (grant EP/J500847) as well as the EDF Energy R&D UK Centre.

References

[1] Wind Europe. "The European offshore wind industry - Key trends and statistics 2016". Wind Europe 2017.

[2] Offshore Renewable Energy Catapult. "Offshore Wind Cost Reduction Task Force Report". Offshore Renewable Energy Catapult 2012.

[3] Ozkan D. "Financial Analysis and Cost Optimization of Offshore Wind Energy under Uncertainty and in Deregulated Power Markets". The Faculty of The School of Engineering and Applied Science of the George Washington University, 2011.

[4] Herman SA. "Probabilistic Cost Model for Analysis of Offshore Wind Energy Costs and Potential". ECN 2002.

[5] Zaaijer MB,Kooijman HJT,Herman SA, HB Hendriks. "How to benefit from cost modelling of offshore wind farms?". Delft University of Technology and ECN 2003.

[6] BVG Associates. "DECC Offshore Wind Programme - Simple Levelised Cost of Energy Model. Revision 3 - 26/10/2015 ". Last accessed 01/06/2017. http:/www.demowind.eu/LCOE.xlsx

[7] Ioannou A, Angus A, Brennan F. "Stochastic Prediction of Offshore Wind Farm LCOE through an Integrated Cost Model". 3rd International Conference on Energy and Environment Research, ICEER 2016, 7-11 September 2016, Barcelona, Spain.

[8] Shafiee M,Brennan F, Armada Espinosa I. "A parametric whole life cost model for offshore wind farms". LCA for Energy Systems and Food Products 2016.

[9] Balks M, Grasse J. "Aggregierte Risiken fur Offshore-Wind-Investitionen - eine Simulation". Analysen und Berichte 2016. (German)

[10] Kaiser MJ, Snyder BF. "Offshore Wind Energy Cost Modeling - Installation and Decommissioning". Springer 2012.

[11] AACE International Recommended Practice. Engineering, Procurement, and Construction for the Process Industries, TCM Framework: 7.3 - Cost Estimating and Budgeting". ACCE International Recommended Practices 2005.

[12] Crundwell FK. "Finance for Engineers - Evaluation and Funding of Capital Projects". Springer 2008.

[13] Gerrard AM. "A Guide to Capital Cost Estimating". IChem and ACostE 2000.

[14] Gonzalez-Rodriguez A. "Review of offshore wind farm components". Energy for Sustainable Development 2016.

[15] Rocquigny E, Devictor N, Tarantola S. "Uncertainty in Industrial Practice - A guide to quantitative uncertainty management". Wiley 2008.

[16] Pasanisi A. "An Industrial Viewpoint on Uncertainty Quantification Simulation: Stakes, Methods, Tools, Examples". Working Conference on Uncertainty Quantification in Scientific Computing -Boulder. International Federation for Information Processing (IFIP), 2011.

[17] The Crown Estate. "Offshore Wind Path Reduction: Pathways Study". The Crown Estate, 2012.

[18] KIC InnoEnergy and BVG associates. "Future Renewable Energy Costs: 51 technology innovations that will have greater impact on reducing the cost of electricity from European offshore wind farms". KIC InnoEnergy and BVG associates, 2016.

[19] Kisiala Jakob. "Conditional Value-at-Risk: Theory and Applications". Dissertation Presented for the Degree of MSc in Operational Research at the University of Edinburgh, 2015.

Applied Energy 252 (2019) 113419

Contents lists available at ScienceDirect

Applied Energy

journal homepage: www.elsevier.com/locate/apenergy

The effects of mean wind speed uncertainty on project finance debt sizing for offshore wind farms

Esteve Borràs Mora[a,b,*], James Spelling[b], Adriaan H. van der Weijde[c,d], Ellen-Mary Pavageau[b]

[a] Industrial Doctoral Centre for Offshore Renewable Energy (IDCORE), The University of Edinburgh, Edinburgh EH9 3JL, UK
[b] EDF Energy R&D UK Centre, Interchange, 81-85 Station Road, Croydon CR0 2AJ, UK
[c] Institute for Energy Systems, School of Engineering, University of Edinburgh, Faraday Building, The King's Buildings, Mayfield Road, Edinburgh EH9 3DW, UK
[d] The Alan Turing Institute, British Library, 96 Euston Rd, London NW1 2DB, UK

HIGHLIGHTS

- Reducing estimated mean wind speed uncertainty does not always lead to better LCOEs.
- Additional measurement becomes more valuable as the maximum gearing increases.
- Consolidation of Floating LIDAR technology as the optimal measurement campaign.

ARTICLE INFO

Keywords:
Offshore wind project finance
Wind speed uncertainty
Decision-making processes under uncertainty

ABSTRACT

Financing costs for offshore projects depend, among many other variables, on the quality of mean wind speed predictions. Financial institutions determine the amount of debt that can be reasonably supported by the project, based on probabilistic cash flow metrics derived from estimated mean wind speeds. Within the offshore wind industry, it is widely believed that longer wind resource campaigns or more precise wind measurement devices that decrease mean wind speed uncertainty lead to lower LCOE values. This paper shows that this is not always true, while a decrease in mean wind speed uncertainty may result in better financing conditions, it typically requires higher development expenditure. We build a theoretical cost modelling framework, which includes detailed project financing constraints, and then apply this to an industrial case study to analyse project financing of different types of offshore wind farms. We show that developers need to find the right balance between a decrease in financing costs and an increase in development expenditure. For projects limited by the maximum gearing or with an unfavourable trade-off between the development expenditure and the increased P90 annual energy production, more precise resource estimation can result in higher LCOE values. This paper suggests a new way of understanding the effects of wind resource assessment campaigns by integrating project finance constraints into cost calculations and highlighting the importance of detailed cost modelling for optimal design of offshore wind farms.

1. Introduction

The importance of project finance for renewable energy projects has been highlighted in [1]. It is understood that project finance could be instrumental in increasing the availability of capital for a successful energy transition, of which offshore wind projects could benefit from. Large-scale offshore wind is often developed through stand-alone project companies, owned by the project investors. A project company, also

Abbrevation: AEP, Annual Energy Production; AEP_{P50}, Annual Energy Production based on P50 estimated mean wind speed; AEP_{P90}, Annual Energy Production based on P90 estimated mean wind speed; BHHMM, Below Hub Height Met Mast; CAPEX, Capital Expenditure; CFADS, Cash Flow Available for Debt Service; DECEX, Decommissioning Expenditure; DEVEX, Development Expenditure; DSCR, Debt Service Coverage Ratio; EPCM, Engineering Procurement and Construction Management; FCF, Free Cash Flows; FID, final Investment Decision; FLIDAR, Floating Light Detection and Ranging; HAFLIDAR, High Accuracy Commercial Floating LIDAR; HMM, Hub Height Met Mast; HVAC, High Voltage Alternating Current; IAV, Inter-annual Variability; LAFLIDAR, Low Accuracy Commercial Floating LIDAR; LCOE, Levelised Cost of Energy; NPV, Net Present Value; O&M, Operations and Maintenance; OPEX, Operational Expenditure; OWCAT, Offshore Wind Cost Analysis Tool; SPV, Special Purpose Vehicle

* Corresponding author.
E-mail address: E.Borras-Mora@ed.ac.uk (E.B. Mora).

https://doi.org/10.1016/j.apenergy.2019.113419
Received 17 December 2018; Received in revised form 7 May 2019; Accepted 31 May 2019
Available online 22 June 2019
0306-2619/

referred to as a SPV, has its own revenues and balance sheet and therefore the ability to raise funding on its own merits. An SPV can raise two discrete categories of funding: equity and debt. In this paper, project finance, or non-recursive financing, is considered for the development of offshore wind farms. As the offshore wind industry grows and more banks are involved in non-recourse financing for offshore wind farms [2–4], a better understanding of how wind farms are financed and what the banks' requirements are, is needed. The financial terms offered by the lenders and the ability of the offshore wind farm to meet its financial obligations once operational depend, among many other variables, on uncertain wind-driven revenues. Given the fact that wind power varies with the cube of the wind speed, accurately and precisely determining the wind speed is of utmost importance for both developers and their bankers during the project's planning stage.

Consider a developer that wants to raise money from a bank or another financial institution in order to build an offshore wind farm. If all goes well and the project succeeds, the bank will have the loan repaid with interest. If the project exceeds its performance and generates more revenues than expected, the bank does not take any benefit from additional production - it has limited upside risk. On the contrary, if the project under-performs then the bank can lose up to the full value of the loan - it has full downside risk. Given that the bank has a limited upside but is exposed to a larger downside, it usually puts in place several mitigation measures to control the project risks, one of which is a comprehensive analysis of the wind resource assessment uncertainty. This is typically carried out before the FID and it requires a sound understanding of the uncertainty of the wind speed and energy losses in order to estimate the potential size of the debt funding that can be reasonably supported by the cash flows of the project. Generally speaking, if the bank is satisfied with the level of confidence with which the yield has been evaluated, it might regard the value as a low uncertainty estimate and provide access to higher gearings, i.e. a higher proportion of finance that is provided by debt relative to the finance provided by equity. Since the cost of debt is cheaper than the cost of equity, developers always try to maximize the share of debt. Developers may therefore need to find the right balance between an increase in the development expenditure associated with better wind speed predictions and a decrease in the financing costs to minimise their LCOE.

The effects of mean wind speed uncertainty in project finance for offshore wind farms were first investigated in the work of Schreider [5]. A high-level study was conducted to select the optimal contract strategy for investing in an offshore wind project. Even though the study slightly touched upon mean wind speed uncertainty by considering a downside scenario with P84 instead of the P50 yield in one of the business cases, the study did not go further; it can be considered as a simple downside scenario analysis. However, wind risk has been identified as one of the fundamental pieces of technical due diligence for project finance offshore wind farms [6]. In addition, offshore wind research has devoted considerable efforts to characterise the uncertainty associated with the annual energy production, given by the inherent uncertainty in the resource as shown in [7–9] and the uncertainty in the technology [10].

Furthermore, offshore wind techno-economic models have been developed to offer a basis for objective communication and decision-making, allowing for a greater number of cases to be analysed and when considering new ideas, offering the option to assess the economic feasibility and potential. Examples of those can be found in [11–14]. However, given the multidisciplinary nature of techno-economic modelling activities, studies tend to be either very detailed in the wind resource assessment part while ignoring financial valuation principles or they make use of sound financial models that do not take into consideration fundamental principles of wind resource assessment.

Thus, there is a research gap in the literature when it comes to bringing together the wind resource assessment uncertainty and bank requirements, which have a direct impact on project finance costs. No previous literature has attempted to explain how a reduction in mean wind speed uncertainty can be translated to both an increase in the development expenditure and a reduction in the cost of financing. It is the trade-off between these two ingredients that determines their aggregated contribution to LCOE. Moreover, no previous project finance model has been published in the literature where the relationship between the P50 and P90 estimated mean wind speed is explained. This lack of analysis is probably due to the limited access to detailed industrial cost models, combining enough technical and financial expertise to be able to carry out this study.

When developing an offshore wind farm a trade-off between the wind resource assessment uncertainty and the development expenditure has to be made. That is to say, the developer has to choose a commercial sensing device (e.g. meteorological mast or FLIDAR) to deploy in order to characterize the wind resource in a given zone. The choice of one or another device determines the magnitude of the DEVEX and the uncertainty in the wind speed measurement. Within the offshore wind industry, it is widely believed that longer wind resource campaigns or more precise wind measurement devices that decrease mean wind speed uncertainty lead to lower LCOE values. But is this always the case? In other words, does the deployment of additional advanced sensing technology, which presumably reduces wind speed uncertainty, compensate for the incurred development expenditure?

The current paper is a first attempt to answer these questions, and to include detailed project finance constraints in wind farm planning decisions. Our focus lies on quantifying the impact of mean wind speed estimated uncertainty reduction on the LCOE of offshore wind farms. Naturally, there are many other long-term uncertainties that influence the operational, economical and financial performance of the farm, but, since wind speeds are such a crucial determinant of wind farm performance, we will leave other uncertainties aside in our quantitative analysis; however, we will briefly describe and, where possible, quantify them before moving on. Throughout, we will also assume that the developer has a good track record of projects and that experienced contractors have been appointed; if this is not the case, banks may impose additional requirements beyond the scope of this paper before taking on any investment risk.

The contribution of this paper is the development of a novel theoretical cost modelling framework which includes, detailed considerations of financing requirements that until now have been usually ignored in the offshore wind planning models. The methodology presented here can be applied to any existing standard corporate finance cost model to account for project finance arrangements. At the same time, this cost modelling framework allows policy-makers and developers alike to assess the trade-off between DEVEX and the estimated wind speed uncertainty, leading to more informed decisions that have the potential to drive down the cost of energy.

The rest of this paper is organised as follows: Section 2 introduces the widely used concepts of P50, P90 and some fundamentals of project finance. Section 3 describes the offshore wind cost modelling tool and provides a high-level overview of its inputs, outputs and the interplay between them. Section 4 describes the formation of the financial module within the tool, which is a key ingredient to understand and quantify the effects of the estimated mean wind speed uncertainty in obtaining better financing conditions. Following this, engineering techniques and financial methods are brought together to understand the implications of the mean wind speed uncertainty reduction in the LCOE, as shown in Section 5. Finally, the findings of the paper are exemplified by an industrial case study throughout Section 6.

2. Project finance for offshore wind farms

The profits of an offshore wind project are wind-driven. Given the uncertain nature of the wind, developers use probabilistic metrics to characterise the wind resource at a given site. AEP_{p50} is associated with a P50 estimated mean wind speed $\overline{v_{P50}}$, meaning that this is the mean wind speed that is expected to be exceeded in 50% of the estimates. It is important to highlight that this is the estimated mean wind speed and

not the measured mean wind speed, which would follow a different probability distribution function such as Rayleigh or Weibull. To put it in other words, this is the median mean wind speed estimate since half of the estimates are expected to be below this value and the other half are predicted to be above it. Although this metric is typically considered from a developer's point of view when doing corporate finance, banks prefer a rather conservative approach; reasons for this are explained in Section 1. Thus, banks use the AEP_{p90}, which is the AEP associated with an estimated mean wind speed that is expected to be exceeded in 90% of the estimates $\overline{v_{P90}}$. The mean wind speed estimated uncertainty is assumed to be characterized by a normal probability distribution, as it is shown in the following relationship 1:

$$\overline{v_{PX}} = \overline{v_{P50}} - \sqrt{2}\cdot\sigma\cdot erf^{-1}[1 - 2\cdot F_X] \;\forall\, X \in [0, 100] \tag{1}$$

where σ is the given level of uncertainty expressed as a percentage of the wind speed representing one standard deviation and X is the level of exceedance requested by the bank. In particular, when looking at a level of exceedance of 90% or P90, Eq. (2) results in:

$$\overline{v_{P90}} = \overline{v_{P50}} - 1.2816\sigma \tag{2}$$

Fig. 1 shows the relationship between a $\overline{v_{P50}}$ of 9 m/s and its associated $\overline{v_{P90}}$ for a given σ of 4%, 6%, and 8%. Reducing the uncertainty increases the $\overline{v_{P90}}$ value as well as the AEP_{p90}.

The AEP uncertainty, represented by its probability distribution function, is determined by propagating the mean wind speed estimated uncertainty together with the uncertainty in the energy factors. However, given the scope of the paper, the energy factors have been held constant throughout the study and considered as known techno-economic assumptions (for instance, X% availability, Y% wake effect losses, Z% electrical losses). This means that the normality hypotheses assumed for the wind speed uncertainty are not applied in the energy factors. In this way, the uncertainty is propagated from the mean wind speed to the AEP based on these known techno-economic assumptions.

Debt sizing determines the maximum amount of project finance debt that an offshore wind farm can sustain based on the banks' requirements. Project lenders usually determine the borrowing capacity on the basis of debt service ratios and covenants. Covenants are restrictions that specify certain limitations, such as the size and use of the loan. Financial institutions have to have an idea of the amount of debt that can be reasonably supported by the project and typically base their limitation on probabilistic metrics such as the P50 and P90 mean wind speed. That is the reason why uncertainty plays a key role in determining the amount of debt.

In project finance, the most common debt service ratios are the Debt Service Coverage Ratio and the maximum gearing. While the gearing is expressed as a percentage of the total project debt the owners are allowed to take on, the DSCR is defined as the Cash Flow Available for Debt Service divided by the debt service (which is calculated as the principal $P_{(t)}$ plus interest $I_{(t)}$) for any given period t. DSCR metrics are typically used in private infrastructure project debt [15], in particular in offshore wind projects [16]. Financial institutions might then decide upon the lower debt size resulting out of the two debt-sizing techniques [17]. They also determine what CFADS is its mean wind speed estimate based on; typically a P50 or P90 mean wind speed. In this paper it is assumed that CFADS is based on P90 cash flows, that is to say, cash flows based on a P90 mean wind speed.

The notion of deriving the debt repayments together with the debt size in order to meet a single or multiple DSCR ratios is known as debt sculpting. When sculpting debt, principal repayments are being manipulated so that the total debt service matches the CFADS for any given period. As a consequence, the DSCR follows the desired target profile. By increasing the DSCR target, debt repayments are reduced in each period, but the last. As debt repayment are reduced, the span of time needed to fully repay the debt increases, which looks appealing from the sponsor point of view. On the other hand, lower DSCR targets increase repayments, resulting in the debt being repaid earlier. The limiting DSCR is given by the bank in conjunction with a constraint in the maximum gearing, since the debt has to be repaid within the debt tenor. When assuming a constant DSCR target, the following Eq. (3) holds for every cash flow period t:

$$DSCR = \frac{CFADS_{(t)}}{P_{(t)} + I_{(t)}} \;\forall\, t \tag{3}$$

From Eq. (3), it is seen that, if this is true for every time period, the sum of the cash flows follows the relationship displayed in Eq. (4), where k is the number of cash flow periods. Thus, by limiting the amount of gearing that a project can take on, a new DSCR is obtained, shown in Eq. (5).

$$DSCR = \frac{\sum_{t=1}^{k} CFADS_{(t)}}{\sum_{t=1}^{k} P_{(t)} + \sum_{t=1}^{k} I_{(t)}} \tag{4}$$

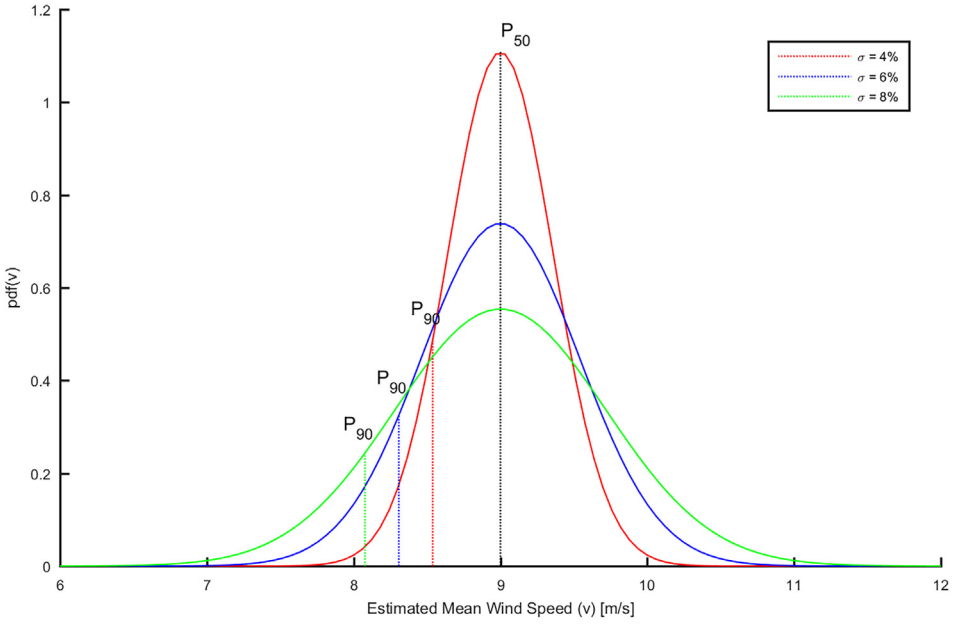

Fig. 1. Relationship between P50 and P90 estimated mean wind speeds for different uncertainties.

$$DSCR = \frac{\sum_{t=1}^{k} CFADS_{(t)}}{gearing \cdot debtservice} \quad (5)$$

This means that the minimum DSCR target used in the financial calculation should be the minimum of the one imposed by the bank, which we define as $DSCR_1$, and the one calculated based on Eq. (5), which we define as $DSCR_2$. Therefore, the resulting DSCR of a project is displayed in Eq. (6).

$$DSCR = min(DSCR_1, DSCR_2) \quad (6)$$

If $DSCR_2$ is higher than $DSCR_1$, the debt cannot be repaid before maturity; that is why the minimum of the two DSCRs is used in the financial calculation. For a developer, the lower the DSCR, the better the offshore wind investment is, as the DSCR measures how many times the cash flows after debt service can repay the scheduled debt service. The approach taken so far consisted in explaining how a limitation in the maximum gearing is reflected into the DSCR in order to be able to take the most restrictive covenant based on a DSCR criteria. This can also be done based on a gearing criteria. A maximum gearing is given by the bank, so we can now find an equivalent gearing given by a DSCR condition, following the same rationale explained in Eq. (5). This relationship is shown in Eq. (7).

$$gearing = \frac{\sum_{t=1}^{k} CFADS_{(t)}}{DSCR \cdot debtservice} \quad (7)$$

As a consequence, if we define the maximum gearing imposed by the bank as $gearing_1$ and the maximum gearing given a DSCR condition based on Eq. (7) as $gearing_2$, the resulting gearing for a project is obtained from the most restrictive covenant, shown in Eq. (8).

$$gearing = min(gearing_1, gearing_2) \quad (8)$$

In addition, bank requirements for different types of infrastructure asset classes such as offshore wind projects evolve with time. It is well understood that the risks involved when building, commissioning and operating an offshore wind project are reflected in the cost of capital. In this regard, the offshore industry has entered a maturation phase and a strong group of actors has emerged. These range from developers to independent power producers, from institutional banks to commercial banks, from suppliers of wind turbines to cables. Over the last few years, this strong group of actors has acquired experience and knowledge about what it takes to bring a project to commissioning or to deal with the marine construction risk. All of this supported by a strong track record of projects being delivered on time and on budget. As these risks are being better understood by the financial institutions and there is a strong track record of successful projects, the bank requirements are being reduced. This maturation phase of the sector is reflected in better financing conditions as shown in Table 1.

Typical DSCR constraints are now 1.50 with P50 and 1.30 with P90. This arises from the fact that financial institutions see no or very limited price risk on the revenue side, a net availability in the 92–95% range, conservative O&M cost assumptions and a full insurance package included [19].

Table 1
Typical project finance conditions for offshore wind farms from 2006 to 2017 [18].

Period	Gearing	Maturity post-completion	Pricing
2006–2007	60:40	10–15 years	150–200 bps
2009–2011	65:35	10–15 years	300 bps
2012–2013	70:30	10–15 years	300–375 bps
2014–2015	70:30	10–15 years	200–250 bps
2016–2017	75:25	15–17 years	150–225 bps

3. Offshore wind cost modelling tool

The modelling approach to offshore wind cost analysis presented in this paper is based around the Offshore Wind Cost Analysis Tool developed at the EDF Energy R&D UK Centre [20]. This cost modelling tool has been used in the past for comparative evaluation of multiple sites, detailed evaluation of specific project layouts and sensitivity studies on both design/technology choices and cost variations. The tool has been validated against cost data from the Navitus Bay, Courseulles-sur-Mer and Neart na Gaoithe projects and shown to be accurate within ±15% for these cases.

The model consists of three main modules: a wind farm design module, a cost calculation module and a financial module. The first stage of the module concerns the wind farm design. In order to evaluate the costs of the project, it is necessary to understand the number and type of wind turbines, foundations, inter-array cabling and the export system. In other words, the wind farm itself must be modelled. Designing an offshore wind farm requires interaction between teams from different disciplines; for example, the wind turbine team will have to interact with the foundation team to make sure that the loads of the turbine are correctly passed onto the foundation, and the foundation team will need to make sure that the electrical connections are correctly secured within the foundation. As such, a cost model must capture the same interactions as the design process and cannot be a simple accumulation of models from separate disciplines.

The design outputs of the first module are fed as inputs into the second module, which calculates the costs of the different offshore wind farm components. The cost module can be divided into DEVEX, CAPEX, OPEX and DECEX. DEVEX covers the costs of all the processes up to the financial close or placing firm orders to proceed with wind farm construction. CAPEX calculates the supply and installation costs of the wind farm; including wind turbines, foundations, inter-array cables, offshore substations, export cables and onshore substations. Indirect costs such as EPCM costs and insurance are also included in the CAPEX breakdown. OPEX includes direct costs for the operation and maintenance of the wind farm, as well as transmission charges, insurance, taxes and royalties. DECEX accounts for the decommissioning of the wind turbines, foundations and offshore substations.

The cost outputs of the second module are passed into the third module, which accounts for the financial model of the wind farm project. The financial model takes into consideration the different cash flows throughout the life of the wind farm, as well as the financing structure put in place to supply the initial capital investment. Based on the resulting free cash flows and financing costs, the LCOE can be determined, together with other financial performance indicators. The financial module allows for corporate and project financing modelling.

The OWCAT input data structure is shown in Fig. 2.

- (i) Project Specifications
- (ii) Technical Specifications
- (iii) Economic and Financial Specifications
- (iv) Vessel Specifications
- (v) Structural Masses and Electrical Components Database

(i) refers to the project offshore wind farm characteristics such as the capacity of the farm, the wind speed at a given referenced height, the average water depth, the soil conditions, the distance from shore, the wind turbine model, foundation type and export system specifications among others. Since no two projects have the same characteristics, project specifications attempt to model each particular site. (ii) addresses the details of the offshore wind technology, representing wind turbine, foundation, inter-array cable, export system and grid parameters. For example, as far as the wind turbine is concerned, parameters such as the wind turbine availability, the installation vessel associated with the wind turbine, the average loading, installation and commissioning times are accounted for. In addition, a decommissioning

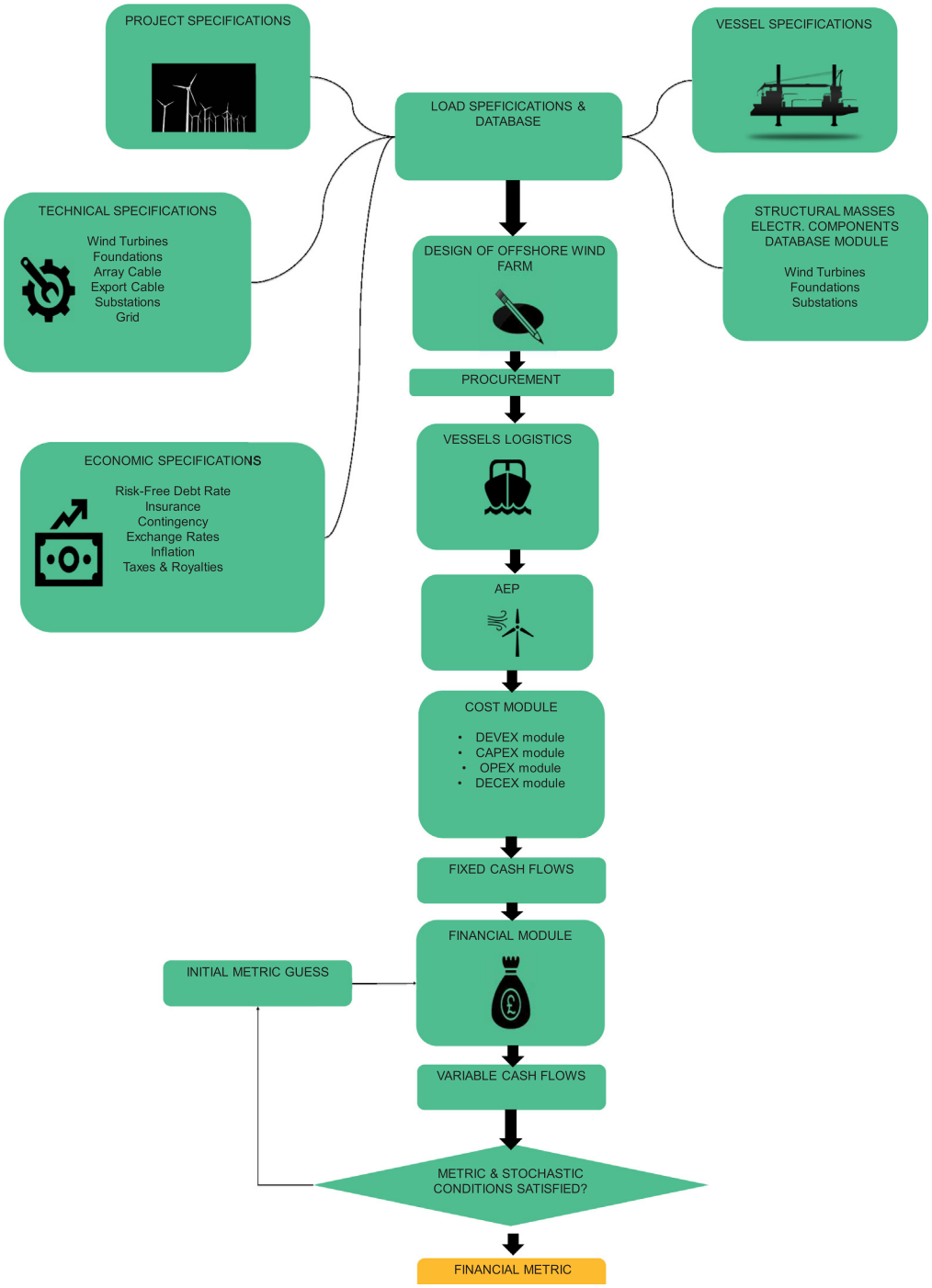

Fig. 2. High level structure of cost modelling tool.

factor is used for all offshore wind farm components to account for a reduction in time from the installation phase. (iii) concerns the reference year for real prices, the risk-free rate and cost of debt, insurance and insurance premium tax rates, contingency requirements, corporation taxes, depreciation, seabed rent, exchange rates and inflation. (iv) involves the different vessel characteristics used in the installation and decommissioning of the offshore wind farms. As an example, heavy-lift jack-up vessel parameters would comprise of the day rate, vessel transit speed, vessel positioning time, vessel mobilisation time, operational weather window and carrying capacities in regard to different components. (v) consists of the data used to establish the foundation mass correlations, which are the basis for the CAPEX estimation in the foundation procurement. It also considers the correlations used to estimate the cost of different electrical components.

The final design contains not only the design of the offshore wind farm, where the foundations masses, inter-array and export system are sized, but also the procurement, vessel charter model and the AEP as displayed in Fig. 2. Procurement stores all information concerning wind turbines, foundations and the electrical system, in terms of the type, number of elements and size (also length if required), giving rise to a procurement catalogue which forms the basis for the cost module. The vessel charter model is based on the work of Kaiser et al. [21], whereas the AEP is built upon industry's best practices assuming respectively either a logarithmic- or power-law wind profile in conjunction with a

Rayleigh or Weibull probability distribution to model the wind speed. Wake losses and electrical losses are also accounted for in the AEP submodule.

4. Formation of the financial module

As far as project evaluation is concerned, given a set of cash flows it is relatively easy to calculate several financial metrics such as the Net Present Value, Internal Rate of Return, Payback Period or Profitability Index. These financial metrics are worked out by projecting backwards in time a set of cash flows, resulting into its present value. In addition, they not only depend on the profile of the cash flows but also on a given discount factor.

A financial metric typically used in the energy sector to evaluate the financial performance of a project is the LCOE. The LCOE is a metric for which an equal-valued fixed revenue delivered over the life of the asset's generating profile would cause the project to break even. Eq. (9) translates the LCOE definition into a mathematical formula, where TOTEX is the total expenditure and NPV is an operator which converts a set of cash flows to present value, given a discount rate. Bearing in mind that the discounted sum of the revenue cash flows should be equal to the discounted sum of expenditures, the right-hand side of Eq. (9) is obtained. It is important to notice the fact that the LCOE is a constant value, and therefore, $NPV\,(LCOE{\cdot}AEP) = LCOE{\cdot}NPV\,(AEP)$ and also that the revenue is expressed by $LCOE{\cdot}AEP$ (in currency units) and accounts for the profit earned by electricity sales.

$$LCOE = \frac{NPV\,(TOTEX)}{NPV\,(AEP)} \rightarrow NPV\,(Revenue) = NPV\left(LCOE{\cdot}AEP\right) = NPV\,(TOTEX) \tag{9}$$

The financial module output of the cost modelling tool is the LCOE, which is a universal metric used for comparison of energy costs, and represents a single, constant, inflation-adjusted price available over the entire lifetime of the project, that also takes into consideration the full range of project cash flows based on its characteristics. The LCOE is used for decision making and is made up of Revenue and TOTEX cash flows. TOTEX can in turn be broken down into DEVEX, CAPEX, OPEX, and DECEX. If TOTEX would not depend on the LCOE, then the problem would be trivial and the left-hand side of Eq. (9) would give us a methodology to work out the LCOE. However, this is not the case. Although DEVEX and DECEX are fixed items, and such can be assessed without any iterative method, CAPEX and OPEX comprise fixed and non-fixed costs, resulting in functions of the LCOE.

In other words, numerical techniques are needed to work out the LCOE. The first step to calculate the LCOE is to define the free cash flows. Although there is more than one way to define the FCF, in this paper it is assumed that the FCF are calculated as the cash flow from operations minus the offshore wind farm's capital expenditures. In this way, the LCOE can be calculated by finding the zero of the function given by the sum of the discounted FCF, as shown in Eq. (10).

$$FCF =_{def} \; LCOE{\cdot}AEP - TOTEX = 0 \rightarrow NPV\,(FCF) = 0 \tag{10}$$

The financial module consists of fixed and variable cash flows. Fixed cash flows are those that do not depend on the LCOE, whereas variable cash flows are a function of the LCOE. Therefore, whereas variable cash flows need to be recalculated at each iteration, fixed cash flows can be calculated only once at the beginning of the iterative process to improve the efficiency of the tool. Fixed cash flows are shown in Fig. 3. DEVEX is displayed in red to highlight that different sensing devices will result in different development expenditure.

The financial appraisal for project finance arrangements entails not only one but twofold iterative processes. On the first hand, the external loop consists of determining the value of λ that makes Eq. (11) equal to 0, where its initial guess λ_0 is obtained from a simplified financial module. Each iteration of the external loop is linked with an internal

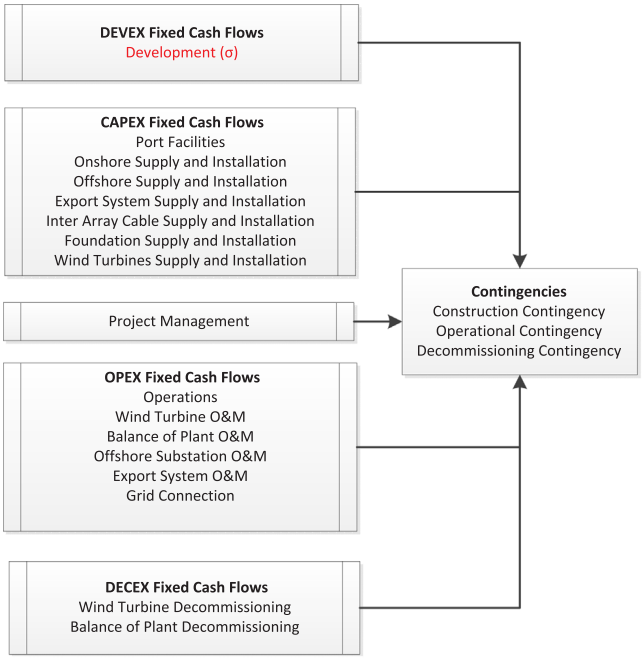

Fig. 3. Fixed cash flows within cost modelling tool.

iterative process for debt sizing. The internal loop is only used for project finance arrangements and concerns the debt sizing or sculpting, which determines the maximum amount of project finance debt that the offshore wind farm can sustain based on the bank's requirements. Project lenders usually specify the borrowing capacity on the basis of debt service ratio and covenants. As such, parameters like the DSCR, the maximum leverage and CFADS have been considered. A priori, the variable λ is unknown, meaning that it will take several external and internal iterations to come up with the zero of Eq. (11). In other words, the LCOE is calculated as the constant real electricity price required to meet the desired Minimum Acceptable Rate of Return, and not the other way around as usually considered. Given that it is inflation-adjusted, it means that a reference year must be defined (typically FID year is used).

$$LCOE = \lambda \left| \sum_{t=1}^{n} \frac{FCF_t(t)}{(1 + MARR)^t} = 0; \right. \tag{11}$$

This high-level iterative process is described in Fig. 4. Further information regarding the details of the different calculations for the internal loop is shown in Fig. 5.

The OWCAT financial model for a generic offshore wind farm is displayed in Fig. 5. Two main areas can be identified–the area outside the purple dashed lines, representing a standard corporate finance model based on P50 cash flows and the area inside the purple dashed lines, representing a part of a project finance model or what is referred in this paper as a Project Finance Add-in based on P90 cash flows. These P50 and P90 cash flows stem from the P50 and P90 AEP values which are the output of the Annual Energy Production module. These P50 and P90 AEP values come in turn from the estimated mean wind speed uncertainty, influenced by several uncertainty drivers. An LCOE value needs to be assumed in order to transform AEP values to revenue cash flows. This is represented in Fig. 5 by a red circle–value that changes from iteration to iteration until the numerical scheme converges (see figure above for the explanation on the twofold iterative calculation).

The standard corporate finance model calculates the different variable cash flows that are required to work out the NPV of the project – seabed rent, fixed cash flows, construction and operational insurances and taxes. Given a discount rate, an iterative process is required to work out the LCOE that makes the cumulative free cash flows zero at the end of the project. The standard corporate finance calculation requires one

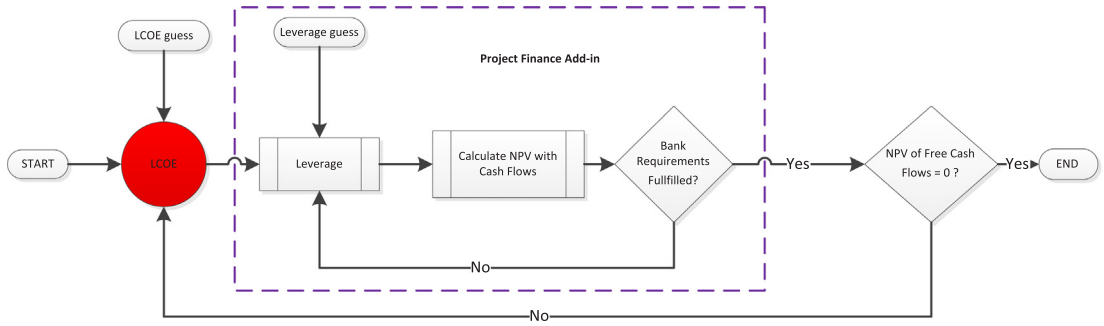

Fig. 4. Double loop iterative project finance modelling.

iterative calculation, whereas the Project Finance Add-in adds an additional loop by working out the amount of debt that the financial institution provides to the project. In cases where the offshore farm is financed via corporate finance arrangements, only the left hand side of the financial model is needed. However, this paper's objective is to understand the effect of the mean wind speed estimated uncertainty on debt sizing for offshore wind farms – so the full financial model needs to be taken into consideration.

The purpose of the Project Finance Add-in (displayed within purple dashed lines) is to estimate the amount of debt that can be reasonably supported by the project based on the probabilistic metric given by the P90 estimated mean wind speed. The output of the Project Finance Add-in is the Debt Finance, Operational and Construction Interest and the Financing Fees cash flows. Without the Project Finance Add-in it would not be possible to estimate the P90 cash flows that are required by the financial institution to support the non-recourse financing of the offshore wind farm. Cash flows in red are key to understand the effect of the estimated mean wind speed on debt sizing for offshore wind farms. These come into play from two sides. On the one side the development expenditure, which is influenced, to some extent, by the cost of the sensing device selected by the developer to characterise the wind speed uncertainty for a given site. On the other side, the changes on the financing costs represented by the four outputs from the Project Finance Add-in: the Debt Finance, Construction and Operational Interest and the Financing Fees. Given the iterative process of the financial modelling, these four cash flows are displayed in blue and are worked out via standard debt sculpting techniques.

It is important to bear in mind that when carrying out an offshore

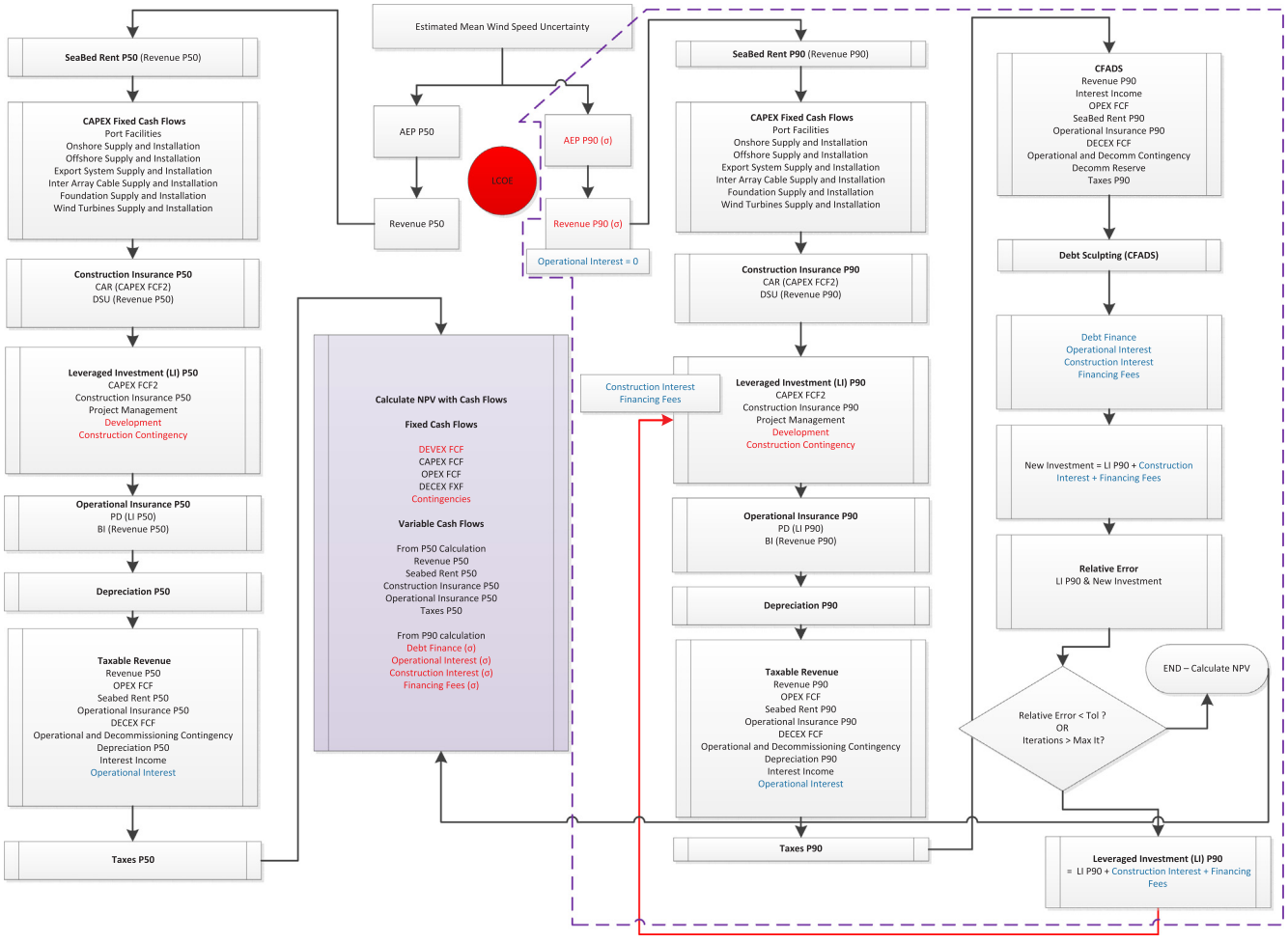

Fig. 5. Project finance structure within cost modelling tool.

wind farm project evaluation via project finance arrangements, both areas of the financial model need to be taken into consideration. The Project Finance Add-in works out the Debt Finance, Construction and Operational Interest and Financing Fees P90 cash flows and the standard corporate finance calculates all the remaining P50 cash flows that are then fed into the NPV operator. Eq. (12) splits the cash flows between these two P50 and P90 categories. Therefore, the developer selects a measuring campaign strategy to measure the mean wind speed estimated uncertainty which directly affects the FCF_t^{P50}. Eq. (13) illustrates that the P50 free cash flows are a function of the DEVEX incurred by the developer. At the same time, the mean wind speed estimated uncertainty, represented here with σ, has an indirect effect on the P90 free cash flows - the financing conditions such as Debt Finance, Construction and Operational Interest and Financing Fees cash flows. Eq. (14) illustrates that the P90 free cash flows are a function of the mean wind speed estimated uncertainty.

This type of modelling integrates the wind resource assessment at the heart of the cost calculations through project finance constraints and allows to quantify and investigate the effect of the mean wind speed estimated uncertainty in debt sizing for offshore wind farms.

$$LCOE = \lambda \left| \sum_{t=1}^{n} \frac{FCF_t^{P50} + FCF_t^{P90}}{(1 + MARR)^t} = 0; \right. \tag{12}$$

$$FCF_t^{P50} = FCF_t^{P50}(DEVEX(\sigma)) \tag{13}$$

$$FCF_t^{P90} = FCF_t^{P90}(\sigma) \tag{14}$$

5. Relationship between mean wind speed estimated uncertainty and debt sculpting

This section builds on Section 4 to derive some theoretical relationships between the mean wind speed estimated uncertainty and the debt sculpting, which gives rise to the curves depicted in Fig. 6. Fig. 6 is used as a reference figure for this section. Let us put aside the red lines for the moment. The top right chart shows the relationship between the DEVEX and the uncertainty in the mean wind speed. Longer wind campaigns and the use of more precise sensing devices allow for a reduction in uncertainty; however, this comes at a cost. A met mast is much more expensive than a Floating LIDAR, which in turn is much more expensive than mesoscale modelling. However, mesoscale modelling is much less precise than a Floating LIDAR, which itself is less precise than a met mast. In general, higher development expenditure results in a decrease in uncertainty. Also, in general, uncertainty is dependent on the quality of the resulting data and the successfulness of the campaign. However, for the sake of simplicity, it is assumed that all campaigns are equally successful, with high availability of data.

The top left chart shows the theoretical relationship between the AEP_{P90} and the uncertainty in mean wind speeds. As the uncertainty decreases, the v_{P90} and the AEP_{P90} increases. This relationship is a direct consequence of what has been displayed in Fig. 1, where a smaller σ would give higher values of v_{P90}. It is worth keeping in mind that all the other factors affecting the AEP have been kept constant here.

Two constraints imposed by banks are applied: the maximum gearing and the DSCR. For further details and description of these terms, see Section 2 above. Consider an offshore wind project for which the binding constraint on debt sizing is the DSCR. As we have seen in the previous section, a limitation on the DSCR can be translated into a limitation on the gearing. If the gearing obtained by the DSCR is lower than the maximum gearing allowed by the bank, this means that extra money could be lent if the CFADS increased. The CFADS is directly related to the wind speed uncertainty as the revenue stream calculated by the banks is based on a AEP_{P90}. Consequently, when the mean wind speed estimated uncertainty is reduced, a higher CFADS becomes available, and this in turn increases the gearing. The bottom left chart shows the relationship between gearing and uncertainty in the estimated mean wind speed. As can be seen in the same chart, the project reaches a point where a further reduction in uncertainty does not give rise to a higher gearing - this uncertainty threshold is defined as U^*. Reaching U^* means that the maximum gearing has been met.

The bottom right chart combines the rest of the charts to calculate the LCOE as a function of the mean wind speed uncertainty. This chart can be divided into two regions. The first region has values of uncertainty higher than U^*. In this case, a higher development expenditure gives rise to a reduction in uncertainty, which increases the AEP_{P90}. That means that a higher gearing can be obtained, decreasing the LCOE. In the second region, to the left of U^*, higher development expenditures also lead to higher AEP_{P90}. However, in this case, since the project is limited by the maximum gearing, no extra gearing is reached. As we reduce the uncertainty further there is an increase in the development expenditure but this does not lead to more favourable financial conditions. The LCOE therefore increases as mean wind speed uncertainty is reduced.

In the above, U^* is the optimal level of uncertainty. However, for some projects, it may be optimal to choose a higher level of uncertainty, depending on how sensitive variations or incremental costs and AEP values are to uncertainty. As an example, consider the red lines in Fig. 6. These exemplify a project not limited by the maximum gearing. For this project, an increase in the DEVEX still leads to an increase in the AEP_{P90}. As a result better financing conditions are reached. But despite this, the LCOE reaches an optimal before the maximum gearing is obtained. The reason for this may be, for instance, that the increase in DEVEX is not compensated by the estimated resource.

In this case, $U_2^* > U^*$ is the optimal amount of uncertainty. In general, whatever the characteristics of the sensitivities of DEVEX and financing costs to uncertainty, it is never optimal to reduce uncertainty below U^*. This conventional wisdom that better mean wind speed predictions are always worth the increased development expenditure is not true. The next section considers cost modelling for real offshore wind farm projects, where these relationships in Fig. 6 are investigated.

6. Case study

The average size of European commercial offshore wind farms commissioned in the year 2017 is 500 MW [2]; we therefore chose the same size as a reference in our case study. The case study is based on three commercial offshore wind farms with the following characteristics: Project A represents our reference offshore wind farm, which is representative of UK round 2 offshore wind projects. Project B represents an offshore wind farm located near the coast, meaning that only a relatively small amount of CAPEX is required to develop the project. However, it is assumed that the site has a poorer wind resource. Finally, Project C represents an offshore wind farm located very far from shore. Project C has a high CAPEX, but it also has access to higher wind resource than previous A and B projects. To some extent, Project C is representative of German offshore wind farms. All projects are assessed with a generic 8.3 MW wind turbine with a rotor diameter of 164 m. We also assume, for the sake of simplicity, that the export cable length, construction and operational port distances are equal to the distance from shore. Whereas Project A and B wind turbines are commissioned atop monopile foundations, project C uses jackets due to water depth requirements. The project specifications of the offshore wind farms are shown in Table 2.

The modelling approach to offshore wind cost analysis presented in this paper is based around OWCAT developed at the EDF Energy R&D UK Centre. Further information on the tool can be found in Section 3 as well as [20]. The only parameters that are modified within the tool are the development expenditure and the uncertainty in the estimated mean wind speed (apart from the site specifications for the different cases). All other uncertain parameters such as the availability of the offshore wind farm, wake losses, are assumed to be the same in all three

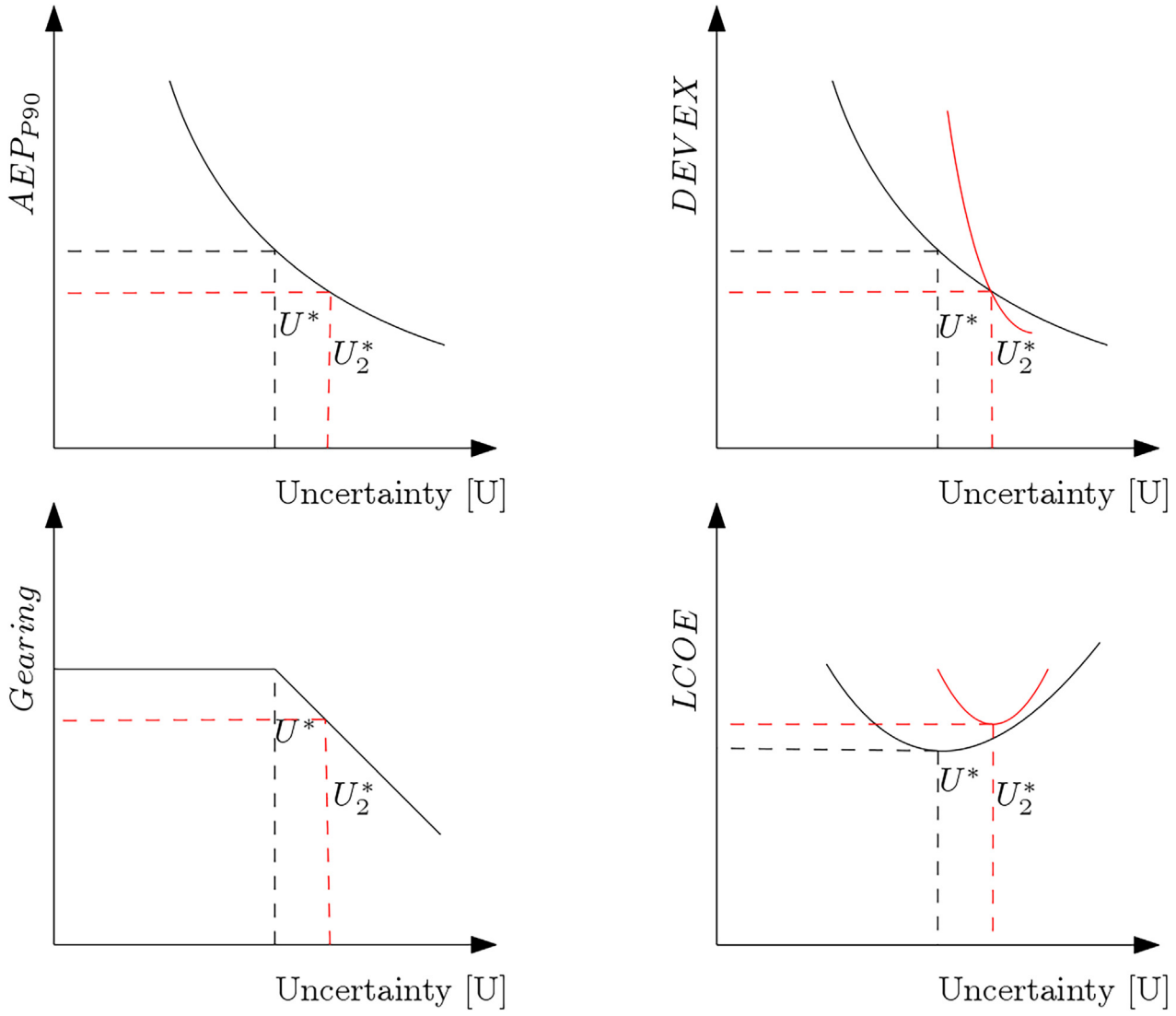

Fig. 6. Theoretical mean wind speed uncertainty – AEP_{P90}, DEVEX, Gearing and LCOE curves, all the other factors being equal.

Table 2
Project A, B and C specifications.

Parameter	Project A	Project B	Project C
Water Depth [m]	25	15	40
Distance from shore [km]	25	15	100
Wind Speed @ 100 m [m/s]	9	8	10
Foundation Type	Monopile	Monopile	Jacket
Electrical Infrastructure	HVAC	HVAC	HVAC
Wind Turbine Type	164–8.3 MW	164–8.3 MW	164–8.3 MW
CAPEX [2015/kW]	2600	2500	3300
OPEX [2015/kW/yr]	85	80	100

cases. We also assume that the availability of the offshore wind farm does not depend on the distance from shore, and therefore, that the technical performance of project A, B and C is similar.

In order to reflect the recent changes in financing conditions displayed in Table 1, we consider two scenarios. The first scenario assumes a gearing representative of the period between 2014 and 2015 (70:30). A second scenario is representative of more recent gearings (75:25).

The aim of the current paper is to reflect the changes of the mean wind speed estimated uncertainty in the LCOE, and not to analyse detailed site-specific uncertainties. In consequence, the emphasis has been placed on the choice of measurement devices, which developers face once a site has been selected. Individual devices are assumed to be deployed in the centre of the offshore wind farm so as to avoid comparisons that favour horizontal extrapolations above others. In this case study, the developer considers the following available options to assess the wind speed of projects A, B and C. A HHMM, a HAFLIDAR that has a shorter mast than HHMM, a HAFLIDAR, a LAFLIDAR and Mesoscale modelling are assumed. Mesoscale modelling is considered as a service provided to the developer. Table 3 shows the respective costs of these methods. The difference between HHMM and BHHMM is the cost of having a taller mast, which allows wind speeds to be measured closer to hub height. The difference between HAFLIDAR and LAFLIDAR is their degree of precision. The developer may opt for a cheaper and less precise device or for a more expensive and precise one.

These cost estimates have been derived from [22–26] as well as from discussion with experts in the field of wind resource assessment. If bigger offshore wind farms were to be analysed, then economies of scale in the cost of the devices should be considered as reflected in [27].

Table 3
Development expenditure for the different wind measurement campaigns.

Cost [£m 2017]	HHMM	BHHMM	HAFLIDAR	LAFLIDAR	Mesoscale
DEVEX	10	9	1.2	1	0.15

Table 4
Breakdown of the device-specific uncertainties for the different measurement campaigns, based on DNV GL [33,7,25].

Uncertainty [%]	HHMM	BHHMM	HAFLIDAR	LAFLIDAR	Mesoscale
Instrument Accuracy	2	2	3	4	10
Measurement Interference	1.5	1.5	0.5	0.5	0
Data Quality & Metadata	1	1	1	1	0
Vertical Extrapolation	0	1	0	0	3
Horizontal Extrapolation	1.5	1.5	1	1	0
Total Wind Speed Measurement	3.08	3.24	3.35	4.27	10.44

In order to represent current technology trends, and given that the first offshore wind project to be built using the AEP_{P90} on wind resource data from a Floating LIDAR was Burbo Bank Extension in the UK, in 2014 [28], two different types of Floating LIDAR are considered in this study. According to the Carbon Trust Offshore Wind Accelerator [26], a pre-commercial LIDAR has an indicative measurement uncertainty range between 4 to 7%, whereas a commercial one can achieve a range between 2 to 4%. The Floating LIDAR industry has benefited from research and development programmes and has reached the commercialisation stage [29,30,25]. This is the reason why two commercial LIDARs are considered. More recently, it was announced that AXYS FLIDAR met the commercialisation stage of the Carbon Trust Offshore Wind Accelerator [31], meaning that uncertainties between 3 and 4% in instrument accuracy for a Floating LIDAR is a sensible choice according to the current state of technology.

A section on the classification and description of wind speed uncertainties is out of the scope of this research paper, however wind speed uncertainties have been estimated based on the classification provided by DNV GL [32,7,25] as well as discussions with industry experts. Those values are displayed in Table 4. The different site-specific uncertainties for A, B and C are shown in Table 5 and are independent of the device. Table 6 shows the devices ordered in terms of total precision, HHMM is the most precise one (4.25%) and Mesoscale the less precise (10.84%). All uncertainties are expressed as a percentage of the standard deviation of the mean wind speed and are combined by assuming they are independent and normally-distributed.

The relationship between cost and mean wind speed estimated uncertainty for the different campaigns is given in Fig. 7. It is shown that this relationship follows a negative concave trend hypothesised in Section 5 on the top right of Fig. 6.

The case study consists on selecting the sensing device that minimises the LCOE, which is a real-world problem faced by developers in the offshore wind industry. Three representative commercial offshore wind farms are selected whose characteristics are shown in Table 2.

Table 5
Breakdown of the site-specific uncertainties for the different measurement campaigns [33].

Description for A, B and C Projects	Uncertainty [%]
Representativeness of Data Period	1.5
Consistency & Quality of Reference Data	1
Correlation	0.5
On-site data	0.5
Wind Frequency Distribution - Past	0.5
Wind Frequency Distribution - Future	0.5
IAV of the Wind - Future	1.5
Climate Change	1.5
Total Site	2.92

Table 6
Breakdown of the total uncertainties for the different measurement campaigns.

Uncertainty [%]	HHMM	BHHMM	HAFLIDAR	LAFLIDAR	Mesoscale
Total Wind Speed	4.25	4.36	4.45	5.17	10.84

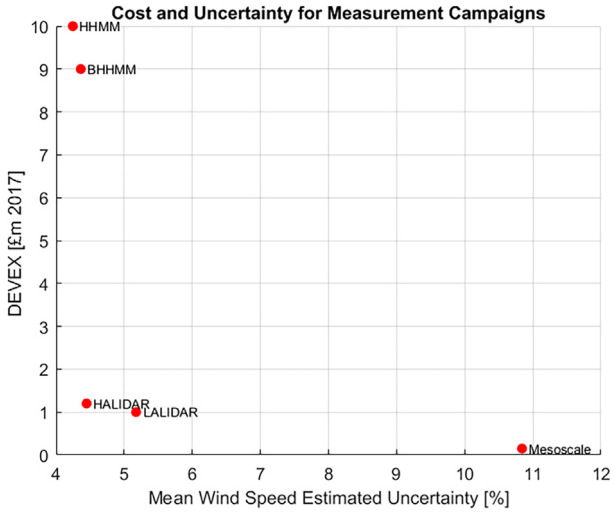

Fig. 7. Relationship between DEVEX and wind speed measurement uncertainty for different wind measurement campaigns.

These sites attempt to be representative for different types of site-specific characteristics. Five commercial sensing devices are available for conducting the wind campaigns, capturing well established devices such as met masts and the latest developments in FLIDAR technology. In addition, two scenarios are assumed with different gearing regimes, that reflect a reduction on the perceived risk from financial institutions when investing in offshore wind.

6.1. Scenario 1: maximum gearing of 0.70

Fig. 8 shows the first set of results, assuming 0.70 maximum gearing. All charts show the relationship between the uncertainty in the estimated mean wind speed (on the horizontal axis), the gearing (the right vertical axis) and the LCOE (the left vertical axis) for all three projects. The continuous black line depicts the gearing for different levels of uncertainty, whereas the dashed red line highlights the lowest LCOE that can be achieved in each project.

Starting off with the Mesoscale Modelling campaign on the right in all three projects, none of the projects are limited by the gearing and hence a further reduction in uncertainty may lead to a reduction in financing costs that more than compensates the higher development expenditure. In all projects, using LAFLIDARs allows the developer to reach the point where projects become limited by the gearing. Although HAFLIDARs are more precise than LAFLIDAR, they are not the optimal choice, since the further reduction in uncertainty they achieve do not decrease financing costs, while they do increase development expenditure.

In all cases, the optimal device is the LAFLIDAR. A slightly higher LCOE is obtained by using a HAFLIDAR. The slopes of maximum gearing are affected by the type of offshore wind farm. Higher wind resource results in flatter slopes for the maximum gearing, whereas poor wind results in steeper slopes. Project B has a lower CAPEX and lower wind resource than the other projects. For this reason, the maximum gearing of the project is achieved with a lower uncertainty, since the effect of improving financing conditions by reducing the uncertainty is weaker. Project C, with high CAPEX and a high wind resources, achieves maximum gearing at a higher uncertainty, since the

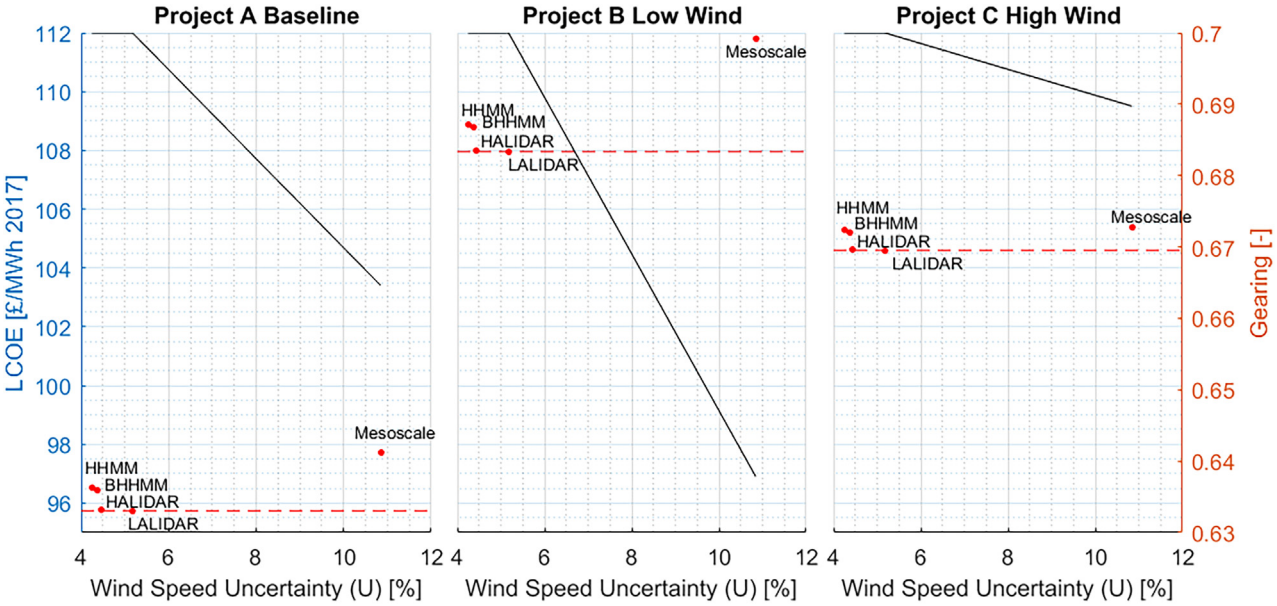

Fig. 8. Project A, B and C relationship between Uncertainty, Gearing and LCOE for a maximum gearing of 0.70.

effect of improving the financing conditions by reducing the uncertainty is stronger – for the same level of uncertainty, a higher level of production can be obtained.

6.2. Scenario 2: maximum gearing of 0.75

Fig. 9 shows the results of a similar exercise, but with a more recent gearing of 0.75. As above, all charts show the relationship between the uncertainty in the estimated mean wind speed (on the horizontal axis), the gearing (the right vertical axis) and the LCOE (the left vertical axis) for all three projects. The continuous black line depicts the gearing for different levels of uncertainty, whereas the dashed red line highlights the lowest LCOE that can be achieved in each project.

The main difference with the previous results is that the point where project A becomes limited by the gearing has moved from the LAFLIDAR to the BHHMM. However, given the unfavourable trade-off between uncertainty and DEVEX, the HAFLIDAR is the optimal choice. Project B, characterized by a poor wind resource, also does not reach maximum gearing, with the HAFLIDAR being LCOE optimal. In both cases, this happens because of the steep slope of the trade-off between DEVEX and uncertainty as displayed in Fig. 7. If the developer wants to slightly reduce the uncertainty from HAFLIDAR, a very large increase in DEVEX is incurred. In Project C the maximum gearing of the project is achieved with a higher uncertainty, since the effect of improving the financing conditions by reducing the uncertainty is stronger, and therefore the project also reaches its minimum LCOE with a HAFLIDAR.

7. Conclusions

We have shown that offshore wind projects can be categorised into two different types, based on project finance conditions. The first type is limited by the DSCR, whereas the second is limited by the maximum gearing offered by the bank. For projects limited by the maximum gearing the costs of decreasing mean wind speed uncertainty only

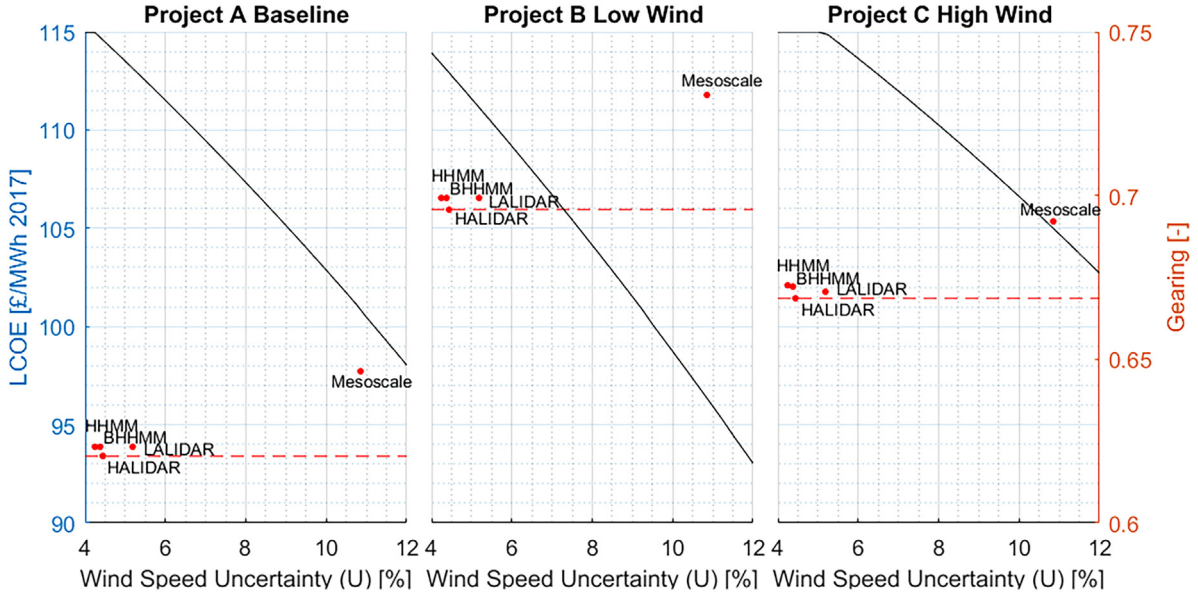

Fig. 9. Project A, B and C relationship between Uncertainty, Gearing and LCOE for a maximum gearing of 0.75.

increase the LCOE, whereas for projects limited by the DSCR the effect of decreasing the LCOE depends on the trade-off between the DEVEX and the mean wind speed estimated uncertainty. This is represented in Fig. 7 and more theoretically on the top right of Fig. 6. This means that it is never optimal to reduce uncertainty as far as possible, as it is commonly believed in the industry.

In a realistic case study, we have further explored this effect. Interestingly, this case study suggests that it is never optimal to use met masts to obtain the most reliable mean wind speed estimates. Commercial LIDARs are optimal in all cases, highlighting the maturation phase of this technology. Differences between different offshore wind farms specifications are reflected in the slope of the gearing and the point at which maximum gearings are reached. High wind resource offshore wind farms will have higher gearings than other average-wind farms for the same level of uncertainty. Conversely, poor wind resource offshore wind farms may not reach the gearing limit or reach it for smaller levels of uncertainty than average-wind farms.

In addition, the maximum gearing has a big effect on the financial conditions and on optimal wind speed estimation techniques. As we have seen, the maximum gearing is increasing, as banks are becoming more familiar with offshore wind projects. This means that additional measurements become more valuable. In our case study, the optimal device for a maximum gearing of 0.75 is the more precise and expensive HAFLIDAR, whereas for a gearing of 0.70 it is the cheaper and less precise LAFLIDAR. This illustrates that a detailed understanding of project finance constraints is necessary to optimally plan and execute offshore wind projects.

This paper has presented the development of a novel theoretical cost modelling framework which includes detailed considerations of financing requirements that until now have been usually ignored in the offshore wind planning models. The methodology presented here links these financing requirements such as the DSCR and the maximum gearing to the cash flow metrics, while considering the development expenditure incurred in choosing a wind speed measurement device and its mean wind speed estimated uncertainty represented by the P50 and P90 metrics. This methodology can be applied to any existing standard corporate finance cost model to account for project finance arrangements. At the same time, this cost modelling framework allows policy-makers and developers alike to assess the trade-off between DEVEX and the estimated wind speed uncertainty, leading to more informed decision that have the potential to drive down the cost of energy.

It has been assumed in this study that the DSCR metric is based on P90 cash flows. However, in reality, projects might be evaluated against two DSCRs metrics based on P50 and P90 cash flows; this imposes an additional constraint. Further work should include the ability to incorporate these two constraints as well as a description of the different uncertainties that characterise the mean wind speed and energy factors.

Acknowledgements

This article is based on work sponsored by EDF Energy R&D UK at the Industrial Doctoral Centre for Offshore Renewable Energy (IDCORE), a consortium of the University of Exeter, University of Edinburgh and University of Strathclyde. IDCORE is funded by both the Energy Technologies Institute and the Research Councils Energy Programme through Grant No. EP/J500847/1. Additional support came from the UK Engineering and Physical Sciences Research Council through Grant No. EP/P001173/1 (CESI). Special thanks go to Hugo Herrmann for reading the manuscript and for his constructive suggestions.

References

[1] Steffen Bjarne. The importance of project finance for renewable energy projects. Energy Econ 2018;69:280–94. https://doi.org/10.1016/j.eneco.2017.11.006. ISSN: 0140-9883.
[2] Wind Europe. Financing and investment trends: the European wind industry in 2017. Tech. rep.; 2018. p. 32. https://doi.org/10.1080/00218460701751855. URL: https://windeurope.org/wp-content/uploads/files/about-wind/reports/Financing-and-Investment-Trends-2017.pdf.
[3] IEA – RETD Renewable Energy Technology Deployment. Gusts of change: How effective policy is catalysing a booming offshore wind sector. Tech. rep.; March 2017.
[4] Wind Europe. Offshore Wind in Europe: Key Trends and Statistics 2017. Tech. rep.; 2018.
[5] Schreider Achim, Sedlacek Mirko. Project financing offshore wind farms: risk analysis for a structured finance. In: European Offshore Wind 2009 Conference. Stockholm; 2009. p. 1–10.
[6] Wadham David. Finandg Offshore Wind: Plain sailing? Tech. rep. 20; 2018.
[7] Foussekis D et al. Uncertainty estimations for offshore wind resource assessment and power verification. In: EERA Deep Wind 18. Trondheim; 2018.
[8] Loukatou Angeliki, et al. Stochastic wind speed modelling for estimation of expected wind power output. Appl Energy 2018;228(May):1328–40. https://doi.org/10.1016/j.apenergy.2018.06.117.
[9] Crockford Anthony et al. Estimated uncertainty for various wind measurement strategies including floating LiDAR at the Hollandse Kust Zuid offshore wind farm zone. Tech. rep.; 2016.
[10] Yan Jie, et al. Uncertainty estimation for wind energy conversion by probabilistic wind turbine power curve modelling. Appl Energy 2019;239(September 2018):1356–70. https://doi.org/10.1016/j.apenergy.2019.01.180. ISSN: 03062619.
[11] Gavin Smart. Offshore Wind Cost Reduction: Recent and future trends in the UK and Europe. Tech. rep.; November. 2016. p. 1–10.
[12] BVG associates. Future renewable energy costs: offshore wind. Tech. rep.; 2017. p. 80.
[13] Mytilinou Varvara, Kolios Athanasios J. Techno-economic optimisation of offshore wind farms based on life cycle cost analysis on the UK. Renew Energy 2019;132:439–54. https://doi.org/10.1016/j.renene.2018.07.146. ISSN: 18790682.
[14] Ioannou Anastasia, Angus Andrew, Brennan Feargal. A lifecycle techno-economic model of offshore wind energy for different entry and exit instances. Appl Energy 2018;221(November 2017):406–24. https://doi.org/10.1016/j.apenergy.2018.03.143. ISSN: 03062619.
[15] EDHEC Infrastructure Institute-Singapore. Cash Flow Dynamics of Private infrastructure Project Debt. Tech. rep.; March. 2016. p. 1–108.
[16] Green Giraffe. Project finance for German offshore wind. Tech. rep.; February 2017.
[17] Bodmer Edward. Debt Sculpting in a Project Finance Model. In: Corporate and project finance modeling. Theory and practice; 2015. p. 515–37. ISBN: 9781118854365. DOI: https://doi.org/10.1002/9781118957394. URL: https://drive.google.com/open?id=0B544TwTVwnWkN2ZlSm9YZHZxSG8 (chap. 41).
[18] Green Giraffe. Offshore wind finance – evolution and outlook. Tech. rep; September 2017.
[19] Green Giraffe. Introduction to wind project finance. Tech. rep.; March 2017.
[20] Mora Esteve Borràs. Transition from deterministic to stochastic cost models for offshore wind farms. In: Offshore wind energy conference; June 2017.
[21] Kaiser Mark J, Snyder Brian F. Offshore wind energy cost modeling- installation and decommissioning; 2012. 248 p. ISBN: 9781608052851. DOI: https://doi.org/10.2174/97816080528511060101. URL: http://www.benthamdirect.org/pages/content.php?9781608052851.
[22] Clive Peter et al. Offshore power curve tests for onshore costs: a real world case study. Tech. rep.; 2014. p. 1–9. DOI: https://doi.org/10.1177/1066480709355039.
[23] BVG Associates. Value breakdown for the offshore wind sector. Tech. rep.; February 2010. p. 1–20. URL: https://www.gov.uk/government/uploads/system/uploads/attachment%7B%5C_%7Ddata/file/48171/2806-value-breakdown-offshore-wind-sector.pdf.
[24] Cool GA. Floating LiDAR technology: oceanographic parameters influencing accuracy ol wind vector reconstruction. PhD thesis; 2016.
[25] Herrmann Hugo et al. Floating LiDAR Uncertainty Assessment Wind Europe – Resource Assessment March 2017; March 2017.
[26] Carbon Trust. Carbon Trust Offshore Wind Accelerator Program. Tech. rep.; 2017. URL: https://www.carbontrust.com/offshore-wind/owa/.
[27] Electricity Market Reform. Supply Chain Plan Consultation; November 2013.
[28] Offshorewindbiz. Burbo Bank Extension First FLWAR-Calculated OWF to Be Built; 2015. URL: https://www.offshorewind.biz/2015/04/24/burbo-bank-extension-first-flidar-calculated-owf-to-be-built/.
[29] Gottschall J, et al. Results and conclusions ol a floating-lidar offshore test. Energy Procedia 2014;53(C):156–61. https://doi.org/10.1016/j.egypro.2014.07.224. ISSN:18766102.
[30] Gottschall Julia, et al. Floating lidar as an advanced offshore wind speed measurement technique: current technology status and gap analysis in regard to lull maturity. Wiley Interdiscipl Rev Energy Environ 2017;6(5). https://doi.org/10.1002/wene. 250. ISSN: 2041840X.
[31] Offshorewindbiz. Axys FLIDAR Reaches Stage 3 on Carbon Trust Roadmap; 2018. URL: https://www.offshorewind.biz/2017/06/06/axys-flidar-reaches-stage-3-on-carbon-trust-roadmap/.
[32] DNV KEMA ENERGY & SUSTAINABILITY. Framework for the Categorisation of Losses and Uncertainty for Wind Energy Assessments. Tech. rep. 2013. URL: http://www.sgurrenergy.com/wp-content/uploads/2013/02/Loss-and-Uncertainty-Definitions-Report-05Feb2013.pdf.
[33] DNV GL. Study on UK Offshore Wind Variability. Tech. rep. L2C124303-UKBR-R-01, Issue B; 2016.

Environmental Modelling and Software 122 (2019) 104556

Contents lists available at ScienceDirect

Environmental Modelling and Software

journal homepage: http://www.elsevier.com/locate/envsoft

Benchmarking the PAWN distribution-based method against the variance-based method in global sensitivity analysis: Empirical results

Esteve Borràs Mora [a,b,*], James Spelling [b], Adriaan H. van der Weijde [c,d]

[a] Industrial Doctoral Centre for Offshore Renewable Energy (IDCORE), The University of Edinburgh, Edinburgh, EH9 3JL, UK
[b] EDF Energy R&D UK Centre, Interchange, 81-85 Station Road, Croydon, CR0 2AJ, UK
[c] Institute for Energy Systems, School of Engineering, University of Edinburgh, Faraday Building, The King's Buildings, Mayfield Road, Edinburgh, EH9 3DW, UK
[d] The Alan Turing Institute, British Library, 96 Euston Rd, London, NW1 2DB, UK

ARTICLE INFO

Keywords:
Global sensitivity analysis
PAWN distribution-based method
Variance-based sensitivity analysis

ABSTRACT

The search for new and more efficient global sensitivity analysis methods has led to the development of the PAWN distribution-based method. This method has been proven to overcome one of the main limitation of variance-based methods – the moment independent property. In this regard, the distribution-based method has outperformed the variance-based method for some highly-skewed or multi-modal distributions. However, despite its increasing popularity, there is a lack of understanding about the performance and properties of the distribution-based method. The benchmark presented in this paper is an attempt to remedy this. We compare the distribution-based method against the variance-based method for a set of well-known test functions. We show that, whereas the distribution-based method can be used as a complementary approach to variance-based methods, which is especially useful when dealing with highly-skewed or multi-modal distributions, it fails to rank different inputs that have different orders of magnitude in their contribution of the response.

1. Introduction

Global Sensitivity Analysis (GSA) methods are used to study how different sources of uncertainty in model output can be apportioned to the different sources of uncertainty in model input by exploring the combined space formed by all parameters in the domain (Cacuci, 2003) (Saltelliet al., 2008). Before starting a GSA, it is imperative to define which research question needs to be answered and which risk metrics are to be used to quantify uncertainty. Different research questions and risk metrics will lead to different answers, and therefore this is something that has to be established from the very beginning.

In the context of this paper, the research question GSA attempts to aswer is to determine the most relevant input variables to an output behaviour, as well as to identify those variables whose contribution can be neglected. By ranking the model inputs in order of importance, useful insights into the model can be gained, especially when the system is not well known or the model is in the early stages of development. The process of ranking these inputs is also referred to as **Factor Prioritization** (Saltelliet al., 2008). Prioritization leads naturally to the idea of important inputs but also to negligible inputs or factors whose variability has a negligible effect on the output. Very often the inputs into a model follow very asymmetric distributions of importance, with few inputs accounting for most of the output uncertainty and most inputs playing little or no role (de Rocquigny et al., 2008). By identifying those parameters that have no significant contribution to the model output, the complexity of the model can be reduced. This is also known as **Factor Fixing** (Saltelliet al., 2008).

It is similarly important to define the risk metric. A number of methods have been developed. One of the most well-established and extensively used GSA method is the Sobol or variance-based method, developed in 1990 by Ilya Meyerovich Sobol (1993). The Sobol method decomposes the variance of the model output in terms of the input variances. The method is model independent and therefore, it can be applied to any model regardless of the response function of the input-outputs. In addition, it is easy to interpret and to implement, making it the cornerstone of GSA. However, one of the key limitations of the method concerns the fact that the method needs a moment of the output distribution to fully characterise the output uncertainty.

Moment independent techniques arose from the works of Borgonovo (Borgonovo et al., 2011) and Liu (Liu et al., 2006), where highly-skewed distributions were analysed to examine how its variance is decomposed. When using conventional variance-based GSA techniques both works

* Corresponding author. Industrial Doctoral Centre for Offshore Renewable Energy (IDCORE), The University of Edinburgh, Edinburgh, EH9 3JL, UK.
E-mail address: E.Borras-Mora@ed.ac.uk (E.B. Mora).

https://doi.org/10.1016/j.envsoft.2019.104556
Received 20 September 2019; Accepted 9 October 2019
Available online 17 October 2019

concluded that identifying variance with uncertainty might lead to misleading conclusions. The first set of results showed that the unconditional variance was lower that the conditional variance at a given conditioning value, implying that the variance of the output increases when removing the uncertainty from one of the inputs; an example of that can be found in (Saltelliet al., 2008) for non-additive models. The second example failed to rank the importance of the different input uncertainties. Therefore, decision makers might be given a false sense of security, whereby attempting to fix/reduce some of the input uncertainty may result in higher variability of the output. These findings prompted the research community to investigate methods that remove the dependence on a single moment. As such, moment independent techniques are not affected by the presence of correlations and can provide a solution for those distributions that are not well represented by its variance, avoiding costly pitfalls.

As a consequence, several GSA methods were developed (citing here just a few) such as the entropy-based and the δ-sensitivity to overcome the moment dependent property (Borgonovo et al., 2011; Liu et al., 2006). However, the practical implementation of those methods has been quite limited (Pianosi and Wagener, 2015). This is thought to be related with the computational cost of calculating many Probability Distribution Functions (PDFs). Later on, the PAWN method was published in 2015, coined under the name of "A simple and efficient method for GSA based on CDFs" (Pianosi and Wagener, 2015). The innovative idea was to use the Cumulative Distribution Function (CDF) instead of the PDF in order to apportion the uncertainty of the output into the different inputs. The underlying reason for choosing CDFs over PDFs is based on the fact that CDFs are much easier to approximate than PDFs (Pianosi and Wagener, 2015). PDFs are usually unknown and must be estimated empirically. An easier way to calculate an empirical PDF would be to use a histogram of the data sample, whose resulting shape will be conditioned on both the position of the first bin and the size of the bin. However, obtaining values that correctly represent the empirical PDF may be difficult. A different way to estimate the PDFs would be to use the Kernel Density Estimation (KDE) methods, which would only require the estimation of a single parameter – the bandwidth. Another approach that has been used in the past is to first estimate the CDFs, and then use derivation techniques to work out the empirical PDFs (Liu et al., 2006). Given that the calculation of PDFs has to be repeated many times, it must be as computationally inexpensive as possible. As a result, it seems logical to compute CDFs instead of PDFs at no extra cost and without the need for tuning parameters. Not only does the PAWN method claimed to address the complexity of previous moment independent methods; its authors also provided several examples where the method outperforms the variance-based method for those PDF model output distributions that were highly-skewed or multi-modal, suggesting that, in these cases, variance was not a good proxy for uncertainty.

Findings that more theoretical understanding is needed in order to employ CDF-based sensitivity measures are available in the existing literature as shown in (Borgonovo, 2007; Baucells and Borgonovo, 2013; Plischke et al., 2013). Nevertheless, given its advantages, moment independent techniques are continuously being applied to tackle complex problems. In 2016 the PAWN method was used in a techno-economic optimal wind-energy converter, where its model exhibited an output PDF which was not symmetric but right-skewed (Hollet al., 2016). As a result, negative values were obtained for those cases were the conditional variance exceeded the unconditional variance; result of which was driven by a numerical approximation due to the limited sample size. In 2017, the Sobol and PAWN GSA techniques were compared for a hydrological model called Soil and Water Assessment Tool (Farkhondeh Khorashadi Zadesh, 2017). The comparison was undertaken in terms of the convergence rate, parameter ranking and screening results. It was shown that there were no differences between the two methods as for the convergence rate and screening results. However, PAWN and Sobol came up with a different ranking of the model inputs importance. The paper emphasised that this was due to the underlying assumption that Sobol considers variance as a good proxy for uncertainty, whereas in reality this may not be the case; at the same time the paper suggested that the variance-based and PAWN methods may be regarded as complementary approaches to study the sensitivity of model output.

Although the PAWN method has been widely adopted, a major limitation of PAWN was perceived by the authors regarding the need for a tailored sampling strategy to approximate the sensitivity indices. PAWN required to tune the triplet *Nu*, *Nc* and *n* to compute its PAWN indices. However, no one has yet analysed how to choose the values for the triplet. In addition, given the tailored sampling strategy, it is difficult to apply several GSA methods to the same problem, as PAWN requires dedicated model evaluations. In 2018, the authors addressed these two issues by developing a generic approach of the PAWN method, called the distribution-based global sensitivity analysis. This generic approach provides a solution for these two limitations as shown in (Pianosi and Wagener, 2018). On a separate note, Gamboa et al. investigated in 2018 the generalisation of the so-called Sobol indices to higher moments, where its index appears to be more general than Sobol as it takes into consideration the whole distribution and not the second moment (Gamboaet al., 2018).

Given the number of people that use the PAWN distribution-based method in the field of environmental modelling (Pianosi et al., 2015), the authors would like to limit the scope of this paper to benchmark the PAWN distribution-based against the variance based. Even though the one from Gamboa is well suited for this comparison, this will be considered in future work. Further research is necessary to compare the PAWN distribution-based method against the well-established Sobol method, before the former can be widely adopted by the community. Therefore, a wider set of reference test functions has to be used to benchmark these two methods for those cases where the analytical variances of the test functions are known. In other words, the community needs to know how the PAWN distribution-based method compares to Sobol for those cases where Sobol has worked well and also which are the advantages of the PAWN distribution-based over Sobol. The aim of the current paper is to remedy this lack of understanding by providing this benchmark. We then show its properties, and suggest where the method is appropriate.

The rest of this paper is organised as follows: Section 2 and 3 introduces the fundamentals of variance-based and PAWN distribution-based GSA, respectively. Following this, a set of well-known test functions is introduced in Section 4 and used to benchmark the two methods. Results and discussions are shown in Section 5. Conclusions are drawn in Section 6.

2. Sobol method

2.1. Introduction

The Sobol method, or variance-based sensitivity analysis, is a form of global sensitivity analysis that focus on decomposing the variance of the model outputs in terms of the variance of the model inputs. The following formulation is reproduced from (Sobol, 1993). Let us assume that a mathematical model can be represented by Equation (1), which is made of summands of increased dimensionality. This is also called a High Dimensional Model Representation (HDMR), where the total number of summands in Equation (1) is 2^N. Let us also consider that the model input $\mathbf{X}$ belongs to the n-dimensional unit hypercube domain I^N, which is expressed as: $X_i \in [0,1]\ \forall i \in 1,\ldots,N$. $f(\mathbf{X})$ is the model under study and the number of elements of increasing dimensionality grows as a function of $\binom{N}{i}\ \forall i \in 1,\ldots,N$.

$$Y = f(\mathbf{X}) = f_0 + \sum_i f_i(X_i) + \sum_{i<j} f_{i<j}(X_i, X_j) + \ldots + f_{12\ldots n}(X_1, X_2 \ldots, X_N) \qquad (1)$$

As a result, the total number of summands (apart from f_0) is given by

Table 1
Statistical measures and interpretation.

ID	Mathematical notation	Interpretation
1	$\mathbf{V}_{X_i}(\mathbf{E}_{\mathbf{X}_{\sim i}}[Y\|X_i])$	Expected reduction in variance that would be obtained if x_i could be fixed.
2	$\mathbf{E}_{\mathbf{X}_{\sim i}}(\mathbf{V}_{X_i}([Y\|X_{\sim i}]$	Expected variance that would be left if all factors but x_i could be fixed.
3	$\mathbf{V}_{X_{\sim i}}(\mathbf{E}_{\mathbf{X}_i}[Y\|X_{\sim i})$	Expected variance that would be obtained if all factors but x_i could be fixed.
4	$\mathbf{E}_{\mathbf{X}_i}(\mathbf{V}_{X_{\sim i}}([Y\|X_i]$	Expected reduction in variance that would be left if x_i could be fixed.

Equation (2).

$$\sum_{i=1}^{N}\binom{N}{i} = 2^N - 1 \tag{2}$$

If the following requirement in Equation (3) can be satisfied, then the representation of the model is called Analysis of Variance (ANOVA) HDMR. This means that the variables are considered to be mutually independent and it has been proven that this decomposition is unique (Sobol, 2003).

$$\int_0^1 f_{i_1\ldots i_s} dX_k = 0 \quad \text{for} \quad k = i_1, \ldots i_s \tag{3}$$

From assumption 3 and Equation (1), it follows the following relationships 4 to 7, where X_i is the i-th factor, $X_{\sim i}$ denotes all the factors but the i-th and $\mathbf{E}$ is the expectation operator.

$$\mathbf{E}[Y] = \int_{I^N} f(\mathbf{X}) = f_0 \tag{4}$$

$$\mathbf{E}_{\mathbf{X}_{\sim i}}[Y|X_i] = \int_{I^N} f(\mathbf{X}) \prod_{k\neq i} dX_k = f_0 + f_i(X_i) \tag{5}$$

$$\mathbf{E}_{\mathbf{X}_{\sim i,j}}\left[Y\middle|X_i, X_j\right] = \int_{I^N} f(\mathbf{X}) \prod_{k\neq i,j} dX_k = f_0 + f_i(X_i) + f_j\left(X_j\right) + f_{ij}\left(X_i, X_j\right) \tag{6}$$

$$\begin{aligned}\mathbf{E}_{\mathbf{X}_{\sim i,j,l}}\left[Y\middle|X_i, X_j, X_l\right] = \int_{I^N} f(\mathbf{X}) \prod_{k\neq i,j,l} dX_k = f_0 + f_i(X_i) + f_j\left(X_j\right) + f_l(X_l) + \\ f_{ij}\left(X_i, X_j\right) + f_{il}(X_i, X_l) + f_{jl}\left(X_j, X_l\right) + f_{ijl}\left(X_i, X_j, X_l\right)\end{aligned} \tag{7}$$

Equation (4) shows that, when integrating the HDMR, all the terms cancel out apart from the constant f_0. The differential x $dX_k\ \forall k \in 1, \ldots, N$ concerns the integration of the model respect those k variables. It becomes apparent that when fixing a variable, the integration does not lead to a 0 contribution as per assumption 3. The procedure is continued until all $(N-1)$-dimensional summands are defined, and then for the last member $f_{12\ldots N}(X_1, X_2 \ldots, X_N)$ Equation (1) is used. By regrouping the terms and calculating the multidimensional integrals, the different HDMR functions can be obtained in a recursive way.

2.2. Construction of ANOVA in HDMR

If we now assume that the input parameters are independent random variables uniformly distributed over $[0, 1]$, as expressed in 8, as well as that $f(\mathbf{X})$ is square integrable (so are all the terms), then the following Equations hold. The expectation of this function is given in Equation (9), where $f_X(\mathbf{X})$ is the pdf of x and by construction this is equal to 1.

$$\mathbf{X} = \left\{X_1, \ldots, X_N^T\right\}, X_i \sim \mathscr{U}(0,1), \forall i \in 1, \ldots, N \tag{8}$$

$$\mathbf{E}[f(X)] = \int_{I^N} f(\mathbf{X}) f_X(\mathbf{X}) dX = \int_{I^N} f(\mathbf{X}) dX = f_0 \tag{9}$$

The total variance of the function can be defined in Equation (10).

$$\mathbf{V}[Y] = \int f(\mathbf{X})^2 dX - f_0^2 \tag{10}$$

Taking the different functional components of the HDMR $\{f_0, f_i, f_{ij}, \ldots\}$, partial variances V_i,V_{ij} can be calculated as in Equations (11) and (12). In addition, the total variance $V(Y)$ can be decomposed using Equation (13).

$$V_i = V(f_i(X_i)) = \mathbf{V}_{X_i}(\mathbf{E}_{\mathbf{X}_{\sim i}}[Y|X_i]) \tag{11}$$

$$\begin{aligned}V_{ij} = V\left(f_{i,j}\left(X_i, X_j\right)\right) = \mathbf{V}_{X_i X_j}\left(\mathbf{E}_{\mathbf{X}_{\sim ij}}\left[Y\middle|X_i, X_j\right]\right) - \mathbf{V}_{X_i}(\mathbf{E}_{\mathbf{X}_{\sim i}}[Y|X_i]) \\ - \mathbf{V}_{X_j}\left(\mathbf{E}_{\mathbf{X}_{\sim j}}\left[Y\middle|X_j\right]\right)\end{aligned} \tag{12}$$

$$\mathbf{V}[Y] = \sum_i V_i + \sum_{i<j} V_{i,j} + \ldots + V_{12\ldots n} \tag{13}$$

2.3. Sensitivity indices

The decomposition of variance used in the previous section allows to define the following sensitivity analysis indices: the first and total order sensitivity coefficients. Whereas the first order S_i coefficient measures the part of variance which is caused by X_i, it does not take into account the interaction with the other variables. When considering the order 2 coefficient S_{ij}, it not only takes into account the part of variance caused by X_i and X_j, but also the interaction between X_i and X_j. The order 3 sensitivity coefficient S_{ijk} includes the variance of the output Y, resulting from the interactions of the three variables X_i, X_j and X_k, which is not explained by neither considering the single variables nor by the interaction of two variables. This can be generalised until the highest order.

The first sensitivity index is defined in Equation (14). Regardless of the interactions in the model, S_i is a measure of the main effect. In other words, it gives information on how much output variance could be reduced when fixing the input model X_i.

$$S_i = \frac{\mathbf{V}_{X_i}(\mathbf{E}_{\mathbf{X}_{\sim i}}[Y|X_i])}{V(Y)} = \frac{V_i}{V(Y)} \tag{14}$$

Where X_i is the i-th factor and $X_{\sim i}$ denotes all the factors but the i-th. The expectation of Y is taken over all the possible values of $X_{\sim i}$ while keeping X_i fixed. The outer variance is taken over all possible values of X_i. Although the total effects S_{T_i} are a direct consequence from Sobol's decomposition, they weren't explicitly mentioned until the work of Homma and Saltelli (1996). It is worth remembering that the number of coefficients to be computed grows exponentially according to 2^N, where N is the number of uncertain variables. Consequently, computing all Sobol components can be prohibitive if the model has many inputs. For this reason, and as a means to overcome this challenge, the total effect index was introduced, as defined in Equation (15). The total effect index takes into account the total contribution of the output variation due to the factor X_i, which includes the first-order effect as well as all higher-order interactions.

$$S_{T_i} = 1 - S_{\sim i} \tag{15}$$

Where $S_{\sim i}$ is the sum of all $S_{i_1\ldots i_s}$ that do not include the index i. A different formalism for it is shown in Equation (16) as in the work of Sudret (Bruno, 2007).

$$S_{T_i} = \sum_{I_i} \frac{V_{i_1\ldots i_s}}{V(Y)} \qquad I_i = \{\{i_1, \ldots, i_s\} \supset \{i\}\} \tag{16}$$

In order to be consistent with the first order mathematical definition, the total order index can be defined in Equation (17).

$$S_{T_i} = \frac{\mathbf{E}_{\mathbf{X}_{\sim i}}(\mathbf{V}_{X_i}([Y|X_{\sim i}])}{V(Y)} = 1 - \frac{\mathbf{V}_{\mathbf{X}_{\sim i}}(\mathbf{E}_{X_i}([Y|X_{\sim i}])}{V(Y)} \tag{17}$$

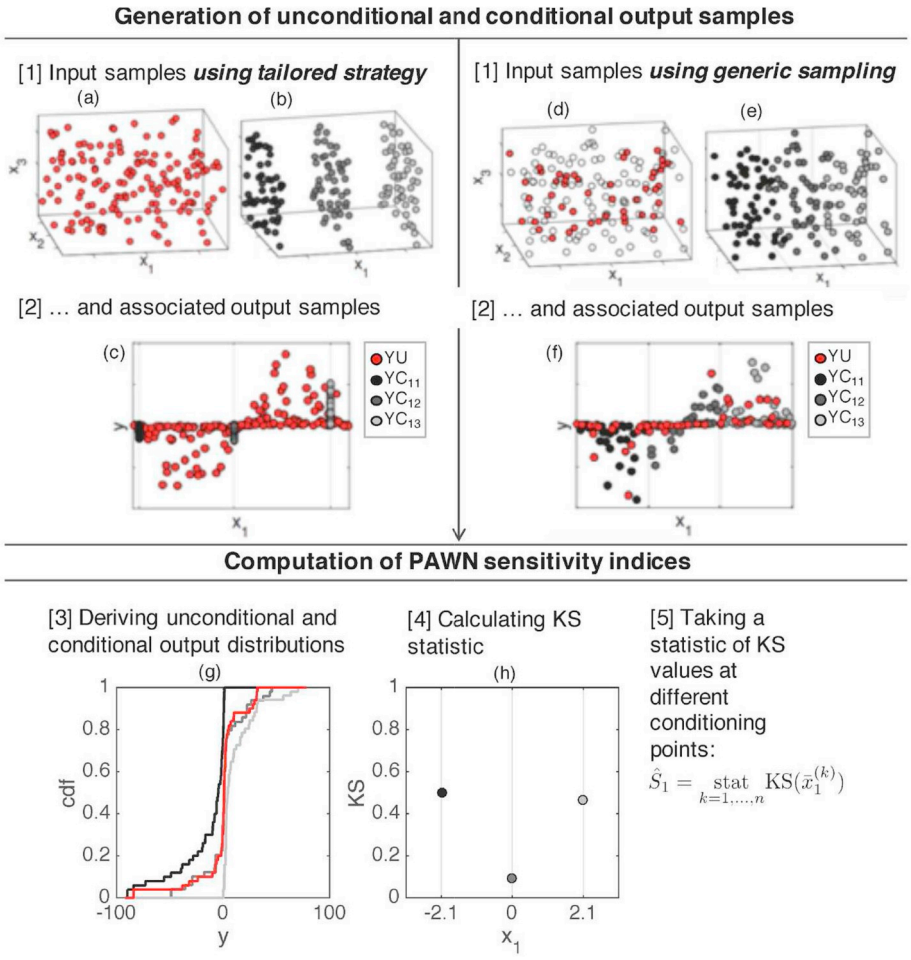

Fig. 1. Comparison between the tailored and generic approach for the distribution-based method.

Table 2
Analytical variance for Ishigami-Homma test function.

X_i	ST[%]
1	55.76
2	44.24
3	24.37

As described in (Saltelliet al., 2010), a way to visualise the total order index is to consider $\mathbf{V}_{\mathbf{X}_{\sim i}}(\mathbf{E}_{X_i}([Y|X_{\sim i}])$ as the first effect order of the $X_{\sim i}$. If we were to subtract this value from $V(Y)$, this would mean that the remaining variance should be the contribution of all terms in the decomposition that include X_i.

A summary of the different statistical measures and its interpretations is given in Table 1. It is important to notice that the Law of Total Variance can be applied for 1&4 as well as 2&3.

2.4. Latest results on the Sobol method

Since Sobol first published his work, many different estimators have appeared in the literature attempting to increase the efficiency of the method in computing the sensitivity indices. The latest estimators and designs are found in (Saltelliet al., 2010) (Campolongo et al., 2011): the radial sampling versus the winding stairs. These show that a radial design outperforms winding stairs. Therefore, this paper also adopts the same principle as a comparator.

Given two independent sampling matrices **A** and **B**, a_{ji} and b_{ji} are the generic elements of the matrices, where j is a dummy variables that varies from one to the number of simulations (N) and i is a second dummy variable that varies between one and the number of input variables (k). The generic elements of the matrix are obtained using Sobol's quasi-random numbers, or the so-called shifted LP_t sequences. The use of these low discrepancy series speeds up the performance of conventional Monte Carlo sampling. There are open-source libraries that generate this sequences based on (M SobolYu and V Leviatan, 1992). We can now define $\mathbf{A}_{\mathbf{B}}^{(\mathbf{i})}$ as the matrix **A**, where the only difference is that column i belongs to **B**. By using the notation at matrix or component level, the total sensitivity indices S_{T_i} are estimated by Jansen (1999) and displayed in 18 and 19 respectively.

$$\mathbf{E}_{\mathbf{X}_{\sim i}}\left(\mathbf{V}_{X_i}([Y|X_{\sim i}]) = \frac{1}{2N}\sum_{j=1}^{N}\left[f(\mathbf{A})_j - f\left(\mathbf{A}_{\mathbf{B}}^{(\mathbf{i})}\right)_j\right]^2 \tag{18}$$

$$\mathbf{E}_{\mathbf{X}_{\sim i}}\left(\mathbf{V}_{X_i}([Y|X_{\sim i}]) = \frac{1}{2N}\sum_{j=1}^{N}\left[\left(a_1^{(j)}, a_2^{(j)}, \ldots, a_k^{(j)}\right) - y\left(a_1^{(j)}, a_2^{(j)}, \ldots, b_i^{(j)}, \ldots, a_k^{(j)}\right)\right]^2 \tag{19}$$

Further information and details on the implementation of Sobol can be found in (Saltelliet al., 2010) (Campolongo et al., 2011).

3. PAWN distribution-based method

3.1. Introduction

We now describe the PAWN distribution-based method. The un-

Table 3
Parameters and analytical variance for K, B, G_4^* and G_{10}^* test functions.

X_i	K	B		ST[%]	G_4^*	α	ST[%]	G_{10}^*	α	ST[%]
	ST[%]	$\overline{X_i}$	σ_{X_i}		a			a		
1	75.00	0	0.5	0.39	100	1	0	100	1	0
2	25.00	0	0.5	0.62	0	4	67.44	0	4	75.49
3	8.33	0	1	1.55	100	1	0	100	1	0
4	2.78	0	1	1.55	100	1	0	100	1	0
5	0.93	0	2	12.41	100	1	0	100	1	0
6	0.31	0	2	22.34	100	1	0	100	1	0
7	0.10	0	1	3.49	1	0.5	3.19	1	0.4	2.56
8	0.03	0	0.5	1.40	0	3	59.28	10	3	1.24
9	0.01	0	1.5	20.25	100	1	0	0	0.8	23.30
10	0	0	2	36.00	100	1	0	0	0.7	20.00
11	0	1	2	0.31	0	2	46.83	9	2	0.94
12	0	2	2	0.31	100	1	0	0	1.3	37.68
13	0	2	1	0.31	100	1	0	100	1	0
14	0	2	1	0.31	100	1	0	100	1	0
15	0	3	1	1.24	1	0.5	3.19	4	0.3	0.26
16	0	3	3	11.17	100	1	0	100	1	0
17	0	1.5	3	2.79	100	1	0	100	1	0
18	0	3	3	0.70	0	1.5	37.94	7	1.5	1.03
19	0	2	5	17.46	100	1	0	100	1	0
20	0	2	5	31.03	1	0.5	3.19	2	0.6	2.11

Table 4
Analytical variance for highly-skewed test function.

X_i	ST[%]
1	54.50
2	54.60

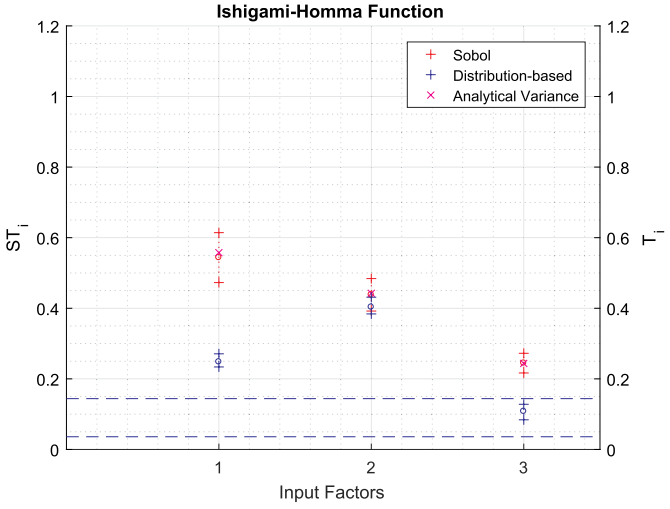

Fig. 2. Benchmarking the distribution-based with $N = 5000n = 20$ and $k = 3$ against VBSA with $N = 1250$ samples. Both result into 5000 model evaluations.

conditional cumulative distribution function (UCDF) of the output y is represented by $F_y(y)$, whereas the conditional cumulative distribution function (CCDF) of the output when x_i has been fixed is represented by $F_{y|x_i}(y)$. The logic behind this GSA technique consists of assessing the distance between $F_y(y)$ and $F_{y|x_i}(y)$; this distance accounts for the variability of the output that has been reduced due to fixing variable x_i, providing an importance measure of x_i on the output.

Let us imagine that $F_y(y)$ and $F_{y|x_i}(y)$ are almost the same, i.e., that the distance between these two statistics is close to zero. This would mean that the amount of output variability reduction because of fixing the value x_i is negligible, which in turns implies that this parameter has almost no contribution to the output and could well be screened out. Conversely, if the distance of the two CDFs is large, this would mean that almost all the variability of the output can be explained by this parameter. The distance between the UCDF and the CCDF is measured through the Kolmogorov-Smirnov (KS) statistic. Formula 20 defines the KS statistic for a given x_i value.

$$KS(x_i) = \left| F_y(y) - F_{y|x_i}(y) \right| \tag{20}$$

It is important to bear in mind that the KS distance depends on the value upon which it has been conditioned. If we were to use the KS statistic as it is defined in Equation (20), this would mean that the model would be conditional on an assumed value, which is not desirable. The metric could give different results based on the conditioning value. As a way to uncondition the previous definition or remove the dependency of x_i, a statistic for the KS (for instance, the median) is used.

$$T_i = stat_{x_i} |KS(x_i)| \tag{21}$$

This index T_i, shown in Equation (21), has several characteristics: It is global, so the input variations take place in the entire feasible space; it is quantitative, model independent, unconditional, easy to interpret and implement, stable and moment independent. The last property is the main difference between the distribution-based and the variance-based techniques. Considering the fact that the analytical computation of the index T_i is impossible in most cases, the following numerical techniques attempt to estimate it.

$$\widehat{KS(x_i)} = \left| \widehat{F_y(y)} - \widehat{F_{y|x_i}(y)} \right| \tag{22}$$

Equation (22), describes the formulation, where $\widehat{F_y(y)}$ and $\widehat{F_{y|x_i}(y)}$ are the empirical UCDF and CCDF approximated by a finite number of samples. Whereas the UCDF is approximated using N_u output evaluations by sampling the entire output feasibility space, the CCDF is approximated using N_c output evaluations by sampling all but x_i inputs. Consequently, the conditional KS can be transformed to an unconditional KS by means of a statistic, as displayed in Equation (23). However, it is important to notice that the choice of conditioning points will have an effect on the result. Both T_i and S_{Ti} metrics range from 0 to 1.

$$\widehat{T}_i = stat_{x_i = x_i^{(1)}, \ldots, x_i^{(n)}} |\widehat{KS(x_i)}| \tag{23}$$

The implementation of PAWN has been made available in (Pianosi et al., 2015). This version of PAWN is now considered as the tailored sampling approach method and futher information can be found in

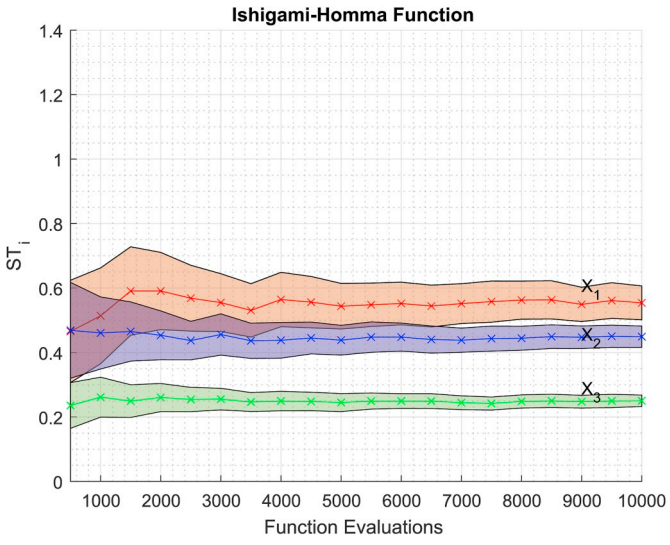

(a)

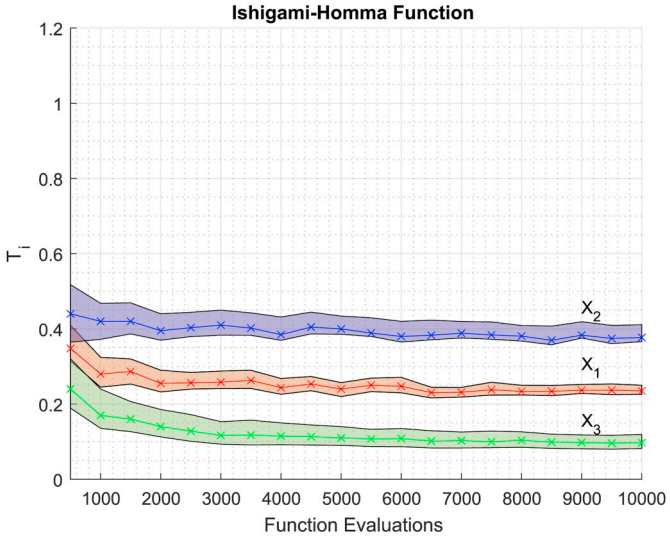

(b)

Fig. 3. Covergence analysis for Ishigami-Homma function. Comparison of distribution-based T_i and Sobol S_i indices for input factors X_1, X_2 and X_3.(a): VBSA (b): distribution-based.

(Pianosi and Wagener, 2015; Pianosiet al., 2016). More recently in 2018, as mentioned in the introduction, a new implementation of PAWN, called the distribution-based method, addressed the limitations of the old version; this can found in (Pianosi and Wagener, 2018). The distribution-based method splits the range of variation of each input factor x_i into n equally spaced intervals I_k and define the conditional samples YC_{ik} accordingly. The unconditional sample YU can coincide with the entire sample Y or with a subsample of it. This is represented in Equation (24).

$$\widehat{S}_i = stat_{k=1,\ldots,n} KS(I_k) \; where \; KS(I_k) = \left| \widehat{F_y(y)} - F_{y|x_i}\widehat{(y)} \in I_k \right| \tag{24}$$

The main difference between the old and new version of PAWN is shown in Fig. 1, sourced from (Pianosi and Wagener, 2018). "Example of using a tailored sampling strategy (left) and generic sampling (right) to approximate the PAWN index of input x1 in a case of M = 3 input factors. Left (tailored): (a) Input samples used to derive the unconditional output sample YU. These are generated by randomly sampling the entire space of input variability. (b) Input samples used to derive three conditional samples YC11, YC12 and YC13. These are generated by fixing x1 at selected conditioning values (for the sake of clarity, only n = 3 conditioning values are shown here). (c) Scatter plot of the unconditional (red) and conditional (grey) output samples YU, YC11, YC12 and YC13 against x1. Right (generic): similar to the left hand side but this time the input samples in (d) and (e) are the same. A random subset (highlighted in red) is used to derive YU, and the three subsets obtained by splitting the variability range of x1 into 3 intervals (grey) are used to derive YC11, YC12 and YC13. After sampling, the approximation of the PAWN sensitivity index follows the same steps: (g) unconditional output distribution (red) and the three conditional distributions (grey) when x1 is fixed to a given value (interval). (h) KS statistic (maximum absolute difference) between the unconditional distribution and each of the three conditional ones, plotted against the conditioning value (centre of the interval)".

4. Test functions

A set of well-studied test functions is investigated to benchmark the distribution-based against the reference Variance-based sensitivity analysis (VBSA). The following functions are briefly described below for the sake of completeness.

Function 1: The Ishigami function is one of the most common benchmark test functions because it exhibits strong non-linearity and non-monotonicity (Ishigami and Homma, 1990), as displayed in Equation (25). It has already been used as a benchmark by the distribution-based method in (Pianosi and Wagener, 2018). Parameters $a = 7$ and $b = 0.1$ are assumed and $X_i \sim U(-\pi,\pi)$; its analytical variance is displayed in Table 2.

$$Y = sin(X_1) + asin^2(X_2) + bX_3^4 sin(X_1) \tag{25}$$

Function 2: The K function was introduced by Bratley et al. (Paul, 1992) and used for GSA in (Saltelliet al., 2010). The K function is displayed in Equation (26).

$$K = \sum_{i=1}^{k} (-1)^i \prod_{j=1}^{i} X_j \tag{26}$$

X_i is uniformly distributed in the interval [0,1]. In this test function there are few dominant variables: X_1 and X_2 account for most of the uncertainty band. Moreover, the degree of interaction increases with higher index variables due to the construction of the function. The analytical variance is displayed in Table 3.

Function 3: The non-additive B function was proposed by Saltelli et al. in (Saltelliet al., 2008) and displayed in Equation (27).

$$B = \sum_{i=1}^{m} X_i \cdot X_{m+i} \tag{27}$$

Where $m = k/2$ (k being even), $X_i \sim N(\overline{X_i}, \sigma_{X_i}), i = 1, 2, \ldots, k$ and $N(\overline{X_i}, \sigma_{X_i})$ concerns the mean and standard deviation of a normal distribution. The choice of the different normal distribution parameters condition the number of important factors. Contrary to the G^* and K functions, non-relevant parameters have a non-nihil effect. The same parameters as (Campolongo et al., 2011) for the B function are kept and shown in Table 3.

Function 4 & 5: The G* function is a modified version of the G-Sobol function and it was introduced in (Saltelliet al., 2010). This function is shown in Equations (28) and (29).

$$G^*(X_1, \ldots, X_k; a_1, \ldots, a_k, \delta_1, \ldots, \delta_k, \alpha_1, \ldots, \alpha_k) = \prod_{i=1}^{k} g_i^* \tag{28}$$

where g_i^* is defined as:

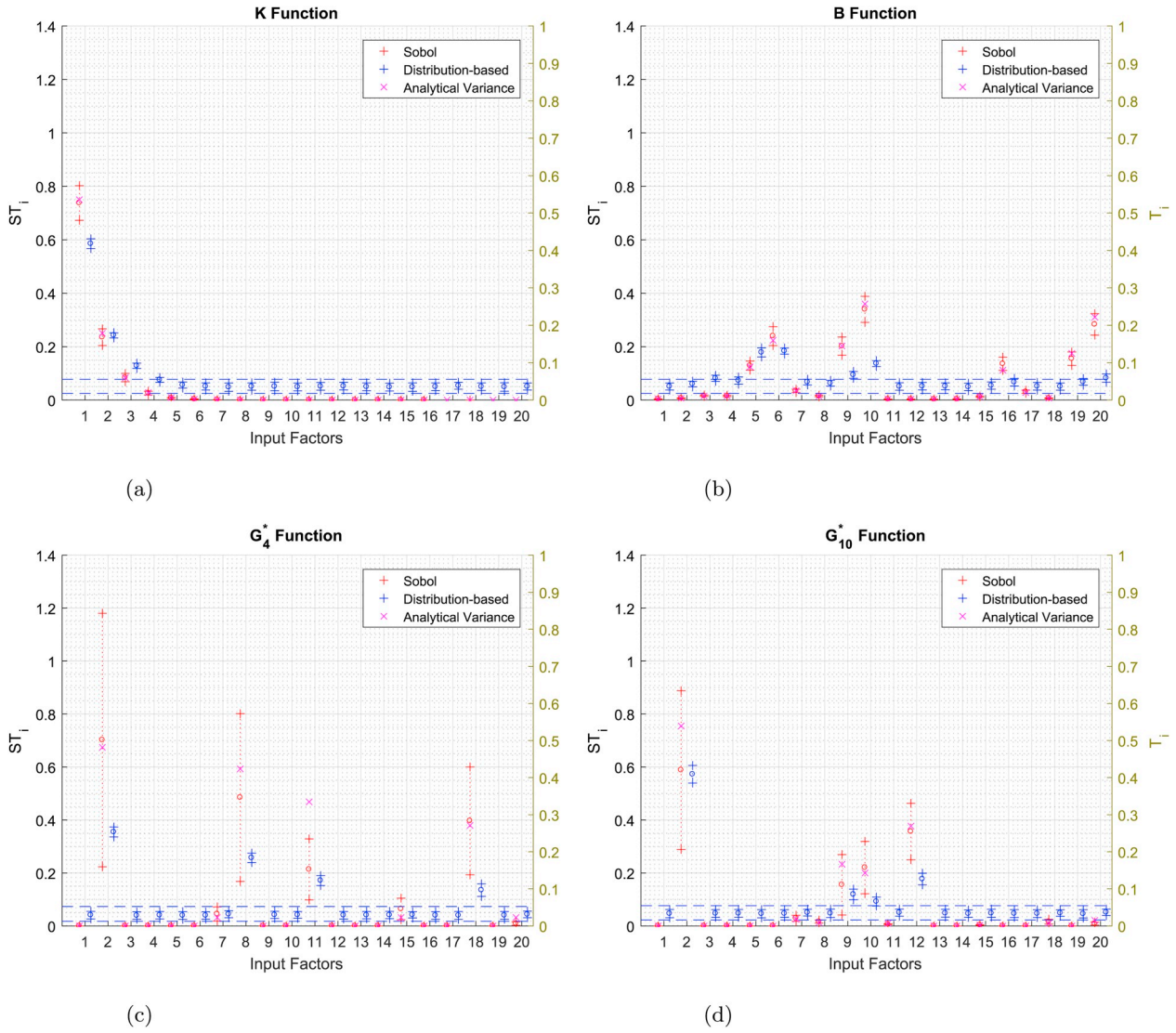

Fig. 4. Benchmarking the distribution-based with $N = 25200$ and $k = 20$ against VBSA with $N = 1200$ samples. Both result into 25200 model evaluations. (a): K Function (b): B Function (c): G_4^* Function (d): G_{10}^* Function.

$$g_i^* = \frac{(1+\alpha_i)\cdot|2(X_i+\delta_i - I[X_i+\delta_i]-1|^{\alpha_i}+a_i}{1+a_i} \tag{29}$$

Where X_i are the input factors, uniformly distributed between $[0,1]$, $a_i > 0$ are the traditional G functional parameters, $\delta_i \in [0,1]$ and $\alpha_i > 0$ are the shift and curvature parameters, respectively. $\delta_i s$ are randomly chosen since the uncertainties propagate independently of them. The mathematical meaning of $I[X_i + \delta_i]$ refers to the integer part of $X_i + \delta_i$. It is also worth adding that the relative importance of the factors directly depends on the choice of the parameters. For this reason, two functions are considered for benchmarking purposes with 4 and 10 important factors: 4 (G_4^*) and 10 (G_{10}^*), whose parameters and analytical variance are displayed in Table 3.

Function 6: A highly-skewed test function defined in Equation (30) was proposed in (Liu et al., 2006).

$$y = \frac{x_1}{x_2} \tag{30}$$

Where $x_1 \sim \chi^2(d_1)$ and $x_2 \sim \chi^2(d_2)$ follow Chi-square distributions with d_1 equal to 10 and d_2 13.978. The quotient of two Chi-square distributions is F-distributed. Hence analytical values are shown in Table 4 and its formulation is presented in the Appendix for the sake of completeness. If d_1 was 10 and d_2 14, the ST would be 54.5454% for both inputs. However, it has been purposely chosen to set d_2 smaller than 14 so that the theoretical variance of input factor 2 is greater than input factor 1.

5. Results and discussion

5.1. Ishigami-Homma function

In order to allow for a fair comparison between the VBSA and the PAWN distribution-based, the same number of model evaluations is considered. The benchmark is carried out by taking the distribution-based with $N = 5000$ and $n = 20$ against the VBSA with $N = 1250$ samples. Both result into approximately 5000 model evaluations. Results are displayed in Fig. 2. Total sensitivity indices ST_i (small circles in red) are estimated via Monte Carlo method (by means of the Sobol low-discrepancy sequence) for input factors X_i $i = 1, \ldots, 3$. 95% confidence intervals (vertical dashed lines in red) are estimated by bootstrapping 1000 replicas. Analytical variances (crosses in magenta) are given for all input factors. Total Kolmogorov Smirnov (KS) statistics T_i (small circles in blue) are estimated via random Monte Carlo sampling. 95% confidence intervals (vertical dashed lines in blue) are estimated by

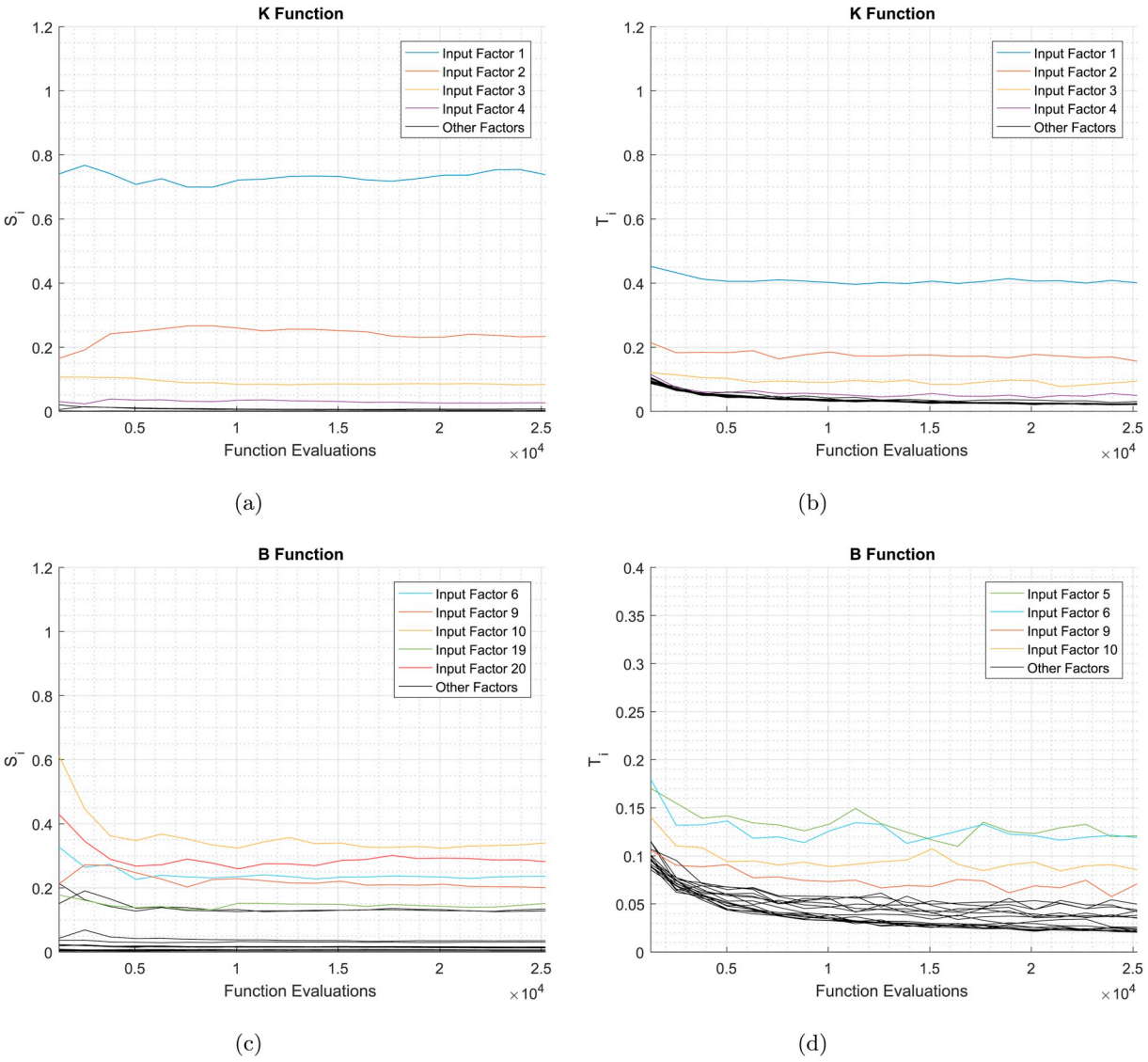

Fig. 5. Covergence analysis for K Function (a,b) and B Function (c,d). Comparison of distribution-based T_i and Sobol S_i indices.(a,c): VBSA (b,d): distribution-based.

bootstrapping 1000 replicas. The level of noise for the distribution-based method (horizontal dashed lines in blue) is calculated by the introduction of a dummy variable. This level of noise is bootstrapped 1000 times and results into the upper and lower horizontal dashed lines in blue. This means that, if the T_i was comprised between the upper and lower bound, we wouldn't be able to say if this is due to the importance of the input or the level of noise of the method.

Fig. 2 also shows that the analytical variance is inside the confidence level for the variance-based method. If we were to rank the importance of the inputs based on the two measures, we would obtain different results - the distribution-based method captures the non-linearity of the second input factor X_2 and places more weight on its uncertainty than the variance-based method. Also, the distribution-based method is not able to capture the importance of X_2 as it falls below the upper level of noise. A convergence analysis in VBSA is conducted by increasing the sample size from 125 to 2500 by steps of 125. In addition to this, 95% confidence intervals are estimated by bootstrapping 1000 replicas in each case. This is shown in Fig. 3(a). The same process is repeated for the distribution-based. Whereas the left axis is used for Sobol with ST_i, the right one is used for distribution-based with T_i. The number of conditioning points has been kept to 20, whereas N is increased from 500 to 10000 by steps of 500, as shown in Fig. 3(b). As expected, when we increase the number of samples, the range of the confidence intervals is reduced. ST_i and T_i remain stable for the Ishigami-Homma function across the different simulations.

5.2. *K, B G_4^* and G_{10}^* function*

The same number of model evaluations is considered for the following 4 functions in order to allow for a fair comparison between the VBSA and the distribution-based. The benchmark is carried out by taking the distribution-based with $N = 25200$ and $n = 20$ against VBSA with $N = 1200$ samples. Both result into approximately 25200 model evaluations. Results are displayed in Fig. 4. Total sensitivity indices ST_i (small circles in red) are estimated via Monte Carlo(by means of the Sobol low-discrepancy sequence) for input factors X_i $i = 1, \ldots, 20$. 95% confidence intervals (vertical dashed lines in red) are estimated by bootstrapping 1000 replicas. Analytical variances (crosses in magenta) are given for all input factors. Total Kolmogorov Smirnov (KS) statistics T_i (small circles in blue) are estimated via random Monte Carlo sampling. 95% confidence intervals (vertical dashed lines in blue) are estimated by bootstrapping 1000 replicas. The level of noise for the distribution-based method (horizontal dashed lines) is calculated by the introduction of a dummy variable. This level of noise is bootstrapped

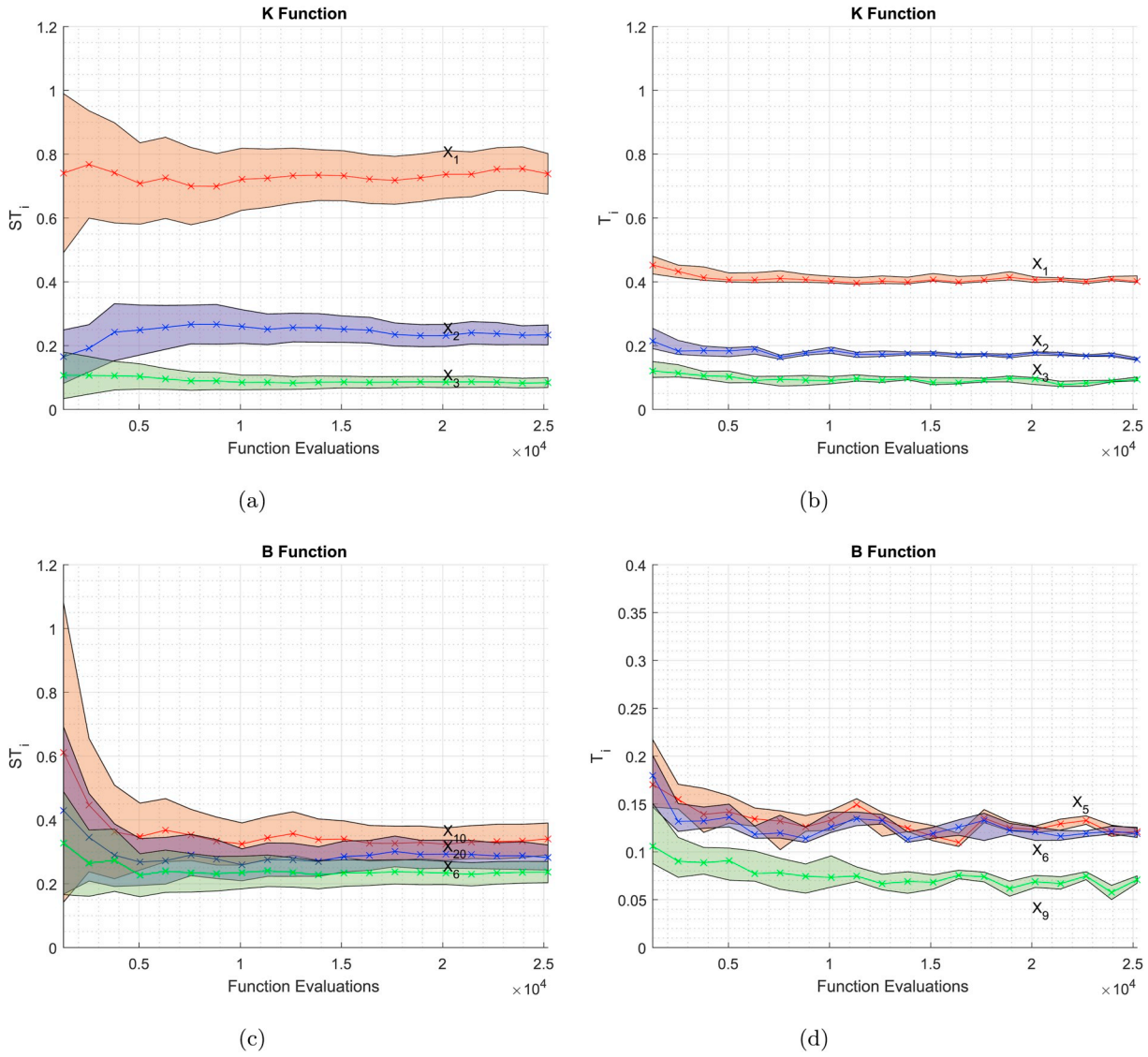

Fig. 6. Covergence analysis for K Function (a,b) and B Function (c,d) for its three main inputs. Comparison of distribution-based T_i and Sobol S_i indices.(a,c): VBSA (b,d): distribution-based.

1000 times and results into the upper and lower horizontal dashed lines in blue, as previously done for the Ishigami - Homma test function.

As far as the K function is concerned, only the first 9 inputs contribute to the variance of the output, which is reflected in Table 2. Input X_1 has a greater contribution than X_2 and X_2 has a greater contribution than X_3, and so on and so forth. However, when the distribution-based method is used, only $X_{1,2,3}$ can be considered within the validity of the method. The level of noise of the method doesn't allow us to say, for example, that input X_4 has a greater contribution than input X_{15}. Consequently, the method fails to rank inputs that have different order of magnitude in the contribution of the response. When applied to the B function, the distribution-based method allows to identify $X_{5,6,9,10}$ but fails to rank three of the most relevant contributors to the variance: $X_{16,19,20}$. As for the G_4^* function, the distribution-based method allows to identify $X_{2,8,11,18}$ but it does not capture the small contributions represented by $X_{7,15,20}$. Finally as far as the G_{10}^* function is concerned, the distribution-based method allows to identify $X_{2,9,10,12}$ but it doesn't capture the small contributions represented by $X_{7,8,11,15,18,20}$.

Fig. 4 also shows that the analytical variance is inside the confidence level in VBSA for all but one input factor - X_{11} from the B function. It has been checked that increasing the number of model evaluations leads to the analytical variance falling inside the confidence level for all input factors. A convergence analysis in VBSA is conducted by increasing the sample size from 60 to 1200 by steps of 60, leading to a total of 25200 model evaluations in the last case. Confidence intervals are estimated by bootstrapping 1000 replicas in each case. Whereas Fig. 5 doesn't display the confidence interval for a better interpretation, Fig. 6 does display it for its main three inputs resulting. The same process is repeated for the distribution-based. The number of conditioning points has been kept to 20, whereas N is increased from 1260 to 25200 by steps of 1260, as shown in Fig. 5(b,d). ST_i remain stable for both the K and B Function across the different simulations. T_i is also stable and changes only occur in X_5 and X_6 for the B function, as they have similar KS values. This is basically due to the fact that the 20 conditioning points (n) play a role in exploring the search space. These conditioning points are evenly spaced within the domain, but change from simulation to simulation. Finally, it is also worth noticing that in Fig. 6(d) the main input factors from Sobol cannot be recognised in function B once the confidence levels are plotted.

5.3. *Highly skewed function*

The empirical PDF of the highly-skewed function (Equation (30)) is

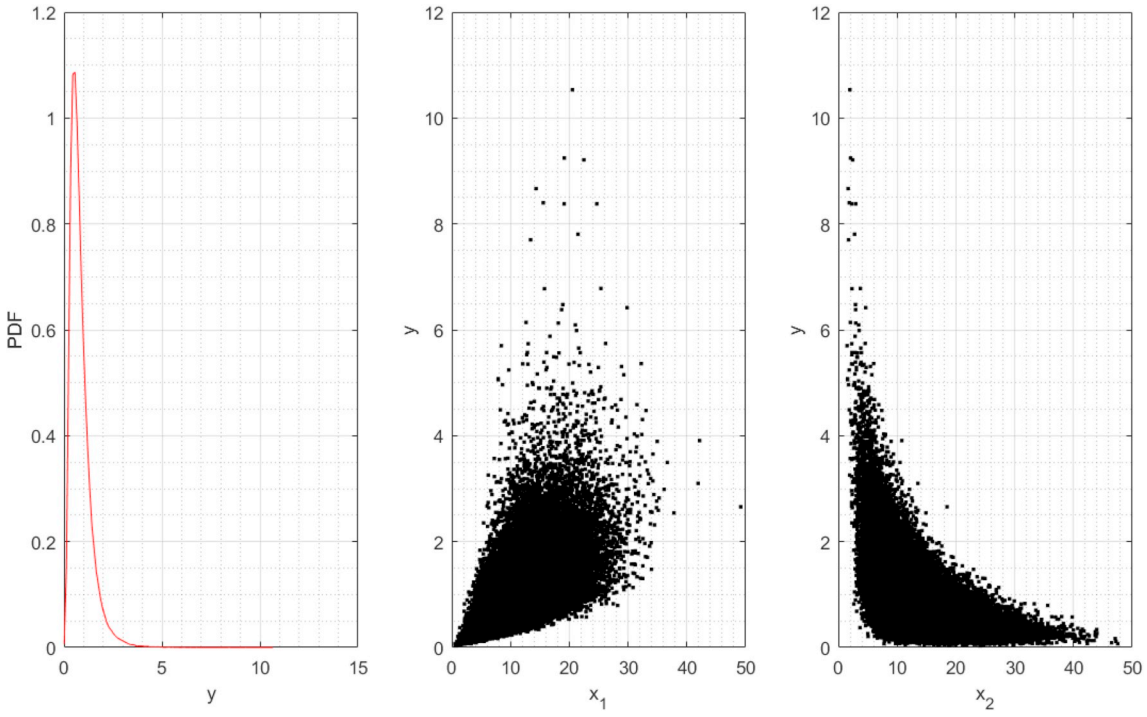

Fig. 7. Empirical PDF of Function 6 and associated scatter plots with 100000 samples.

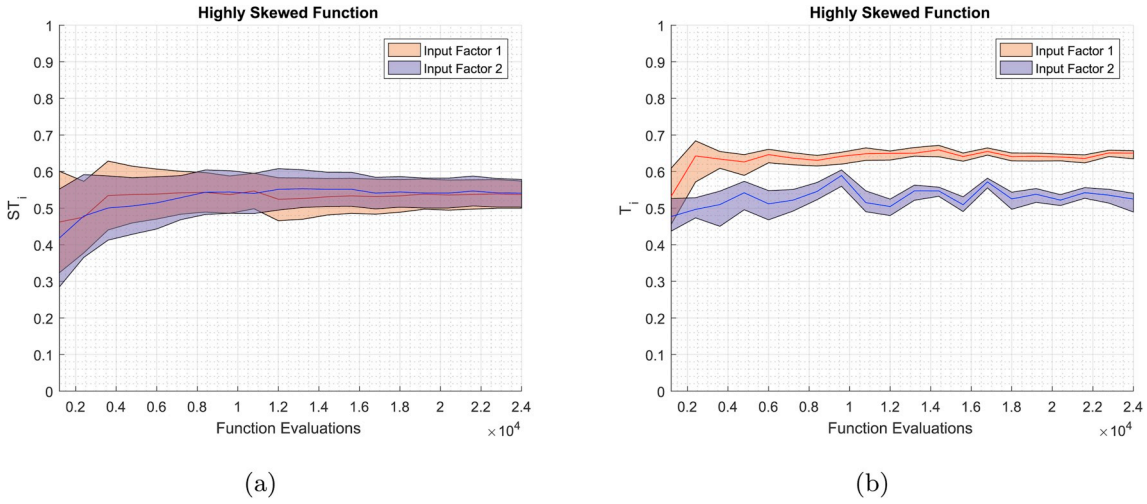

Fig. 8. Covergence analysis of PAWN T_i and Sobol S_i indices for a highly-skewed function. (a): VBSA (b): distribution-based.

displayed on the left hand side of Fig. 7, together with the associated scatter plots which confirm the importance of X_1 over X_2, as studied in (Liu et al., 2006).

Fig. 8 shows a convergence analysis for the same highly-skewed function using the VBSA and the distribution-based. 95% confidence intervals are represented with coloured patch. It is seen that whereas the Sobol method shows that X_1 and X_2 input factors are equally important, the distribution-based generally recognises the input factor importance X_1 over X_2, as it is shown in (Pianosi and Wagener, 2015). A convergence analysis in VBSA is conducted by increasing the sample size from 400 to 8000 by steps of 400, leading to a total of 24000 model evaluations in the last case. Distribution-based convergence analysis is carried out in a similar way with 10 conditioning points.

5.4. Discussion

From the results it is clear that the PAWN distribution-based method has an inherent high level of noise. A dummy variable X_d is considered to assess the level of noise for both methods. When assuming a dummy variable for the VBSA method, matrix A and A_B differ in column B. If column B contains a dummy variable, then, when evaluating the response of the model y_A, this will be equal to y_{A_B}, resulting in a nil contribution to the variance, as shown in Equation (31). Therefore there is no inherent level of noise associated with the variance-based method.

$$\mathbf{E}_{\mathbf{X}_{\sim i}}\left(\mathbf{V}_{X_i}([Y|X_{\sim i}]) = \frac{1}{2N}\sum_{j=1}^{N}\left[y\left(a_1^{(j)}, a_2^{(j)}, \ldots, a_k^{(j)}\right) - y\left(a_1^{(j)}, a_2^{(j)}, \ldots, b_i^{(j)}, \ldots, a_k^{(j)}\right)\right]^2 \tag{31}$$

On the other hand, the distribution-based's difference between the

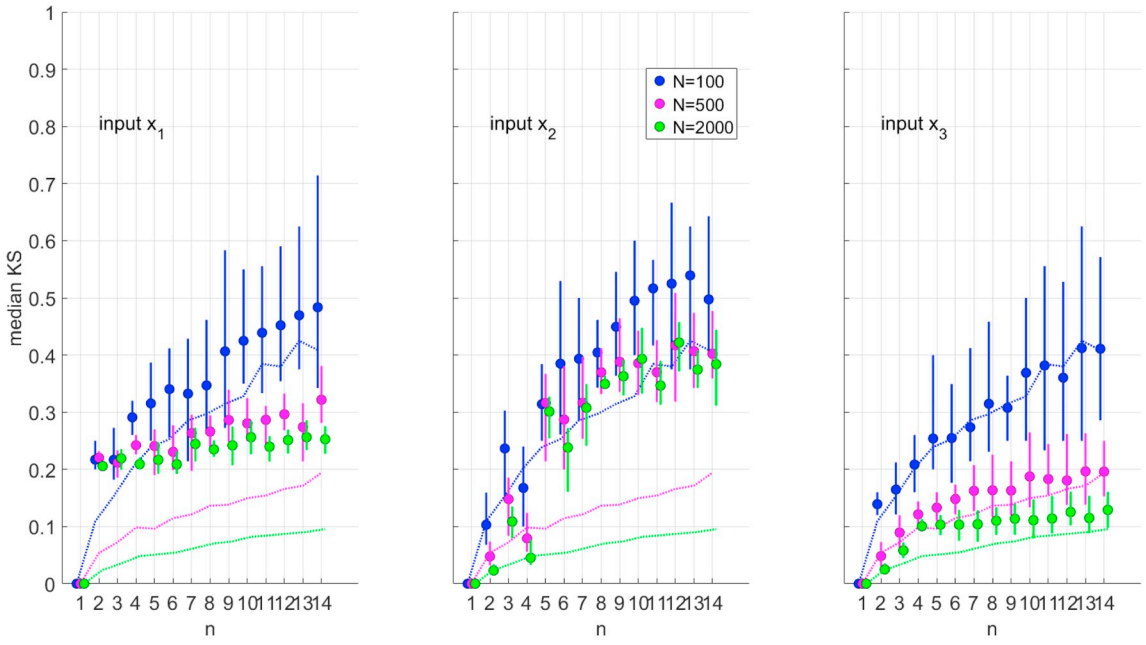

Fig. 9. Level of noise as a function of conditioning points and number of samples.

UCDF and CCDF provides a metric as to how important an input is. Even if the two CDFs were the same - under the assumption of a dummy variable - the fact that the variable must be conditioned results into a level of noise. However, since we expect the input samples to be uniformly spread in the given dataset we may also expect the size of the conditional sample to be approximately equal to N/n. This means that the user is able to increase the resolution of the conditional sample at the expense of a higher computational cost by controlling both N and n. This rationale is tested on the Ishigami-Homma function. The level of noise is measured by the mean of the KS statistic, which is in turn based on the maximum distance of several conditioning points; this is displayed in Equation (32).

$$\widehat{T_{dummy}} = mean_{1,2,\ldots,n} max\left|\widehat{F_y(y)} - \widehat{F_{y|x_i}(y)}\right| \tag{32}$$

Fig. 9 shows the distribution-based indices for the three input factors of the Ishigami-Homma function. Each subplot report results for one input factor. Indices are approximated using an increasing sample size N and increasing number of conditioning intervals n. For each combination of (N,n), bootstrapping is used to estimate the 95% confidence interval (vertical line) and mean value (circle) of each distribution-based index. Dashed lines show the KS of the dummy parameter at each combination of (N,n). The number of conditioning points bears almost no effect as long as n is greater than 5; this figure has been reproduced from the work of (Pianosi and Wagener, 2018), changing the Ishigami-Homma parameters as defined in the test function.

Furthermore, the computational complexity of the VBSA and distribution-based methods is displayed in Equations (33) and (34), where N is the number of samples, n is the number of conditioning points for the distribution-based method and k is the number of model inputs.

$$F_{eval} = N^*(k+1) \tag{33}$$

$$F_{eval} = N \tag{34}$$

Given that the aim of the paper is to allow for a fair benchmark between the two methods, the total number of model evaluations has been kept the same in all the cases. One of the main advantages of the distribution-based method is that it does not require tailored evaluations of the model; in other words, given an input-output sample is possible to determine the T_i coefficients.

6. Conclusions

Global sensitivity analysis such as the variance-based and distribution-based methods are widely adopted by the research community in order to identify key input drivers. However, in order for the results to be reproducible all parameters used in either method need to be provided. In addition, bootstrapping should be used to assess the confidence intervals and, where the computational complexity of the problem allows for it, a convergence analysis should be conducted. Given a set of model evaluations, the distribution-based method can be applied at no extra cost, adding value to the global sensitivity analysis and complementing the variance-based method. This paper benchmarks establish a framework on how methods should be compared against each other. It also shows that while the distribution-based method can be used as a complementary approach to the variance-based, as it has the potential to characterise those probability functions that are highly-skewed or multi-modal, it fails to rank different inputs when these have different order of magnitude in their contribution of the response. This has been documented by using well-established test functions, whose analytical variances are known.

Future work

Future work will focus on adding the CDF-based measure following the ideas of Gamboa, Klein and Lagnoux (2018): “Sensitivity analysis based on Cramér–von Mises distance”, which augments the Sobol’ method with a CDF-based indicator (Gamboaet al., 2018). Gamboa et al. investigated in 2018 the generalisation of the so-called Sobol indices to higher moments, where its index appears to be more general than Sobol as it takes into consideration the whole distribution and not the second moment.

Acknowledgements

This article is based on work sponsored by EDF Energy R&D UK at the Industrial Doctoral Centre for Offshore Renewable Energy (IDCORE), a consortium of the University of Exeter, University of Edinburgh and University of Strathclyde. IDCORE is funded by both the Energy Technologies Institute and the Research Councils Energy Programme through grant number EP/J500847/1. Additional support came

from the UK Engineering and Physical Sciences Research Council through grant number EP/P001173/1 (CESI).

Appendix

Analytical variances for the Ishigami-Homma function can be found in (Jean-Marc Baudin and Matinez, 2013), whereas analytical variances for the K, B and G* functions are given in the work of (Saltelliet al., 2010). This appendix includes the analytical variances for the highly-skewed test function, where $x_1 \sim \chi^2(d_1)$ and $x_2 \sim \chi^2(d_2)$ follow chi-square distributions with d_1 and d_2 degrees of freedom.

$$y = \frac{x_1}{x_2}$$

Then, if we assume that U_1 is a chi-square distribution with d_1 degrees of freedom, U_2 is a chi-square distribution with d_2 degrees of freedom, and that U_1 and U_2 are independent. The distribution of

$$Y = \frac{U_1/d_1}{U_2/d_2}$$

is F-distributed with d_1 degrees of freedom in the numerator and d_2 degrees of freedom in the denominator. The total variance can be calculated as:

$$V(Y) = \frac{2d_2^2 \cdot (d_1 + d_2 - 2)}{d_1 \cdot (d_2 - 2)^2 (d_2 - 4)} \; if \; d_2 > 4$$

Using the independence property between U_1 and U_2, the moment generating function of the chi-square distribution as well as some of the properties of the gamma function below:

$$E\left[U_2^{-1}\right] = \frac{1}{d_2 - 2}$$

$$E\left[X^k\right] = 2^k \frac{\Gamma(n/2 + k)}{\Gamma(n/2)}$$

$$\Gamma(n) = (n-1)\Gamma(n-1)$$

Total sensitivity indices S_{Ti} can be calculated as the sum of first order indices S_i together with the interactions between the two variables:

$$S_{T1} = S_1 + S_{12} = \frac{d_2 - 4}{d_1 + d_2 - 2} + \frac{2}{d_1 + d_2 - 2} = \frac{d_2 - 2}{d_1 + d_2 - 2}$$

$$S_{T2} = S_2 + S_{12} = \frac{d_1}{d_1 + d_2 - 2} + \frac{2}{d_1 + d_2 - 2} = \frac{d_1 + 2}{d_1 + d_2 - 2}$$

References

Baucells, Manel, Borgonovo, Emanuele, 2013. Invariant probabilistic sensitivity analysis. In: Management Science, vol. 59, pp. 2536–2549.

Borgonovo, Emanuele, 2007. A new uncertainty importance measure. In: Reliability Engineering & System Safety, vol. 92, pp. 771–784. https://doi.org/10.1016/j.ress.2006.04.015.

Borgonovo, Emanuele, Castaings, William, Tarantola, Stefano, 2011. Moment independent importance measures: new results and analytical test cases. In: Risk Analysis. ISSN: 02724332, vol. 31, p. 404428. https://doi.org/10.1111/j.1539-6924.2010.01519.x, 3.

Bruno, Sudret, 2007. Uncertainty Propagation and Sensitivity Analysis in Mechanical Models Contributions to Structural and Stochastic Spectral Methods. PhD thesis. Universite BLAISE PASCAL - Clermont II, p. 252.

Cacuci, Dan G., 2003. Sensitivity & Uncertainty Analysis, Volume I: Theory. CHAPMAN & HALL/CRC A, ISBN 1584881151, p. 285. https://doi.org/10.1201/9780203911396.ch10.

Campolongo, Francesca, Saltelli, Andrea, Cariboni, Jessica, 2011. From screening to quantitative sensitivity analysis. A unified approach, 4. In: Computer Physics Communications. ISSN: 00104655, vol. 182, pp. 978–988. https://doi.org/10.1016/j.cpc.2010.12.039. URL, 10.1016/j.cpc.2010.12.039.

de Rocquigny, E., Devictor, N., Tarantola, S., 2008. Uncertainty in Industrial Practice: a Guide to Quantitative Uncertainty Management, ISBN 0470770740, p. 364. https://doi.org/10.1002/9780470770733.

Farkhondeh Khorashadi Zadesh, 2017. Comparison of variance-based and moment-independent global SA approached by the application of SWAT model. In: Environmental Modelling and Software, vol. 91, pp. 210–222.

Gamboa, Fabrice, et al., 2018. Sensitivity analysis based on Cramer von Mises distance e. In: SIAM/ASA Journal on Uncertainty Quantification, vol. 6, pp. 522–548.

Holl, Mario, et al., 2016. Sensitivity analysis of a techno-economic optimal wind-energy converter. In: International Conference on Next Generation Wind Energy (ICNGWE). I, pp. 1–24.

Homma, T., Saltelli, Andrea, 1996. Importance measures in global sensitivity analysis of nonlinear models. In: Reliability Engineering & System Safety. ISSN: 09518320, vol. 52, pp. 1–17. https://doi.org/10.1016/0951-8320(96)00002-6. URL. http://www.sciencedirect.com/science/article/pii/0951832096000026.

Ishigami, T., Homma, T., 1990. An Importance Quantification Technique in Uncertainty Analysis for Computer Models. Tech. Rep. Japan Atomic Energy Research Institute, pp. 398–403.

Jansen, Michiel J.W., 1999. Analysis of variance designs for model output, 1. In: Computer Physics Communications. ISSN: 00104655, vol. 117, pp. 35–43. https://doi.org/10.1016/S0010-4655(98)00154- 4.

Jean-Marc Baudin, Michael, Matinez, January. 2013. Introduction to sensitivity analysis with NISP. Tech. Rep. 73. http://forge.scilab.org/index.php/p/nisp/downloads/get/nisp{/_}introsensal{/_}-{/_}v0.4.pdf.

Liu, Huibin, Chen, Wei, Sudjianto, Agus, 2006. Relative entropy based method for probabilistic sensitivity analysis in engineering design, 2. In: Journal of Mechanical Design. ISSN: 10500472, vol. 128, p. 326. https://doi.org/10.1115/1.2159025. URL. http://mechanicaldesign.asmedigitalcollectionasme.org/article.aspx?articleid=1448867.

M Sobol, I., Yu, Turchaninov, V Leviatan, B., 1992. Quasi random sequence generator. In: Keldysh Institute of Applied Mathematics, Russian Accademy of Sciences, Moscow.

Paul, Bratley, 1992. Implementation and tests of low-discrepancy sequences. In: ACM Transactions on Modeling and Computer Simulation, vol. 2, pp. 195–213, 3.

Pianosi, Francesca, Wagener, Thorsten, 2015. A simple and efficient method for global sensitivity analysis based oncumulative distribution functions. In: Environmental Modelling and Software. ISSN: 13648152, vol. 67, pp. 1–11. https://doi.org/10.1016/j.envsoft.2015.01.004. URL, 10.1016/j.envsoft.2015.01.004.

Pianosi, Francesca, Wagener, Thorsten, 2018. Distribution-based sensitivity analysis from a generic input-output sample. August 2018. In: Environmental Modelling and Software. ISSN: 13648152, vol. 108, p. 197207. https://doi.org/10.1016/j.envsoft.2018.07.019. URL, 10.1016/j.envsoft.2018.07.019.

Pianosi, Francesca, Sarrazin, Fanny, Wagener, Thorsten, 2015. A matlab toolbox for global sensitivity analysis. In: Environmental Modelling and Software. ISSN: 13648152, vol. 70, pp. 80–85. https://doi.org/10.1016/j.envsoft.2015.04.009 arXiv: NIHMS150003. URL, 10.1016/j.envsoft.2015.04.009.

Pianosi, Francesca, et al., 2016. Sensitivity analysis of environmental models: a systematic review with practical workflow. In: Environmental Modelling and Software. ISSN: 13648152, vol. 79, pp. 214–232. https://doi.org/10.1016/j.

envsoft.2016.02.008 arXiv: j.envsoft.2016.02.008 [10.1016]. URL, 10.1016/j-envsoft.2016.02.008.

Plischke, Elmar, Borgonovo, Emanuele, Smith, Curtis L., 2013. Global sensitivity measures from given data, 3. In: European Journal of Operational Research. ISSN: 03772217, vol. 226, pp. 536–550. https://doi.org/10.1016/j.ejor.2012.11.047. URL, 10.1016/j-ejor.2012.11.047.

Saltelli, Andrea, et al., 2008. Global sensitivity analysis. The primer, pp. 237–275. https://doi.org/10.1002/9780470725184.

Saltelli, Andrea, et al., 2010. Variance based sensitivity analysis of model output. Design and estimator for the total sensitivity index, 2. In: Computer Physics Communications. ISSN: 00104655, vol. 181, p. 259270. https://doi.org/10.1016/j.cpc.2009.09.018. URL, 10.1016/j.cpc.2009.09.018.

Sobol, I.M., 1993. Sensitivity analysis for nonlinear mathematical models. In: Math. Model. Com- puter.Exp 1, vol. 4, pp. 407–414. https://doi.org/10.18287/0134-2452-2015-39-4-459461 arXiv: arXiv : 1305 . 4373v1. URL, 0234–0879. https://max2.ese.u-psud.fr/epc/conservation/M0DE/Sobol0riginalPaper.pdf{/%}0A. https://www.mathnet.ru/eng/mm2320.

Sobol, I.M., 2003. Theorems and examples on high dimensional model representation, 2. In: Reliability Engineering & System Safety. ISSN: 09518320, vol. 79, pp. 187–193. https://doi.org/10.1016/S0951-8320(02) 00229-6. URL. https://www.sciencedirect.com/science/article/pii/S0951832002002296.

How does risk aversion shape overplanting in the design of offshore wind farms?

IOP Conf. Series: Journal of Physics: Conf. Series **1356** (2019) 012026 doi:10.1088/1742-6596/1356/1/012026

How does risk aversion shape overplanting in the design of offshore wind farms?

Esteve Borràs Mora[1,2], James Spelling[2] and Adriaan H. van der Weijde[3]

[1] Industrial Doctoral Centre for Offshore Renewable Energy (IDCORE), The University of Edinburgh, Edinburgh, EH9 3JL, UK
[2] EDF Energy R&D UK Centre, Interchange, 81-85 Station Road, Croydon, CR0 2AJ, UK
[3] University of Edinburgh School of Engineering and the Alan Turing Institute, Faraday Building, The King's Buildings, Mayfield Road, Edinburgh, EH9 3DW, UK

E-mail: E.Borras-Mora@ed.ac.uk

Abstract. Offshore wind farms are subjected to a maximum export capacity set in their connection agreement with the Transmission System Operator (TSO). Generators can export up to their contracted maximum export capacity, with any additional generation curtailed by the TSO. However, given the fact that the majority of the time offshore wind farms are not generating at full power, overplanting wind farms by installing a higher wind farm capacity compared to the fixed electrical infrastructure can result in better overall economics despite power output being curtailed at generations' peaks. The objective of this paper is to provide a framework to assess overplanting in the design of offshore wind farms when the underlying variables, such as wind speed and availability rates among others, are uncertain. The paper integrates site characteristics, technology specificities and financing constraints grounded in the mathematical framework of uncertainty quantification at the heart of the decision-making process. Generally speaking, the role of determining the optimal amount of overplanting comes down to the risk appetite of the developer, which in this paper is represented by a linear combination of the risk aversion and risk neutrality setting. A case study for a commercial offshore wind farm shows a 2% optimal overplanting for a Monte Carlo simulation, whereas this is found at 4% for a double Monte Carlo loop simulation regardless of the risk appetite considered. Furthermore, overplanting the farm by any value from 2% to 8% gives a better result than with no overplanting for a risk neutral setting. This paper will be of interest to developers, policy-makers and regulatory bodies confronted with uncertainty in overplanting the design of offshore wind farms.

1. Introduction

The connection of offshore wind farms is subjected to a maximum export capacity (MEC) set in their connection agreement with the Transmission System Operator (TSO). Generators can export up to their contracted MEC, with any additional generation curtailed by the TSO. For this reason, it has been common practice to size the capacity of offshore wind farms to its MEC, even though the majority of the time they are not generating at full power. Little thought has been put into designing offshore wind farms which optimise its farm capacity in regard to the fixed electrical connection capacity. In this paper, overplanting is defined as the process of installing additional wind farm capacity compared to its MEC.

In 2008, while planning the UK Offshore Wind Round 3, it came to the attention of National Grid that installing a higher installed generating capacity than the connection capacity could result in better overall economics for the development of offshore wind farms despite power being constrained at generations peaks [1]. In that report, a high level study was undertaken in Appendix 1 where 12% overplanting was suggested as an optimal setup, which meant that 1200 MW of offshore wind should be built for 1000 MW of grid connection. The report also looked at the sensitivity of ratio of connection costs to installed wind turbine costs, average wind speed and wind turbine availability. The findings of the study showed that (i) as the cost ratio increases there's an asymptotic trend for the optimum size of the wind farm towards 111%, (ii) as the average wind speed increases there is little change in the optimum size, but if the mean wind speed is less than 9 m/s then the optimum size increases in order to maximise the utilisation of the available capacity and (iii) as the percentage of the wind turbine availability decreases, the installed capacity needs to increase to maximise the utilisation of the available capacity. Although this was a high level study and some of the assumptions are a bit conservative at the current state of the offshore wind sector, it opened up further points for analysis.

In 2011, The Irish Commission for Energy Regulation (CER) published a report where generators were allowed to overplant their onshore wind farm capacity up to 5%, value driven by wind farm cabling and transformer losses which would compensate for losses on the generator's side of the grid connection and would allow the developer to export up to its MEC at the connection point [2]. In 2014, CER decided to update the earlier decision in light of potential economic benefits by increasing overplanting to 20% [3].

In 2012, Forewind looked at overplanting by factoring a number of variables: different turbine types, export and inter-array cable losses, wake losses, grid connection downtime and the total cost for wind turbines, including construction, operation and maintenance [4]. In this study it was also shown that adding more wind turbines improves the economics of the project, however further conclusions could not be drawn given the dependence of many site and technology-specific variables. Similar studies have mentioned the economic benefits of overplanting [5].

A clear example of overplanting in the offshore wind industry is given in the Netherlands for the Wind Farm Zone Borssele. The wind farm is divided into 5 sites. Site I, II and IV can accommodate 350 MW plus 30 MW of overplanting, whereas Site III can accommodate 330 MW plus 30 MW of overplanting. This is around 9 % of overplanting for both cases. TenneT, the Dutch TSO, contemplated the option of dynamic loading of the export cables. Namely, in case that Site I, II and IV was producing at full power, which would see a load of 380 MW being transferred through one of the export cables, this electricity could be handled by the cable and sent to the grid [6]. However, the capacity in excess of 350 MW is not always guaranteed by TenneT, but it is subjected to some constraints linked to the final soil resistivity values, temperature of the cable, final design of the cable system and voltage level of the system.

More recently, some authors have attempted to model overplanting for onshore and offshore wind farms [7, 8]. However, the models utilised in assessing overplanting did not capture the complex relationships between offshore wind engineering variables and financing constraints. Whereas the work of McInerney et al [7] sought to emphasize the benefits of overplanting from the economical point of view, it didn't consider technical variables. Conversely, the work of Wolter et al [8] placed more weight on the technical variables but left aside important financing constraints. Nevertheless, there is enough evidence to suggest that overplanting can lead to further cost reductions in the maturing offshore wind sector. However, a tailored techno-economic model that integrates site characteristics, technology specificities and financing constraints is

needed to demonstrate the benefits of overplanting. Furthermore, this techno-economic model should be grounded in the framework of uncertainty quantification, where its model inputs are represented by probability distribution functions.

The contribution of the current paper is to provide a framework to assess overplanting under uncertainty in the design of offshore wind farms; allowing developers and regulatory bodies to identify pareto-optimal trade-offs between cost and uncertainty when deploying additional turbines for a given electrical infrastructure. The rest of this paper is structured as follows: Section 2 describes the detailed modelling of overplanting and its main assumptions. Section 3 applies the modelling techniques to a case study. Finally, a brief discussion and conclusions are drawn in Section 4.

2. Methodology

The modelling approach to assess overplanting is based around the Offshore Wind Cost Analysis Tool (OWCAT) developed at the EDF Energy R&D UK Centre. Further information regarding its inputs, outputs and interplay between them can be found in Appendix A.

2.1. Factors Affecting Overplanting

Overplanting is mainly driven by the following factors:

- Ratio of wind turbine expenditure to electrical infrastructure: higher costs of installing an additional turbine for a given electrical infrastructure makes it more difficult for developers to consider this option.
- Wind speed distribution: it describes the variation of wind speeds for a given site. Sites with low mean wind speed mean that the share of time generating at its MEC is low and so is the amount of curtailment; this encourages developers to increase the installation of additional capacity. On the contrary, sites with high mean wind speed mean that the share of time generating at its MEC is high and so is the amount of curtailment; this doesn't favour the installation of additional capacity.
- Wind turbine availability: it is defined as the amount of time that the turbine is able to operate over a certain period of time divided by the total time in that period. Farms with high availability values mean that more turbines are operational at a given point in time and therefore it is expected a higher share of curtailment when overplanting. Likewise, low availabilities result in less amount of curtailment and favour overplanting.
- Inter-array cable availability: same rationale as wind turbine availability.
- Wake effect: they reduce the wind speed downstream a generating wind turbine. At high wind speeds the farm is able to produce at rated power. However, wake effects need to be taken into consideration for low wind speeds, which is the amount of generation that is not constrained.
- Electrical losses: they take place in transformers, collection wiring, substation and cables. Higher losses will encourage developers to overplant to be able to generate at MEC at the connection point.
- Degradation factor: wind turbine blades are subjected to environmental conditions that result in blade degradation over time, which directly reduces energy production and encourages overplanting.

2.2. Modelling of Overplanting

In order to determine the optimal size of an offshore wind farm relative to the electrical infrastructure it is important to capture the elements described in Section 2.1 within the modelling process. Two types of modelling are considered. Modelling Type 1 is based on constraining individual power curves as a function of the number of turbines and its MEC. As the number of additional turbines to the given MEC increases, the power that can be generated per turbine is reduced due to the electrical constraint of the connection capacity, as shown in Figure 1. In addition, wind turbine and inter-array cable availabilities are assumed to be fixed, following the work of National Grid [1]. Modelling Type 2 takes advantage of the stochastic capabilities of the cost modelling tool and propagates the uncertainties of the wind speed and availabilities to the power output via Monte Carlo simulation. Then, the resulting aggregated power transferred to the grid is obtained by constraining all those ocurrences that are higher than the MEC, as shown in Figure 2.

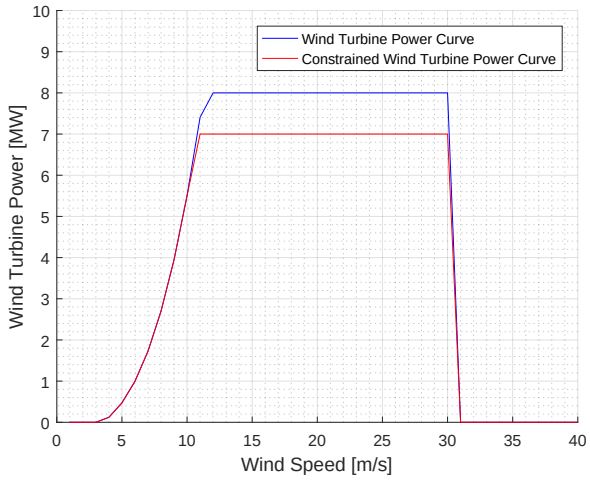

Figure 1. 8MW wind turbine constrained to 7MW due to overplanting in Modelling Type 1.

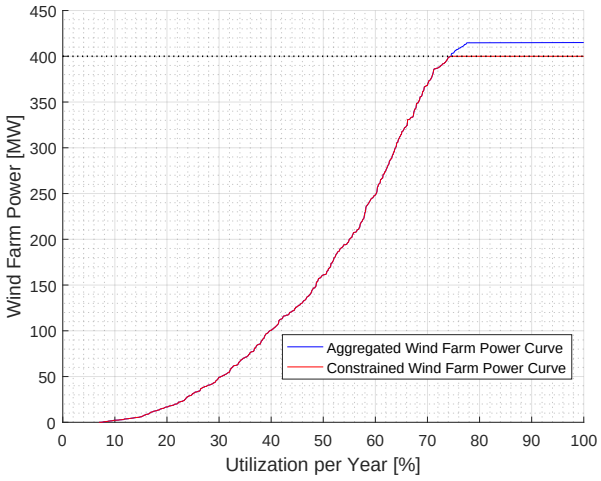

Figure 2. 52 8MW wind turbines constrained to a MEC of 400 MW in Modelling Type 2.

The philosophy of modelling the wake effects lies on decreasing the energy available in the wind so that the total losses are equal to the known wake effects calculated through standard commercial tools f_{wake}. Since it is assumed that each turbine produces the same energy over the lifetime of the farm, wake effects are obtained at wind farm level and not at individual turbines. The power output $P(v)$ produced by a single turbine is modelled by a theoretical power curve, which is a function of the rated power P_{rated}, cut-in speed v_{cut-in}, cut-off speed $v_{cut-off}$, Betz efficiency C_{eff}, the air density ρ_{air}, parameter $\alpha = 1$, wind speed v and the rotor diameter D, according to Equation 1.

The cut-in speed is defined as the speed at which the turbine begins to rotate, when applying sufficient torque on the rotor to generate power. At the other side of the curve, when the speed increases beyond a given threshold or cut-off speed, putting the integrity of the rotor at risk, the braking system is employed to bring the rotor to a standstill. Both situations result in a nil amount of power being produced. Otherwise, when the wind speed is found between the cut-in and cut-off speed, then the production is governed by Equation 1. It is worth noting that, whereas the Betz limit is a theoretical maximum of the wind energy that can be extracted, the Betz efficiency or C_{eff} has been considered as the efficiency of the wind turbine generator. From Equation 1 it is also possible to make a distinction between the energy available in the wind

and the energy produced by a wind turbine generator, which is a preliminary step to model the wake effects in the cost modelling tool. We've assumed a parameter $\alpha = 1$, the challenge is now to work out α so that the total losses are equal to the known wake effects calculated through standard commercial tools f_{wake}. In order to solve this problem and obtain alpha, an iterative method is conducted and displayed in the flowchart of Figure 3.

$$P(v) = min\left(P_{rated}, \alpha\frac{1}{2}\cdot C_{eff}\frac{16}{27}\cdot\pi\rho_{air}\frac{D^2}{2}(v^3 - v_{cut-in}^3)\right)\forall v \in (v_{cut-in}, v_{cut-off}) \quad (1)$$

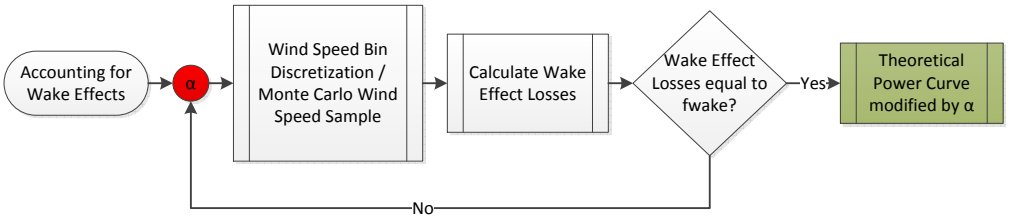

Figure 3. Wake Effects Flowchart

Figure 4 shows a wind speed distribution associated with a given site. Figure 5 displays the theoretical wind turbine power curve for different alpha coefficients. An alpha coefficient of 1 means that there are no wake effects, while decreasing values imply higher wake effects. Figure 6 shows the aggregated power curve distribution for a 400 MW farm and alpha coefficients. Figure 7 shows the losses incurred for each alpha parameter. Once alpha has been determined, it is fixed for the rest of the calculations.

On another note, availability is defined in this paper as the amount of time that a component is able to operate over a certain period, divided by the amount of the time in the period. Whereas a constant wind turbine availability rate is assumed for Modelling Type 1, its stochastic counterpart, Modelling Type 2, uses a binomial distribution to represent the number of wind turbines and inter-array cables available for energy production at a given point in time. Figure 8 displays the cumulative distribution functions of the number of wind turbines available for energy production for given wind turbine availability rates. It becomes apparent that higher availability rates lead to a higher share of time where the same number of wind turbines are available. Modelling Type 1 assumes the expected value of the number of wind turbines available for energy production. However, overplanting means that we need to be careful on how to determine the share of time the electrical connection is constrained.

Adding additional turbines to a fixed electrical infrastructure and assuming constant availability rates could lead to an overestimation of the annual energy production. Firstly, there are times where the power produced by the number of available wind turbines is higher than the MEC, resulting in some curtailment by the TSO. Secondly, there are also times where the power flowing through the connection point is less than the MEC, meaning that less wind turbines are available for production than its expected number. Figure 9 shows the difference between considering a fixed wind turbine and inter-array cable availability rates and modelling its stochastic counterparts; this is to say Modelling Type 1 is compared against Modelling Type 2. Even though it is possible for a developer to optimise an offshore wind farm so that its aggregated power curve matches the MEC at its expected value, the full information on the stochastic behaviour should also be considered. Modelling Type 1 leads to the aggregated power curve in blue, whereas the one in red represents Modelling Type 2. In order to avoid an overestimation of the energy production, Modelling Type 2 is considered for the rest of the paper despite requiring a higher computational cost.

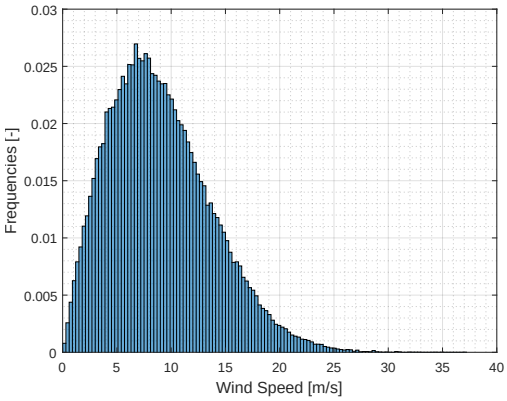

Figure 4. Wind speed represented by a Rayleigh distribution associated with a mean wind speed of 9 m/s.

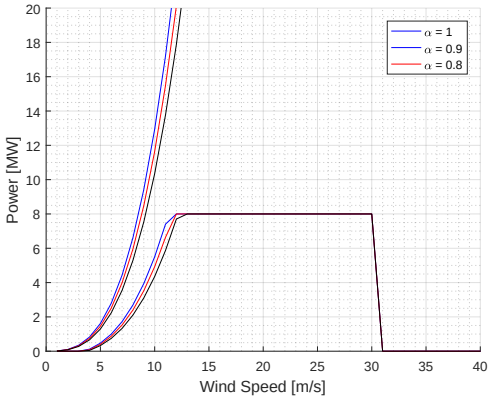

Figure 5. Theoretical wind turbine power curve for different alpha coefficients.

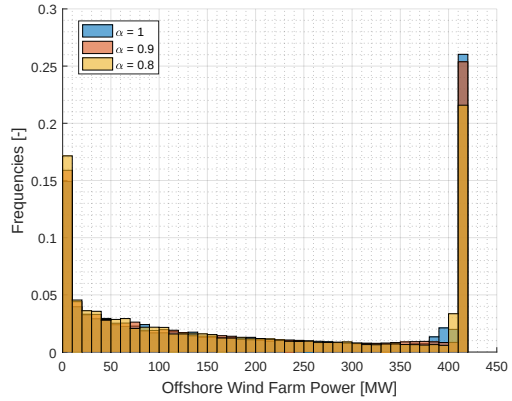

Figure 6. Wind power output distribution for different alpha coefficients.

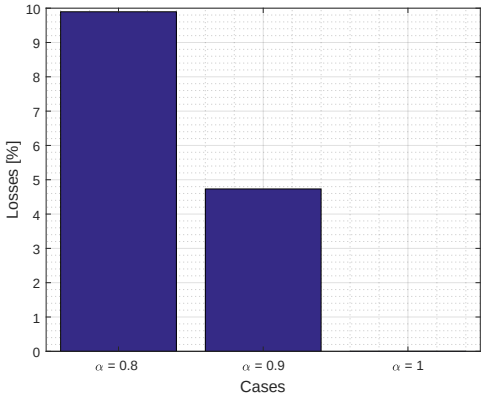

Figure 7. Incurred losses for different alpha coefficients.

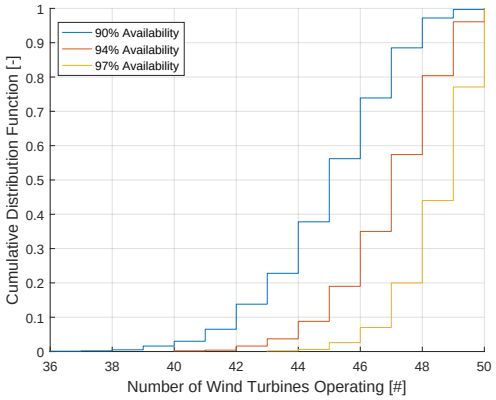

Figure 8. Binomial Cumulative Distribution Function of 50 WTG farm for given WTG availability rates.

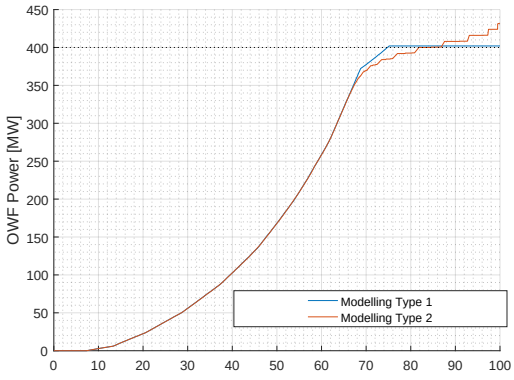

Figure 9. Modelling Type 1 against Modelling Type 2; limitations of considering fixed availability rates.

Electrical losses are modelled as a function of the power factor, which is the ratio between the real and reactive power, the cross section of the cables, the operating voltage and efficiencies of the system. The degradation factor is modelled by as a coefficient which decreases the energy production as the asset ages based on the work of Staffell [9].

2.3. Modelling Risk Aversion

Risk aversion is modelled by risk metrics originated in the financial mathematics literature such as the Value at Risk (VaR) and Conditional Value at Risk (CVar). The $\mathbf{VaR}_\alpha$ gives the probability α that a certain outcome is worse than a given threshold. Typically the probability α represents the confidence level and $\mathbf{VaR}_\alpha$ is regarded as the maximum value that will not be exceeded at this given confidence level. Building on $\mathbf{VaR}_\alpha$, $\mathbf{CVaR}_\alpha$ gives the expected outcome given that the value is worse than $\mathbf{VaR}_\alpha$. The concept was first introduced in Rockafellar [10] and further developed by him in [11]. The mathematical formulation for $\mathbf{VaR}_\alpha$ and $\mathbf{CVaR}_\alpha$ for continuous functions is given in Equation 2 and 3, respectively.

$$\mathbf{VaR}_\alpha(LCOE) = min\left(c : P(LCOE \leq c) \geq \alpha\right). \tag{2}$$

$$\mathbf{CVaR}_\alpha[LCOE] = \mathbf{E}[LCOE | LCOE \geq \mathbf{VaR}_\alpha(LCOE)] \tag{3}$$

Where LCOE is the Levelised Cost of Energy, $P(LCOE \leq c)$ is the probability of the LCOE being less or equal than c and $\mathbf{E}$ is the mathematical expectation operator. One of the main shortcomings of the $\mathbf{VaR}_\alpha$ is that it provides no information on the extent to which values might materialise beyond the threshold amount indicated by the $\mathbf{VaR}_\alpha$ itself, whereas $\mathbf{CVaR}_\alpha$ does. In addition, $\mathbf{CVaR}_\alpha$ has superior mathematical properties since this measure is coherent in the sense of Artzner [12]. For this reason, we've selected $\mathbf{CVaR}_\alpha$ as the preferred financial risk metric. In this approach risk aversion is modelled as a weighted average λ of the **Median** and $\mathbf{CVaR}_\alpha$ of the LCOE values. Parameter λ can be varied from 0 (in a risk neutrality setting) to 1 (extreme risk aversion), based on the work of Munoz [13] and displayed in Equation 4.

$$\boldsymbol{\rho}_\alpha[\lambda, LCOE] = \lambda \mathbf{CVaR}_\alpha[LCOE] + (1 - \lambda)\mathbf{Median}[LCOE] \tag{4}$$

3. Case Study and Results

The case study is based on a 400MW commercial offshore wind farm; its project specifications are shown in Table 1. It is assumed, for the sake of simplicity, that the export cable length, construction and operational port distances are equal to the distance from shore. The MEC is 400MW and offshore wind farm capacities are varied from 400MW to 456MW, or from 0% to 14% of overplanting. The estimated mean wind speed is represented by a normal distribution with mean (μ) and standard deviation (σ) as $\mathcal{N}(\mu, \sigma^2)$[1]. Likewise, availabilities are represented by uniform distributions with lower(a) and upper(b) bounds as $\mathcal{U}(a, b)$.

Table 1. Offshore wind farm project specifications.

Characteristic	Value	Uncertainty
Water Depth [m]	25	None
Distance from shore [km]	25	None
Mean Wind Speed @ 100m [m/s]	9	$\mathcal{N}(9, 0.1^2)$
Wind Turbine Availability [%]	95	$\mathcal{U}(90, 97)$
Inter-Array Cable Availability [%]	99	$\mathcal{U}(97, 99)$
Foundation Type [-]	Monopile	None
Electrical Infrastructure [-]	HVAC	None
Wind Turbine Type [-]	164-8 MW	None
Wake effect [%]	10	None
Degradation Factor [%]	0.05	None

[1] 0.1 m/s is a representative value combined from independent uncertainties, individually determined by normal distributions as seen in [14, 15, 16]. A different choice doesn't affect the optimal overplanting, as suggested by the sensitivity analysis on the mean wind speed

The reference case is calculated through a Monte Carlo simulation with input parameters from Table 1 (without uncertainties). Figure 10 shows the difference between the unconstrained and constrained yield as a function of overplanting; the amount of constraint is minimum up to 2% overplanting, where the two lines start to diverge. This point is also reflected in Figure 11, suggesting that additional energy produced by the over installation of turbines doesn't outweigh its wind turbine expenditure; a 2% overplanting is considered optimal for this farm.

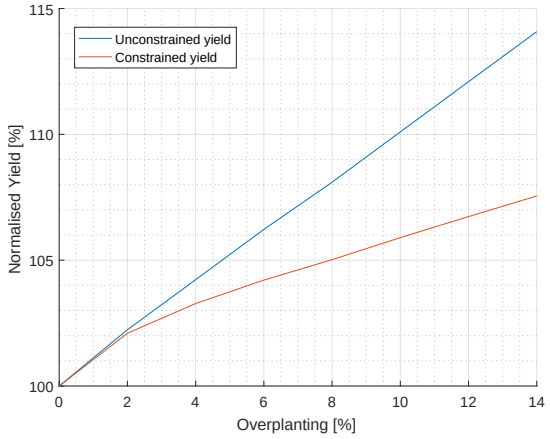

Figure 10. Unconstrained versus constrained normalised yield as a function of overplanting.

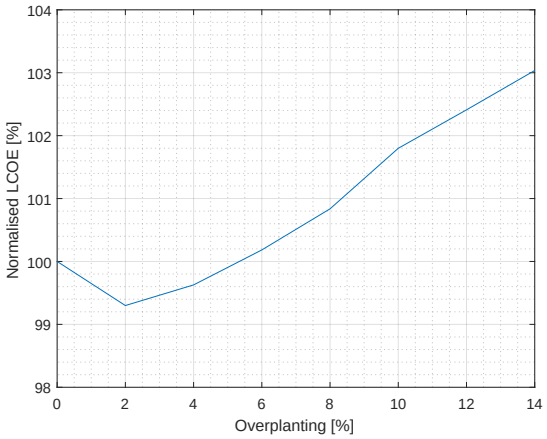

Figure 11. Reference case LCOE values as a function of overplanting.

A local sensitivity analysis on the wind speed, wake effects and wind turbine and inter-array cable availability has been conducted. Figure 12 shows the effects of an estimated mean wind speed of 8, 9 and 10 m/s, where the optimal amount of overplanting remains at 2%. Similar results are obtained by investigating the sensitivity of the wake effects and inter-array cable availability. However, as far as the wind turbine availability is concerned, this parameter is much more sensitive, resulting in an optimal overplanting of 6% when the availability is as low as 90%, as shown in Figure 13.

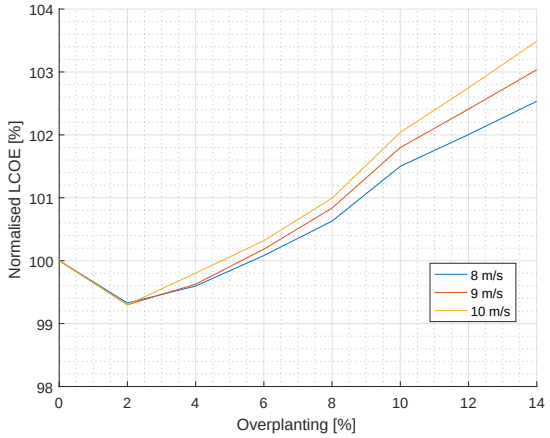

Figure 12. Local Sensitivity Analysis on mean wind speed.

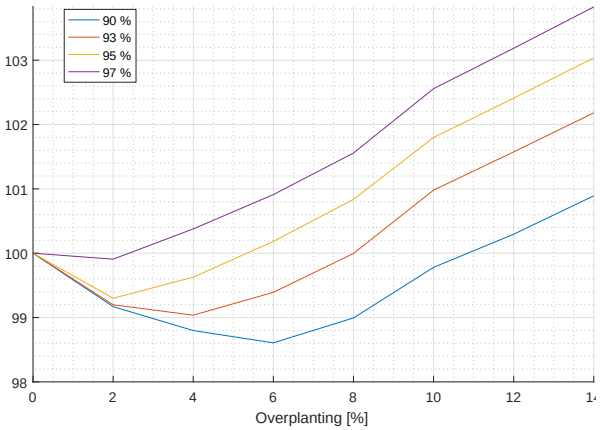

Figure 13. Local Sensitivity Analysis on wind turbine availability.

Figure 14 shows the yearly cumulative utilization rate of the connection capacity for an estimated mean wind speed of 9 and 10 m/s and varying wind farm capacities. Although higher wind speeds lead to hitting the MEC cap earlier, they also produce more power for a

given utilization rate. The area underneath the aggregated power curve represents the total energy produced and overplanting is concerned about maximising this area. Since a change in wind speed does not significantly change this area, it remains a second order parameter to overplanting. On the contrary, overplanting low wind turbine availabilities significantly changes this area, as reflected in Figure 13. Notice that the same sequence of random numbers within the inner Monte Carlo has been used to generate the wind speed distributions for the different capacities so as to avoid the introduction of additional noise - otherwise the aggregated power curves may overlap.

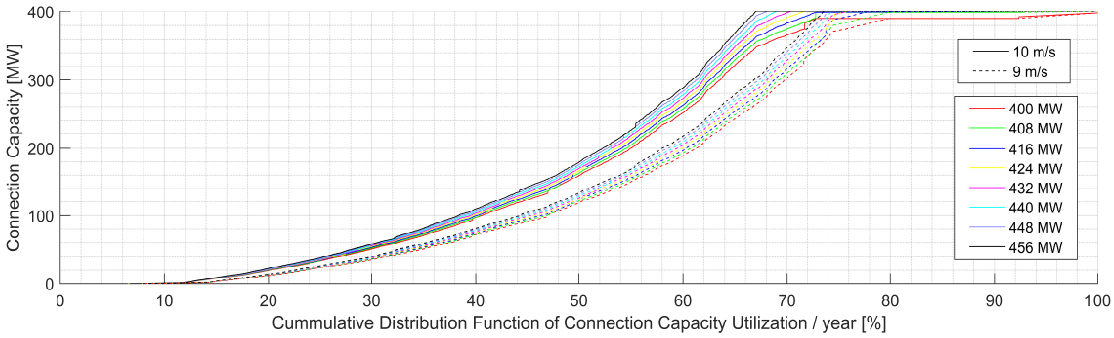

Figure 14. Utilization Rate Cummulative Distribution Function for 9 and 10 m/s wind speeds.

For a clearer interpretation of the findings we have conditioned the LCOE distribution given the base case wind speed. The kernel density function (KDF) for wind speeds equal or greater than 9 m/s is given in Figure 15, whereas for less than 9 m/s is shown in Figure 16. Both figures reflect that when overplanting with a small amount, there's a shift to the left in the KDF. However, for larger amounts of overplanting, the KDF is shifted to the right well beyond the reference case represented in blue.

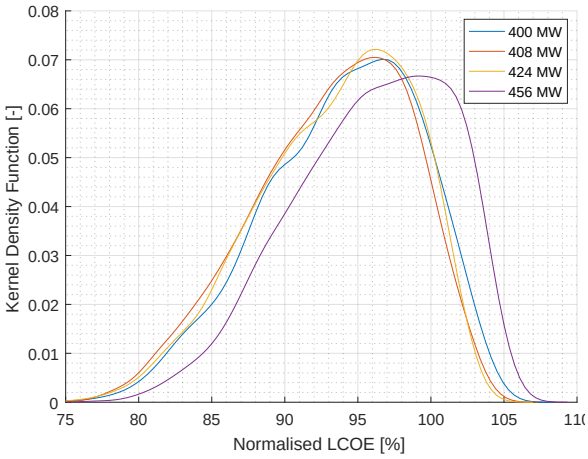

Figure 15. KDF sensitivity to overplanting for wind speeds equal or greater than 9 m/s.

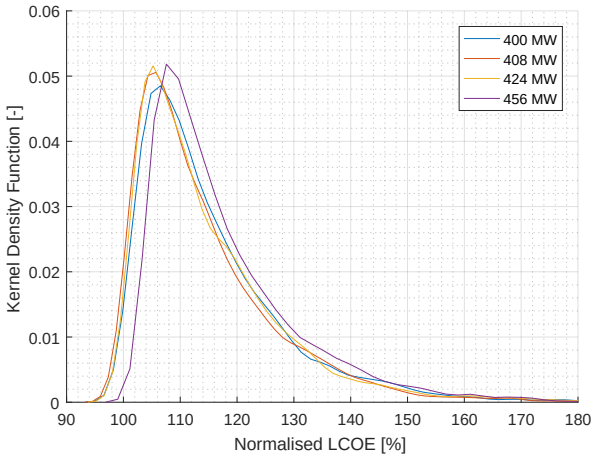

Figure 16. KDF sensitivity to overplanting for wind speeds less than 9 m/s.

The probability distribution function of the LCOE is obtained by 20,000 model evaluations of an outer Monte Carlo loop with parameters displayed in Table 1. It is worth bearing in mind that, for each model evaluation, an inner Monte Carlo simulation propagates the wind speed and availabilities with another 10,000 model evaluations within the Annual Energy Production module; this process is repeated for several degrees of overplanting. The risk metrics given by the expression $\lambda\mathbf{CVaR}_{\alpha=0.05}[LCOE] + (1-\lambda)\mathbf{Median}[LCOE]$ are normalised with respect to the values obtained when no overplanting is applied, as displayed in Figure 17. Overplanting the farm from 2% to 8% results in risk metrics (in a risk neutrality setting) that improve the economics of the farm. However, the optimal design is found at 4% of overplanting regardless of the risk appetite.

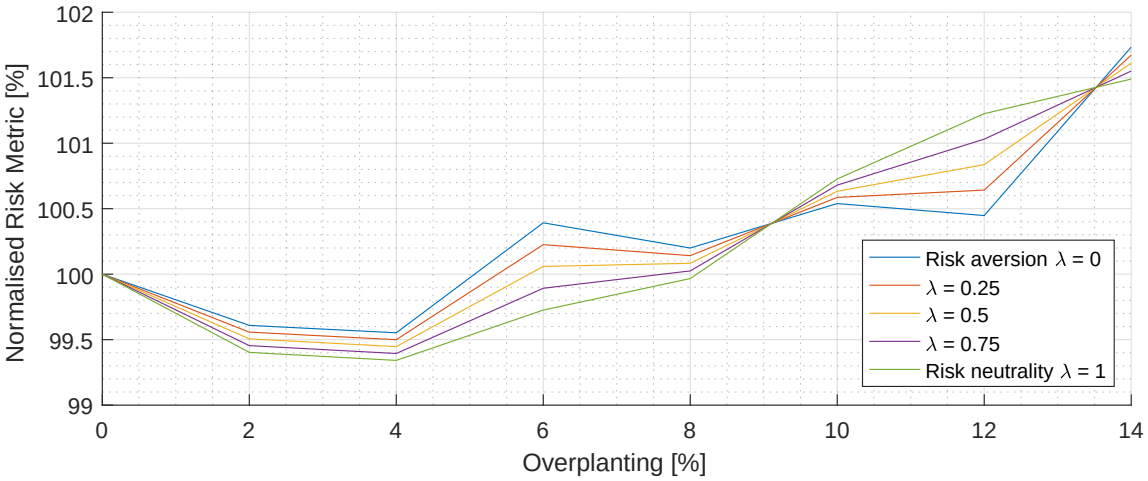

Figure 17. Risk aversion represented by $\boldsymbol{\rho}_{\alpha}[\lambda, overplanting]$.

4. Discussion and Conclusion

This paper has presented the development of a novel framework to assess overplanting in the design of offshore wind farms when the underlying variables, such as the wind speed and availability rates, among others, are uncertain. Two types of modelling have been compared, taking into consideration the estimated mean wind speed, wind speed distribution, availability rates, electrical losses, wake effects and a degradation factor. Although Modelling Type 1 is easier to implement than Modelling Type 2, it can lead to an overestimation of the annual energy production. Modelling Type 2 addresses this problem via an inner Monte Carlo simulation despite requiring higher computational costs by assessing the percentage of time the MEC is constrained, and it has therefore been the preferred method for this paper.

A local sensitivity analysis has revealed that the wind turbine availability is the most sensitive parameter to overplanting, whereas the estimated mean wind speed, wake effects and inter-array cable availability play a secondary role. As the wind turbine availability increases, overplanting becomes less valuable. This suggests that previous studies on overplanting, which were based on low wind turbine availabilities rates from UK Round 1 offshore wind farms (in the order of 90%) or on Modelling Type 1, need to be revisited. New studies on overplanting must consider current offshore wind turbine availability rates as well as Modelling Type 2 or a similar methodology whereby the effects of uncertainty are integrated in the decision-making process.

Without considering the uncertainties in the different parameters represented by the outer Monte Carlo loop, it appears that the optimal amount of overplanting is 2% for our reference offshore wind farm. Generally speaking, the role of determining the optimal setup comes down to the risk appetite of the developer, which in this case is represented by a linear combination of the risk aversion and risk neutrality setting, governed by the λ parameter. However, when conducting the double loop Monte Carlo simulation, the optimal setup is found at 4% regardless of the risk appetite considered. Furthermore, overplanting the farm by any value from 2% to 8% gives a better result than with no overplanting for a risk neutral setting, meaning that overplanting can be used as a hedging instrument.

Future work will take advantage of the framework developed in this paper to investigate several offshore wind farm configurations in terms of its suitability to overplanting. How is overplanting influenced by larger wind turbines and sites located further from shore? and how does risk aversion influence the investment decision for these new sites? we will investigate the ratio of wind turbine expenditure to electrical infrastructure. Also, the degradation factor has been taken into account after the constraint, but we would expect greater amounts of overplanting if this was taken before the constraint.

Acknowledgments
This article is based on work sponsored by EDF Energy R&D UK at the Industrial Doctoral Centre for Offshore Renewable Energy (IDCORE), a consortium of the University of Exeter, University of Edinburgh and University of Strathclyde. IDCORE is funded by both the Energy Technologies Institute and the Research Councils Energy Programme through grant number EP/J500847/1. Additional support came from the UK Engineering and Physical Sciences Research Council through grant number EP/P001173/1 (CESI).

Appendix A. Offshore Wind Cost Modelling Tool

The Offshore Wind Cost Analysis Tool (OWCAT) developed at the EDF Energy R&D UK Centre has been used in the past for comparative evaluation of multiple sites, detailed evaluation of specific project layouts and sensitivity studies on both design/technology choices and cost variations [17]. The tool has been validated against cost data from the Navitus Bay, Courseulles-sur-Mer and Neart na Gaoithe projects and shown to be accurate within ± 15% for these cases.

The cost modelling tool consists of four main modules: a wind farm design module, a cost calculation module, a financial module and an overarching stochastic module which allows inputs to be represented by probability distribution functions. The first stage of the module concerns the wind farm design. In order to evaluate the costs of the project, it is necessary to have information about the number and type of wind turbines, foundations, inter-array cabling and the export system. In other words, the wind farm itself must be modelled. Designing an offshore wind farm requires interaction between teams from different disciplines; for example, the wind turbine team will have to interact with the foundation team to make sure that the loads of the turbine are correctly passed onto the foundation, and the foundation team will need to make sure that the electrical connections are correctly secured within the foundation. As such, a cost model must capture the same interactions as the design process and cannot be a simple accumulation of models from separate disciplines.

The design outputs of the first module are fed as inputs into the second module, which calculates the costs of the different offshore wind farm components. The cost module can be divided into Development Expenditure (DEVEX), Capital Expenditure (CAPEX), Operational Expenditure (OPEX) and Decommissioning Expenditure (DECEX). DEVEX covers the costs of all the processes up to the financial close or placing firm orders to proceed with the construction. CAPEX calculates the supply and installation costs of the wind farm, including wind turbines, foundations, inter-array cables, offshore substations, export cables and onshore substations. Indirect costs such as Engineering, Procurement, and Construction Management (EPCM) costs and insurance are also included in the CAPEX breakdown. OPEX includes direct costs for the operation and maintenance of the wind farm, as well as transmission charges, insurance, taxes and royalties. DECEX accounts for the decommissioning of the wind turbines, foundations and offshore substations.

The cost outputs of the second module are passed into the third module, which is the financial model of the wind farm project. The financial model takes into consideration the different cash flows throughout the life of the wind farm, as well as the financing structure put in place to supply the initial capital investment. Based on the resulting free cash flows and financing costs, the LCOE can be determined, together with other financial performance indicators. The financial module allows for corporate and project financing modelling.

The OWCAT structure is shown in Figure A1. This information has been divided into:

- (i) Project Specifications
- (ii) Technical Specifications
- (iii) Economic and Financial Specifications
- (iv) Vessel Specifications
- (v) Structural Masses and Electrical Components Database

(i) refers to the project offshore wind farm characteristics such as the capacity of the farm, the wind speed at a given referenced height, the average water depth, the soil conditions, the distance from shore, the wind turbine model, foundation type and export system specifications among others. Since no two projects will have the same characteristics, project specifications attempt to model each particular site.(ii) addresses the details of the offshore wind technology, representing wind turbine, foundation, inter-array cable, export system and grid parameters. For example, as far as the wind turbine is concerned, parameters such as the wind turbine availability, the installation vessel associated with the wind turbine, the average loading, installation and commissioning times are accounted for. In addition, a decommissioning factor is used for all offshore wind farm components to account for a reduction in time from the installation phase.(iii) concerns the reference year for real prices, the risk-free rate and cost of debt, insurance and insurance premium tax rates, contingency requirements, corporation taxes, depreciation, seabed rent, exchange rates and inflation.(iv) involves the different vessel characteristics used in the installation and decommissioning of the offshore wind farms. As an example, heavy-lift jack-up vessel parameters comprise the day rate, vessel transit speed, vessel positioning time, vessel mobilisation time, operational weather window and carrying capacities in regard to different components.(v) consists of the data used to establish the foundation mass correlations, which are the basis for the CAPEX estimation in the foundation procurement. It also considers the correlations used to estimate the cost of different electrical components.

The final design contains not only the design of the offshore wind farm, where the foundations masses, inter-array and export system are sized, but also the procurement, vessel charter model and the Annual Energy Production (AEP) as displayed in Figure A1. Procurement stores all the information concerning wind turbines, foundations and the electrical system, in terms of the type, number of elements and size (also length if required), giving rise to a procurement catalogue which forms the basis for the cost module. The vessel charter model is based on the work of Kaiser [18], whereas the AEPs is built upon industry's best practices assuming respectively either a logarithmic- or power-law wind profile in conjunction with a Rayleigh or Weibull probability distribution to model the wind speed. Wake losses and electrical losses are also accounted for in the AEP submodule.

As far as the financial module is concerned, the calculation itself entails not only one but a twofold iterative process. The external loop consists of determining the value of λ that makes Equation A.1 equal to 0.

$$LCOE = \lambda | \sum_{t=1}^{n} \frac{FCF_t(t)}{(1+MARR)^t} = 0; \tag{A.1}$$

Where FCF are the free cash flows, $MARR$ is the desired Minimum Acceptable Rate of Return (MARR) and λ_0 is the intial guess obtained from a simplified financial model. The LCOE financial metric is calculated as the constant inflation-linked real electricity price required to meet the desired MARR. The internal loop is used in the project finance setting and concerns the debt sizing or sculpting, which determines the maximum amount of project finance debt that the offshore wind farm can sustain based on the bank's requirements. Project lenders usually specify the borrowing capacity on the basis of debt service ratio and convenants. As such, parameters such as the Debt Service Coverage Ratio (DSCR), the maximum leverage and the Cash Flow Available for Debt Service (CFADS) have been considered.

Lastly, the stochastic module (depicted in orange in Figure A1) allows the model to be embedded in the framework of uncertainty quantification.

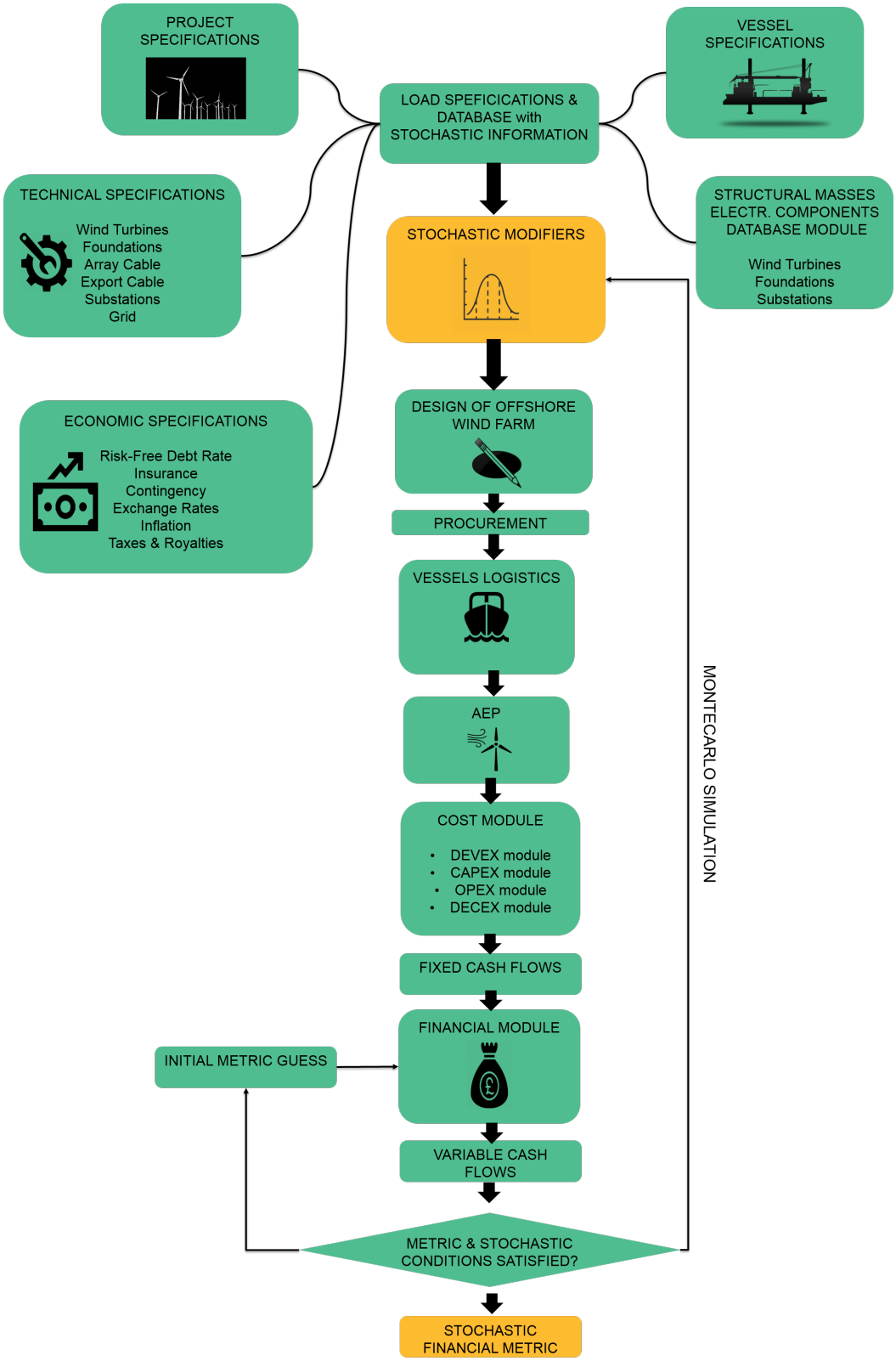

Figure A1. Stochastic OWCAT Structure

References

[1] 2008 Round 3 Offshore Wind Farm Connection Study Tech. rep.
[2] Brid ODonovan 2011 Connection Offer Policy & Process (COPP) Tech. rep. Commission for Energy Regulation
[3] Morris N 2014 Decision on Installed Capacity Cap Installed Capacity Cap Tech. rep. Commission for Energy Regulation
[4] Forewind 2014 Environmental Statement Chapter 6 Appendix B Offshore Project Boundary Selection Report Tech. Rep. March
[5] SMart Wind L 2015 **5** 19
[6] TenneT 2015 POSITION PAPER Overplanting Tech. rep. TenneT URL https://www.tennet.eu/fileadmin/user_upload/Our_Grid/Offshore_Netherlands/Consultatie_proces_net_op_zee/Technical_Topics/ 50_ONL_15-083-T11_Overplanting_PP_v2.pdf
[7] Mcinerney C and Bunn D W 2017 *Energy Economics* **61** 87–96 ISSN 0140-9883 URL http://dx.doi.org/10.1016/j.eneco.2016.10.022
[8] Wolter C, Jacobsen H K, Rogdakis G, Zeni L and Cutululis N 2016 *15th Wind Integration Workshop* **49** 0–4
[9] Staffell I and Green R 2014 *Renewable Energy* **66** 775–786 ISSN 0960-1481 URL http://dx.doi.org/10.1016/j.renene.2013.10.041
[10] Rockafellar R T and Uryasev S 2000 *The Journal of Risk* **2** 21–41 ISSN 14651211 (*Preprint* arXiv:1011.1669v3) URL http://www.risk.net/journal-of-risk/technical-paper/2161159/optimization-conditional-value-risk
[11] Rockafellar R T and Uryasev S 2002 *Journal of Banking & Finance* **26** 1443–1471
[12] Artzner P, Delbaen F, Eber J M and Heath D 1999 *Mathematical Finance* **9** 203–228 ISSN 09601627
[13] Munoz F D, Hendrik A, Weijde V D, Hobbs B F and Watson J p 2017 *Energy Economics* **64** 213–225 ISSN 0140-9883 URL http://dx.doi.org/10.1016/j.eneco.2017.03.025
[14] Jain P 2017 Wind Resource Assessment : A Key Step in Wind Projects Green Energy Financing Workshop Asia Clean Energy Forum
[15] Gribben B, Joyce M and Frazer-Nash Consultancy 2011 Uncertainty analysis to support asset procurement decisions in offshore wind Tech. rep.
[16] Zhang M H 2015 Wind Park Production Estimate *Wind Resource Assessment and Micro-sitting* chap 7, pp 143–167
[17] Borras Mora E 2017 Transition from Deterministic to Stochastic Cost Models for Offshore Wind Farms *Offshore Wind Energy Conference* June
[18] Kaiser M J and Snyder B F 2012 *Offshore wind energy cost modeling- Installation and decommissioning* ISBN 9781608052851 URL http://www.benthamdirect.org/pages/content.php?9781608052851

IAEE International Conference 2019 - Local Energy, Global Markets

Cost and Uncertainty in Overplanting the Design of Offshore Wind Farms

Esteve Borràs Mora[1,2*] , James Spelling[2], Adriaan H. van der Weijde[4], Marie Berthelot[2]

[1] Industrial Doctoral Centre for Offshore Renewable Energy (IDCORE), The University of Edinburgh, Edinburgh, EH9 3JL, UK
[2] EDF Energy R&D UK Centre, Interchange, 81-85 Station Road, Croydon, CR0 2AJ, UK
[3] School of Engineering, University of Edinburgh, and The Alan Turing Institute, London. Faraday Building, The King's Buildings, Mayfield Road, Edinburgh, EH9 3DW, UK

Abstract

To date the connection of offshore wind farms is subjected to a Maximum Export Capacity (MEC) set in their connection agreement with the Transmission System Operator (TSO). Generators can export up to their contracted MEC, with any additional generation curtailed by the TSO. However, the share of time an offshore wind farm is generating at its MEC tends to be low. Overplanting the offshore wind farm by installing a higher wind farm capacity compared to the fixed electrical infrastructure can result in better overall economics, but because wind speeds and wind farm component availabilities are uncertain, there are trade-offs between the probability of additional revenue produced by capturing more wind and higher capital costs of over-installation of turbines. Nevertheless, there is enough evidence to suggest that overplanting can lead to further cost reductions in the maturing offshore wind sector. The percentage of time an offshore wind farm operates at its MEC is an indication of the extent to which the asset can profit from higher transmission utilisation rates. This paper provides a framework to assess overplanting when developers, policy-makers or regulatory bodies are confronted with trade-offs between cost and uncertainty. The paper sheds light onto which sites and technology-specific factors make overplanting a viable option. Finally, the findings of the paper are exemplified by an industrial case study where several offshore wind farms configurations are analysed.

Keywords: Overplanting, offshore wind, decision-making under uncertainty, risk aversion

*Corresponding author.
Email: E.Borras-Mora@ed.ac.uk.
Tel: +44 (0)7470 023 829

1 Introduction

The connection of offshore wind farms is subjected to a maximum export capacity (MEC) set in their connection agreement with the Transmission System Operator (TSO). Generators can export up to their contracted MEC, with any additional generation curtailed by the TSO. For this reason, it has been common practice to size the capacity of offshore wind farms to its MEC, even though the majority of the time they are not generating at full power. Little thought has been put into designing offshore wind farms which optimise its farm capacity in regard to the fixed electrical connection capacity. In this paper, overplanting is defined as the process of installing additional wind farm capacity compared to its MEC.

In 2008, while planning the UK Offshore Wind Round 3, it came to the attention of National Grid that installing a higher installed generating capacity than the connection capacity could result in better overall economics for the development of offshore wind farms despite power being constrained at generations peaks [14]. In that report, a high level study was undertaken in Appendix 1 where 12% overplanting was suggested as an optimal setup, which meant that 1200 MW of offshore wind should be built for 1000 MW of grid connection. The report also looked at the sensitivity of ratio of connection costs to installed wind turbine costs, average wind speed and wind turbine availability. The findings of the study showed that (i) as the cost ratio increases there's an asymptotic trend for the optimum size of the wind farm towards 111%, (ii) as the average wind speed increases there is little change in the optimum size, but if the mean wind speed is less than 9 m/s then the optimum size increases in order to maximise the utilisation of the available capacity and (iii) as the percentage of the wind turbine availability decreases, the installed capacity needs to increase to maximise the utilisation of the available capacity. Although this was a high level study and some of the assumptions are a bit conservative at the current state of the offshore wind sector, it opened up further points for analysis.

In 2011, The Irish Commission for Energy Regulation (CER) published a report where generators were allowed to overplant their onshore wind farm capacity up to 5%, value driven by wind farm cabling and transformer losses which would compensate for losses on the generator's side of the grid connection and would allow the developer to export up to its MEC at the connection point [4]. In 2014, CER decided to update the earlier decision in light of potential economic benefits by increasing overplanting to 20% [9].

In 2012, Forewind looked at overplanting by factoring a number of variables: different turbine types, export and inter-array cable losses, wake losses, grid connection downtime and the total cost for wind turbines, including construction, operation and maintenance [5]. In this study it was also shown that adding more wind turbines improves the economics of the project, however further conclusions could not be drawn given the dependence of many site and technology-specific variables. Similar studies have mentioned the economic benefits of overplanting [15].

A clear example of overplanting in the offshore wind industry is given in the Netherlands for the Wind Farm Zone Borssele. The wind farm is divided into 5 sites. Site I, II and IV can accommodate 350 MW plus 30 MW of overplanting, whereas Site III can accommodate 330 MW plus 30 MW of overplanting. This is around 9 % of overplanting for both cases. TenneT, the Dutch TSO, contemplated the option of dynamic loading of the export cables. Namely, in case that Site I, II and IV was producing at full power, which would see a load of 380 MW being transferred through one of the export cables, this electricity could be handled by the cable and sent to the grid [16]. However, the capacity in excess of 350 MW is not always guaranteed by TenneT, but it is subjected to some constraints linked to the final soil resistivity values, temperature of the cable, final design of the cable system and voltage level of the system.

More recently, some authors have attempted to model overplanting for onshore and offshore wind farms [8, 17]. However, the models utilised in assessing overplanting did not capture the complex

relationships between offshore wind engineering variables and financing constraints. Whereas the work of McInerney et al [8] sought to emphasize the benefits of overplanting from the economical point of view, it didn't consider technical variables. Conversely, the work of Wolter et al [17] placed more weight on the technical variables but left aside important financing constraints. Nevertheless, there is enough evidence to suggest that overplanting can lead to further cost reductions in the maturing offshore wind sector. However, a tailored techno-economic model that integrates site characteristics, technology specificities and financing constraints is needed to demonstrate the benefits of overplanting. Furthermore, this techno-economic model should be grounded in the framework of uncertainty quantification, where its model inputs are represented by probability distribution functions.

The contribution of the current paper is to provide a framework to assess overplanting under uncertainty in the design of offshore wind farms; allowing developers and regulatory bodies to identify pareto-optimal trade-offs between cost and uncertainty when deploying additional turbines for a given electrical infrastructure. The rest of this paper is structured as follows: Section 2 explains the main factors driving overplanting. Section 3 describes the detailed modelling of overplanting and its main assumptions. Section 4 benchmarks the current model against previous studies on overplanting. Section 5 applies the modelling techniques to different wind farm configurations. Finally, conclusions are drawn in Section 6.

2 Factors Affecting Overplanting

Overplanting is mainly driven by the following factors:

- Ratio of wind turbine expenditure to electrical infrastructure: higher costs of installing an additional turbine for a given electrical infrastructure makes it more difficult for developers to consider this option.
- Wind speed distribution: it describes the variation of wind speeds for a given site. Sites with low mean wind speed mean that the share of time generating at its MEC is low and so is the amount of curtailment; this encourages developers to increase the installation of additional capacity. On the contrary, sites with high mean wind speed mean that the share of time generating at its MEC is high and so is the amount of curtailment; this doesn't favour the installation of additional capacity.
- Wind turbine and inter-array availability: it is defined as the amount of time that the turbine/cable is able to operate over a certain period of time divided by the total time in that period. Farms with high availability values mean that more turbines/cables are operational at a given point in time and therefore it is expected a higher share of curtailment when overplanting. Likewise, low availabilities result in less amount of curtailment and favour overplanting.
- Wake effect: they reduce the wind speed downstream a generating wind turbine. At high wind speeds the farm is able to produce at rated power. However, wake effects need to be taken into consideration for low wind speeds, which is the amount of generation that is not constrained.
- Electrical losses: they take place in transformers, collection wiring, substation and cables. Higher losses will encourage developers to overplant to be able to generate at MEC at the connection point.
- Degradation factor: wind turbine blades are subjected to environmental conditions that result in blade degradation over time, which directly reduces energy production and encourages overplanting.

3 Modelling

The modelling approach to assess overplanting is based around the Offshore Wind Cost Analysis Tool (OWCAT) developed at the EDF Energy R&D UK Centre. Further information regarding its inputs, outputs and interplay between them can be found in Appendix 8. In addition, details on the modelling of overplanting approach can be found in [2]. Modelling Type 2, as referred to in [2], is considered for the rest of the paper in order to take advantage of the full stochastic behaviour of the model inputs despite requiring a higher computational cost.

Stochastic Modelling

The transition from deterministic to stochastic models requires an added level of complexity that can be justified by three of the following features, as suggested in [13]. First, a pre-existing model that captures the relationship between inputs and outputs. Second, a variety of sources of uncertainty affecting the model inputs, which in this case are represented by probability distribution functions and finally, industrial stakes and decision-making circumstances motivating the uncertainty assessment, leading to a better understanding on cost and uncertainty in overplanting the design of offshore wind farms. OWCAT is a numerical model linking inputs (uncertain $\underline{x}$ or fixed variables $\underline{d}$) to outputs $\underline{z}$ (from which decision criteria can be established). This can be formally defined in Equation 1.

$$\underline{x}, \underline{d} \Longrightarrow \underline{z} = OWCAT(\underline{x}, \underline{d}) \tag{1}$$

It is worth noting the difference between these two sets of inputs. Whereas some inputs have uncertainty associated to them, others may be fixed – as they will play another role in the model, those are represented with notation $\underline{d}$. This is the case when: (i) model inputs represent variables under full control: for example the vessel associated with the installation of a monopile foundation, (ii) the uncertainties affecting the model inputs are considered to be negligible and (iii) the decision process conventionally fixes some variables for comparative purposes and time constraints: for example the discount rate may be set by the developer. However, it is important to bear in mind that a distinction between "uncertain" and "fixed" variables usually involve an iterative process by means of sensitivity analyses of the model which is out of the scope of this paper. The methodology of quantitative uncertainty management is a staged process. First, the specification of the problem needs to be considered. This is mathematically represented as the OWCAT model. After that, the uncertainty in the inputs is quantified and modelled by probability distributions. Once this is done, the propagation of uncertainty sources to the quantities of interest in the outputs can be carried out via MonteCarlo or other propagation techniques, resulting in a spread of project performance.

Modelling Risk Aversion

Risk aversion is modelled by risk metrics originated in the financial mathematics literature such as the Value at Risk (VaR) and Conditional Value at Risk (CVar). The $\mathbf{VaR}_\alpha$ gives the probability α that a certain outcome is worse than a given threshold. Typically the probability α represents the confidence level and $\mathbf{VaR}_\alpha$ is regarded as the maximum value that will not be exceeded at this given confidence level. Building on $\mathbf{VaR}_\alpha$, $\mathbf{CVaR}_\alpha$ gives the expected outcome given that the value is worse than $\mathbf{VaR}_\alpha$. The concept was first introduced in Rockafellar [12] and further developed by him in [11]. The mathematical formulation for $\mathbf{VaR}_\alpha$ and $\mathbf{CVaR}_\alpha$ for continuous functions is given in Equation 2 and 3, respectively.

$$\mathbf{VaR}_\alpha(LCOE) = min\left(c : P(LCOE \leq c) \geq \alpha\right). \tag{2}$$

$$\mathbf{CVaR}_\alpha[LCOE] = \mathbf{E}[LCOE | LCOE \geq \mathbf{VaR}_\alpha(LCOE)] \tag{3}$$

Where LCOE is the Levelised Cost of Energy, $P(LCOE \leq c)$ is the probability of the LCOE being less or equal than c and $\mathbf{E}$ is the mathematical expectation operator. One of the main shortcomings of the $\mathbf{VaR}_\alpha$ is that it provides no information on the extent to which values might materialise beyond the threshold amount indicated by the $\mathbf{VaR}_\alpha$ itself, whereas $\mathbf{CVaR}_\alpha$ does. In addition, $\mathbf{CVaR}_\alpha$ has superior mathematical properties since this measure is coherent in the sense of Artzner [1]. For this reason, we've selected $\mathbf{CVaR}_\alpha$ as the preferred financial risk metric. In this approach risk aversion is modelled as a weighted average λ of the **Median** and $\mathbf{CVaR}_\alpha$ of the LCOE values. Parameter λ can be varied from 0 (in a risk neutrality setting) to 1 (extreme risk aversion), based on the work of Munoz [10] and displayed in Equation 4.

$$\boldsymbol{\rho}_\alpha[\lambda, LCOE] = \lambda \mathbf{CVaR}_\alpha[LCOE] + (1-\lambda)\mathbf{Median}[LCOE] \tag{4}$$

4 Benchmark against National Grid

National Grid conducted a high level study on the optimal amount of overplanting for the UK Round 3 offshore wind farms [14]. The findings of the study suggested a 12% overplanting. However these findings are based on the following parameters: 5MW wind turbine, 90% wind turbine availability, 1.1GW of total capacity and an average wind speed of 9 m/s, which meant that 1200 MW of offshore wind should be built for 1000 MW of grid connection. Assuming the same base parameters, Figure 1 and 2 were obtained using our cost modelling tool. Figure 1 shows the difference between the unconstrained and constrained yield as a function of overplanting; the amount of constraint is minimum up to 8% overplanting, where the two lines start to diverge. This point is also reflected in Figure 2, suggesting that additional energy produced by the over installation of turbines doesn't outweigh its wind turbine expenditure; a 9% overplanting is considered optimal for this farm. Although the OWCAT modelling provides similar levels of overplanting as National Grid, some of the assumptions are a bit conservative in the current state of the offshore wind sector. For example, the rated capacity of wind turbines has almost double since 2010, moving from 5MW to 10MW wind turbines. Moreover, wind turbine availability rates have also increased from 90 to 95% or above. This suggests that past studies on overplanting based on these assumptions needs to be revisited.

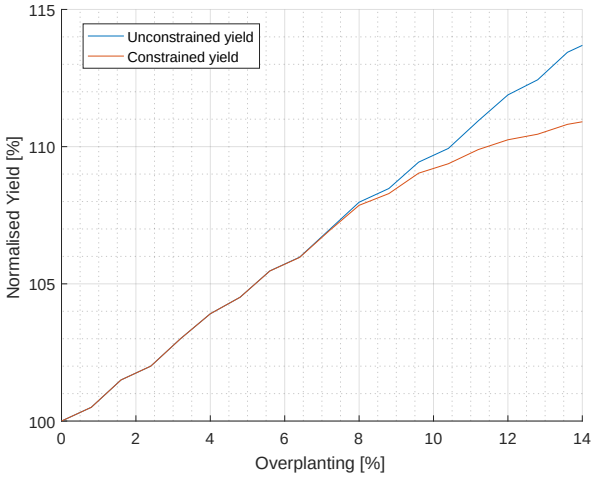

Figure 1: Unconstrained versus constrained normalised yield as a function of overplanting.

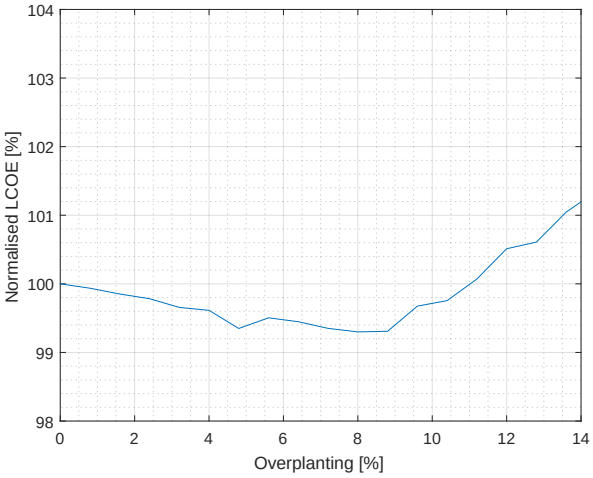

Figure 2: Reference case LCOE values for National Grid as a function of overplanting

5 Case Study

Several offshore wind farm configurations are analysed in terms of its suitability to overplanting; its project specifications are shown in Table 1. It is assumed, for the sake of simplicity, that the export cable length, construction and operational port distances are equal to the distance from shore. The MEC is 400MW, 1GW and 2GW and offshore wind farm capacities are varied from 0% to 14% in overplanting. The estimated mean wind speed is represented by a normal distribution with mean (μ) and standard deviation (σ) as $\mathcal{N}(\mu, \sigma^2)$[1]. Likewise, availabilities are represented by uniform distributions with lower(a) and upper(b) bounds as $\mathcal{U}(a, b)$.

Table 1: Offshore wind farm project specifications.

Characteristic	Value	Uncertainty
Water Depth [m]	25	None
Distance from shore [km]	25	None
Mean Wind Speed @ 100m [m/s]	9	$\mathcal{N}(9, 0.1^2)$
Wind Turbine Availability [%]	95	$\mathcal{U}(90, 97)$
Inter-Array Cable Availability [%]	99	$\mathcal{U}(97, 99)$
Foundation Type [-]	Monopile	None
Electrical Infrastructure [-]	HVAC	None
Wind Turbine Type [-]	164-8 MW	None
Wake effect [%]	10	None
Degradation Factor [%]	0.05	None

The reference case is calculated through a Monte Carlo simulation with input parameters from Table 1 (without uncertainties). Figure 3 shows the difference between the unconstrained and constrained yield as a function of overplanting; the amount of constraint is minimum up to 2% overplanting, where the two lines start to diverge. This point is also reflected in Figure 4, suggesting that additional energy produced by the over installation of turbines doesn't outweigh its wind turbine expenditure; a 2% overplanting is considered optimal for this farm. This is considerably lower compared to National Grid. As shown in Borras [2], several technology-specific factors were investigated in terms of its suitability to overplanting: wind speed, wake effects and wind turbine and inter-array cable availability. It was shown that the most sensitive parameter to overplanting is the wind turbine availability, which has been fixed to 95% for the local sensitivity in this study. The purpose of this paper is to expand this study to examine parameters such as wind farm capacity, wind turbine size, average water depth and average distance from shore, in order to provide some insight on how overplanting is influenced by larger turbines and sites located further from shore. In order to do so, the following number of combinatorial configurations (81), displayed in Table 2, have been examined.

Figure 5 shows the optimal amount of overplanting as a function of the wind farm total capacity and distance from shore. For a 25km distance from shore, overplanting the farm results in overall economic benefits. As the wind farm size increases so does the optimal amount of overplanting, moving from 2% to 4%. On the contrary, for 50 and 75km distance from shore, the optimal amount of overplanting remains at %2 for 400 MW while higher capacities lead to a negative overplanting effect; to the extend that for a 75km from distance any amount of overplanting results in a negative effect. For a given

[1] 0.1 m/s is a representative value combined from independent uncertainties, individually determined by normal distributions as seen in [7, 6, 18]

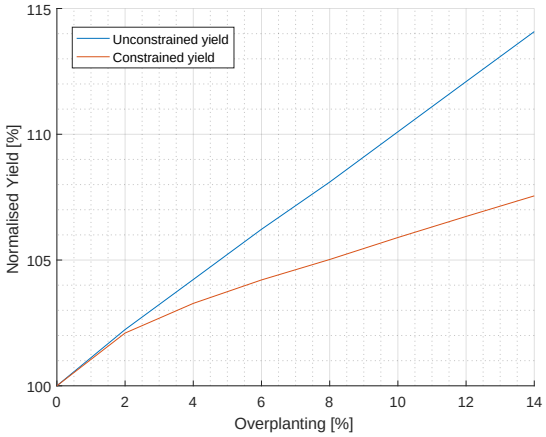

Figure 3: Unconstrained versus constrained normalised yield as a function of overplanting.

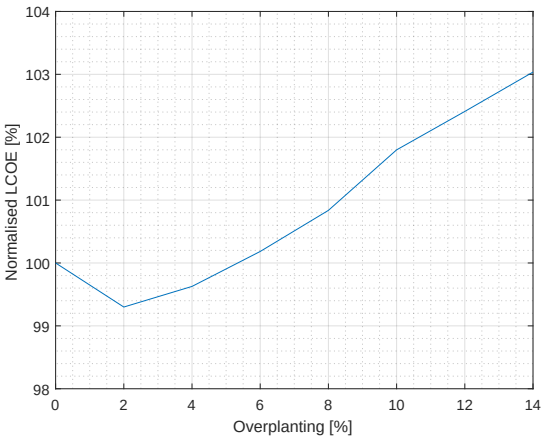

Figure 4: Reference case LCOE values as a function of overplanting.

Table 2: Wind farm configurations.

OWF Capacity[MW]	WTG Size[MW]	Distance Shore[km]	Water Depth[m]
400	4	25	25
1000	8	50	40
2000	12	75	60

site, the further from shore, the higher are the installation costs of the wind turbines. Given that the wind resource remains constant for all cases (at 9m/s mean wind speed), increasing the distance from shore, reduces the amount of optimal overplanting. In addition, the increase in wind farm size acts as a catalyst, increasing the effects of overplanting - derived from its economies of scale. Figure 6 takes advantage of the same data as Figure 5; however these are display holding wind farm capacity constant for every subplot. Figure 7 shows the optimal amount of overplanting as a function of the number of wind turbines for several wind farm sizes. Although the amount of overplanting changes depending on the size of the wind turbines, this effect is reduced as the the size of the farm grows. Figure 8 shows the optimal amount of overplanting as a function of the water depth and distance from shore in a 400 MW farm, whereas Figure 9 represents the same data but for a 2000 MW farm. Both figures suggest that the water depth has a neglegible effect on the optimal amount of overplanting.

The probability distribution function of the LCOE is obtained by 20,000 model evaluations of an outer Monte Carlo loop with parameters displayed in Table 1. It is worth bearing in mind that, for each model evaluation, an inner Monte Carlo simulation propagates the wind speed and availabilities with another 10,000 model evaluations within the Annual Energy Production module; this process is repeated for several degrees of overplanting. The risk metrics given by the expression $\lambda \mathbf{CVaR}_{\alpha=0.05}[LCOE] + (1-\lambda)\mathbf{Median}[LCOE]$ are normalised with respect to the values obtained when no overplanting is applied, as displayed in Figure 10. Overplanting the farm from 2% to 8% results in risk metrics (in a risk neutrality setting) that improve the economics of the farm. However, the optimal design is found at 4% of overplanting regardless of the risk appetite. Figure 11 includes the case when a 0.05 m/s mean wind speed uncertainty is given - the optimal amount of overplanting remains constant.

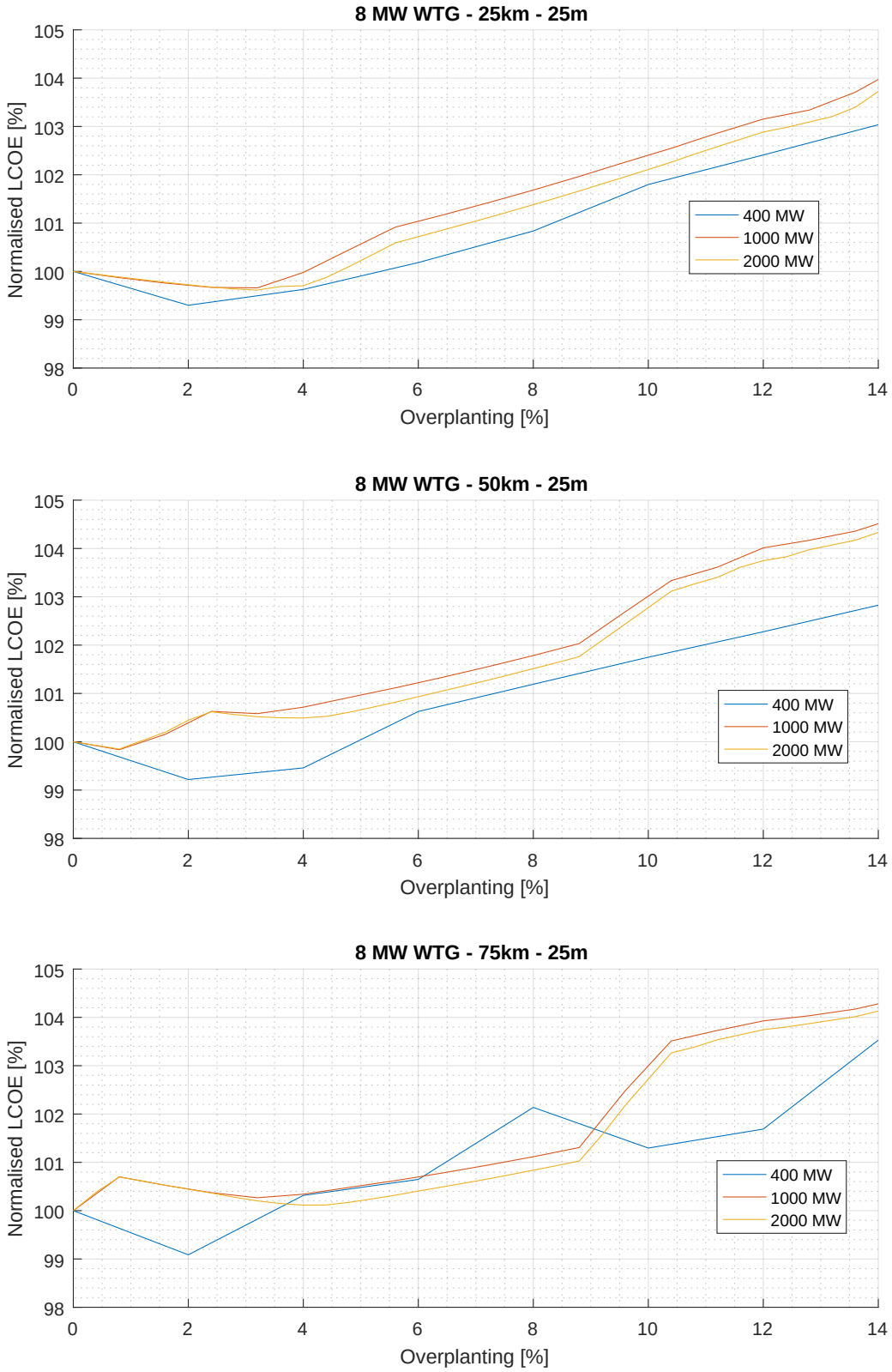

Figure 5: Influence of wind farm capacity and distance from shore to the optimal amount of overplanting.

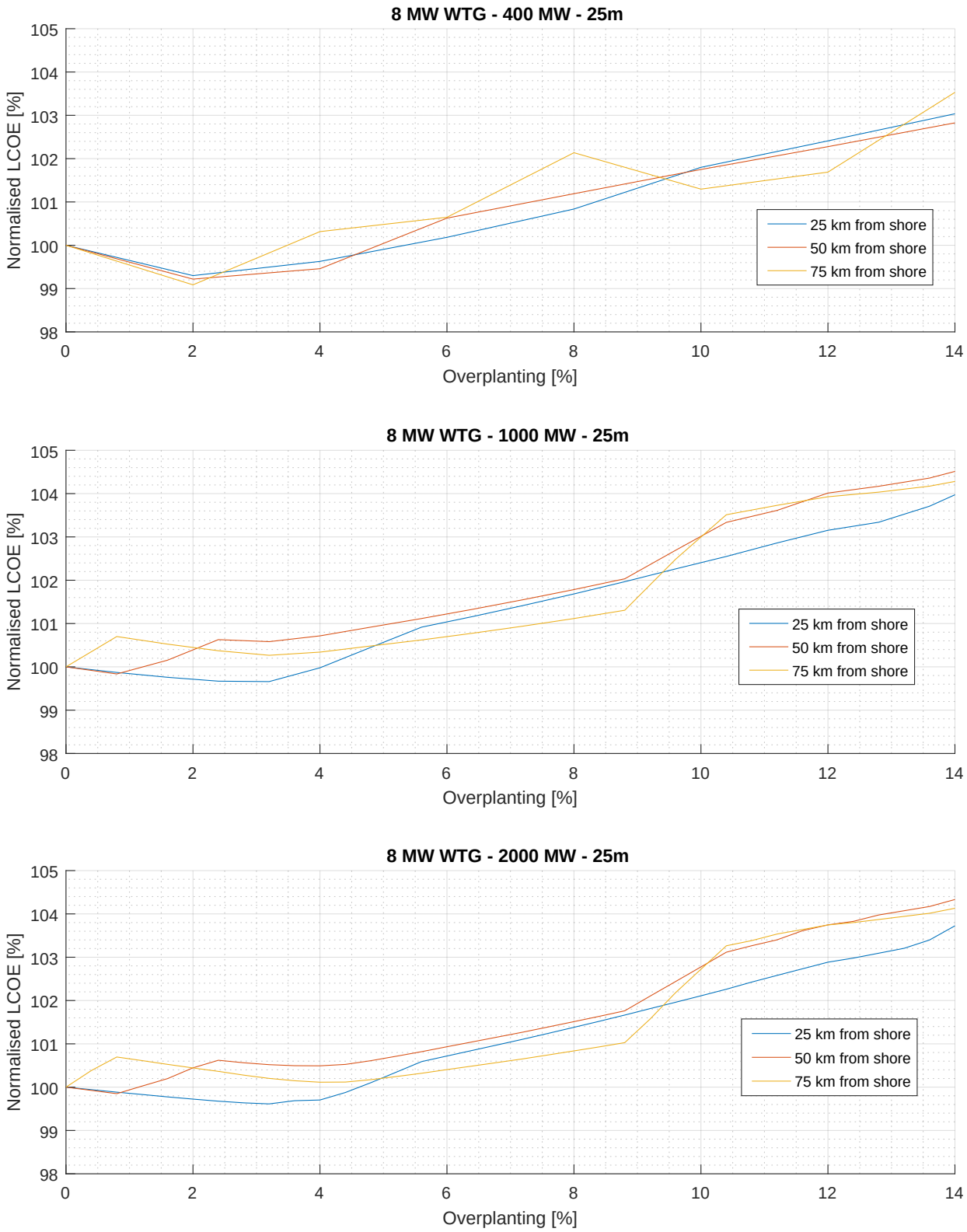

Figure 6: Influence of wind farm capacity and distance from shore to the optimal amount of overplanting.

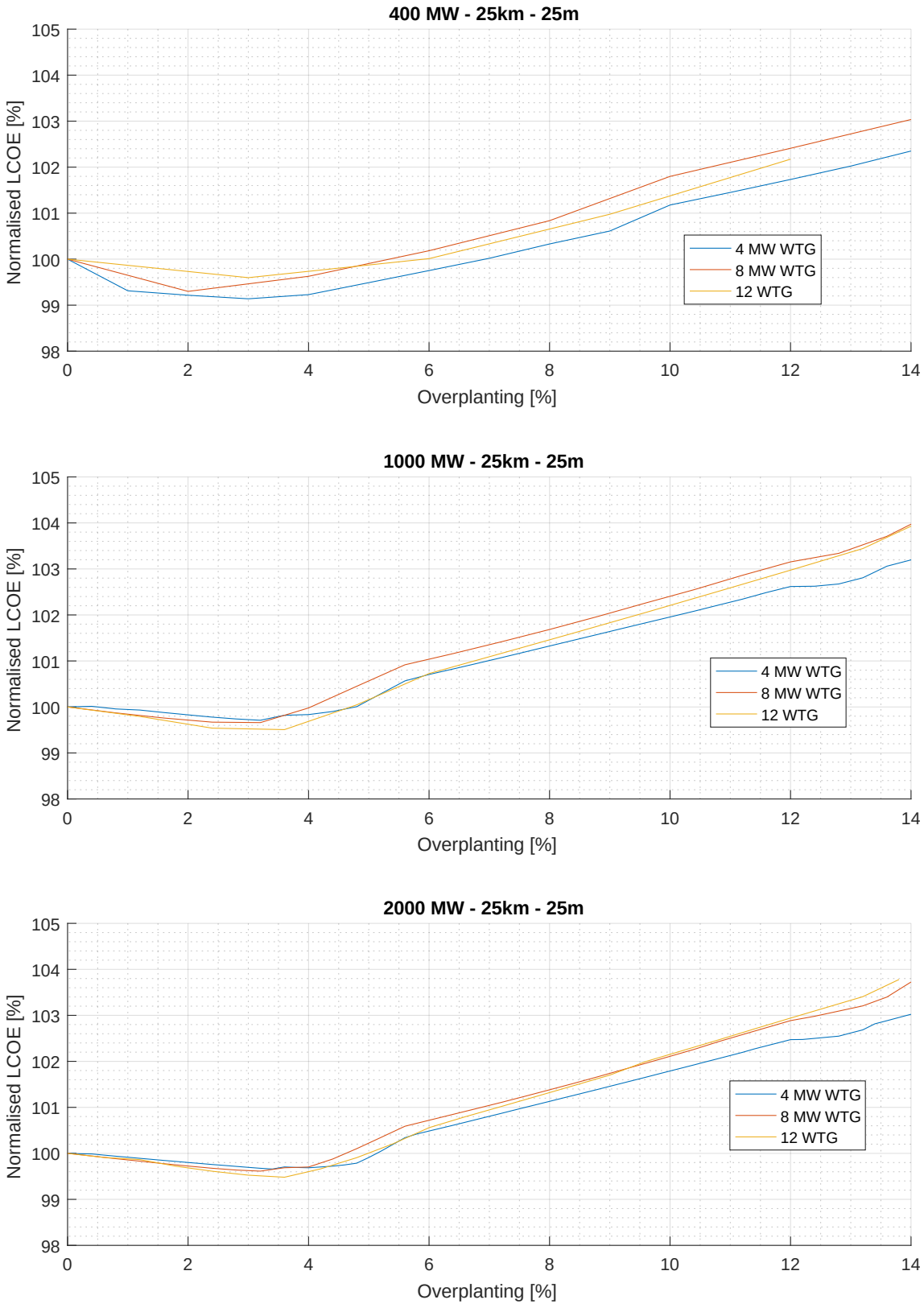

Figure 7: Influence of wind turbine size to the optimal amount of overplanting.

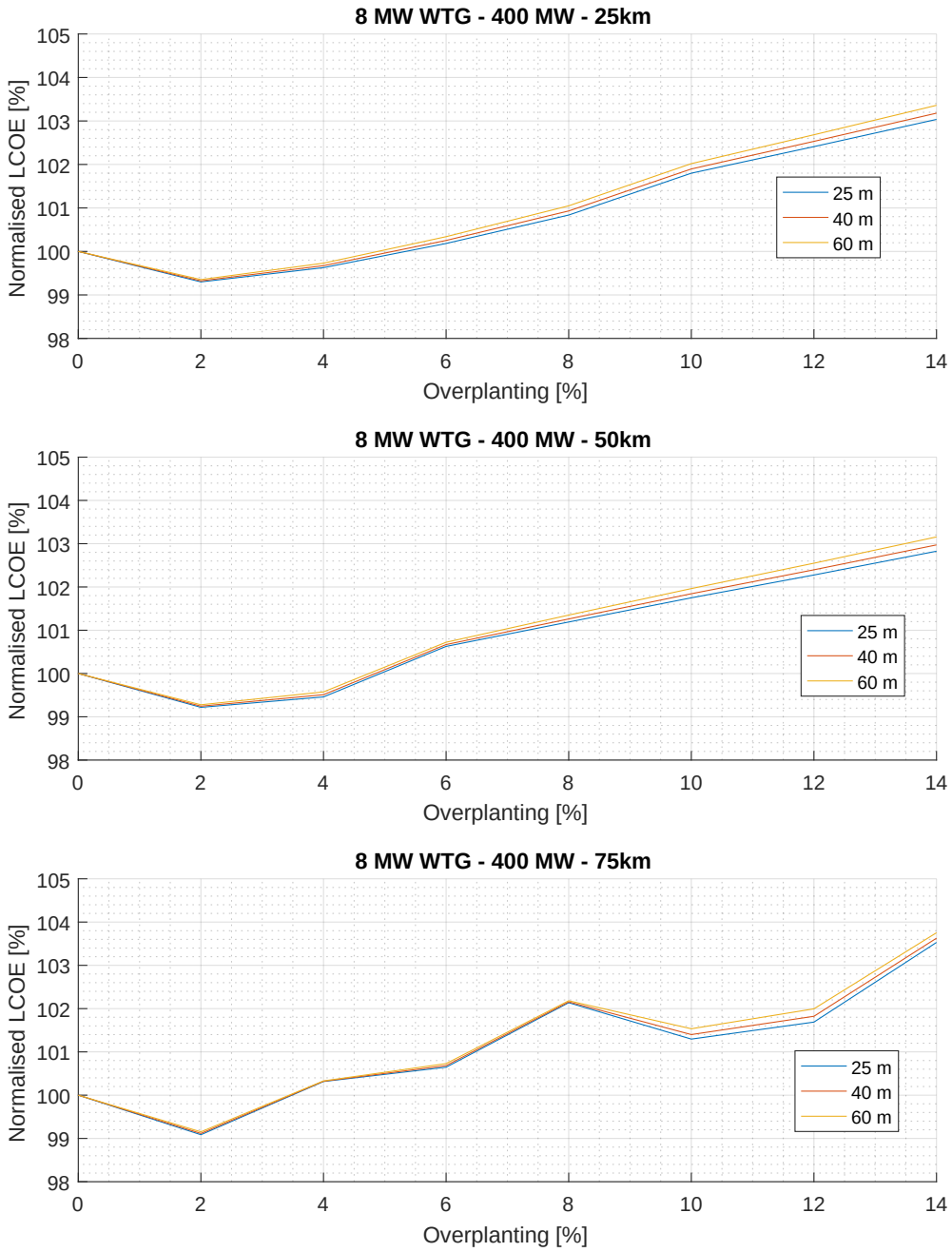

Figure 8: Influence of water depth to the optimal amount of overplanting in 400 MW farm.

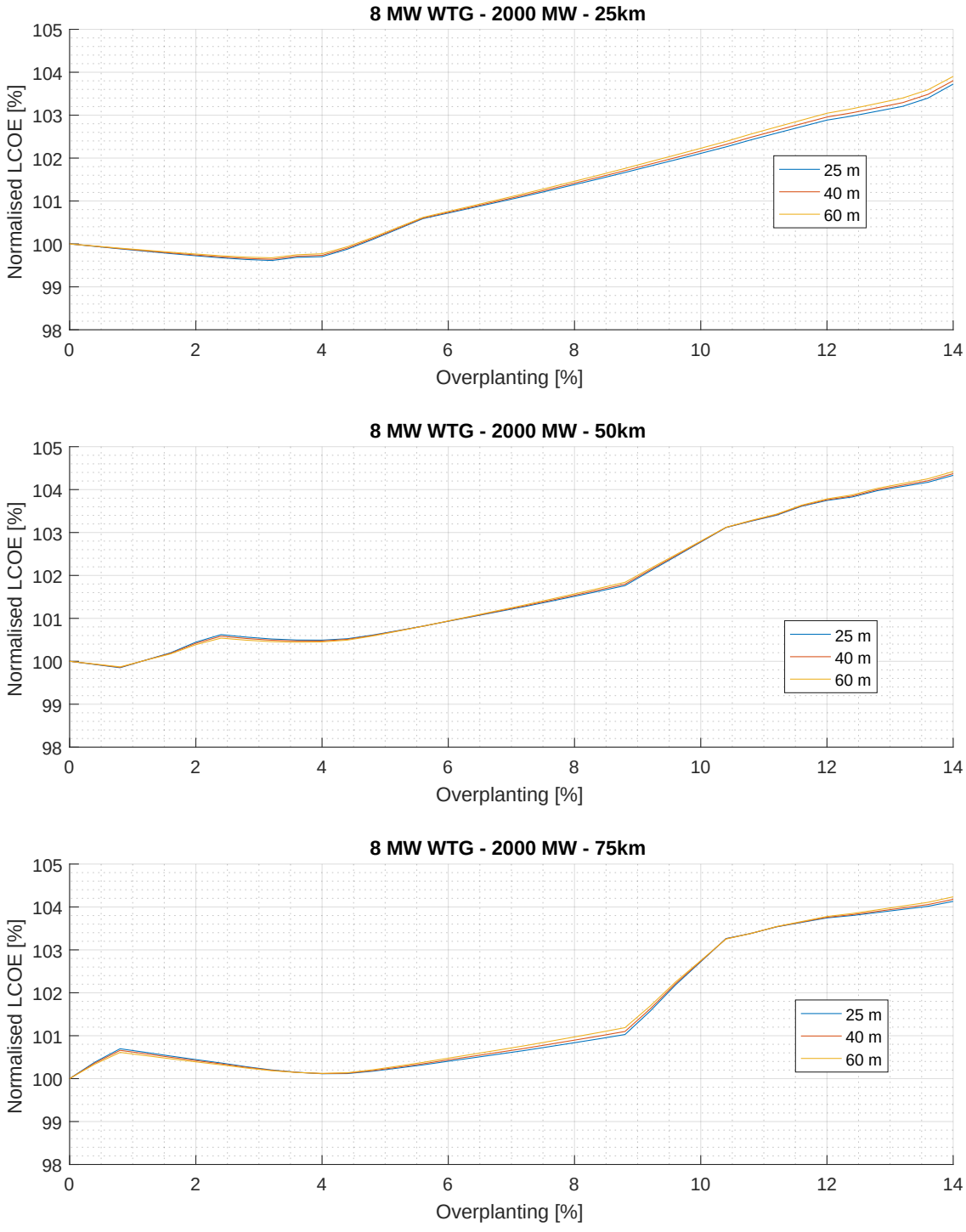

Figure 9: Influence of water depth to the optimal amount of overplanting in 2000 MW farm.

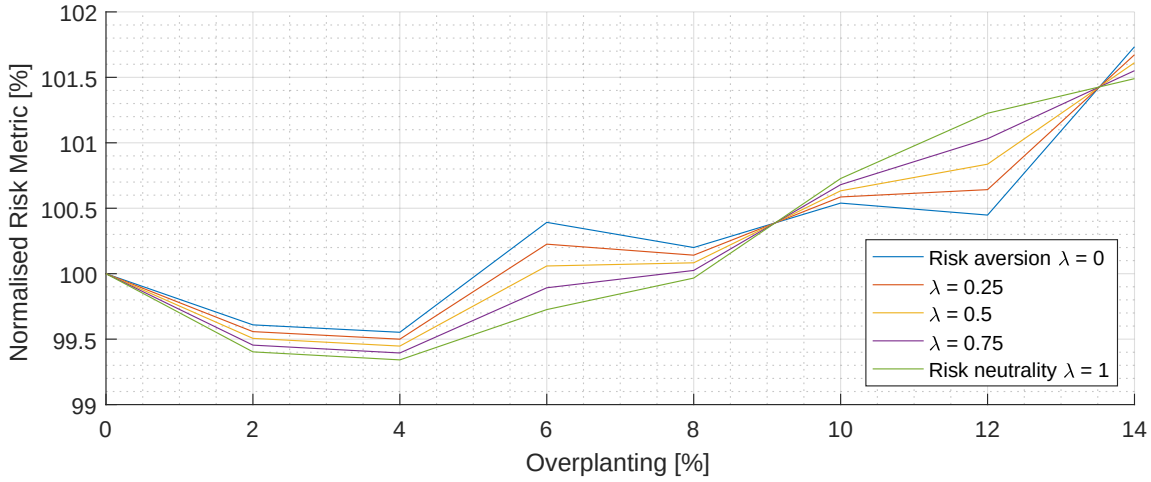

Figure 10: Risk aversion represented by $\boldsymbol{\rho}_\alpha[\lambda, overplanting]$ - 0.1 m/s mean wind speed uncertainty.

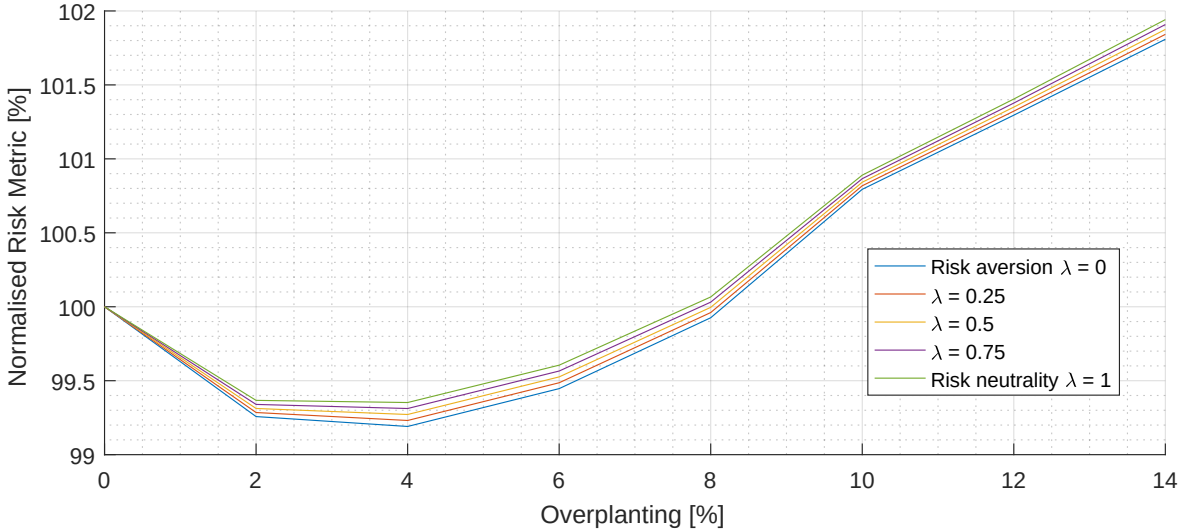

Figure 11: Risk aversion represented by $\boldsymbol{\rho}_\alpha[\lambda, overplanting]$ - 0.05 m/s mean wind speed uncertainty.

6 Conclusions

This paper has presented the development of a novel framework to assess overplanting in the design of offshore wind farms when the underlying variables, such as the wind speed and availability rates, among others, are uncertain. As seen by a benchmark with National Grid, as the wind turbine availability increases, overplanting becomes less valuable. This suggests that previous studies on overplanting, which were based on low wind turbine availabilities rates from UK Round 1 offshore wind farms (in the order of 90%), need to be revisited.

A local sensitivity analysis has revealed that wind farm capacities, turbine sizes and distances from shore are sensitive parameters to overplanting, whereas water depths play a secondary role. For a given site, wind farm sizes act as a catalyst for overplanting - increasing the positive or negative effects depending on the wind farm configuration. In addition, bigger wind turbine sizes reduce the effect of overplanting. Finally, the further the distance from shore, the higher installation costs of the wind turbines are and when holding wind resource constant, it reduces the amount of optimal overplanting. As a consequence, it is expected that sites located further from shore, with bigger wind turbines and less units for a given wind farm capacity will most likely have small benefits from overplanting.

Without considering the uncertainties in the different parameters represented by the outer Monte Carlo loop, it appears that the optimal amount of overplanting is 2% for our reference offshore wind farm. Generally speaking, the role of determining the optimal setup comes down to the risk appetite of the developer, which in this case is represented by a linear combination of the risk aversion and risk neutrality setting, governed by the λ parameter. However, when conducting the double loop Monte Carlo simulation, the optimal setup is found at 4% regardless of the risk appetite considered. Furthermore, overplanting the farm by any value from 2% to 8% gives a better result than with no overplanting for a risk neutral setting, meaning that overplanting can be used as a hedging instrument. Sensitivities on wind speed uncertainty do not change the optimal amount of overplanting.

Future work will take advantage of the framework developed in this paper to quantify how risk aversion influences the investment decision for the local sensitivity analysis carried out in this study. Also, the degradation factor has been taken into account after the constraint, but we would expect greater amounts of overplanting if this was taken before the constraint.

7 Acknowledgements

This article is based on work sponsored by EDF Energy R&D UK at the Industrial Doctoral Centre for Offshore Renewable Energy (IDCORE), a consortium of the University of Exeter, University of Edinburgh and University of Strathclyde. IDCORE is funded by both the Energy Technologies Institute and the Research Councils Energy Programme through grant number EP/J500847/1. Additional support came from the UK Engineering and Physical Sciences Research Council through grant number EP/P001173/1 (CESI).

8 Appendix A - Offshore Wind Cost Modelling Tool

The Offshore Wind Cost Analysis Tool (OWCAT) developed at the EDF Energy R&D UK Centre has been used in the past for comparative evaluation of multiple sites, detailed evaluation of specific project layouts and sensitivity studies on both design/technology choices and cost variations [3]. The tool has been validated against cost data from the Navitus Bay, Courseulles-sur-Mer and Neart na Gaoithe projects and shown to be accurate within ± 15% for these cases.

The cost modelling tool consists of four main modules: a wind farm design module, a cost calculation module, a financial module and an overarching stochastic module which allows inputs to be represented by probability distribution functions. The first stage of the module concerns the wind farm design. In order to evaluate the costs of the project, it is necessary to have information about the number and type of wind turbines, foundations, inter-array cabling and the export system. In other words, the wind farm itself must be modelled. Designing an offshore wind farm requires interaction between teams from different disciplines; for example, the wind turbine team will have to interact with the foundation team to make sure that the loads of the turbine are correctly passed onto the foundation, and the foundation team will need to make sure that the electrical connections are correctly secured within the foundation. As such, a cost model must capture the same interactions as the design process and cannot be a simple accumulation of models from separate disciplines.

The design outputs of the first module are fed as inputs into the second module, which calculates the costs of the different offshore wind farm components. The cost module can be divided into Development Expenditure (DEVEX), Capital Expenditure (CAPEX), Operational Expenditure (OPEX) and Decommissioning Expenditure (DECEX). DEVEX covers the costs of all the processes up to the financial close or placing firm orders to proceed with the construction. CAPEX calculates the supply and installation costs of the wind farm, including wind turbines, foundations, inter-array cables, offshore substations, export cables and onshore substations. Indirect costs such as Engineering, Procurement, and Construction Management (EPCM) costs and insurance are also included in the CAPEX breakdown. OPEX includes direct costs for the operation and maintenance of the wind farm, as well as transmission charges, insurance, taxes and royalties. DECEX accounts for the decommissioning of the wind turbines, foundations and offshore substations.

The cost outputs of the second module are passed into the third module, which is the financial model of the wind farm project. The financial model takes into consideration the different cash flows throughout the life of the wind farm, as well as the financing structure put in place to supply the initial capital investment. Based on the resulting free cash flows and financing costs, the LCOE can be determined, together with other financial performance indicators. The financial module allows for corporate and project financing modelling.

The OWCAT structure is shown in Figure 12. This information has been divided into:

- (i) Project Specifications
- (ii) Technical Specifications
- (iii) Economic and Financial Specifications
- (iv) Vessel Specifications
- (v) Structural Masses and Electrical Components Database

(i) refers to the project offshore wind farm characteristics such as the capacity of the farm, the wind speed at a given referenced height, the average water depth, the soil conditions, the distance from shore, the wind turbine model, foundation type and export system specifications among others. Since no two projects will have the same characteristics, project specifications attempt to model each particular site.(ii) addresses the details of the offshore wind technology, representing wind turbine, foundation, inter-array cable, export system and grid parameters. For example, as far as the wind turbine is concerned, parameters such as the wind turbine availability, the installation vessel associated with the wind turbine, the average loading, installation and commissioning times are accounted for. In addition, a decommissioning factor is used for all offshore wind farm components to account for a reduction in time from the installation phase.(iii) concerns the reference year for real prices, the risk-free rate and cost of debt, insurance and insurance premium tax rates, contingency requirements, corporation taxes, depreciation, seabed rent, exchange rates and inflation.(iv) involves the different vessel characteristics used in the installation and decommissioning of the offshore wind farms. As an example, heavy-lift jack-up vessel parameters comprise the day rate, vessel transit speed, vessel positioning time, vessel mobilisation time, operational weather window and carrying capacities in regard to different components.(v) consists of the data used to establish the foundation mass correlations, which are the basis for the CAPEX estimation in the foundation procurement. It also considers the correlations used to estimate the cost of different electrical components.

The final design contains not only the design of the offshore wind farm, where the foundations masses, inter-array and export system are sized, but also the procurement, vessel charter model and the Annual Energy Production (AEP) as displayed in Figure 12. Procurement stores all the information concerning wind turbines, foundations and the electrical system, in terms of the type, number of elements and size (also length if required), giving rise to a procurement catalogue which forms the basis for the cost module. The vessel charter model is based on the work of Kaiser [**Kaiser2012**], whereas the AEPs is built upon industry's best practices assuming respectively either a logarithmic- or power-law wind profile in conjunction with a Rayleigh or Weibull probability distribution to model the wind speed. Wake losses and electrical losses are also accounted for in the AEP submodule.

As far as the financial module is concerned, the calculation itself entails not only one but a twofold iterative process. The external loop consists of determining the value of λ that makes Equation 5 equal to 0.

$$LCOE = \lambda | \sum_{t=1}^{n} \frac{FCF_t(t)}{(1 + MARR)^t} = 0; \tag{5}$$

Where FCF are the free cash flows, $MARR$ is the desired Minimum Acceptable Rate of Return (MARR) and λ_0 is the intial guess obtained from a simplified financial model. The LCOE financial metric is calculated as the constant inflation-linked real electricity price required to meet the desired MARR. The internal loop is used in the project finance setting and concerns the debt sizing or sculpting, which determines the maximum amount of project finance debt that the offshore wind farm can sustain based on the bank's requirements. Project lenders usually specify the borrowing capacity on the basis of debt service ratio and convenants. As such, parameters such as the Debt Service Coverage Ratio (DSCR), the maximum leverage and the Cash Flow Available for Debt Service (CFADS) have been considered.

Lastly, the stochastic module (depicted in orange in Figure 12) allows the model to be embedded in the framework of uncertainty quantification.

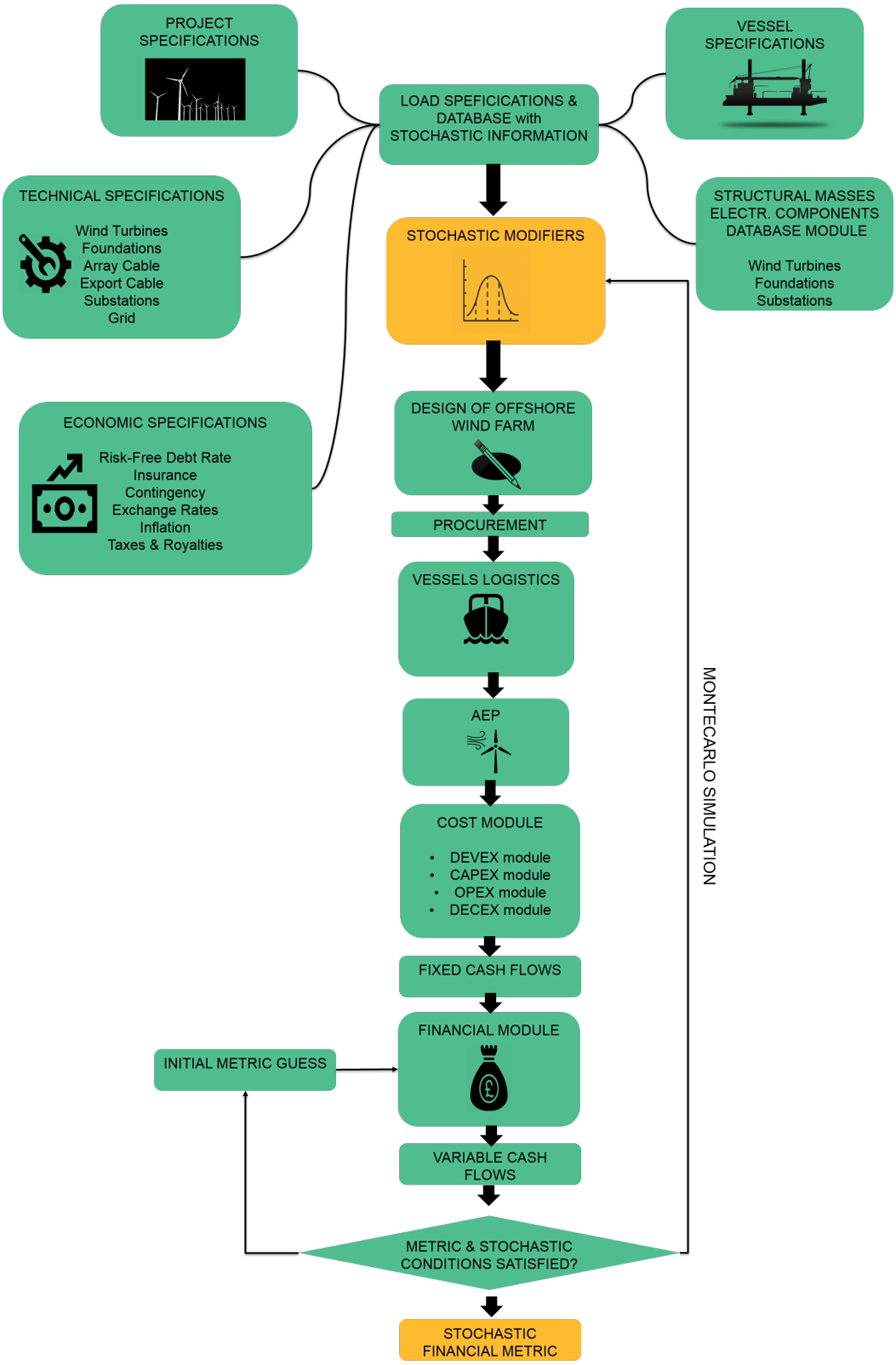

Figure 12: Stochastic OWCAT Structure

References

[1] Philippe Artzner et al. "Coherent measures of risk". In: *Mathematical Finance* 9.3 (1999), pp. 203–228. ISSN: 09601627. DOI: 10.1111/1467-9965.00068.

[2] Esteve Borras Mora. "How does risk aversion shape overplanting in the design of offshore wind farms ?" In: *Journal of Physics: Conference Series* (2019).

[3] Esteve Borras Mora. "Transition from Deterministic to Stochastic Cost Models for Offshore Wind Farms". In: *Offshore Wind Energy Conference*. June. 2017.

[4] Brid ODonovan. *Connection Offer Policy & Process (COPP)*. Tech. rep. Commission for Energy Regulation, 2011.

[5] Forewind. *Environmental Statement Chapter 6 Appendix B Offshore Project Boundary Selection Report*. Tech. rep. March. 2014.

[6] Brian Gribben, Mark Joyce, and Frazer-Nash Consultancy. *Uncertainty analysis to support asset procurement decisions in offshore wind*. Tech. rep. 2011.

[7] Pramod Jain. *Wind Resource Assessment : A Key Step in Wind Projects Green Energy Financing Workshop Asia Clean Energy Forum*. 2017.

[8] Celine Mcinerney and Derek W Bunn. "Optimal over installation of wind generation facilities". In: *Energy Economics* 61 (2017), pp. 87–96. ISSN: 0140-9883. DOI: 10.1016/j.eneco.2016.10.022. URL: http://dx.doi.org/10.1016/j.eneco.2016.10.022.

[9] Nigel Morris. *Decision on Installed Capacity Cap Installed Capacity Cap*. Tech. rep. Commission for Energy Regulation, 2014.

[10] Francisco D Munoz et al. "Does risk aversion affect transmission and generation planning ? A Western North America case study". In: *Energy Economics* 64 (2017), pp. 213–225. ISSN: 0140-9883. DOI: 10.1016/j.eneco.2017.03.025. URL: http://dx.doi.org/10.1016/j.eneco.2017.03.025.

[11] R Tyrrell Rockafellar and Stanislav Uryasev. "Conditional value-at-risk for general loss distributions". In: *Journal of Banking & Finance* 26 (2002), pp. 1443–1471.

[12] R. Tyrrell Rockafellar and Stanislav Uryasev. "Optimization of conditional value-at-risk". In: *The Journal of Risk* 2.3 (2000), pp. 21–41. ISSN: 14651211. DOI: 10.21314/JOR.2000.038. arXiv: arXiv:1011.1669v3. URL: http://www.risk.net/journal-of-risk/technical-paper/2161159/optimization-conditional-value-risk.

[13] Etienne de Rocquigny, Nicolas Devictor, and Stefano Tarantola. *Uncertainty in Industrial Practice: A Guide to Quantitative Uncertainty Management*. 2008, p. 364. ISBN: 0470770740. DOI: 10.1002/9780470770733. URL: https://books.google.com/books?id=qg8bqw6ByskC%7B%5C&%7Dpgis=1.

[14] *Round 3 Offshore Wind Farm Connection Study*. Tech. rep. 2008.

[15] Limited SMart Wind. "Hornsea Offshore Wind Farm - Project Two". In: 5.January (2015), p. 19.

[16] TenneT Team. *POSITION PAPER Overplanting*. Tech. rep. TenneT, 2015, pp. 1–7. URL: http://www.tennet.eu/nl/fileadmin/afbeeldingen/grid-projects/Net%7B%5C_%7Diop%7B%5C_%7Dzee/Ronde%7B%5C_%7D7/ONL%7B%5C_%7D15-083-T11%7B%5C_%7DOverplanting%7B%5C_%7DPP%7B%5C_%7Dv2.pdf.

[17] C Wolter et al. "Overplanting in Offshore Wind Power Plants in Different Regulatory Regimes". In: *15th Wind Integration Workshop* 49.0 (2016), pp. 0–4. DOI: 10.1146/annurev.matsci.35.100303.110641.

[18] Matthew Huaiquan Zhang. "Wind Park Production Estimate". In: *Wind Resource Assessment and Micro-sitting*. 2015. Chap. 7, pp. 143–167.